

Enhancing Dykeland Resiliency in a Hypertidal Estuary

By
Graeme Matheson

A Thesis Submitted to
Saint Mary's University, Halifax, Nova Scotia
In Partial Fulfillment of the Requirements for
The Degree of Master of Science in Applied Science.

March 2020, Halifax, Nova Scotia

© Graeme Matheson

Approved: Dr. Danika van Proosdij
Supervisor
Department of Geography and
Environmental Studies

Approved: Dr. Jeremy Lundholm
Supervisory Committee Member
Department of Biology

Approved: Tony Bowron MSc.
Supervisory Committee Member
Department of Environmental Science

Approved: Dr. Devon Eulie
External Examiner
Department of Environmental Science
University of North Carolina
Wilmington

March 02nd, 2020

Abstract

Enhancing Dykeland Resiliency in a Hypertidal Estuary

by Graeme Matheson

March 02nd, 2020

DykELANDS are low-lying areas created by the reclamation of saltmarshes by the construction of dykes and other infrastructure which are made resilient to the impacts of climate change by the presence of robust foreshore saltmarshes seaward of dyke infrastructure. This study looked at the impact flood and erosion adaptation strategies have had on hypertidal saltmarshes at various spatial and temporal scales in the Bay of Fundy, Canada. While the primary cause of significant foreshore saltmarsh erosion and progradation were a result of natural processes, several features were found to have precipitated significant changes in the position of the foreshore. Borrow pits, which are excavated swaths of saltmarsh excavated from the foreshore for dyke topping material were also studied using an unmanned-aerial-vehicle and structure-from-motion software. Eight out of the 13 borrow pits studied were found to be infilling at a rate which would only reduce dykeland resiliency in the short-to-medium term.

Keywords: Dykeland, Climate Change, Sea Level Rise, Ecomorphodynamics, Adaptation, Mitigation, Management, Unmanned Aerial Systems, Structure-from-Motion, GIS

Acknowledgements

I would like to thank my supervisor Dr. Danika van Proosdij for her guidance, compassion and continual patience throughout this entire thesis. I would also like to thank my committee members, Dr. Jeremy Lundholm and Tony Bowron for their support and helpful guidance. A big thank you to Logan Horrocks, who helped me with all my field and lab work from day one and Julia Purcell for all her help with processing the hydrodynamic data. Also, I would like to thank “the crew”: Christa Skinner, Julia Purcell, Sam Cunningham, Larissa Sweeny, Reyhan Akyol, Raj Singh Toor, Claire Mercer, and Ashton Baiche for all their help and contributions in the field. Chris Ross was a critical part of my thesis, programming DSAS and AMBUR for the EPR calculation, as well as providing countless GIS tips. And thanks to Greg Baker for all his help with GIS, Pix4D, and piloting the UAV. I would like to thank Jennie Graham and CBWES for their support and help with processing level loggers and the inundation frequency tables. Thank you to the Nova Scotia Department of Agriculture, Kevin Bekkers, Carl Esau, Darrell Hingley, David Smith, Craig Bauchmann, and Cyrus Steele for your expert knowledge and in-kind support. Finally, I would like to thank my parents, David and Yvonne, and my fiancée, Amy Nelson for their endless patience, support, and love while I completed this master’s thesis. This project was funded through AgriRisk and by the Nova Scotia Graduate Scholarship.

Table of Contents

Abstract	ii
Acknowledgements	iii
List of Figures	iv
List of Tables	xi
List of Equations	xiii
Chapter 1: Introduction to Research Project	1
1.1 Introduction.....	1
1.2 Project Context.....	4
1.3 Thesis Organization.....	5
Chapter 2: Ecomorphodynamic response of saltmarshes to natural and anthropogenic modifications in a fetch-limited, highly turbid, hypertidal estuary.....	7
2.1 Introduction	7
2.2 Study Area	16
2.3 Methods and Materials	19
2.3.1 Assessment of error reporting for EPR	26
2.4 Results	27
2.5 Discussion.....	34
2.5.1 Dykes.....	36
2.5.2 Kickers.....	42
2.5.3 Borrow Pits.....	46
2.5.4 Aboiteaux.....	50
2.5.5 Dredging.....	51
2.5.6 Foreshore Rocking.....	54
2.5.7 Managed Realignment.....	56
2.5.8 Channel Migration and Thalweg.....	57
2.6 Conclusion.....	59
Chapter 3: Application of unmanned aerial systems, structure-from-motion, and hydrodynamics to assess the sustainability of borrow pits for dykeland management.....	65
3.1 Introduction	65
3.1.1 Borrow Pits.....	68

3.1.2 Sediment Dynamics.....	74
3.1.3 Unmanned Aerial Systems and Structure-from-Motion.....	76
3.2 Study Area	80
3.3 Methods and Materials	84
3.3.1 Change Detection using UAS-SfM	85
3.3.2 Empirical Measurements of Hydrodynamics	96
3.4 Results	100
3.4.1 Digital Surface Model Accuracy Validation.....	100
3.4.2 Infill Rates and Empirical Measurements of Hydrodynamics	101
3.5 Discussion.....	128
3.5.1 Importance of Suspended Sediment Concentration	129
3.5.2 Borrow Pit Hydrology	133
3.5.3 Role of scour in borrow pit re-vegetation.....	134
3.5.4 The potential impact of seasonal variability.....	134
3.5.5 Efficacy of UAS for saltmarshes and tidal environments.....	135
3.5.6 Volumetric Uncertainty.....	138
3.6 Conclusion.....	140
Chapter 4: Enhancing dykeland resiliency: Guiding principles for dykeland management in a “green-grey” coastal defence system.....	143
4.1 No foreshore saltmarsh should be destroyed to implement coastal defence structures.....	143
4.2 Green and hybrid coastal defence schemes should be implemented wherever possible.....	144
4.3 Borrow Pits.....	147
4.3.1 Dyke topping material should be borrowed from upland source whenever possible.....	148
4.3.2 Borrow pits should only be implemented on robust foreshore saltmarshes with a history of progradation and static change patterns.....	148
4.3.3 Borrow pits should only be implemented in low-energy, highly-turbid systems.....	151
4.3.4 Borrow pits should be based off a scientific framework for implementation.....	155
4.3.5 Adaptive management strategies for failing borrow pits.....	157

4.4 Conclusion.....	158
References	159
Appendix I – EPR Images and Shoreline Position Error.	177
Appendix II – Hydrodynamic Tables by Borrow Pit	179
Appendix III – Predicted cumulative infill and hydroperiod.	185

List of Figures

Figure 1: A list of common structures and strategies implemented in hypertidal estuaries around the world and in the Bay of Fundy. These will be the focus of this study.	12
Figure 2: Study area map showing the location of foreshore saltmarsh and dyke infrastructure as well as the extent of the various process dominated zones in the Cobequid Bay Salmon River Estuary, Nova Scotia, Canada.	18
Figure 3: An example of how transects were edited to be perpendicular to the direction of foreshore processes.	21
Figure 4: Workflow for determining significant change at the saltmarsh scale.	24
Figure 5: Workflow for validating and identifying significant changes at the process dominated zone scale.	25
Figure 6: Percentage of total transects per EPR range and zone.	28
Figure 7: Mean EPR per dyke segment (25m) for marshes in the Tidal/Wave dominated zone. NS064_02, NS064_04, and NS023r are considered fluvial.	29
Figure 8: Mean EPR per dyke segment (25m) for marshes in the mixed zone. NS015_01, NS015_02, NS040_3, and NS040_05 are considered fluvial.	31
Figure 9: Mean EPR per dyke segment (25m) for marshes in the fluvial zone. Other fluvial dominated marshes shown in Figure 7 and 8 include NS015_01, NS015_02, NS023r, NS040_03, NS040_05, NS064_02, and NS064_04.	33
Figure 10: Changes in EPR over decadal scale.	34
Figure 11: Map showing changes in saltmarsh location from 1938 (pink) to 2013 (dark green). Mean EPR between 1975 and 2017 shown below. Significant progradation is	

4.6m·yr⁻¹ and significant erosion is -2.7m·yr⁻¹. Start and end points in map correlate with points in EPR graph.38

Figure 12: Foreshore change at NS114 between 1964 and 2013. Although the relative position of the foreshore edge has stayed the same, there has been a loss of foreshore width and resiliency.39

Figure 13: Map showing changes in saltmarsh location from 1938 (pink) to 2013 (dark green). Mean EPR between 1938 and 2017 shown below. Significant erosion is -11.4m·yr⁻¹. Start and end points in map correlate with points in EPR graph.41

Figure 14: Map showing changes in saltmarsh location from 1938 (pink) to 2013 (dark green). Mean EPR between 1938 and 2017 shown below. Significant progradation is 1.8m·yr⁻¹ and significant erosion is -1.2m·yr⁻¹.43

Figure 15: 1) Bank erosion caused by movement of thalweg. 2) Kicker is installed deflecting thalweg away from bank. 3) Deposition occurs downstream of the kicker. Thalweg position is reinforced by bed scour. 4) Saltmarsh colonizes the newly formed mudflat. Based off Klingemann et al, 1984. Credit: Will Flanagan.....44

Figure 16: Map showing how the implementation of dykes and kickers have stabilized the Salmon River and its thalweg between 1938 and 2015.46

Figure 17: Scouring of backshore saltmarsh caused by the excavation of a borrow pit outlet.47

Figure 18: Foreshore erosion exceeding 10m·yr⁻¹ following the excavation of borrow pits. This is caused by high velocities entering and leaving the borrow pit outlets.....49

Figure 19: The movement of an aboiteau channel at NS012 VDJ Marsh has significantly influenced the position of the foreshore saltmarsh. As the channel migrates toward the foreshore edge it can accelerate erosion rates. When it migrates away from the edge it

leaves behind an area where rapid deposition can occur leading to significant	
progradation when mudflat reaches a suitable elevation for saltmarsh growth.....	51
Figure 20:Significant loss of foreshore saltmarsh caused by dredging followed by a period	
of rapid deposition and saltmarsh growth. Dredging was implemented in an effort to	
mitigate flooding.	53
Figure 21: Dredging of the channel bed, intertidal mudflat, and saltmarsh.	54
Figure 22: Foreshore rocking implemented to prevent erosion was implemented in	
between 2013 and 2014. Although this has temporarily slowed erosion rates, it has	
increased scour at the end of the rocking, removing the intertidal mudflat.....	56
Figure 23: Dynamic rates of change in the location of the foreshore edge caused by ebb	
channel migration.....	58
Figure 24: Extreme rates of progradation (>50m/yr) caused by the rapid colonization of	
an intertidal mudflat by <i>Spartina alterniflora</i>	59
Figure 25:Aerial photographs of borrow pits. A) A borrow pit and dyke supported by a	
rock apron. B) A long borrow pit excavated near Masstown, Nova Scotia. C) A parallel	
borrow pit configuration excavated near Truro, Nova Scotia. D) A borrow pit inundated at	
high tide near Onslow, Nova Scotia.....	69
Figure 26: Borrow pit excavation using a long-reach excavator. Photo credit - Carl Esau,	
NSDA, winter 2015.	71
Figure 27:Study area map showing the locations of marshes with newly excavated borrow	
pits examined in this thesis. Masstown West, Masstown East, VDJ, and Lower Truro are	
all located in the Cobequid Bay Salmon River Estuary while Ryerson-Dugau is located in	
the lower Bay of Fundy in the Annapolis Basin.	82

Figure 28: Borrow pits at A) Masstown West, B) Masstown East, C) Ryerson-Dugau, D) VDJ, and E) Lower Truro marshes.83

Figure 29: Idealized GCP network at Ryerson-Dugau Marsh. GCPs surround the study area and are evenly distributed throughout the site.....86

Figure 30: General method for installing GCPs.....87

Figure 31: Generalized diagram of how the Surface Volume tool in ArcMap10.5 was used to determine volumetric change (ESRI, 2018).91

Figure 32: Fieldwork setup at VDJ Marsh showing the general layout of hydrodynamic equipment used at all sites, including: Acoustic Doppler Current Profiler (ADCP), Acoustic Doppler Velocimeter (ADV), Teledyne ISCO Water Sample, Level Loggers (LL) and Rising Stage Bottles (RSB).97

Figure 33: Rising stage bottles installed 20cm above the channel bed were used to measure incoming SSC.98

Figure 34: DoD showing vertical change at RD_01. Green represents vertical accretion and red represents erosion. The top figure uses all pixels, the bottom shows changes that occurred with 68% confidence (LoD =0.080m).106

Figure 35: SSC vs water level over the tidal period. RD_01 July deployment. Time is relative to the recorded high tide (HT).107

Figure 36: Hydrodynamics during July deployment (T2) at RD_01. Backscatter proxy (top), resolved horizontal velocity (middle), and SSC vs water level (bottom).108

Figure 37: SSC vs water level over the tidal period. VDJ_03 June deployment. Time is relative to the recorded high tide (HT).110

Figure 38: SSC vs water level over the tidal period. MTW_01 June deployment. Time is relative to the recorded high tide (HT).110

Figure 39: Hydrodynamics during May deployment (T1) at MTW_01. Backscatter proxy (top), resolved horizontal velocity (middle), and SSC vs water level (bottom). 111

Figure 40: Hydrodynamics during June deployment (T1) at VDJ_03. Backscatter proxy (top), resolved horizontal velocity (middle), and SSC vs water level (bottom). 113

Figure 41: The borrow pit outlet at MTW_01 significantly widened at either end, or experienced bed scour. This is a result of the volume of the pit being out of hydraulic equilibrium with the size of the outlet channel. 115

Figure 42: DoD showing vertical change at VDJ_01. Green represents vertical accretion and red represents erosion. The top figure uses all pixels, the bottom shows changes that occurred with 68% confidence (LoD =0.170m). 116

Figure 43: DoD showing vertical change at VDJ_03. Green represents vertical accretion and red represents erosion. The top figure uses all pixels, the bottom shows changes that occurred with 68% confidence (LoD =0.170m). 117

Figure 44: DoD showing vertical change at MTW_01. Green represents vertical accretion and red represents erosion. The top figure uses all pixels, the bottom shows changes that occurred with 68% confidence (LoD =0.140m). 118

Figure 45: DoD showing vertical change at MTW_02. Green represents vertical accretion and red represents erosion. The top figure uses all pixels, the bottom shows changes that occurred with 68% confidence (LoD =0.140m). 119

Figure 46: DoD showing vertical change at MTE_01. Green represents vertical accretion and red represents erosion. The top figure uses all pixels, the bottom shows changes that occurred with 68% confidence (LoD =0.120m). 121

Figure 47: DoD showing vertical change at MTE_02. Green represents vertical accretion and red represents erosion. The top figure uses all pixels, the bottom shows changes that occurred with 68% confidence (LoD =0.120m). 122

Figure 48: DoD showing vertical change at MTE_03. Green represents vertical accretion and red represents erosion. The top figure uses all pixels, the bottom shows changes that occurred with 68% confidence (LoD =0.120m). 123

Figure 49: DoD showing vertical change at LT_01, LT_02, LT_03, and LT_04. Green represents vertical accretion and red represents erosion. The top figure uses all pixels, the bottom shows changes that occurred with 68% confidence (LoD =0.070m). 124

Figure 50: DoD showing vertical change at VDJ_02. Green represents vertical accretion and red represents erosion. The top figure uses all pixels, the bottom shows changes that occurred with 68% confidence (LoD =0.170m). 125

Figure 51: SSC throughout the tidal period in LT_01. There is no water depth in this graph due to an equipment malfunction. Time is relative to high tide (HT). 127

Figure 52: Rock aprons implemented across the borrow pit at RD_01 (right). Ebb tide moving over the rock aprons in RD_01 (left). 130

Figure 53: SSC throughout the tidal period for LT_01 (top) and MTW_01 (bottom). Measurements were taking August 2016, May 2017, and June 2017 (MTW_01 only). LT_01 not only had a higher incoming SSC (before high tide), it had similar SSC on the ebb tide except for Tide 3, May 2017, which occurred during a large storm. 132

Figure 54: Predicted cumulative infill and hydroperiod for MTW_01..... 150

Figure 55: Predicted cumulative infill and hydroperiod for VDJ_03. 151

Figure 56: A map showing the deposition of sediment and the recovery of vegetation in two borrow pits in NS024 Noel Shore and NS067 North Onslow marshes. 153

Figure 57: The borrow pit at NS024 Noel Shore (CBWES, 2019)..... 154

Figure 58: Predicted cumulative infill and hydroperiod for LT_01..... 155

List of Tables

Table 1: Summary of common flood and erosion mitigation structures and their recorded influence on saltmarsh ecomorphodynamics.	13
Table 2: EPR Statistics generalized for each process dominated zone. The error associated with mean EPR is the mean of the ESP errors for all years.	27
Table 3: ERP statistics for wave dominated zone. The error associated with mean EPR is the ESP error divided by the range of years between the first and last image.	29
Table 4: EPR statistics for mixed zone. The error associated with mean EPR is the ESP error divided by the range of years between the first and last image.	30
Table 5: EPR statistics for fluvial zone. The error associated with mean EPR is the ESP error divided by the range of years between the first and last image.	32
Table 6: Borrow pits on each marsh and the year they were constructed.	83
Table 7: General hydrodynamic characteristics of each marsh.	84
Table 8: Dates each marsh was surveyed with a UAS.	85
Table 9: Specifications for the DJI Phantom 3 Professional (dji.com, 2018).	88
Table 10: List of hydrodynamic equipment deployed during each field visit. All hydrodynamic data can be found in Appendix 2.	100
Table 11: Accuracy validation for each DSM. "X" indicates when the accuracy assessment was not conducted due to equipment availability. For each flight the number of ground control points (GCPs) and independent check points (n) are listed, along with the mean, standard deviation (SD), root mean squared error of the vertical component (RMSEz), and the mean absolute error (MAE) for each validation.	101

Table 12: Results of the volumetric change analysis for all borrow pits using all pixels and 68% confidence intervals. * represents a manually calculated as-built volume. ¹ represents an “Year 2” infill rate.	103
Table 13: Results of the empirical hydrodynamic measurements in each borrow pit.	104
Table 14: Table comparing Lane et al (2003) and Taylor (1997) equations for volumetric uncertainty.	139
Table 15: Results of EPR in front of borrow pits (BP). Mean, minimum and maximum years before urgency (YBU) was calculated by dividing the width of the foreshore by EPR in the same location. Prograding marshes do not yield an YBU date.	150
Table 16: The hydrodynamic characteristics near NS024 Noel Shore and NS067 North Onslow.	152

List of Equations

Equation 1: Shoreline Position Error (Tibbetts and van Proosdij, 2013).....	19
Equation 2: Equation for calculating End Point Change Rate (EPR).....	22
Equation 3: Potential error in EPR between any two images.	22
Equation 4: Equation for calculating significant change.	23
Equation 5: Volumetric Change in sediment between two DSMs.	91
Equation 6: Root mean square error of the vertical component (Hugenholtz et al, 2013).93	
Equation 7: Volumetric uncertainty added in quadrature (Lane et al, 2003).	94
Equation 8: Uncertainty between two DSMs based on their individual accuracies (Brasington et al, 2003; Lane et al, 2003).....	94
Equation 9:Maximum volumetric uncertainty (Taylor, 1997).	95
Equation 10: Level of detection threshold determined by a "t" value and the uncertainty between two DSMs (Wheaton et al, 2010).	95
Equation 11: Resolved Horizontal Velocity (O’Laughlin and van Proosdij, 2013).....	99
Equation 12: Depth of water based on water and atmospheric pressures and the density of water (nasa.gov, 2014).	99

Chapter 1: Introduction to Research Project

1.1 Introduction

Dykelands are low-lying areas or former saltmarshes that have been removed from intertidal flow by the construction of dykes and other coastal infrastructure (novascotia.ca, 2013). As a result, dykelands reside below high-tide levels making them particularly susceptible to coastal inundation and erosion. This susceptibility is exacerbated by sea level rise (SLR) and other impacts of climate change such as increases in the frequency and magnitude of storm events (Nicholls and Cazenave, 2010). Furthermore, as sea levels increase seaward of the dykes, autocompaction on the landward side of the dykes decreases elevation capital over time via agricultural practices and other human uses (Allen, 2000). As populations increase within the areas protected by dykes, and the disparity between water levels and land elevation increases, dykelands are becoming less resilient to coastal flooding (van Proosdij and Page, 2012). Although many dykes can be topped to prevent coastal flooding, the cost to do so is high, and it is often prohibitive to top all dyke infrastructure in dykelands (van Proosdij and Page, 2012). Fortunately, saltmarsh ecosystems, otherwise known as foreshore marsh, are often present on the seaward side of dykes and can help increase the resiliency of dykelands to climate change, SLR, and storm events (Gedan et al, 2010; Möller et al, 2014; Vuik et al, 2016). This thesis focuses on foreshore marshes in front of dyke infrastructure in order to focus on their role in increasing resiliency in “green-grey” coastal defence systems.

Resiliency is defined as the ability of a system to absorb and recover from the impacts of a hazardous event (IPCC, 2012). An important component in maintaining, or enhancing, coastal resiliency is the presence and promotion of a healthy natural coastal

ecosystem (Sutton-Grier et al, 2015). Saltmarshes, and other ecosystems such as mangroves, provide coastal regions with a myriad of ecosystem services that enhance coastal resiliency by mitigating many negative impacts associated with climate change and sea-level rise (SLR) (Gedan et al, 2011; Temmerman et al, 2013; Vuik et al, 2016; Rendón et al, 2019). Chief amongst these benefits are saltmarshes' capacity to dissipate wave energy (Möller et al, 1996; Gedan et al, 2011; Vuik et al, 2016). The effectiveness of saltmarshes to attenuate waves is controlled by the width of the foreshore marsh, wave height, and the type, rigidity and density of vegetation (Sheppard et al, 2011; Barbier et al, 2011; Möller et al, 2014, Anderson and Smith, 2014). As a result, healthy saltmarsh ecosystems are viewed as a viable source of coastal protection and are being integrated into "green-grey" hybrid coastal defence infrastructures, worldwide (Sutton-Grier et al, 2015; Narayan et al, 2016). In these hybrid systems, saltmarshes act either as the primary or secondary source of coastal protection, depending on the management scheme (van der Nat et al, 2016). In dykelands, saltmarshes explicitly increase dykeland resiliency by reducing the frequency and intensity of wave interaction with dyke infrastructure (Vuik et al, 2016).

Besides wave attenuation, saltmarshes increase the resiliency of dykelands in less direct ways as well. Saltmarshes are also ecosystem engineers that can accrete at a pace similar to, or greater than, SLR given an ample sediment supply (Friedrichs and Perry, 2001; Temmerman et al, 2012; Kirwan et al, 2016). With enough accommodation space, saltmarshes can continue to provide protection to dykes and dykelands in the context of future climate change and sea level rise. Furthermore, unlike hard engineered coastal protection structures, saltmarshes can rebound following a destructive storm event (Sutton-Grier et al, 2015). This makes green-grey hybrid coastal protection systems

inherently more resilient than strictly grey systems, and ultimately enhances the resiliency of dykelands themselves. However, for saltmarshes to be a viable component of coastal protection, they must remain healthy and robust. Changes in the natural drivers and human intervention can impact the integrity of saltmarshes. In the case of the human impacts, the implementation of coastal structures and strategies can positively, or negatively, affect the ecomorphodynamic processes that govern saltmarsh evolution. Specifically, changes in ecomorphodynamics can precipitate or enhance saltmarsh progradation (horizontal growth), accretion, and erosion. Ecomorphodynamics describes interaction of vegetation, hydrology, sediment dynamics and topography to create and influence landform morphology. Furthermore, ecomorphodynamics include the feedback loop created by the formation or changes in landform on the aforementioned drivers. As a result, maladaptation is an obstacle to the successful implementation of nature-based coastal defence.

Ultimately, saltmarshes not only increase dykeland resiliency by reducing the frequency and intensity of wave interaction with dyke infrastructure, but by rebounding following a storm event, and by sequestering carbon from the atmosphere (Sutton-Grier et al, 2015; Vuik et al, 2016; Wollenburg et al 2018). This reduces maintenance costs and reduces the critical dyke elevation to prevent overtopping if the foreshore saltmarsh is wide enough (Vuik et al, 2016). This can allow dykeland managers to focus capital on other dykes, infrastructure, or on projects that address socioeconomic issues in the dykeland, further increasing the resiliency of the dykelands.

1.2 Project Context

Dykeland landscapes exist around the globe including, but not limited to, China, Vietnam, Netherlands, Croatia, France, England, USA, and Canada (van Proosdij and Page, 2012). This thesis examines dykeland adjacent saltmarshes in the Bay of Fundy, Nova Scotia, Canada. The Bay of Fundy is hypertidal with tide ranges that exceed 16m (50ft). The Bay of Fundy has several sub-regions with varying tidal ranges and hydrodynamic characteristics (e.g. suspended sediment concentration, sediment source). The Bay of Fundy also has a long history of dyke building for the creation of agricultural land dating back to the Acadian settlers of the 17th Century (Milligan, 1987; Bleakney, 2004). Since then, saltmarshes in the Bay of Fundy have reduced as much as 80%, most of which has been lost as a result of reclamation (novascotia.ca, 2017). Dyke building has been a continued practice; however, the largest large-scale dyke building endeavor occurred in the 1950's following the implementation of the Maritime Marshlands Rehabilitation Act (MMRA), in 1949 (Milligan, 1987). By the end of this decade, over 225km of new dyke was constructed with over 27,000ha of agricultural land being reclaimed or revamped in Nova Scotia, New Brunswick, and Prince Edward Island (Milligan, 1987). In 1970, the responsibility of dyke maintenance was passed over to the Nova Scotia Department of Agriculture (Milligan, 1987).

Today, Nova Scotia has approximately 241km of dyke infrastructure protecting approximately 20,000ha of land that is under the purview of the Nova Scotia Department of Agriculture, Land Protection Division (van Proosdij and Page, 2012; novascotia.ca, 2018). This responsibility is extended to the maintenance of over 260 aboiteau and implementation of rock armouring on the dykes and foreshore saltmarsh (novascotia.ca, 2018). Many of the dykes in the province have not been topped since their original

construction in the 1950's. Currently, many of the dykes overtop during storm events that occur during a high tide. With sea level rise (SLR) projections for the Bay of Fundy predict levels could increase by as much as 0.79m, by 2055, coastal flooding will increase in Nova Scotia unless the dykes are topped (Greenburg et al, 2012). This constitutes a large endeavor, which is made worse by relatively scarce funding (Sherren et al, 2016). As a result, the NSDA has implemented some creative strategies to protect the dykelands in Nova Scotia including managed realignment of dyke infrastructure, saltmarsh restoration, living shorelines, and borrow pit construction. The NSDA recognizes saltmarshes are an important part of coastal defence and integral in dykeland management. This project received in-kind support and collaboration by the NSDA investigate the common structures and strategies implemented in the Bay of Fundy used to adapt to, and mitigate, coastal flooding and erosion. The goal of this investigation, and thesis, is to identify how these structures and strategies impact saltmarshes so that they can be managed and implemented into the coastal defence strategy, and in doing so, enhancing dykeland resiliency.

1.3 Thesis Organization

This thesis follows a manuscript style format. Ultimately, this thesis will examine how common dykeland practices, implemented in estuaries around the world impact saltmarsh integrity over various time scales. In Chapter 2, an intertidal morphodynamic analysis was implemented to examine how a variety of dykeland management practices have influenced saltmarshes over different temporal (i.e. yearly to decadal) and spatial (i.e. individual marsh to estuarine) scales. This was done using the Digital Shoreline Analysis System (DSAS) (Thieler, 2009) and Analyzing Moving Boundaries Using R

(AMBUR) software (Jackson, 2009) to determine change rates on foreshore saltmarshes. Chapter 3 examines whether borrow pit excavation, a practice not thoroughly researched in the literature, can be considered a sustainable method of obtaining dyke topping material in the context of contemporary dykeland management. To do this, an unmanned aerial system (UAS) and structure-from-motion (SfM) software was used to measure the volumetric change of sediment in the borrow pits following their excavation. These changes were supplemented with measurements of hydrodynamics (e.g. suspended sediment concentration, flow velocity). Chapter 4 will integrate the findings from Chapter 2 and Chapter 3 in order to make broader suggestions related to the implementation of various flood and erosion mitigation structures and strategies in the Bay of Fundy.

Chapter 2:

Ecomorphodynamic response of saltmarshes to natural and anthropogenic modifications in a fetch-limited, highly turbid, hypertidal estuary.

2.1 Introduction

Coastal regions around the world are increasingly concerned about the impacts of contemporary and future climate change; particularly those related to sea-level rise (SLR). Rising sea levels and associated increases in storm surge will exacerbate a number of different threats to coastal regions, including: inundation of low-lying areas, erosion of shorelines, vulnerability to coastal flooding during storms, saltwater intrusion, loss or alteration of coastal ecosystems, damage to existing flood and erosion prevention structures, as well as the potential displacement of millions of people worldwide (Nicholls and Cazenave, 2010; van Proosdij and Page, 2012; Doney et al, 2012; IPCC, 2013). To mitigate and adapt to these impacts, namely those related to coastal flooding and erosion, coastal communities often implement a number of hard engineering structures such as dykes, sea walls, groynes, and shore rocking (Allen, 2000; French, 2001; Bernatchez and Fraser, 2012; van Proosdij and Page, 2012). Building and maintaining these structures is expensive. Many older structures were built without SLR in mind and are no longer adequate to protect coastal regions from current and future flooding extents. Furthermore, hard engineering structures often replace or segment coastal ecosystems – effectively reducing the resiliency of shorelines and their ability to adapt and respond to changes in sea levels and other natural processes or anthropogenic stressors. Natural ecosystems such as saltmarshes, which often grow on the foreshore side of dykes in tidal estuaries, not only provide a significant source of coastal protection but

its capacity to recover from disturbance makes the coastline more resilient (Gedan et al, 2011; Sutton-Grier et al, 2015; Vuik et al, 2016). As such, saltmarshes and other ecosystems such as mangroves represent a cheap and green alternative to conventional hard engineering structures (Costanza et al, 2008; Gedan et al, 2011; Vuik et al., 2016). Saltmarshes are especially resilient to the impacts of climate change and SLR because they are self-engineering ecosystems (Crain and Bertness, 2006; van der Nat et al, 2016). During the wave attenuation process, saltmarshes also promote sediment deposition (Freidrichs and Perry, 2001). This allows saltmarshes to accrete vertically with SLR given an ample sediment supply further adding to the resiliency they contribute to the coastline. Finally, saltmarshes provide several co-benefits that make them a valuable coastal ecosystem in the context of climate change.

Saltmarshes are dynamic ecosystems that offer a myriad of environmental services including carbon sequestration (Chmura et al, 2003; Andrews et al, 2006; Wollenburg et al, 2018), flood abatement, habitat for a variety of flora and fauna (van Eerden et al, 2005) and as a valuable source of coastal protection (Möller et al, 2014; Sutton-Grier, 2015; Sanchez-Arcilla et al, 2017). Several studies have shown that saltmarshes effectively dissipate wave energy during typical over-marsh tides (Möller and Spencer, 2002) and during large storm events (Möller et al, 2014; Vuik et al 2016). If saltmarshes are to be incorporated into a coastal protection strategy it is imperative to understand how saltmarshes respond to both changes in the natural environment and human interventions in the intertidal zone (Bouma et al, 2014). Since foreshore saltmarsh width is a reliable indicator of the effectiveness of a saltmarsh's ability to attenuate waves and provide coastal protection, understanding how natural and man-made drivers impact changes foreshore edge through erosion and progradation is crucial. In this regard, changes in the

position of the foreshore edge reflect the changing efficacy of an individual saltmarsh to provide coastal protection, and therefore, the resiliency of the saltmarsh and dyke infrastructure system.

Saltmarsh erosion and progradation (i.e. the horizontal movement of the foreshore edge) is a dynamic process which can naturally alternate over the decadal scale (Chauhan, 2009; Allen and Haslett, 2014). This autocyclic erosion process can make attributing erosion or progradation at the foreshore edge to any single driver challenging as most marshes will contain some degree of natural variability (Chauhan, 2009). Furthermore, there is often a significant lag between human intervention along the coast and the emergence of a new erosional or progradational state on the foreshore edge. This is because many implementations will alter the bed level morphodynamics of the intertidal mudflat adjacent to the foreshore edge (Willemsen et al, 2018). Recent studies have shown that these changes are often inextricably linked to saltmarsh erosion and progradation due to the role the mudflats play in the autocyclic erosional processes (Chauhan, 2009; Willemsen et al, 2018). Changes in bed level morphodynamics, especially those that promote the growth of intertidal mudflats, can ultimately lead to changes in tidal prism, which is another important control on the evolution of saltmarshes (Dyer and Taylor, 1973; Pye and Blott, 2014). Tidal prism is the volume of water that flows in and out of an estuary (Dyer and Taylor, 1973; Luketina, 1998; Pye and Blott, 2014). Tidal prism can be altered by a change in both natural drivers, such as changes in sea level, and by the implementation of flood defence structures, such as dykes and tidal barriers (van Proosdij et al, 2009; Wang et al, 2015). Ultimately, changes in tidal prism can alter tidal velocities leading to an increase or decrease in sedimentation in the

intertidal zone, which influences where saltmarshes can evolve or where erosion may take place.

Finally, how a saltmarsh responds to an implementation or change in natural driver can be dependent on where in the estuary it is situated (i.e. wave/tidal, mixed, or fluvial dominated). Its position in the estuary will dictate the types and strength of the ecomorphodynamic interactions that ultimately control its morphology.

Ecomorphodynamics involve the interaction between sediment dynamics, hydrology, topography of the antecedent landscape, and vegetation to shape the landscape; this extends to include the feedback landscape change has on said drivers. Applying an ecomorphodynamic analysis at both the saltmarsh and estuarine scale "...provides a process oriented framework from which to better understand the stability of both natural and engineered tidal marshes in terms of what sustainable configuration may accommodate changes that occur in a state of dynamic equilibrium" (Friedrichs and Perry, 2001, p.7). By doing this, it is possible to avoid implementing maladaptive practices.

This thesis will examine the ecomorphodynamic response of foreshore saltmarshes to the implementation of flood and erosion mitigation structures and strategies as well as changes in natural drivers in a fetch limited, highly turbid, hypertidal estuary at both the saltmarsh and estuarine scale. The work presented here will extend the focus of previous morphodynamic analyses by explicitly recognizing and attributing which implementations increase dykeland resiliency (i.e. promote progradation) and which detract from it (i.e. exacerbate erosion) in the context of climate change adaptation.

Figure 1 shows a brief description of common human implementations used to mitigate coastal flooding and erosion. Other implementations are less common but are

prominently featured in the study area of this thesis, which provides a unique opportunity to explore the impact of less-explored implementations. Table 1 provides a brief summary of the morphodynamic response to each implementation found in those studies. It should be noted that several implementations were found to trigger a number of different responses (i.e. erosion and/or progradation) depending on other influencing factors (e.g. placement in the estuary, suspended sediment concentrations, local hydrology). Ultimately, the saltmarsh responses below will be compared to those found in this thesis and discussed later on.







	<p>Dykes: (dikes, levees, embankments) are elevated earthen or engineered walls that prevent coastal flooding. Historically, dykes were used to cut land off from intertidal flow to create agricultural land, in a process called reclamation.</p>	<p>Borrow Pits: Excavated swaths of saltmarsh used for dyke topping material. Borrow pits are a traditional technique in dyke building, and were excavated using dyke spades. Today, borrow pits are excavated using heavy machinery and are much larger as a result of the need for material to adapt to SLR.</p>	
	<p>Dredging: Involves the in-situ removal of material from the estuarine bed and banks. The aim of dredging is often to improve navigation or to expedite flood water away from developed areas.</p>	<p>Managed Realignment: Involves the relocation, or set-back, of dyke infrastructure allowing for reclaimed land to revert back to natural saltmarsh habitat. Saltmarsh habitats provide protection to the dykes and upland by attenuating incoming waves.</p>	
	<p>Rocking: Implemented to stop erosion by hardening the shoreline. Rocking and seawalls are used to prevent both channel and wave erosion. In the Cobequid Bay Salmon River Estuary, rip-rap is used for shoreline and dyke armouring.</p>	<p>Aboiteau: A one-way sluice gate that allows water to drain from the upland during low tides. At high tide the gate closes, preventing tidal flow from entering the upland.</p>	
	<p>Kickers: Structures designed to deflect, or “kick”, channels away from estuarine banks in order to prevent shoreline erosion. Originally implemented as Gaspereau wiers, dykeland managers realized their usefulness as a shoreline protection technique in the early 1900’s.</p>	<p>Photo Credits:</p> <ol style="list-style-type: none"> 1) van Proodij, 2016 2) Matheson, 2014 3) Matheson, 2014 4) Matheson, 2014 5) Bowron, 2016 6) CBWES, 2019 7) Matheson, 2014 	

Figure 1: A list of common structures and strategies implemented in hypertidal estuaries around the world and in the Bay of Fundy. These will be the focus of this study.

Table 1: Summary of common flood and erosion mitigation structures and their recorded influence on saltmarsh ecomorphodynamics.

Structure	System Response	Author(s)
Dykes/Levees	<p>Reclamation: Reclamation involves cutting off a saltmarsh from tidal flow, usually via the construction of a dyke, or embankment. The saltmarsh is drained and the land-use is often converted to agriculture. Over time, saltmarshes on the foreshore side of the reclamation can accrete, while autocompaction on the landward side can cause the land to subside, making the reclaimed less resilient to SLR.</p> <p>Reduction of tidal prism: Dyke effectively reduce the cross-sectional area of estuaries, which decreases the tidal prism and tidal velocities. Deposition occurs when the tidal velocities are no longer adequate to transport sediment. If wave action is limited, the net effect of these changes is sediment deposition, which leads to the creation of new saltmarshes on the foreshore side of the dykes.</p> <p>Coastal Squeeze: Dykes represent a hard boundary that prevent saltmarshes from retreating inland in response to rising sea levels combined with wave action. The limitation of horizontal accommodation space often leads to in situ net losses in saltmarshes. It can lead to overall losses in estuarine saltmarsh if the eroded saltmarsh material cannot adequately deposit in other areas.</p> <p>Alters bathymetry and/or hydrology: In the mixed and fluvial portion of estuaries, dykes can confine the lateral movement of flood and ebb channels. This impacts the location of erosion and deposition occurrence. Furthermore, channels that are confined laterally can transfer erosional energies from the walls of the channels, to the beds. This can lead to channel deepening, and potentially reinforce the location of these channels.</p>	<p>Allen, 2000, Doody, 2008</p> <p>van der Wal et al, 2002; French et al, 2005; van Proosdij and Baker, 2007; van Proosdij et al, 2009</p> <p>Doody, 2004; Wolters et al 2005; Dario and Chmura, 2013</p> <p>van Proosdij and Baker, 2007; Pye and Blott, 2014</p>
Dredging	<p>Sediment removal: Dredging practices aim to remove sediment from an estuary for navigational or flood abatement purposes. If the sediment is not redistributed back into the system, dredging can lead to large net losses of sediment, which can reduce the amount of sediment for saltmarsh platforms.</p>	<p>Blott et al, 2006</p>

	Alters bathymetry and/or hydrology: When dredging practices are isolated to one channel (i.e. ebb channels for navigation), they can potentially influence the capacity of both channels to transport sediment. This can influence the sediment transport patterns within the estuary and can either increase or decrease the amount of available sediment in an estuary.	van der Wal and Pye, 2004; Blott et al, 2006; Wang et al, 2015
Rocking/Seawalls	Alters hydrology: Rocking can significantly reduce the interaction of hydrodynamic forces and saltmarshes or other coastal landscapes. This provides protection for saltmarshes limiting the amount of in situ erosion but can limit the availability of sediment elsewhere in the estuary. Furthermore, the ends of rocking or seawalls can experience scour leading to an increase in erosion that might otherwise occur.	French, 2001; Bernatchez and Fraser, 2012
Kickers (Groynes)	Alter hydrology: Kickers deflect the thalweg away from saltmarshes in the fluvial and mixed portions of an estuary. The result of this is a reduction in ebb velocities, creating an environment that is conducive to sediment deposition and saltmarsh progradation.	Klingeman et al, 1984; van Proosdij and Matheson, 2015; This study
Borrow Pits	Alter sediment transport: By creating artificial tidal channels, or by enhancing existing channels, borrow pits alter sediment transport on the platform by providing a conduit for sediment to the areas of the high marsh it would not normally reach. Also, by deepening the existing channels, borrow pits act as a sediment sink and trap sediments that might reach the platform in a natural tidal creek system. Alter hydrology: Borrow pits can significantly increase velocities within the saltmarsh platform causing scour and erosion in places that may not experience said forces except during large storms. Sediment Loss: Borrow pit excavation constitutes a significant loss of sediment on the saltmarsh-scale. Large borrow pits can represent a loss of >10,000m ³ of sediment in a single marsh.	Pye, 1995; Dale et al, 2018 This study: Chapter 3
Managed Realignment	Saltmarsh restoration: Managed realignment projects reintroduce reclaimed agricultural land to tidal flow. This results in the rapid deposition of sediment creating large intertidal mudflats which are then colonized by saltmarsh vegetation. Increase tidal prism: By opening reclaimed land to tidal flow, the local tidal prism is increased. This can lead to erosion within the restored saltmarsh and in the tidal creek networks of adjacent marshes. Breach channels can also expand into natural marshes if not implemented correctly.	Garbutt et al, 2006; Stronkhorst and Mulder, 2014; Wollenburg et al, 2018 Friess et al, 2014
Aboiteau	Alteration of sediment supply: Aboiteau management has shifted in the past century favouring a fewer amount of larger aboiteau over a higher number of smaller aboiteau. This has consequences on where and how much sediment is introduced into the estuary from the upland. An increase in sediment due to aboiteau alteration can lead to increased availability for mudflat/saltmarsh development, and vice versa.	This study

	Aboiteau channel migration: The channels created by aboiteau can be considerably large depending on the size of the drainage basin they control. During large events, the channels can migrate significantly leading to rapid and significant erosion at the foreshore edge. In areas with high suspended sediment concentrations, the relict aboiteau channel can infill rapidly and lead to significant periods of saltmarsh colonization.	This study
NATURAL DRIVERS		
Natural Channel Migration	Erosion and progradation of foreshore edge: Flood and ebb channels can be move quite dynamically within the estuarine basin leading to significant changes in location of foreshore saltmarsh edges. When channels move landward and interact with the foreshore edge erosion can occur quite rapidly by undercutting saltmarsh cliffs. When the channels move seaward, they can often leave behind a “depositional wedge” which can lead to the rapid accumulation of sediment. Once this sediment reaches an appropriate elevation in the tidal frame, saltmarsh can colonize leading to rapid progradation.	Pringle, 1995; Gabet, 1998; Pedersen and Bartholdy, 2007; Chauhan, 2009.
Wave Action	Erosion at foreshore edge: Wave action is a driver of erosion along the foreshore edge of saltmarshes. Erosion occurs via a few different mechanisms, including the undercutting of foreshore saltmarsh cliffs and through large block failures at the foreshore edge.	Chauhan, 2009; Leonardi and Fagherazzi, 2014; Leonardi et al, 2016.
Tidal Asymmetry	Control on net sediment transportation: In flood-dominated estuaries, the net direction of net sediment transport is usually towards the inner estuary. This typically increases the availability of sediment within the estuary, which is then available for the creation and expansion of intertidal mudflats. These mudflats can be colonized by saltmarsh vegetation. In ebb-dominated estuary, net sediment transport often results in sediment leaving the estuary to the greater basin. This means that sediment lost to erosion may not be re-deposited within the estuary, which leaves less for mudflat/saltmarsh development.	Dronkers, 1986; Fredrichs and Perry, 2001; Dalrymple et al, 2012.

2.2 Study Area

The Cobequid Bay – Salmon River Estuary is in the northeastern portion of the Bay of Fundy, in Nova Scotia, Canada (Figure 2). It is a hypertidal semi-diurnal estuary with a tidal range exceeding 16m (Desplanque and Mossman, 2004). In the winter, ephemeral ice is present throughout the system. The sediment in the Cobequid Bay – Salmon River Estuary consists primarily of coarse and very coarse silt in the outer and mid-estuary (samples taken in May and September) (van Proosdij et al., 2014). The inner estuary consists predominantly of fine to medium gravel in the North River, and the Salmon River consists of medium gravel during the spring but shifts to medium silt by the fall (CBCL, 2015). Suspended sediment concentrations range from $0.5\text{g}\cdot\text{l}^{-1}$ up to $>100\text{g}\cdot\text{l}^{-1}$ in saltmarsh tidal channels around the turbidity maximum, which can vary spatially along the estuary due to the large tidal range (Crewe et al, 2004; Purcell, 2020).

There is a long history of dyke building in the Cobequid Bay Salmon River Estuary, dating back to the 17th Century. Acadian settlers were the first to dyke, or reclaim, saltmarshes and did so until their expulsion in the 1750's (Bleakney, 2004). The practice of dyke building persisted through to the 1950's; however, many dykes in the area fell into a state of disrepair by that time (Milligan, 1987). In this time, the Government of Canada stepped in and established the Maritime Marshlands Rehabilitation Administration (MMRA), which mandated the repair and improvement of agricultural dykes in Nova Scotia and New Brunswick (Milligan, 1987). Most of the dykes in the Cobequid Bay Salmon River Estuary were built between the 1950's and 1970's and are now currently managed by the Nova Scotia Department of Agriculture

(NSDA), Land Protection Division. Many dykes in the province are engineered to an agricultural standard which accepts periodic overtopping (Agricultural Marshland Conservation Act, 2000). However, as development has moved into the natural flood extent these dykes now protect vital infrastructure and commercial interests. The NSDA are also responsible for the maintenance of over 260 aboiteau structures, armouring dykes and foreshore marsh, and the excavation of borrow pits for dyke topping (novascotia.ca, 2018). The NSDA uses several of the structures and strategies outlined in Table 1 to mitigate and adapt to coastal flooding and erosion – including rocking, kickers, dredging (Municipality of Colchester), and managed realignment.

The legacy of dyke building and maintenance has had a lasting impact on the saltmarshes in the Cobequid Bay Salmon River Estuary. An estimated 80% of saltmarshes have been lost in Nova Scotia, with as much as 50% as a result of reclamation (novascotia.ca, 2017). As a result, this study will look to see whether any of the implementations mentioned above can enhance or detract dykeland resiliency by examining how they have influenced saltmarsh erosion and progradation during the past 80 years.

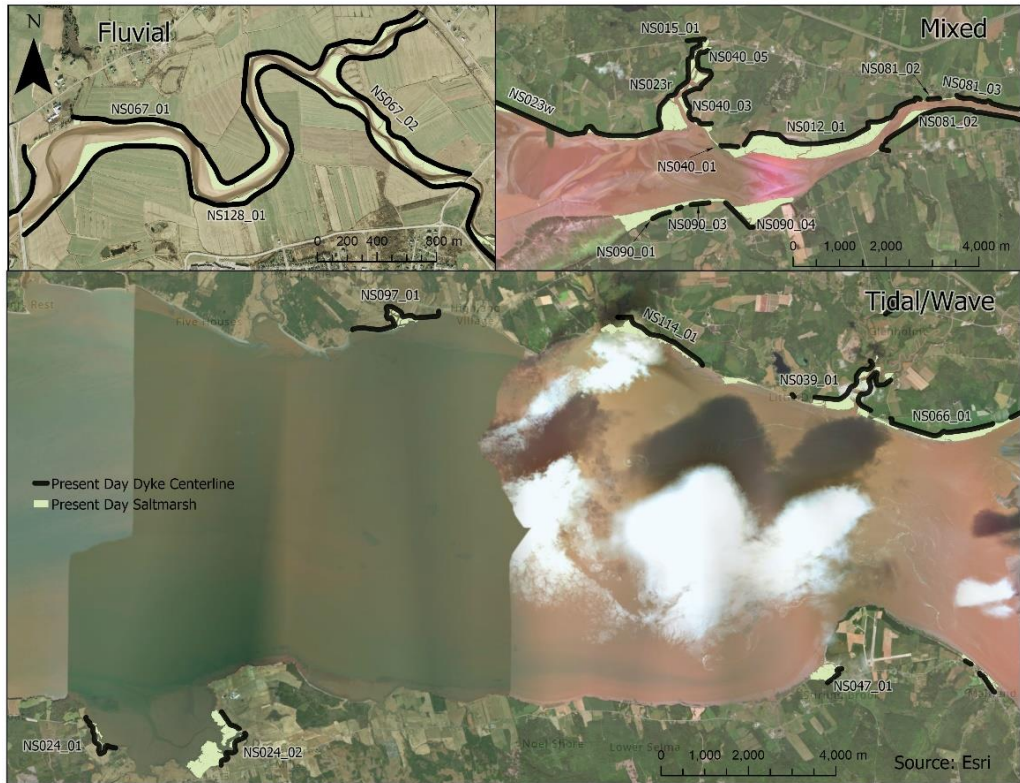
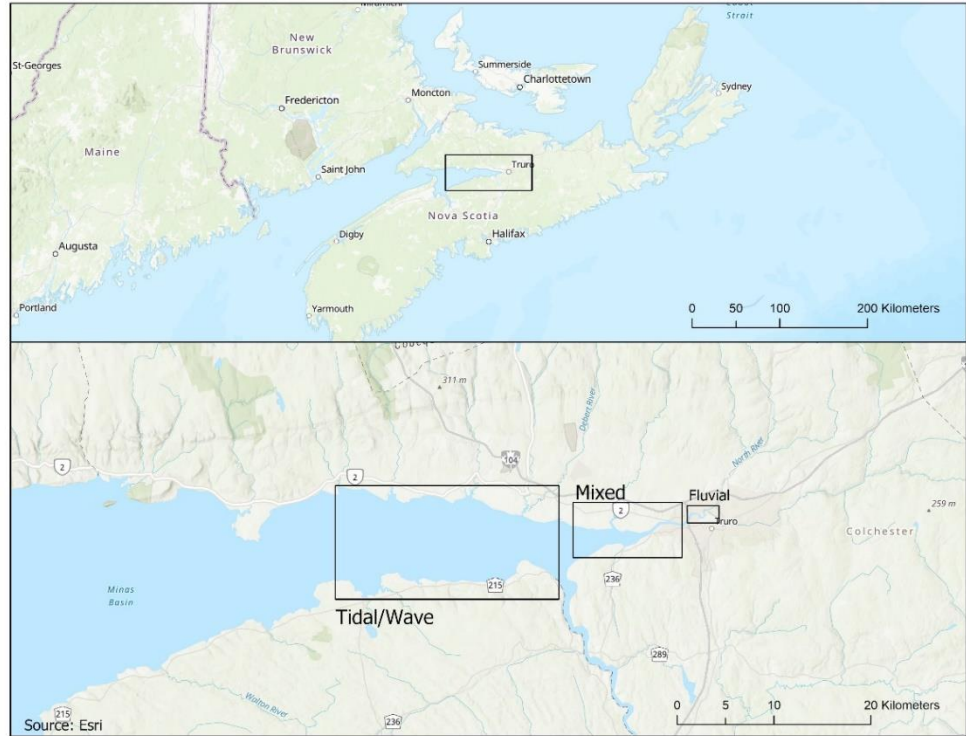


Figure 2: Study area map showing the location of foreshore saltmarsh and dyke infrastructure as well as the extent of the various process dominated zones in the Cobequid Bay Salmon River Estuary, Nova Scotia, Canada.

2.3 Methods and Materials

In order to measure change in the foreshore edge position (i.e. erosion and progradation) a large dataset of imagery was compiled, digitized and analyzed using GIS, Digital Shoreline Analysis System (DSAS) (Theiler et al, 2009) and Analyzing Moving Boundaries Using R (AMBUR) (Jackson, 2009). The measured change was reported as End Point Rate (EPR), which is the rate of change of the foreshore position between successive images along a transect.

The images used in this analysis include aerial photographs, satellite imagery, and imagery obtained from an unmanned aerial vehicle (UAV), all of which were projected into the NAD83 CSRS EPOCH2010 UTM Zone 20 coordinate system. The oldest images date as far back as 1938. The foreshore was manually digitized (i.e. delineated) from these images in ArcMap 10.5, and was double-checked for quality control. Furthermore, images were only used if they were captured during low to mid-tide to ensure the entire foreshore was visible. Since these images were individually georeferenced and/or georectified, and vary in their resolution, each set of foreshore boundaries digitized from a given year has its own level of error (i.e. digitization error) called the Shoreline Position Error (ESP). The ESP associated with set of images can be calculated using equation (1):

Equation 1: Shoreline Position Error (Tibbetts and van Proosdij, 2013).

$$Esp = \sqrt{Er^2 + Ed^2 + Eo^2}$$

where, Esp is the shoreline position error, Er is the root mean squared (RMS) error of the image rectification, Ed is the digitizing error, and Eo is the shoreline proxy offset which is two metres for each image. (Tibbetts and van Proosdij, 2013; van Proosdij et al, 2018). The shoreline proxy offset was generalized based off the entire suite of images.

The resultant shoreline position error for each image used in the analysis is in Appendix 1.

Foreshore change was measured along transects that were cast every 25m along dyke centrelines in the Cobequid Bay Salmon River Estuary. The dyke centreline, which was created using the most recent RTK-GPS surveys, was used as the baseline since this project coincided with another project which examined dyke vulnerability (van Proosdij et al, 2018). DSAS was chosen as the preferred method to cast transects over AMBUR because of the convoluted shape of the baseline (i.e. dyke centreline). Specifically, DSAS allowed for the orientation of the transects to be edited in ArcMap 10.5 to reflect and properly capture the movement of the foreshore saltmarsh (Figure 3). While manually editing the transects introduced user bias and diminished reproducibility, without the manual editing (which AMBUR does not offer) the resultant EPR was often unrealistic and either over-exaggerated or under-exaggerated the amount of change that was occurring at the foreshore edge. In total, 2070 transects were cast. Of those 2070, 266 (12.85%) were removed from the analysis, 954 (46.09%) were modified to capture the direction of foreshore change and 850 (41.06%) remained untouched. The transects were cast using the Smoothed Baseline Cast method and a smoothing distance of 50m.

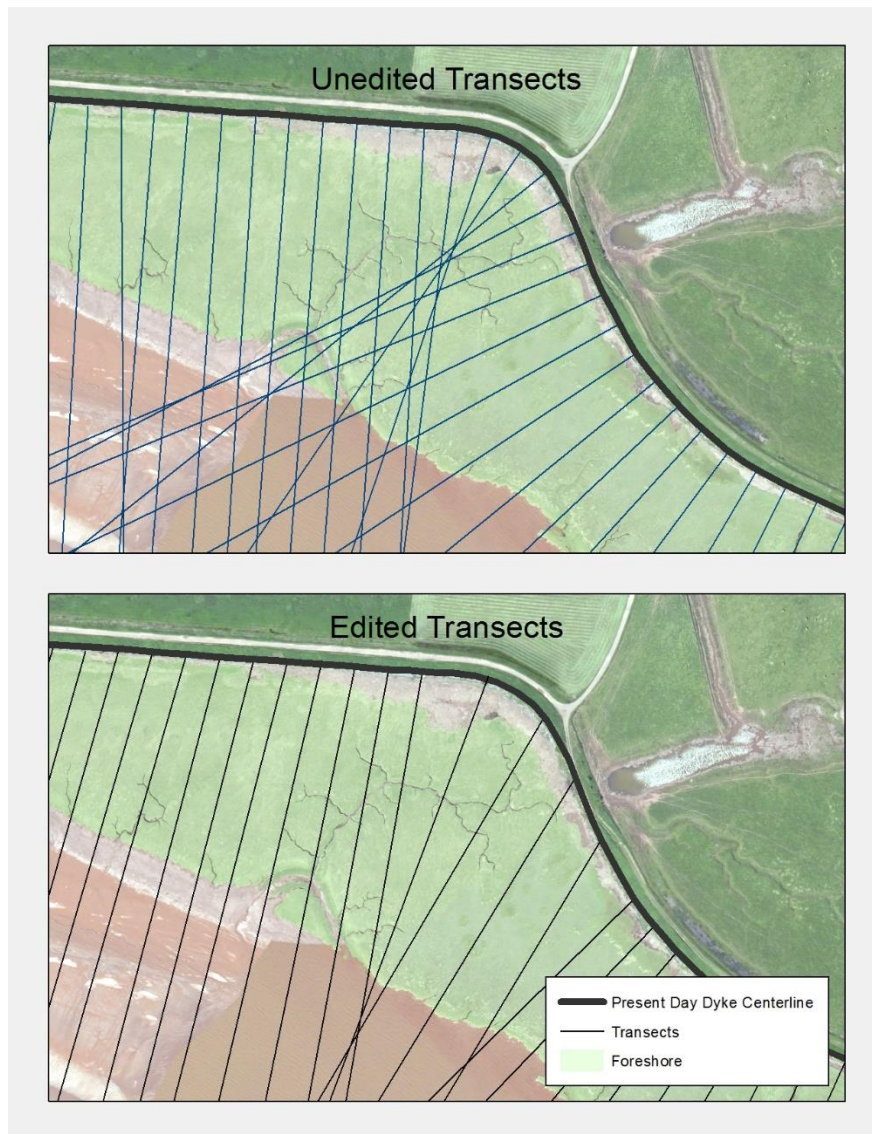


Figure 3: An example of how transects were edited to be perpendicular to the direction of foreshore processes.

Analyzing Moving Boundaries Using R (AMBUR) software was then used to determine the EPR of the foreshore along each transect (Jackson, 2009). EPR represents the rate of change at the foreshore edge along a transect between successive images, whereas mean EPR is the mean change along a transect throughout the entire range of images. AMBUR uses the transects and shorepoints (i.e. where the transects intersect the

digitized saltmarsh polygons) generated in DSAS to obtain statistics regarding each transects' EPR using the basic equation (2):

Equation 2: Equation for calculating End Point Change Rate (EPR).

$$EPR = \frac{D_2 - D_1}{T_2 - T_1}$$

Where D equals the distance along the transect to the shorepoint and T represents the year the image was obtained. Using the ESP values from equation 1, the error in EPR between any successive year can be calculated using the equation (3):

Equation 3: Potential error in EPR between any two images.

$$EPR_{Error} = \frac{\sqrt{ESP_1^2 + ESP_2^2}}{T_2 - T_1}$$

These error values are reported in the Results and Discussion sections when discussing foreshore change. When calculating EPR, the last intersection method was chosen in AMBUR, meaning the EPR were calculated using last shorepoint (i.e. furthest away from the dyke) in each respective saltmarsh polygon (Jackson, 2012). This allows for the calculation of EPR independent of the direction of saltmarsh change. Two separate outputs from AMBUR were used in the analysis: mean EPR of individual transects throughout all images and the foreshore width along all the transects in each corresponding image. The mean EPR of each individual transect was also used to visualize change at the saltmarsh scale throughout the full range of available images. This value was used to characterize the mean direction and magnitude change in each saltmarsh between all the images. It is important to note that most saltmarshes had areas of erosion and progradation even though only one value was reported. To examine the variation in change within each marsh more closely, the mean EPR of each transect within a marsh was also examined to determine significant changes at the saltmarsh level.

Finally, to capture the variability of movement of the foreshore edge the EPR of each transect between all successive images were used to identify significant changes. This allowed for the capture of episodic changes that may have been precipitated by anthropogenic alterations within the intertidal zones or by natural processes.

Significant changes were identified as those that exceeded a two-sigma deviation from the mean change rate measured at both the saltmarsh and process-dominated scales. The two-sigma changes were calculated at the individual saltmarsh level, using the mean EPR and standard deviation of each transect using the equation (4):

Equation 4: Equation for calculating significant change.

$$\frac{\sum EPR_n}{n} \pm 2\sigma$$

Significant changes in the process-dominated zone were calculated using all the EPR between successive years for each transect (Figure 4 and 5). The process-dominated zones were the tidal/wave, mixed, and fluvial dominated zones, which were delineated in Dalrymple et al (1990). This was done because morphodynamic drivers interact differently with the flood and erosion prevention structures in each process-driven zone, impacting EPR and saltmarsh evolution in different ways, leading to varying ecomorphodynamic responses, and ultimately, different magnitudes of EPR. Furthermore, it was expected that rates of change would be greater in the higher energy zones (e.g. tidal/wave) than the low energy zones (e.g. fluvial), particularly regarding erosion. Conditional statements in Excel were used to highlight significant changes along each transect between any two successive years, which were scrutinized to determine if they were real changes, or a false positive as a result of user error (e.g. digitization error, image boundary)

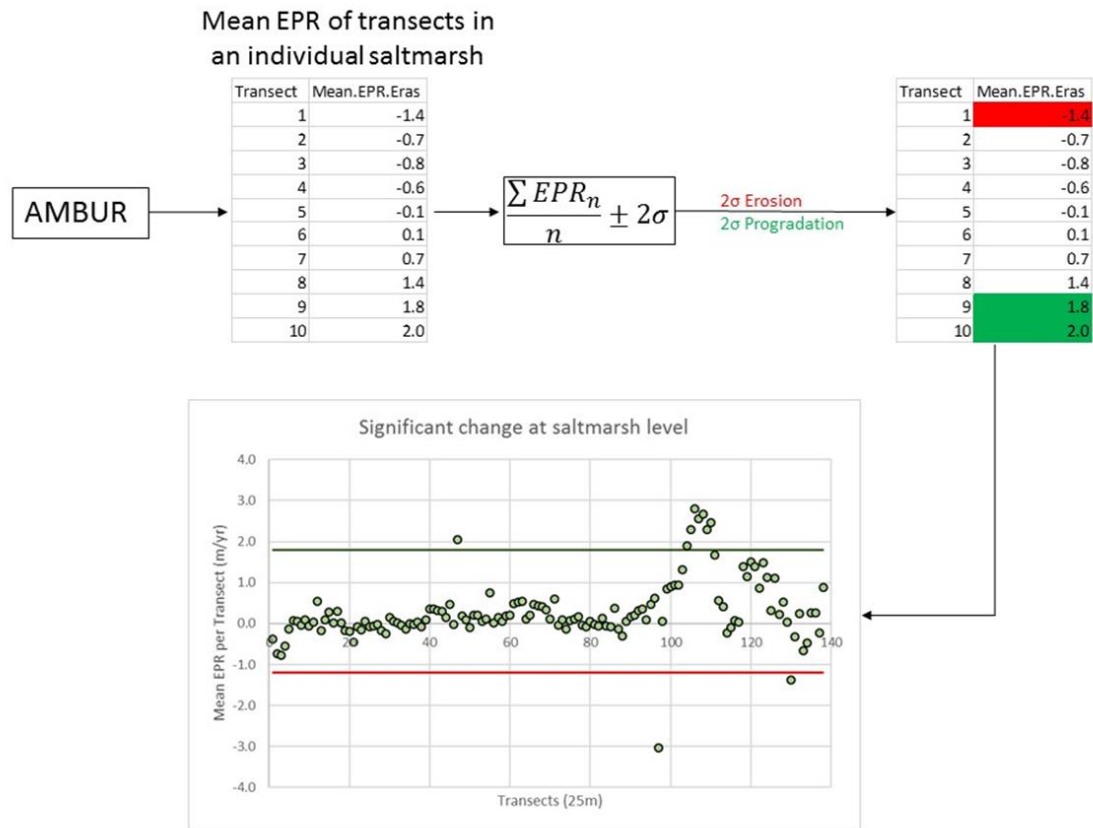


Figure 4: Workflow for determining significant change at the saltmarsh scale.

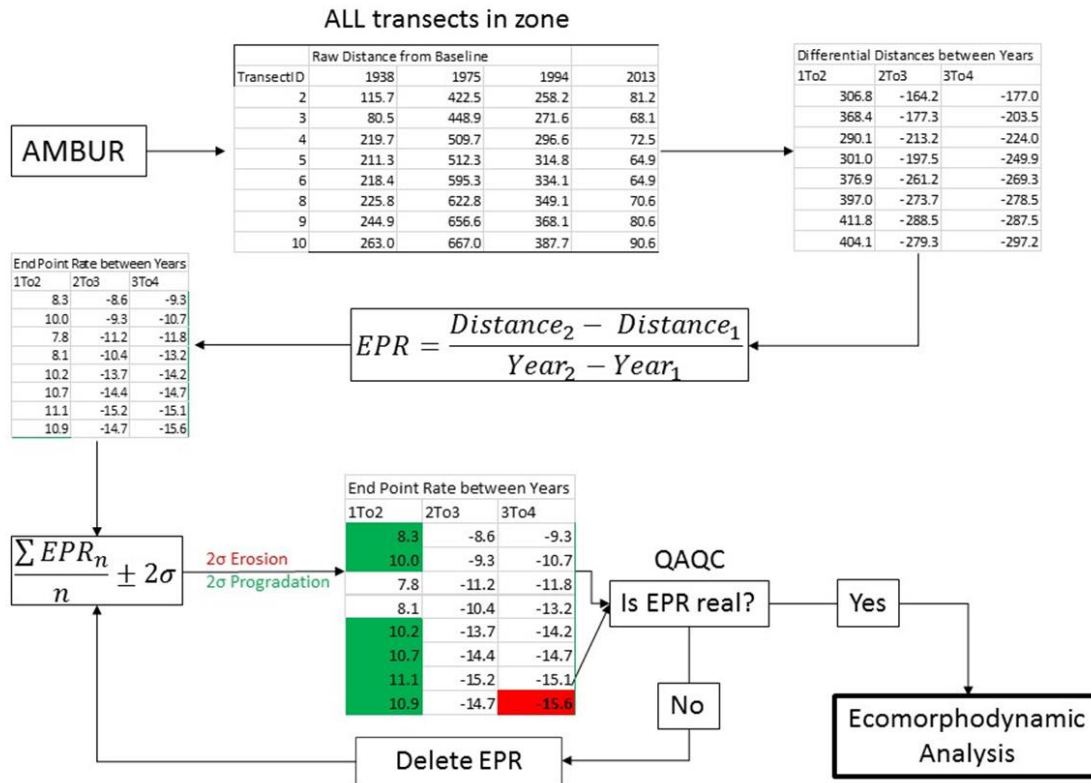


Figure 5: Workflow for validating and identifying significant changes at the process dominated zone scale.

Once the significant changes were verified, they were examined qualitatively using knowledge of the ecomorphodynamic processes that occur in highly turbid, hypertidal estuaries. This method of examining quantitative changes and explaining said changes through the lens of morphodynamics is used in several studies including van der Wal et al (2002), and van Proosdij and Baker (2007). The examination of the foreshore change rates was facilitated by the various imagery as well as a suite of other geospatial data collected for the Marshlands Atlas (van Proosdij et al, 2013). These included the date and location of the implementation, upgrade, or removal of dykes, rockings, kickers, aboiteaux and dredging.

2.3.1 Assessment of error reporting for EPR

The uncertainties in this study should be considered conservative based off the resolution and rectification accuracy of the images used. The over-estimation of error is primarily an artifact of the digitization and shoreline proxy errors used to determine the uncertainty of the foreshore edge location. Shoreline proxy is typically used to determine more ambiguous shorelines, such as the high-water line (HWL) or mean high water (MHW), which is delineated using changes in vegetation or wrack. The delineation of saltmarsh versus mudflat is much less ambiguous, especially in the higher-resolution imagery, yet maintains a value of two metres to cover the uncertainty presented in the black and white, low-resolution, aerial photographs. Future studies should involve photo specific estimations of shoreline proxy and digitization error in addition to rectification error and image resolution.

2.4 Results

In total, the End Point Change Rate (EPR) of 1804 transects were analyzed along 53.8km of dyke. Of those 1804 transects, 932 were eroding and 872 were prograding (Figures 6). The tidal/wave dominated zone in the Cobequid Bay Salmon River estuary was eroding at a mean of $-0.9\text{m}\cdot\text{yr}^{-1} \pm 0.1\text{m}\cdot\text{yr}^{-1}$, while the mixed zone was eroding at a mean rate of $-0.6\text{m}\cdot\text{yr}^{-1} \pm 0.1\text{m}\cdot\text{yr}^{-1}$ (Table 2). The fluvial zone was the only zone that was prograding and was doing so at a rate of $0.1\text{m}\cdot\text{yr}^{-1} \pm 0.1\text{m}\cdot\text{yr}^{-1}$. Furthermore, the mixed zone showed the greatest variation in (EPR) with a standard deviation of $6.1\text{m}\cdot\text{yr}^{-1}$. For context on marsh locations refer to Figure 2.

Table 2: EPR Statistics generalized for each process dominated zone. The error associated with mean EPR is the mean of the ESP errors for all years.

Dominant Process	Number of Marshes	Mean ($\text{m}\cdot\text{yr}^{-1}$)	Standard Deviation ($\text{m}\cdot\text{yr}^{-1}$)	Significant Erosion (-2 Sigma) ($\text{m}\cdot\text{yr}^{-1}$)	Significant Progradation (+2 Sigma) ($\text{m}\cdot\text{yr}^{-1}$)
Tidal/Wave	5	$-0.9 \pm 0.1\text{m}\cdot\text{yr}^{-1}$	3.5	-7.8	6.0
Mixed	13	$-0.6 \pm 0.1\text{m}\cdot\text{yr}^{-1}$	6.1	-12.7	11.5
Fluvial	8	$0.1 \pm 0.1\text{m}\cdot\text{yr}^{-1}$	1.6	-3.2	3.3

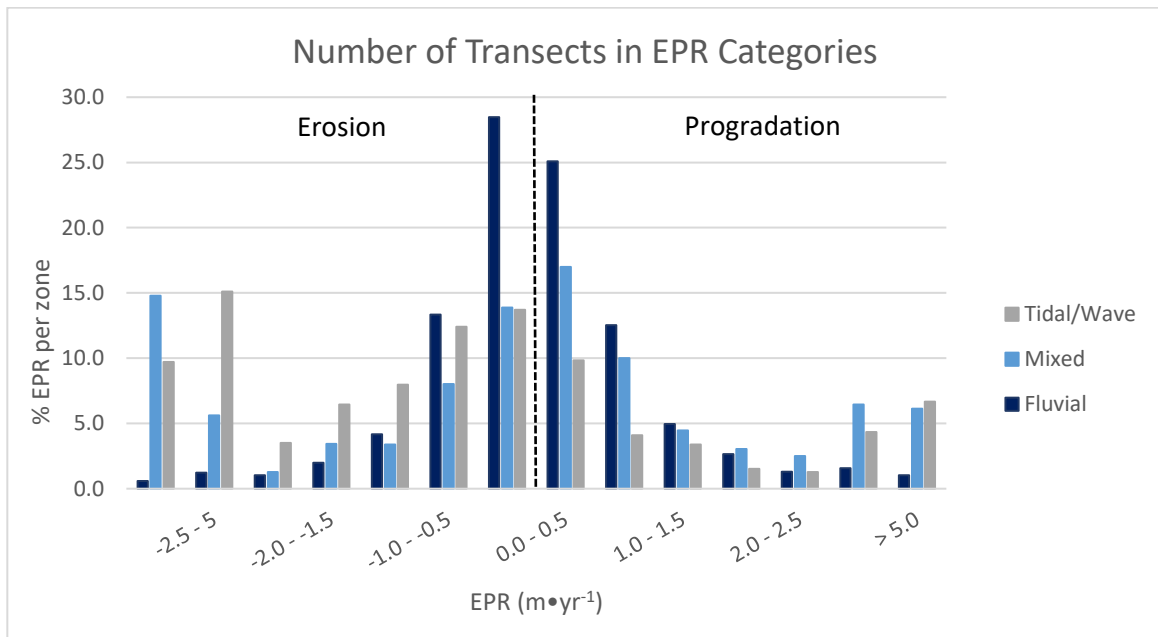


Figure 6: Percentage of total transects per EPR range and zone.

EPR in the tidal/wave dominated section of the Cobequid Bay Salmon River estuary were predominantly negative. Here, average rates of change ranged from $-1.7 \pm 0.1 \text{ m} \cdot \text{yr}^{-1}$ to $0.0 \pm 0.1 \text{ m} \cdot \text{yr}^{-1}$ (Table 3) (Figure 7). The marsh that had the greatest mean erosion was NS066 Round Marsh, which eroded at a rate of $-1.7 \pm 0.1 \text{ m} \cdot \text{yr}^{-1}$ between 1938 and 2013. The greatest rates of erosion occurred between 2011 and 2013, with rates exceeding $-10.0 \text{ m} \cdot \text{yr}^{-1}$ measured in front of 150m of the dyke, reaching as high as $-16.3 \pm 2.4 \text{ m} \cdot \text{yr}^{-1}$. The only marsh edge in the tidal/wave zone that did not retreat was NS114 Great Village, which had mean change of $0.0 \pm 0.1 \text{ m} \cdot \text{yr}^{-1}$ along the entire foreshore. However, this marsh was reclaimed sometime after 1964, which triggered a mean foreshore progradation at a rate of $0.2 \pm 0.4 \text{ m} \cdot \text{yr}^{-1}$ between 1994 and 2013 despite the significant loss of saltmarsh area overall (see 2.5.1 for further discussion).

Table 3: ERP statistics for wave dominated zone. The error associated with mean EPR is the ESP error divided by the range of years between the first and last image.

Marshbody Tract	# Images	Mean (m·yr ⁻¹)	Standard Deviation (m·yr ⁻¹)	Significant Erosion (m·yr ⁻¹)	Significant Progradation (m·yr ⁻¹)	Max Erosion (m·yr ⁻¹)	Max Prog. (m·yr ⁻¹)
NS024_01	3	-0.1±1.6	2.0	-8.3	6.7	-8.1	4.3
NS024_03	3	-0.4±0.1	1.1			-3.0	3.0
NS097_01	4	-0.2±0.1	1.7			-6.6	7.1
NS114_01	5	0.0±0.1	2.2			-6.9	8.8
NS066_01	8	-1.7±0.1	5.1			-16.3	12.2

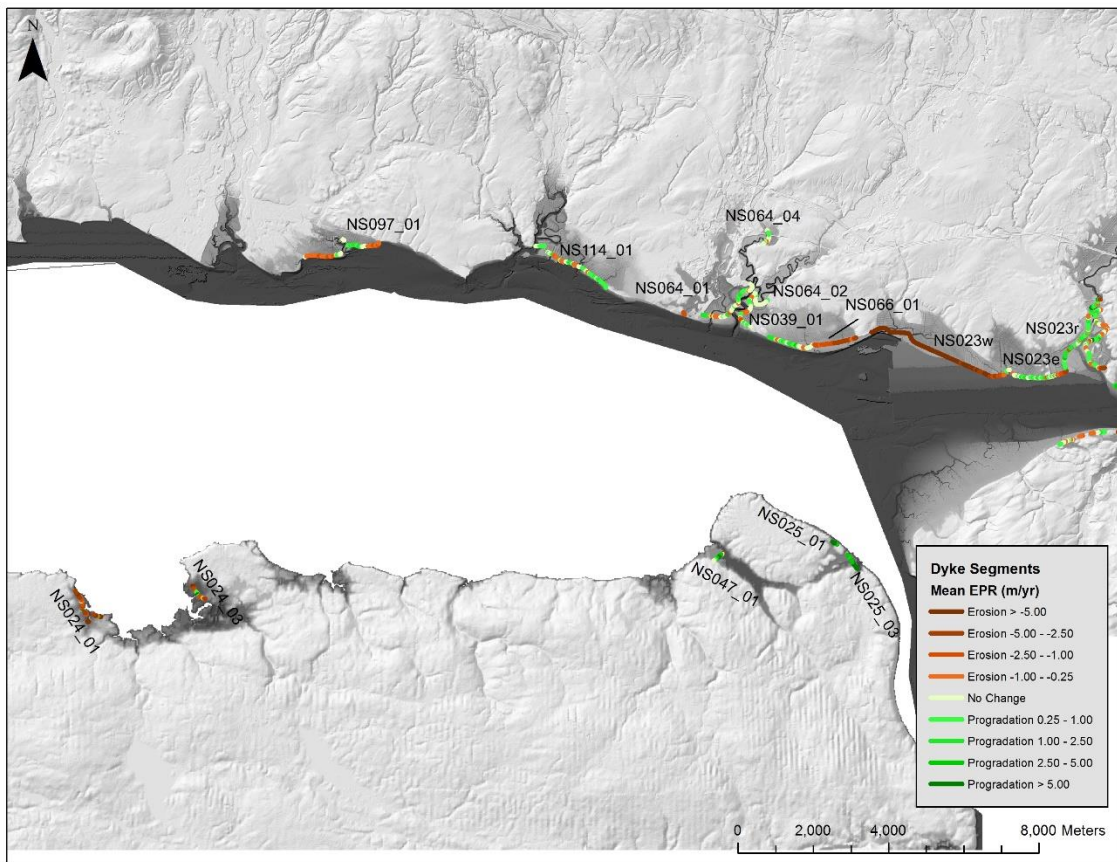


Figure 7: Mean EPR per dyke segment (25m) for marshes in the Tidal/Wave dominated zone. NS064_02, NS064_04, and NS023r are considered fluvial.

The mixed zone had the greatest variation in EPR out of any zone, with mean EPR ranging from $-6.5 \pm 0.1 \text{ m}\cdot\text{yr}^{-1}$ to $8.5 \pm 0.1 \text{ m}\cdot\text{yr}^{-1}$, in NS023w Masstown West Marsh and NS040_01 Fort Lawrence Marsh, respectively (Table 4) (Figure 8). Moreover, these two marshes have the highest rates of erosion and progradation of all the marshes in the Cobequid Bay Salmon River Estuary. The mixed zone had more saltmarshes that had positive EPR rates, even though the average for the entire zone was erosional. This is because Masstown West (NS023w) and Masstown East (NS023e) marshes had the greatest number of transects, skewing the overall average below zero.

Table 4: EPR statistics for mixed zone. The error associated with mean EPR is the ESP error divided by the range of years between the first and last image.

Marshbody Tract	# Images	Mean (m·yr⁻¹)	Standard Deviation (m·yr⁻¹)	Significant Erosion (m·yr⁻¹)	Significant Progradation (m·yr⁻¹)	Max Erosion (m·yr⁻¹)	Max Prog. (m·yr⁻¹)
NS023w	9	-6.5±0.1	6.2	-12.3	11.3	-26.5	13.5
NS023e	9	-0.4±0.1	1.7			-6.2	6.4
NS040_01	6	8.5±0.1	18.6			-1.3	77.3
NS012_01	9	1.7±0.1	6.3			-10.3	48.7
NS086_01	7	0.3±0.1	1.2			-1.6	2.7
NS086_02	4	0.7±0.4	1.0			-0.3	4.4
NS086_03	6	0.2±0.2	0.9			-2.9	6.7
NS086_04	8	0.2±0.2	2.9			-14.5	14.7
NS090_01	5	-1.5±0.1	3.5			-9.2	2.7
NS090_02	5	0.0±0.1	2.9			-3.8	4.9
NS090_03	5	0.6±0.1	1.9			-3.1	5.2
NS081_02	11	0.6±0.1	2.0			-11.6	13.8

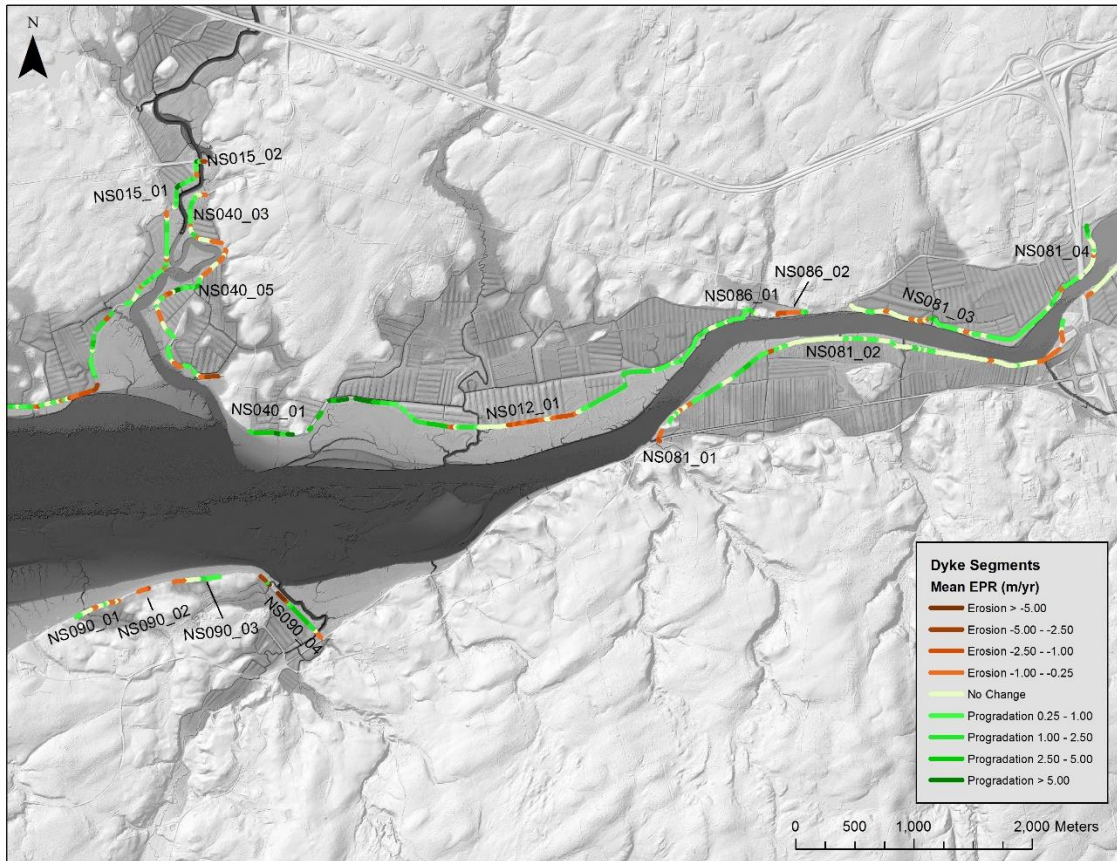


Figure 8: Mean EPR per dyke segment (25m) for marshes in the mixed zone. NS015_01, NS015_02, NS040_3, and NS040_05 are considered fluvial.

The marshes in the fluvial dominated zone of the Cobequid Zone had the least amount of foreshore change overall, with mean foreshore change rates ranging from $0.1 \pm 0.1 \text{ m} \cdot \text{yr}^{-1}$ to $0.5 \pm 0.1 \text{ m} \cdot \text{yr}^{-1}$ in North Onslow Marsh (NS067_01) and Masstown River Marsh (NS023r), respectively (Table 5) (Figure 9). Significant changes in these sections are primarily attributed to the movement of the local ebb channels; however, dredging in the Salmon River (NS067 and NS128) led to significant erosion with subsequent significant progradation. Saltmarsh loss as a result of dredging was based off the imagery and the dates of known dredging endeavors, and will be discussed in section 2.5.5.

Table 5: EPR statistics for fluvial zone. The error associated with mean EPR is the ESP error divided by the range of years between the first and last image.

Marshbody Tract	# Images	Mean (m·yr ⁻¹)	Standard Deviation (m·yr ⁻¹)	Significant Erosion (m·yr ⁻¹)	Significant Progradation (m·yr ⁻¹)	Max Erosion (m·yr ⁻¹)	Max Prog. (m·yr ⁻¹)
NS064_02	3	0.2±0.3	1.1	-3.3	3.5	-5.1	3.1
NS039_01	6	0.0±0.1	1.0			-5.2	3.9
NS023r	8	0.5±0.1	2.4			-11.1	11.0
NS040_03	5	0.5±0.1	1.3			-2.5	5.7
NS040_05	6	0.5±0.1	2.1			-4.3	14.6
NS067_01	9	-0.1±0.1	1.1			-9.8	8.9
NS067_02	9	0.0±0.1	2.9			-25.1	26.0
NS128_01	9	0.0±0.2	0.8			-4.8	2.8

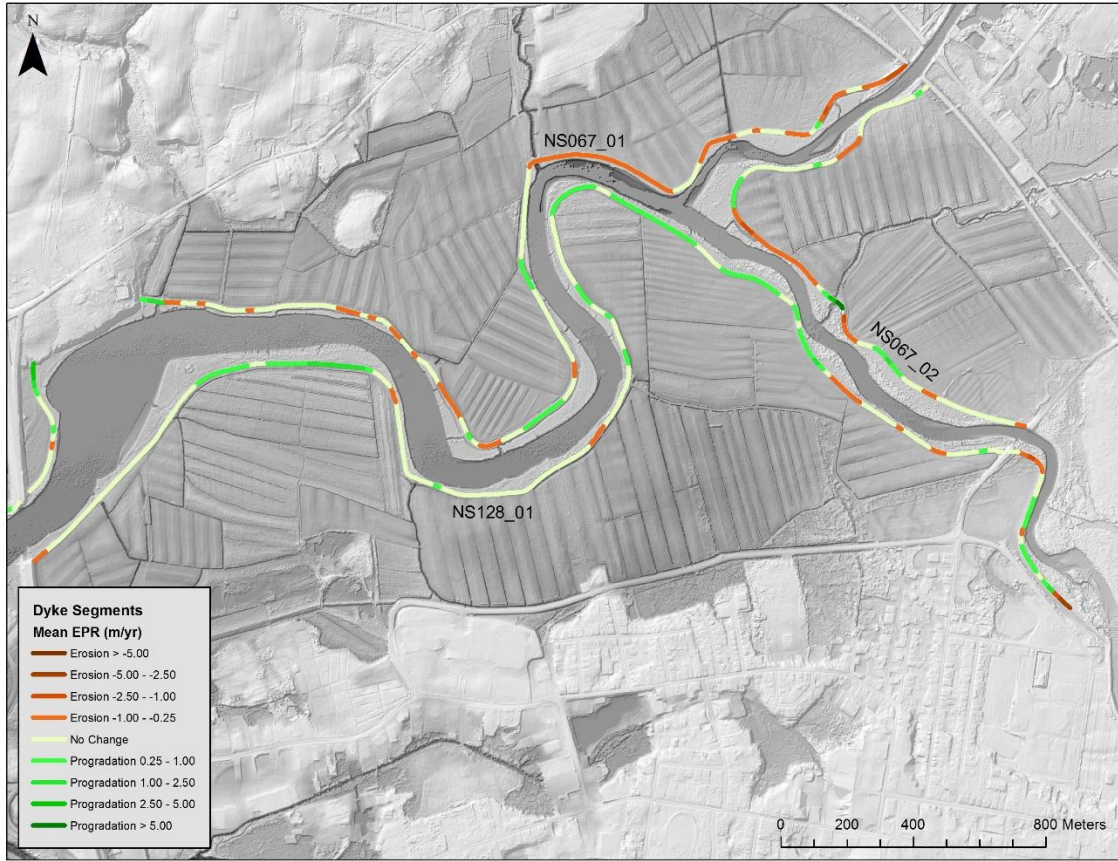


Figure 9: Mean EPR per dyke segment (25m) for marshes in the fluvial zone. Other fluvial dominated marshes shown in Figure 7 and 8 include NS015_01, NS015_02, NS023r, NS040_03, NS040_05, NS064_02, and NS064_04.

There has been an increase in foreshore edge erosion when examining EPR at a decadal scale (Figure 10). Since the dates of the images used to calculate EPR were not consistent across all marshes, EPR was divided into four periods: 1) the 1930's to the 1960's, 2) 1970's, 3) 1990's, and 4) 2000's to 2017. Overall, EPR in the tidal/wave dominated zone of the estuary maintained at approximately $-0.4\text{m}\cdot\text{yr}^{-1}$ from the 1930's to the 1990's, increasing to $-0.5\text{m}\cdot\text{yr}^{-1}$ post-2000's. The mixed zone saw a rapid increase in erosion between the 1970's and 1990's ($-0.9\text{m}\cdot\text{yr}^{-1}$), increasing further post-2000's to a mean rate of $-1.0\text{m}\cdot\text{yr}^{-1}$. The fluvial dominated zone experienced a period of progradation

between the 1930's and 1970's at a mean rate of $0.5\text{m}\cdot\text{yr}^{-1}$. However, this rate ultimately slowed to a rate of $0.1\text{m}\cdot\text{yr}^{-1}$ post-2000.

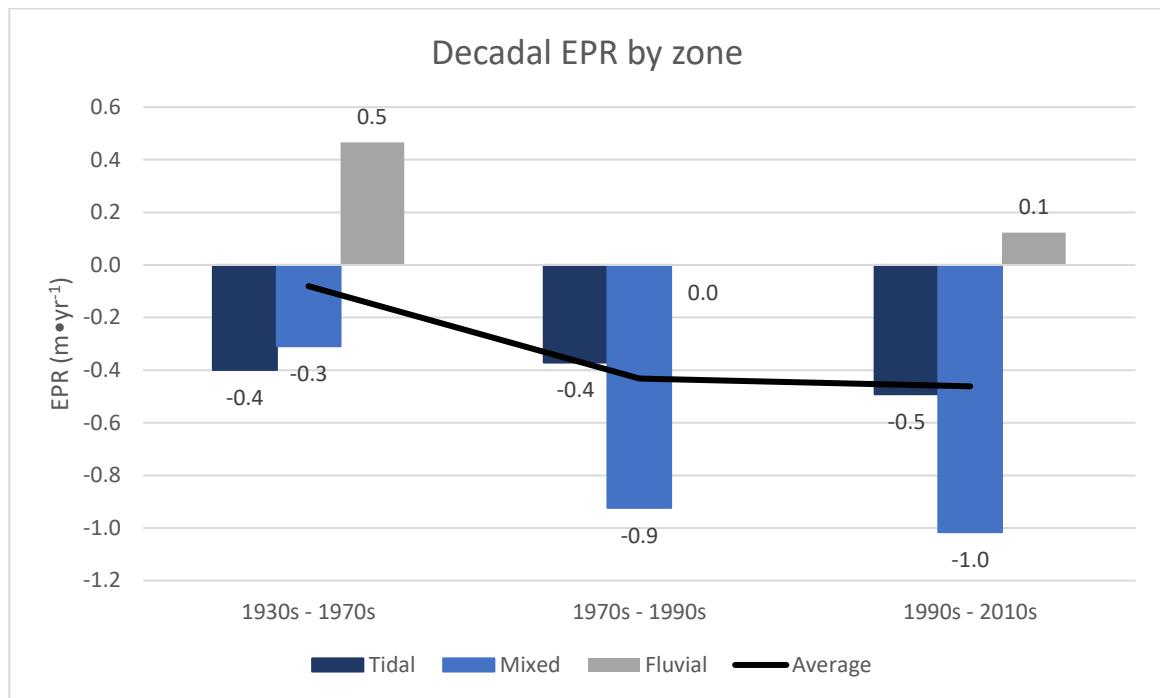


Figure 10: Changes in EPR over decadal scale.

2.5 Discussion

During the past 80 years, there have been significant changes in saltmarsh morphology in the Cobequid Bay Salmon River Estuary. However, the general changes differ depending on the location of the saltmarsh in the estuary. Specifically, there has been an increase in foreshore edge erosion in the tidal/wave dominated and mixed zones of the estuary, while overall, the fluvial dominated zone has experienced a net progradation of the foreshore edge. The continued erosion of the foreshore edge in the tidal/wave dominated zone of the estuary is similar to those found in sandstone cliffs in the Minas Basin, NS, where erosion rates increased from $0.39\text{m}\cdot\text{yr}^{-1}$ to $0.48\text{m}\cdot\text{yr}^{-1}$ from

the 1960's and 1990's, to the 1990's and the 2010's. (Wilson et al, 2017). Figure 10 showed that the saltmarshes in this zone had a mean ERP of $-0.4\text{m}\cdot\text{yr}^{-1}$ and $-0.5\text{m}\cdot\text{yr}^{-1}$ through the same time periods. The fluvial zone was the only part of the estuary to have a net progradation on the foreshore saltmarsh. Most of the progradation occurred during between the 1930's and 1970's, which may have been a result of the reduction of tidal prism downstream and the Cobequid Bay Salmon River estuary's flood dominance transporting sediment upstream (Crewe et al, 2004; Dalrymple et al, 2012). The progradation observed between the 1990's and 2010's is most likely a result of channel migration. With a constant influx of sediment with each tide, mudflats can expand horizontally and accrete vertically. This allows for saltmarsh to colonize and grow in the fluvial zone. The relatively high ERP rate between the 1930's and 1970's ($0.5\text{m}\cdot\text{yr}^{-1}$) may be precipitated by the large-scale efforts to build dykes during the 1950's. This would have decreased the tidal prism significantly in the mixed and fluvial zones, resulting in an influx of sediment deposition in the fluvial sections of the estuary (van der Wal et al, 2002).

Compared to saltmarshes and estuaries elsewhere, several of the end point change rates (ERP) observed in this study showed similarities in terms of the magnitude of change. Using DSAS, McLoughlin et al (2015) measured saltmarsh erosion rates of $-1.0\text{m}\cdot\text{yr}^{-1}$ to $-1.6\text{m}\cdot\text{yr}^{-1}$, over a 50-year period, in Virginia, U.S.A. Although these marshes are in a microtidal environment ($\sim 1.2\text{m}$), their erosion is dominated by wave action (McLaughlin et al, 2015). NS066, which is wave/tide dominated, had a similar ERP, at $-1.7\text{m}\cdot\text{yr}^{-1}$, while other wave/tide dominated marshes in the Cobequid ranged from $0.0\text{m}\cdot\text{yr}^{-1}$ to $-0.4\text{m}\cdot\text{yr}^{-1}$, with a mean change of $-0.6\text{m}\cdot\text{yr}^{-1}$ for all transects in the zone. The Saltfleetby marshes located in the Humber Estuary, U.K., which is a highly turbid,

macrotidal estuary, had extreme progradation rates similar to those observed in NS040_01, and NS090_04 (tide-project.eu, nd; Montreuil and Bullard, 2012). Specifically, Montreuil and Bullard (2012) found that a portion of the Saltfleetby marsh prograded 191.3m over a 16-year period (1994 – 2010). Between 1994 and 2003, NS090_04 had a portion of the marsh prograde 325m over a period of nine years. The mean progradation on Saltfleetby marsh was $1.15 \text{ m}\cdot\text{yr}^{-1}$, which is comparable to NS012_01, at $1.7 \text{ m}\cdot\text{yr}^{-1}$.

While there were some similarities in EPR compared to other marshes, there were instances of changes (both progradation and erosion) in the Cobequid marshes that were greater in both their magnitude and variation. NS023w had a mean EPR of $-6.5 \pm 0.1 \text{ m}\cdot\text{yr}^{-1}$ over 79 years, with maximum EPR between subsequent images measured along one transect of $-26.5 \pm 0.9 \text{ m}\cdot\text{yr}^{-1}$. This results to a mean foreshore loss of over 500m during this time. These rates a higher than those typically found in saltmarsh change literature and are comparable to EPR found in rapidly eroding Arctic barrier island ($-7.2 \pm 0.2 \text{ m}\cdot\text{yr}^{-1}$) and inundated tundra ($-5.8 \pm 0.2 \text{ m}\cdot\text{yr}^{-1}$) coastlines (Irrgang et al, 2018).

2.5.1 Dykes

The construction of dykes for reclamation or flood defence can often lead to the formation, or expansion, of an intertidal mudflat in front of the dyke. Dyke construction precipitates this expansion because it leads to a reduction in the local tidal prism (van der Wal et al, 2002). The reduction of the tidal prism leads to the reduction of tidal velocities and increases the duration of the slack tide (van der Wal et al, 2002; French et al, 2005; Pye and Blott, 2014). This ultimately leads to sediment deposition on the intertidal

mudflat in front of the dyke, and eventually the creation and/or progradation of the foreshore saltmarsh (van der Wal et al, 2002; van Proosdij and Baker, 2007; Pye and Blott, 2014). This pattern of dyke building and subsequent foreshore expansion is apparent on NS012 VDJ Marsh. Since 1938, the foreshore saltmarsh at VDJ has advanced over 750m (Figure 11). In 1955, a large dyke was built approximately 100-200m south of the 1938 foreshore edge. This precipitated the growth and expansion of the foreshore saltmarsh, which averaged a foreshore change rate of $3.3 \pm 0.2 \text{ m}\cdot\text{yr}^{-1}$, with several transects having an EPR exceeding $5.0 \pm 0.2 \text{ m}\cdot\text{yr}^{-1}$ in this period. In 1996, this dyke was realigned in order to reclaim approximately 45ha of the newly created saltmarsh. This realignment further reduced the local tidal prism, allowing for the continued expansion of the intertidal mudflat and the progradation of the foreshore saltmarsh, which averaged a foreshore change rate of $2.3 \pm 0.2 \text{ m}\cdot\text{yr}^{-1}$ for the transects impacted by the realignment. More recently, the foreshore change rates have slowed considerably, with a rate of $0.3 \pm 0.7 \text{ m}\cdot\text{yr}^{-1}$ between 2003 and 2011, and rates of $-0.3 \pm 3.2 \text{ m}\cdot\text{yr}^{-1}$ between 2016 and 2017. The reduction in progradation rates combined with alternating periods of erosion and progradation suggest that the foreshore saltmarsh may be approaching a dynamic equilibrium. This pattern is similar to those found in the Blyth (French et al, 2005), Ribble (van der Wal et al, 2002), the Dee and Wash (Pye and French, 1993) estuaries, in the UK, which found the reduction of tidal prism and the expansion of intertidal mudflats to be a direct morphodynamic response to dyke construction (van Proosdij et al, 2009).

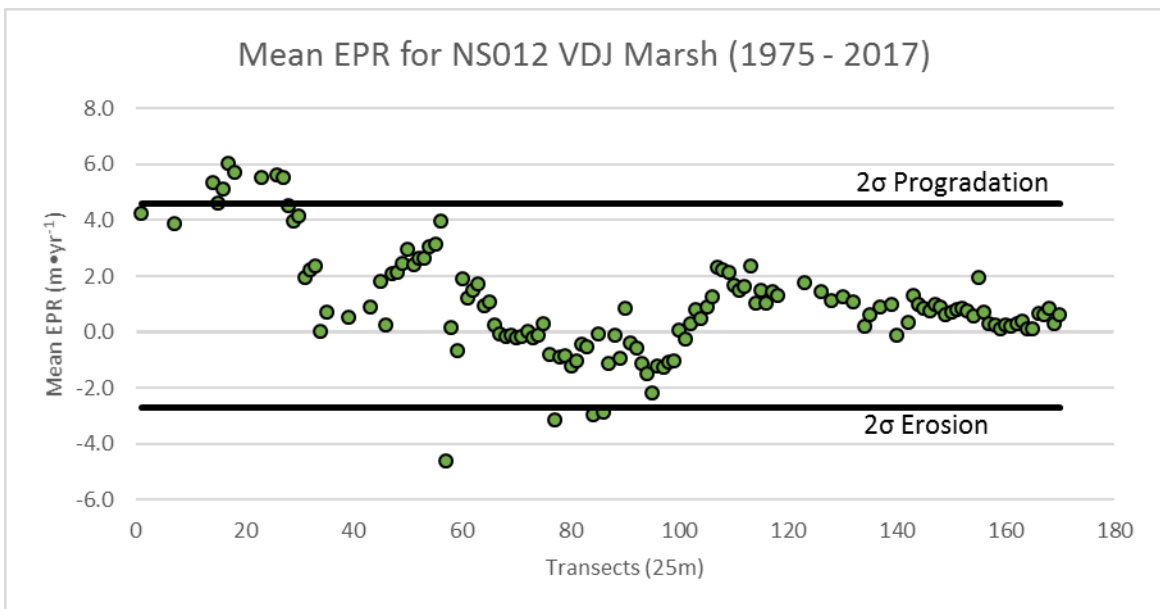
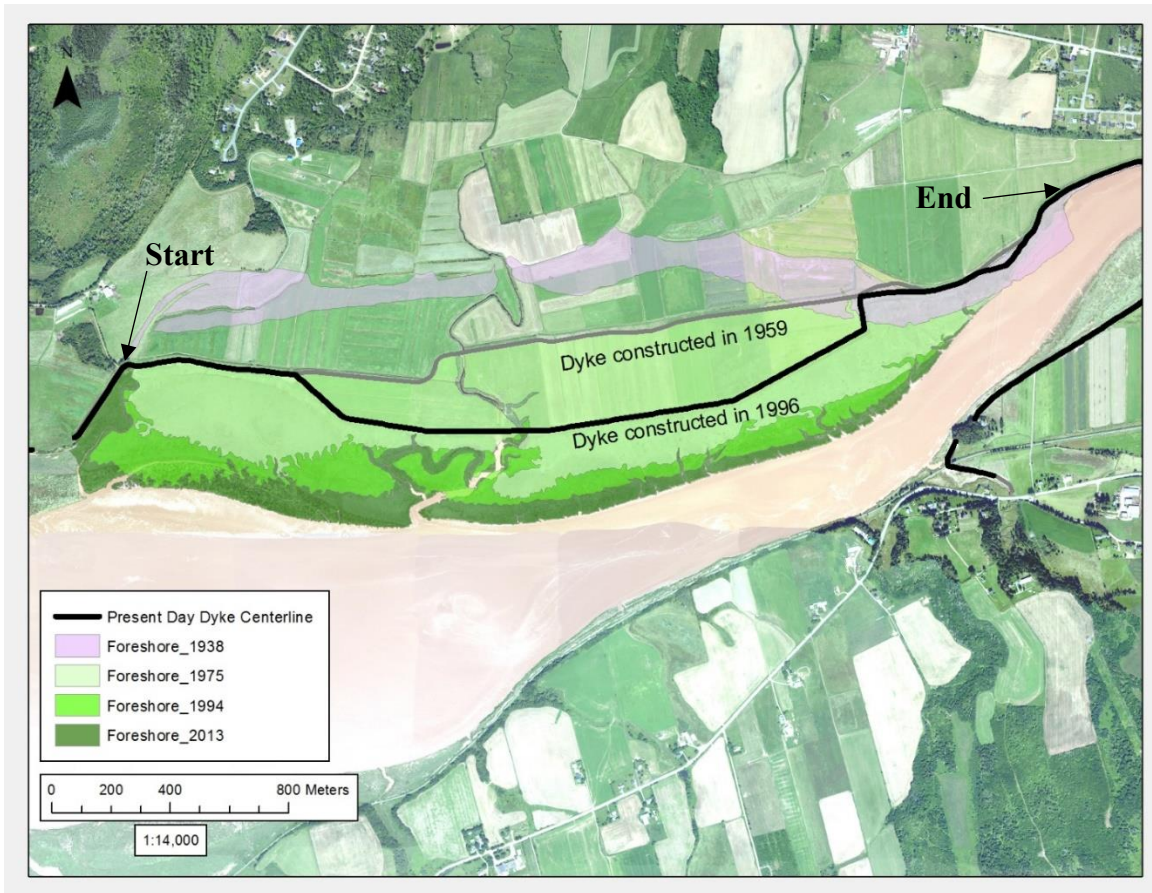


Figure 11: Map showing changes in saltmarsh location from 1938 (pink) to 2013 (dark green). Mean EPR between 1975 and 2017 shown below. Significant progradation is $4.6\text{m}\cdot\text{yr}^{-1}$ and significant erosion is $-2.7\text{m}\cdot\text{yr}^{-1}$. Start and end points in map correlate with points in EPR graph.

Saltmarsh reclamation presents a challenge when it comes to examining dykeland resiliency using EPR. Since dyke construction can precipitate progradation of the foreshore edge, this analysis will see that change as a positive one. However, the progradation that occurs could be at the expense of an overall loss in saltmarsh area, which ultimately makes the dykeland less resilient to SLR, coastal flooding and coastal erosion. This is apparent in NS114, which lost over 80% of its saltmarsh area between 1964 and 1994 despite the foreshore edge remaining in relatively the same position (Figure 12). It is important to be cognizant that while the progradation of a saltmarsh in front of the dyke represents an increase in resiliency, it does not necessarily mean that the system itself is more resilient than if the dyke was closer to the natural backshore.

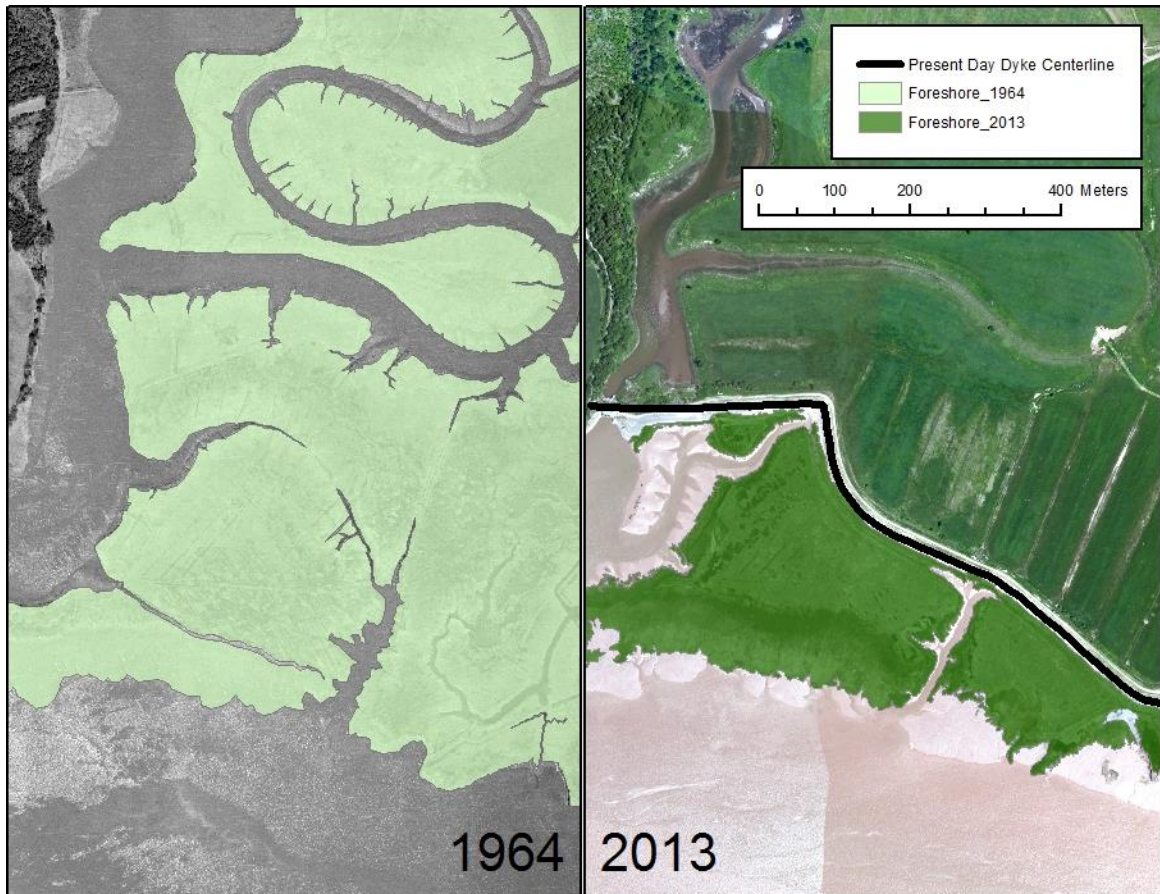


Figure 12: Foreshore change at NS114 between 1964 and 2013. Although the relative position of the foreshore edge has stayed the same, there has been a loss of foreshore width and resiliency.

In some cases, dykes may not directly influence rates of ERP, but the presence of a dyke can exacerbate the loss of resiliency associated with foreshore erosion. In NS023w Masstown West, the mean EPR at the foreshore has been $-6.0 \pm 0.1 \text{ m} \cdot \text{yr}^{-1}$, since 1938, with a number of transects eroding at a rate greater than $-10.0 \pm 0.1 \text{ m} \cdot \text{yr}^{-1}$ (Figure 13). The erosion of the Masstown West saltmarsh is caused by the movement of the ebb channel into the saltmarsh, as well as being orientated close to the dominant fetch direction, making it susceptible to wave erosion. Following the construction of the dyke, in 1953, approximately 138ha of saltmarsh was lost to reclamation. This effectively cut off the horizontal accommodation space the saltmarsh had. At the current rate of foreshore change, it is possible that the foreshore could erode into the dyke by 2030. The reduction of horizontal accommodation space, often called "coastal squeeze", has been identified by a number of studies of as a major contributor to erosion in a number of estuaries (Wolters et al, 2005; Singh et al, 2007; Torio et al, 2013). Since the presence of the dyke does not allow for the saltmarsh to adjust to changes at the foreshore edge, it is effectively a cause of erosion even though it is not actively causing the erosion (Wolters et al, 2005). It should be noted that although the foreshore saltmarsh in front of NS023w has eroded, much of the material has likely transported to a natural marsh directly south, or into the fluvial zone of the estuary.

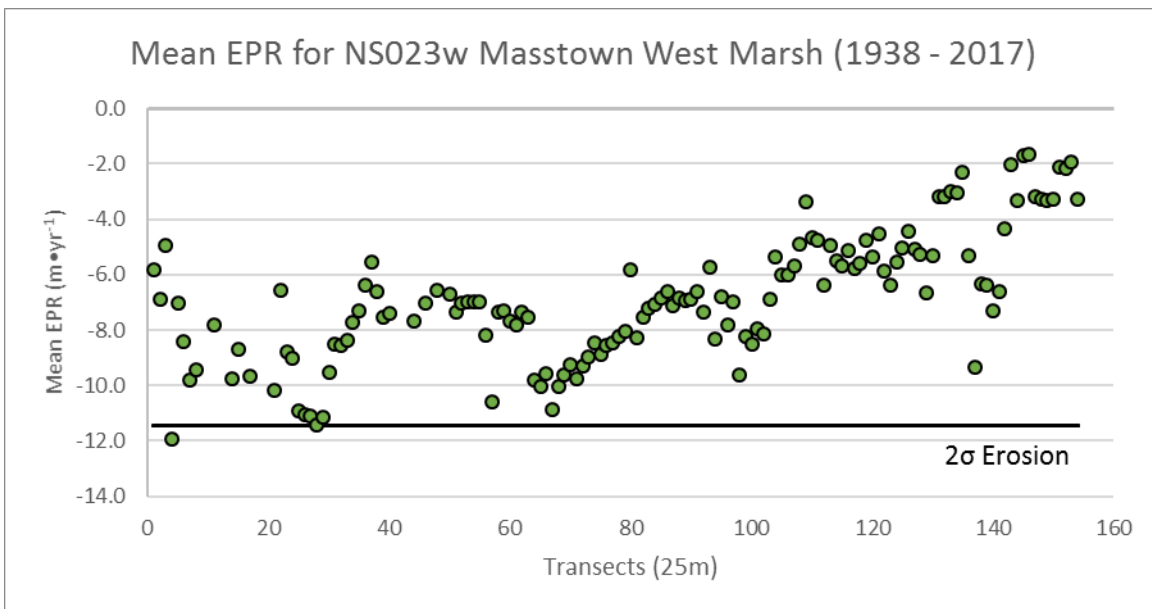
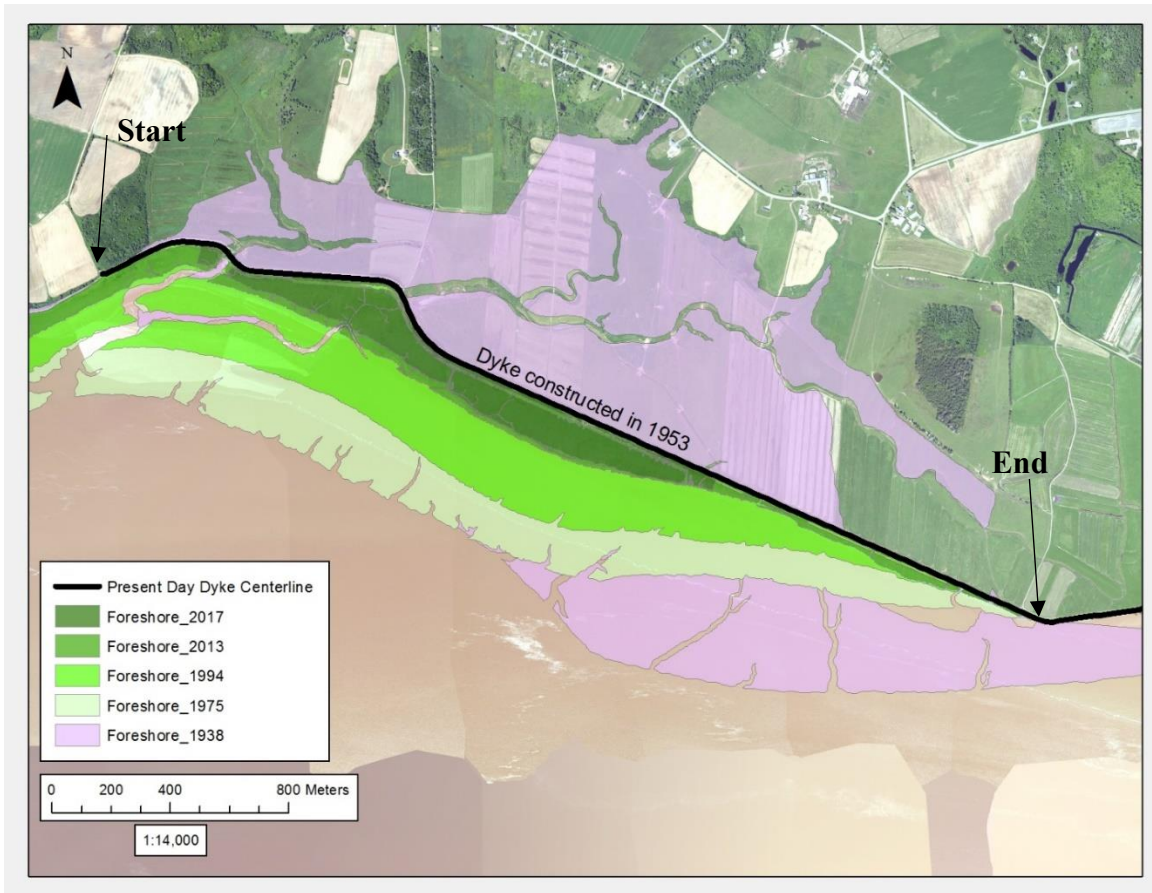


Figure 13: Map showing changes in saltmarsh location from 1938 (pink) to 2017 (dark green). Mean EPR between 1938 and 2017 shown below. Significant erosion is $-11.4\text{m}\cdot\text{yr}^{-1}$. Start and end points in map correlate with points in EPR graph.

2.5.2 Kickers

Kickers have contributed to the progradation of the foreshore saltmarsh in NS081 Lower Truro, which is in the mixed zone of the Cobequid Bay Salmon River Estuary. Specifically, a kicker implemented sometime between 1938 and 1955 has helped deflect the thalweg away from the foreshore edge (Figure 14). As the thalweg moved further away from the foreshore, flow velocity in front of the foreshore slowed down allowing for the accumulation of sediment on the intertidal mudflat (Klingeman et al, 1984) (Figure 15). Slowly, saltmarsh colonized and prograded onto the mudflat at a rate of $2.0 \pm 0.2\text{m}\cdot\text{yr}^{-1}$ between 1975 and 2011. Between 2011 and 2013 significant rates of progradation occurred ($>10 \pm 2.0\text{m}\cdot\text{yr}^{-1}$) as the majority intertidal mudflat reached an elevation that could sustain saltmarsh. This shows the latent response of saltmarshes to certain implementations, as the morphodynamic response of the system was constrained to intertidal mudflats.

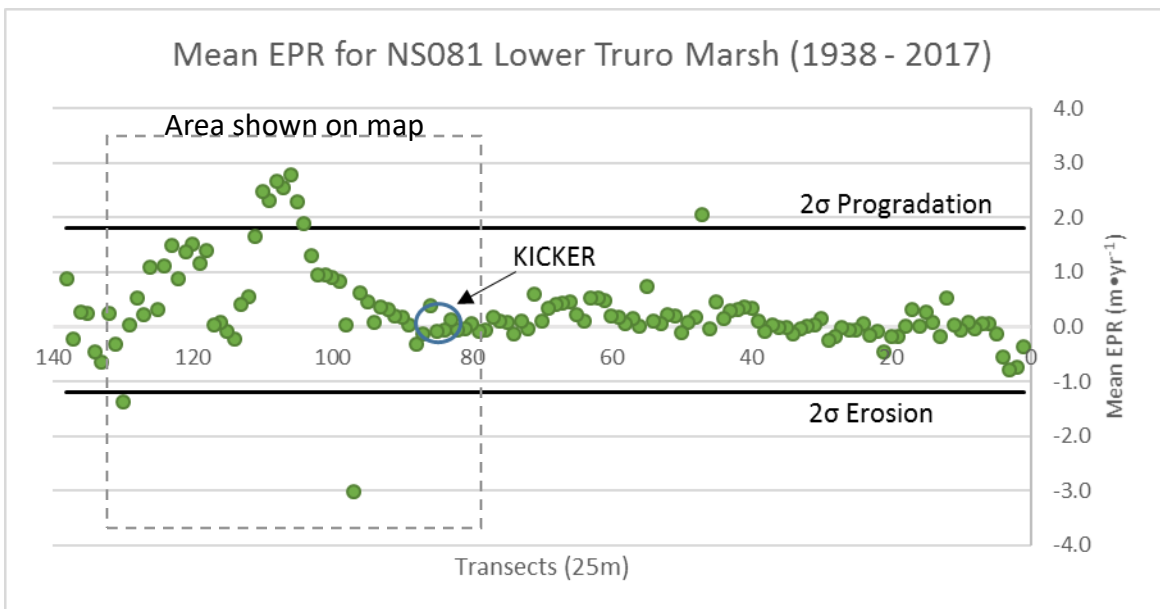


Figure 14: Map showing changes in saltmarsh location from 1938 (pink) to 2013 (dark green). Mean EPR between 1938 and 2017 shown below. Significant progradation is $1.8\text{m}\cdot\text{yr}^{-1}$ and significant erosion is $-1.2\text{m}\cdot\text{yr}^{-1}$.

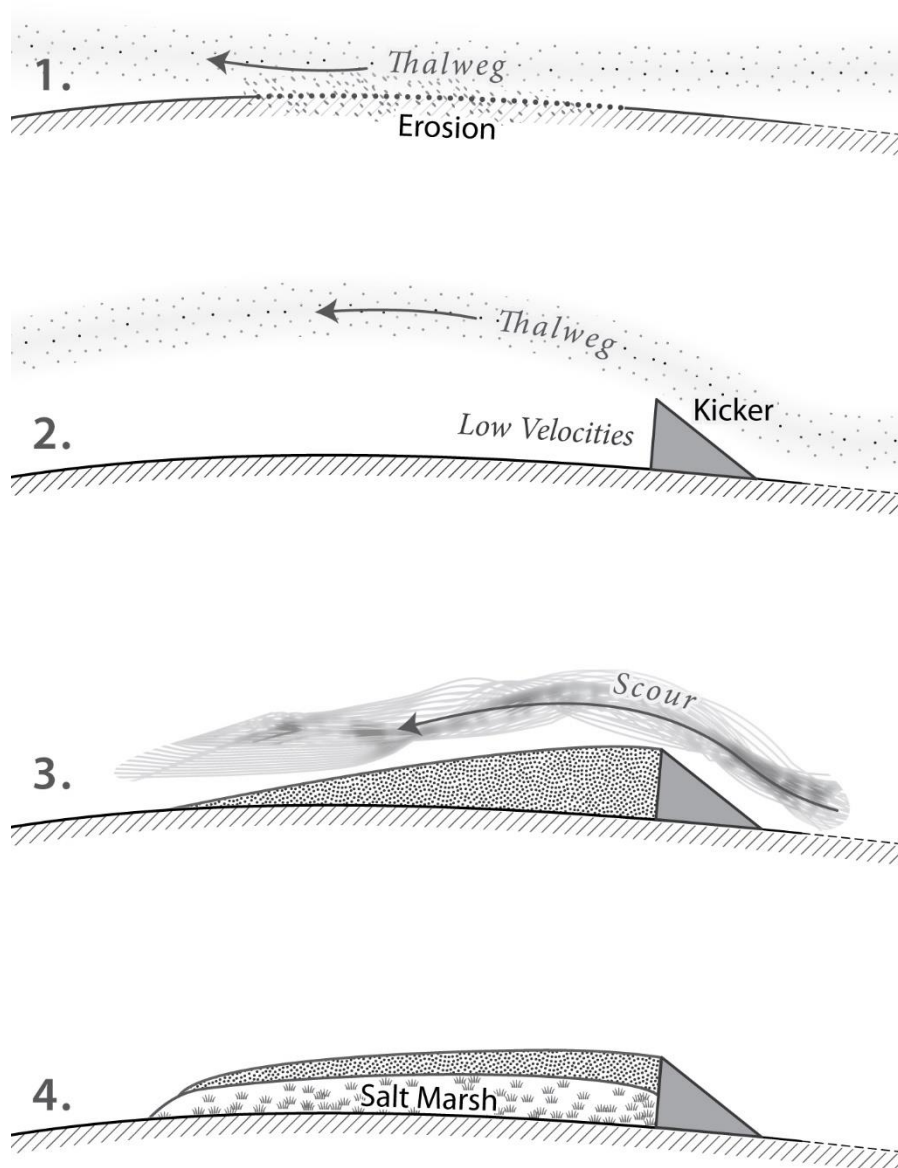


Figure 15: 1) Bank erosion caused by movement of thalweg. 2) Kicker is installed deflecting thalweg away from bank. 3) Deposition occurs downstream of the kicker. Thalweg position is reinforced by bed scour. 4) Saltmarsh colonizes the newly formed mudflat. Based off Klingemann et al, 1984. Credit: Will Flanagan.

In the fluvial dominated zone of the Cobequid Bay – Salmon River estuary, kickers are highly visible in the imagery dating back to 1938 (Figure 16). In this section, the density of kicker implementations is higher, with kickers installed in tandem across the channel. While the implementation of dyke infrastructure helped to confine the river

channel, the kickers help maintain the position of the thalweg within the channel (van Proosdij and Matheson, 2015). As a result, kickers are responsible for stabilizing EPR rather than promoting saltmarsh progradation in the fluvial zone of the estuary (van Proosdij and Matheson, 2015). This is reflected by the mean EPR rates in the Onslow and Cobequid Marsh, which are $-0.1 \pm 0.1 \text{ m} \cdot \text{yr}^{-1}$, $0.0 \pm 0.1 \text{ m} \cdot \text{yr}^{-1}$, and $0.0 \pm 0.2 \text{ m} \cdot \text{yr}^{-1}$ for NS067_01, NS067_02, and NS128_01, respectively. As a result, kickers have a varying function regarding shoreline protection depending on the dominant morphodynamic processes present. In the mixed portion, kickers augment protection by promoting saltmarsh growth, whereas in the fluvial section kickers only reduce the amount of erosion without any significant impact on saltmarsh EPR (van Proosdij and Matheson, 2015).

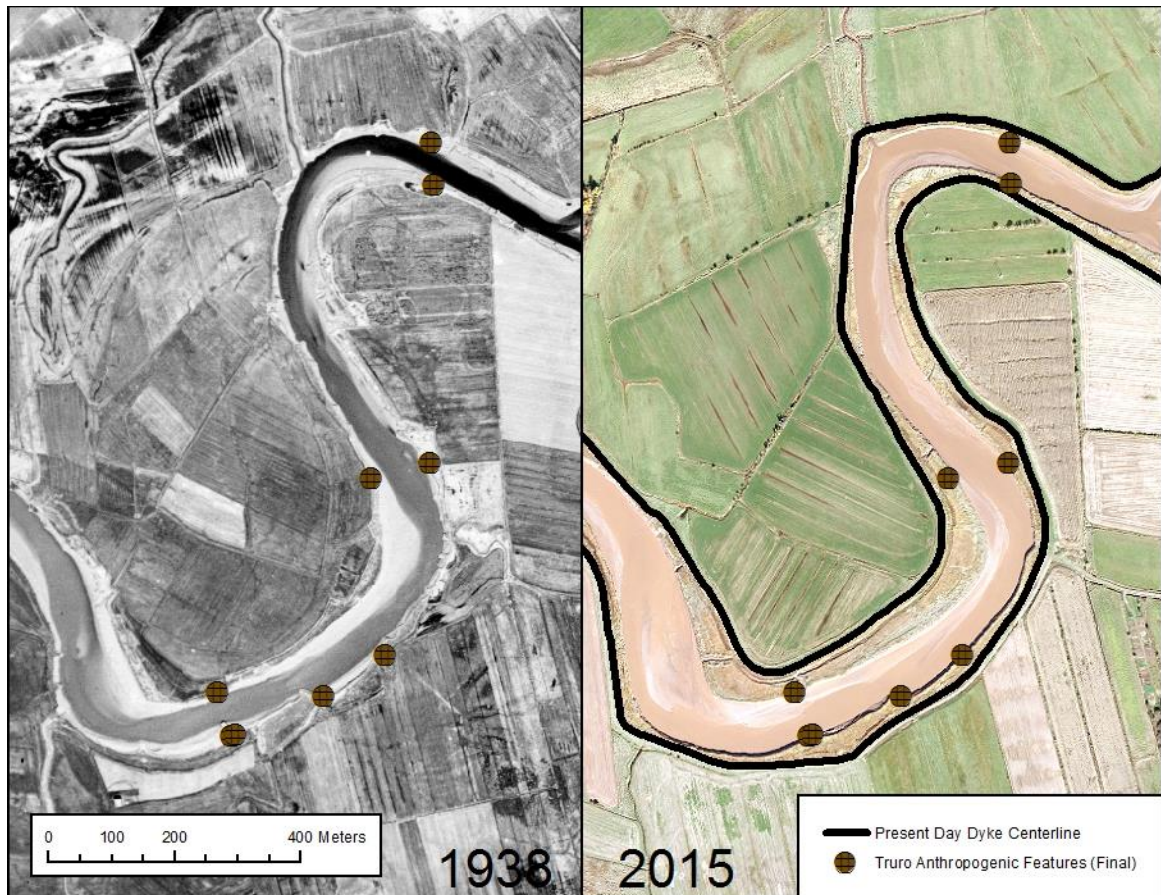


Figure 16: Map showing how the implementation of dykes and kickers have stabilized the Salmon River and its thalweg between 1938 and 2015.

2.5.3 Borrow Pits

Borrow pits have caused localized foreshore erosion in several saltmarshes. In NS023w Masstown West Marsh, a large borrow pit outlet is observed to have significantly increased what was already very high foreshore erosion rates (mean EPR of $-6.5 \pm 0.1 \text{ m} \cdot \text{yr}^{-1}$). The foreshore width in that area can be greatly reduced when borrow pit outlets are excavated perpendicular to the foreshore. Following the excavation of a borrow pit in the early months of 2016, the local foreshore width was reduced by approximately 80m. This led to significant scouring and erosion of saltmarsh material near the backshore, which would have remained undisturbed if the saltmarsh had been left in a natural state (Figure 17). Furthermore, this erosion is occurring within 10m of the toe

of the dyke, potentially putting the infrastructure at risk should it continue. Finally, the outlet channel has nearly doubled in width since 2016, meaning that more of the backshore has become more exposed. This pattern of significant erosion rates near the outlet of borrow pits is also observed on NS023e Masstown East Marsh and NS081 Lower Truro Marsh. In NS023e, there are two borrow pits that intersect the foreshore edge and have caused erosion.



Figure 17: Scouring of backshore saltmarsh caused by the excavation of a borrow pit outlet.

In NS081, borrow pits have led to significant rates of erosion ($-4.0 \pm 2.0\text{m}\cdot\text{yr}^{-1}$ to $-6.8 \pm 2.0\text{m}\cdot\text{yr}^{-1}$) adjacent to the outlet channels as water moves in and out of the borrow pits (Figure 18). Water entering the pits on the rising tide and leaving the pits during the

falling tide can exceed $1\text{ m}\cdot\text{s}^{-1}$ (see Chapter 3.4.3). This causes significant turbulence where the borrow pit flow intersects with the flow in the main channel. This leads to conditions that are conducive to bank scour, resulting in significant loss of foreshore width adjacent to the pits. It is unknown if this erosion is a short-term response to borrow pit excavation, however, as the borrow pits infill as intended, their discharge will decrease as well. This may be enough for the adjacent foreshore edge to rebound given the contemporary erosional or progradational state of the marsh.

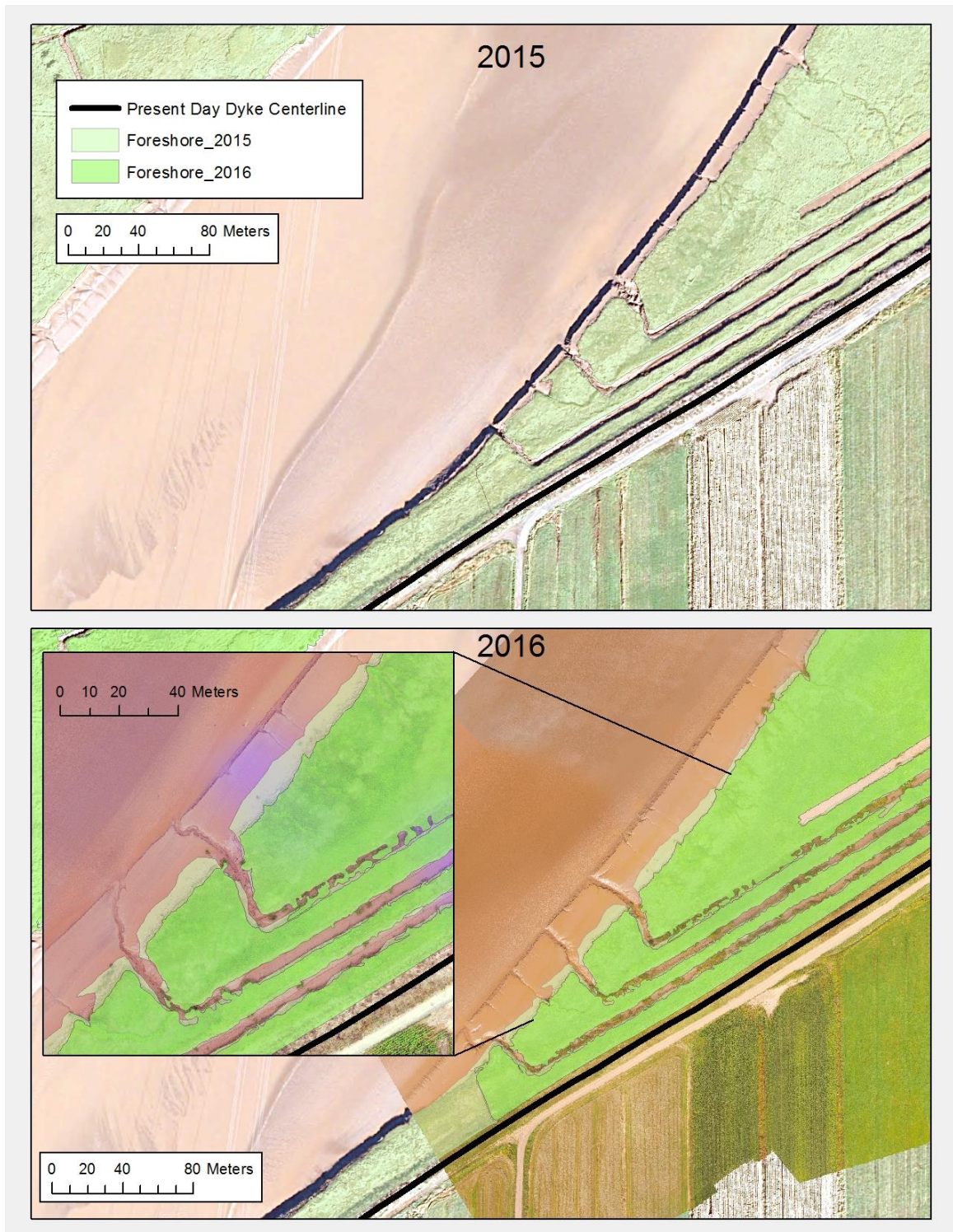


Figure 18: Foreshore erosion exceeding $10\text{m}\cdot\text{yr}^{-1}$ following the excavation of borrow pits. This is caused by high velocities entering and leaving the borrow pit outlets.

2.5.4 Aboiteaux

Aboiteaux were observed to have only influenced EPR at a scale localized to approximately 1000m. Specifically, the implementation of a new aboiteau was found to have precipitated significant erosion rates at several marshes, including: NS012, NS067, NS081, NS086 and NS128. When an aboiteau is removed, the relict outlet channels will often infill, allowing saltmarsh to return and the foreshore to prograde very locally. When a new aboiteau is installed, or the drainage from a removed aboiteau is directed to another, channels can form and widen on the foreshore saltmarsh. Aboiteaux control the location of upland drainage into the main tidal channels, which is followed by the formation of a large outlet channel. When an aboiteau drains a large watershed, the width of the outlet channel can be quite large and have impacts on foreshore change rates elsewhere on the marsh, or on adjacent marshes. In the Cobequid Bay Salmon River Estuary, a large aboiteau located on NS012 VDJ marsh has precipitated significant rates of change on the foreshore saltmarsh since its implementation in the late 1950's, and relocation in 1996 (Figure 19). Specifically, the location and movement of the aboiteau channel has influenced both significant rates of erosion and progradation. Regarding the latter, the location of this aboiteau channel changed substantially between 1994, 2003 and 2015. In 2003 the aboiteau channel was located immediately against the foreshore saltmarsh. In 2015 the aboiteau channel is observed to have migrated east by approximately 1300m. This has allowed deposition to occur on the intertidal mudflat in front of the saltmarsh. Between 2011 and 2013 this mudflat reached an elevation that allowed for the progradation of the foreshore saltmarsh, with rates of change exceeding $40.0 \pm 0.2\text{m}\cdot\text{yr}^{-1}$. Aboiteau migration is predominantly controlled by the magnitude and frequency of higher than average discharge events (Daniel, 1971). It is possible that a

very large event, like Hurricane Juan which moved through the Bay of Fundy in 2003, caused the aboiteau channel to significantly change its course.

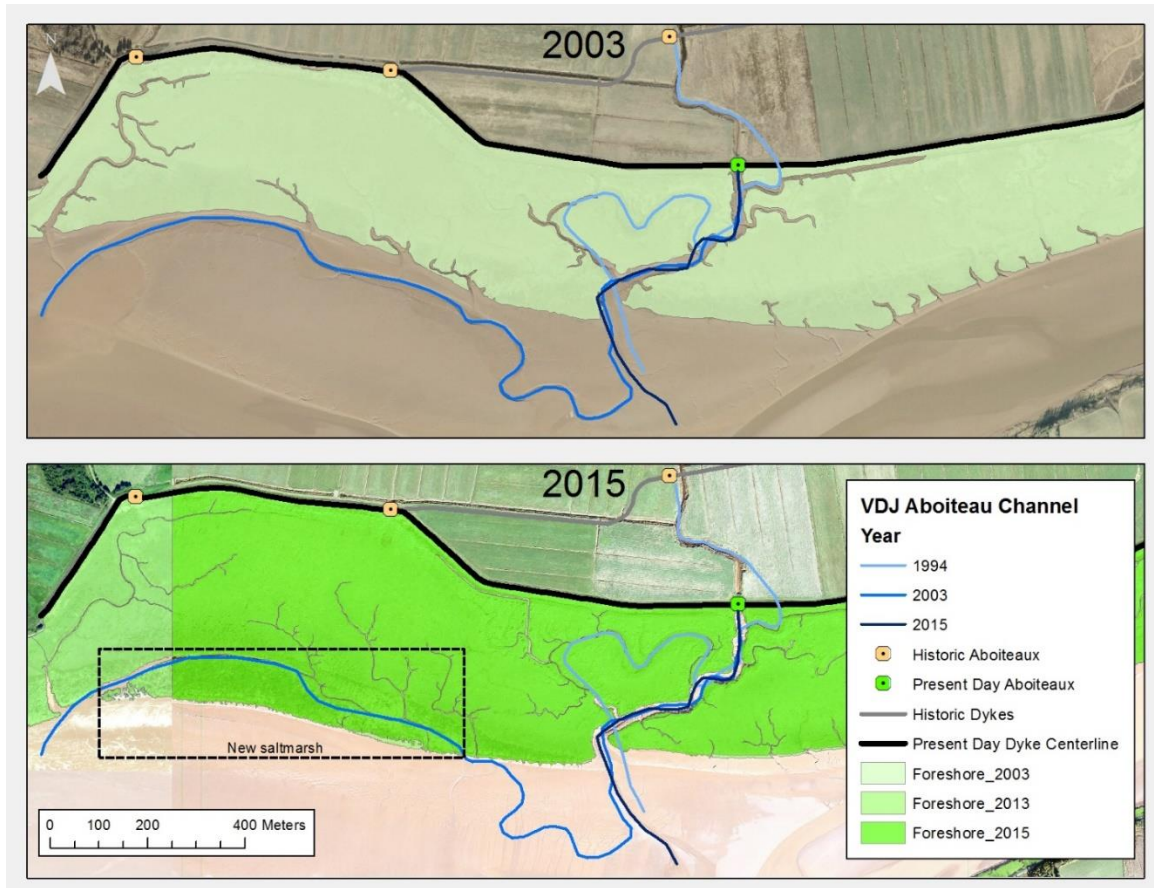


Figure 19: The movement of an aboiteau channel at NS012 VDJ Marsh has significantly influenced the position of the foreshore saltmarsh. As the channel migrates toward the foreshore edge it can accelerate erosion rates. When it migrates away from the edge it leaves behind an area where rapid deposition can occur leading to significant progradation when mudflat reaches a suitable elevation for saltmarsh growth.

2.5.5 Dredging

Dredging activities were observed to have led to significant erosion rates in the fluvial section of the Cobequid Bay – Salmon River estuary (Figure 20). Dredging is implemented to help with flood control in the town of Truro, Nova Scotia, by increasing the cross-sectional area of the Salmon River expediting flow in the downstream direction

(i.e. away from the town) (Figure 21). Dredging was observed to lead to erosion rates of $-3.1 \pm 2.0 \text{ m} \cdot \text{yr}^{-1}$ between 2011 and 2013. Specifically, this comes from the in-situ removal of saltmarsh, intertidal mudflat, and material on the estuarine bed and thalweg. In this case, the material is moved beyond the high marsh and is not redistributed back into the system. This observation is consistent with a few studies which cite dredging as a major source of sediment loss within estuaries worldwide (van der Wal et al, 2004; Blott et al, 2006; Wang et al, 2015). However, since this section of the Cobequid Bay is near the turbidity maxima (Dalrymple et al, 2012) the suspended sediment concentration in this section of the estuary can exceed $100 \text{ g} \cdot \text{l}^{-1}$ (Crewe et al, 2004). This can lead to deposition rates that reach as high as four to five centimetres per tide (Personal Communication, Darrel Hingley, April 27th, 2018; Purcell, 2020). The rapid deposition allows the intertidal mudflats to rebound quickly from dredging, ultimately leading to significant periods of progradation when the mudflat elevation becomes suitable for saltmarsh expansion. As a result, the saltmarsh in the dredged area rebounded at a rate of $3.4 \pm 2.4 \text{ m} \cdot \text{yr}^{-1}$ between 2013 and 2015. It should be noted that this pattern of erosion and deposition was only visible in imagery intervals that were two years apart. This highlights

the importance of developing a frequent monitoring program in order to augment the understanding of how these dynamic systems respond to anthropogenic implementations.

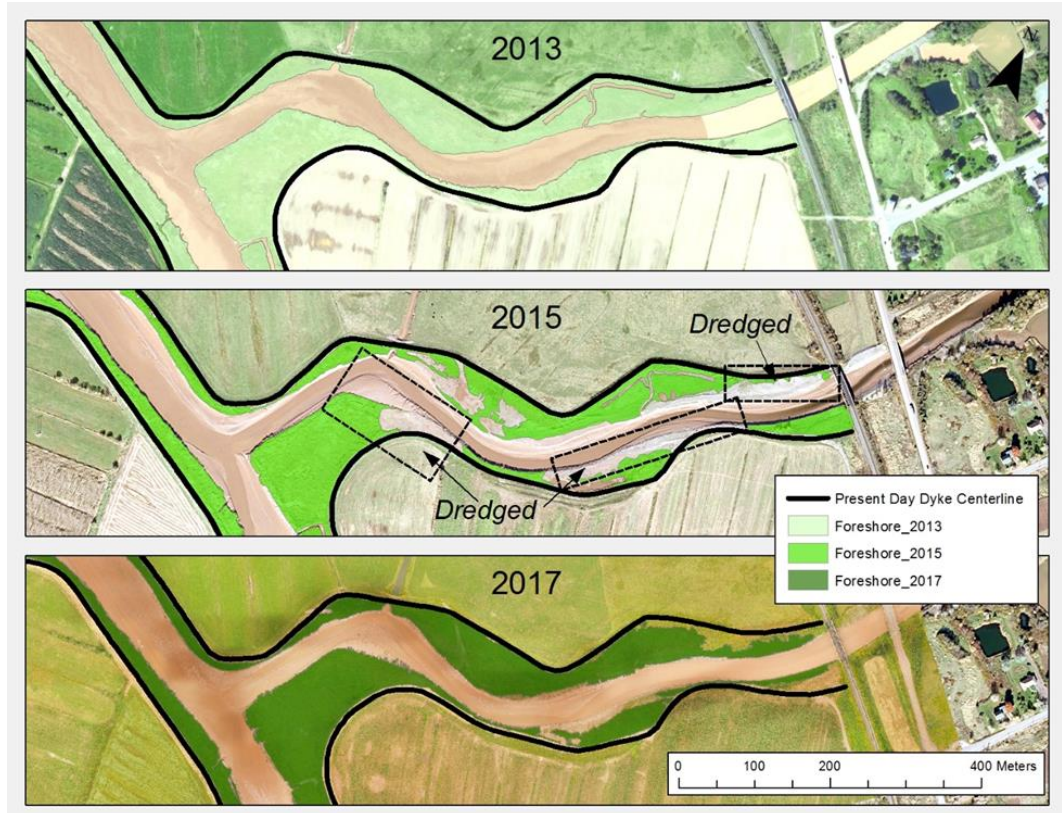


Figure 20: Significant loss of foreshore saltmarsh caused by dredging followed by a period of rapid deposition and saltmarsh growth. Dredging was implemented in an effort to mitigate flooding.



Figure 21: Dredging of the channel bed, intertidal mudflat, and saltmarsh.

2.5.6 Foreshore Rocking

Foreshore rocking did not influence significant changes in foreshore change rate along any of the saltmarshes in the Cobequid Bay – Salmon River estuary. However, due to the relatively short “life expectancy” of foreshore rocking in this macrotidal regime, most of the foreshore rocking projects that were implemented were not visible in the imagery unless the temporal resolution was high (<10 years). This is especially true in the tidal/wave dominated portion of the estuary, where a foreshore rocking project was observed to have degraded over two years. Although foreshore rocking was not shown to have influenced significant foreshore change rates, high resolution imagery obtained using an unmanned aerial vehicle (UAV) revealed that the implementation of rocking precipitated scour in the intertidal mudflat, immediately upstream from the rocking

(Figure 22). The pattern of the scour that forms in the mudflat immediately behind the foreshore rocking is similar to those Bernatchez and Fraser (2012) observed on sandy beaches in the Gulf of Saint Lawrence, Canada. While this has not impacted saltmarsh erosion, it may exacerbate future erosion by eliminating the mudflat in front of the saltmarsh, making it more susceptible to both lateral and wave induced erosion (Chahuan, 2009). This highlights another potentially latent response in saltmarsh EPR to implementations in the intertidal zone. In this case, the process of autocyclic erosion is expected to accelerate due to the erosion of the mudflat precipitated by the implementation of the rocking (Chahuan, 2009).

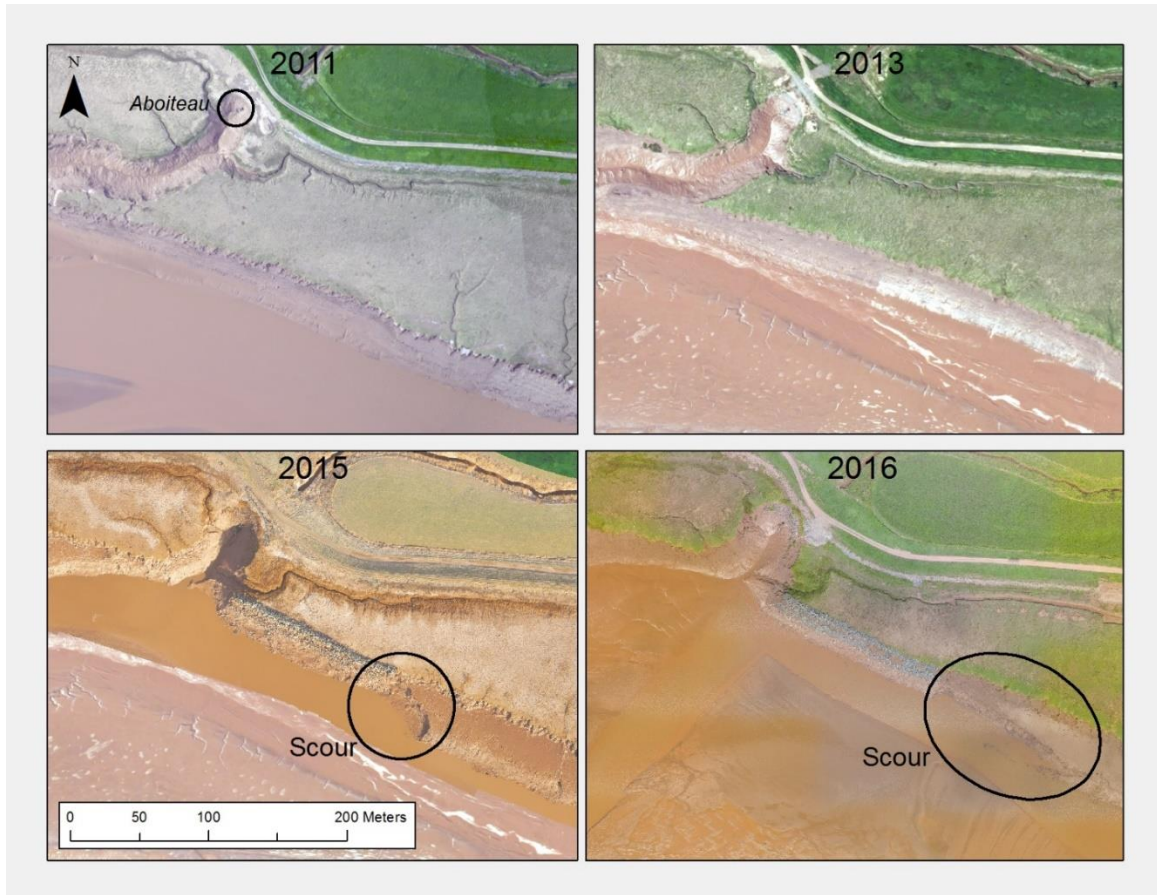


Figure 22: Foreshore rocking implemented to prevent erosion was implemented in between 2013 and 2014. Although this has temporarily slowed erosion rates, it has increased scour at the end of the rocking, removing the intertidal mudflat.

2.5.7 Managed Realignment

During this project, several dykes in the Bay of Fundy have been identified as candidates for managed realignment. In the Cobequid Bay – Salmon River estuary, one dyke has been realigned, although tidal flow has yet to be restored as the final breach designs are still being discussed (Sherren et al, 2019). Theoretically, this managed realignment could create more than 90ha of new saltmarsh, while improving flood abatement locally. In terms of foreshore change rates, it is possible that the realignment of dyke could precipitate foreshore erosion, as the dykes and foreshore rocking will no longer constrain the movement of the channel. Overall, it is expected that the managed

realignment project will increase the resiliency of the dykeland by significantly increasing the foreshore width, despite what may occur at the foreshore edge.

2.5.8 Channel Migration and Thalweg

Perhaps the biggest driver of erosion and progradation in the Cobequid Bay Salmon River Estuary is the movement of the ebb and flood tidal channels. Channel migration is the primary mechanism for the erosion occurring at Masstown West marsh as well as the dynamic movement of the foreshore at Old Barns marsh. Figure 23 shows how the movement of the Salmon River ebb channel has oscillated north and south several 100s of metres since 1975. This movement has resulted in both significant erosion and progradation of the foreshore during this time. It should also be noted that erosion occurs as the thalweg moves into the saltmarsh. However, there is a latency between the movement of the channel away from the saltmarsh and the subsequent progradation. This is because in order for progradation to occur, the intertidal mudflat between the saltmarsh and thalweg must build up to an elevation in which the saltmarsh can colonize it. This is apparent in the 1994 and 2003 images. In both images the ebb channel is relatively in the same position, indicating the majority of the movement occurred prior to 1994. In the 1994 a large mudflat is visible between the foreshore and the thalweg, which is fully colonized by 2003. By 2013, the foreshore has eroded approximately 150m ($1.5 \pm 0.6 \text{m} \cdot \text{yr}^{-1}$) in ten years, as the thalweg migrates southward again and is located immediately adjacent to the saltmarsh. This process of channel movement, mudflat development, and saltmarsh colonization is also responsible for the highest rates of progradation observed in the Cobequid Bay Salmon River Estuary (Figure 24). These

changes occurred at NS040 Fort Belcher marsh, where the saltmarsh prograded at a rate that ranged from $11.1 \pm 2.0\text{m}\cdot\text{yr}^{-1}$ to $77.3 \pm 2.0\text{m}\cdot\text{yr}^{-1}$, from 2011 to 2013

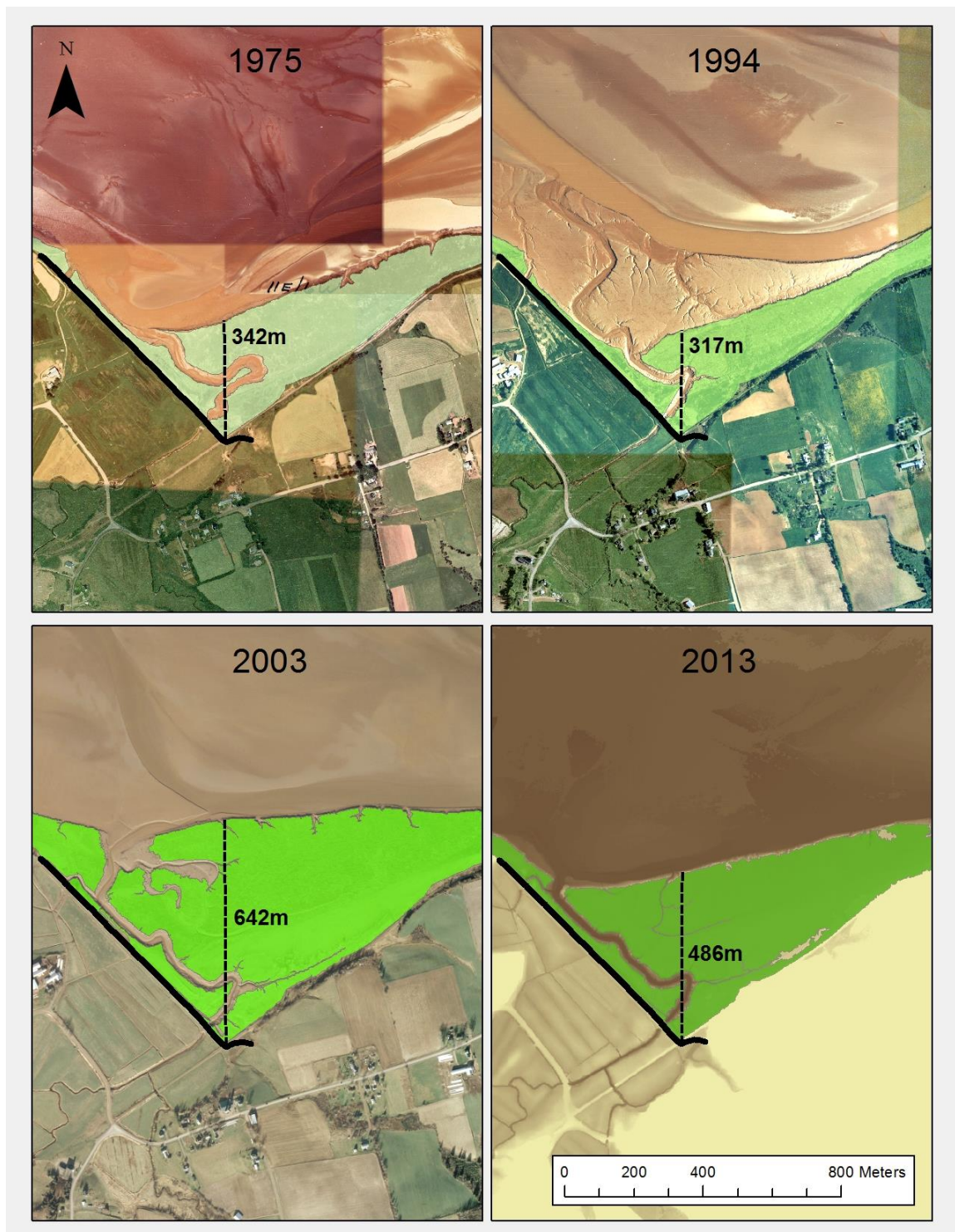


Figure 23: Dynamic rates of change in the location of the foreshore edge caused by ebb channel migration.

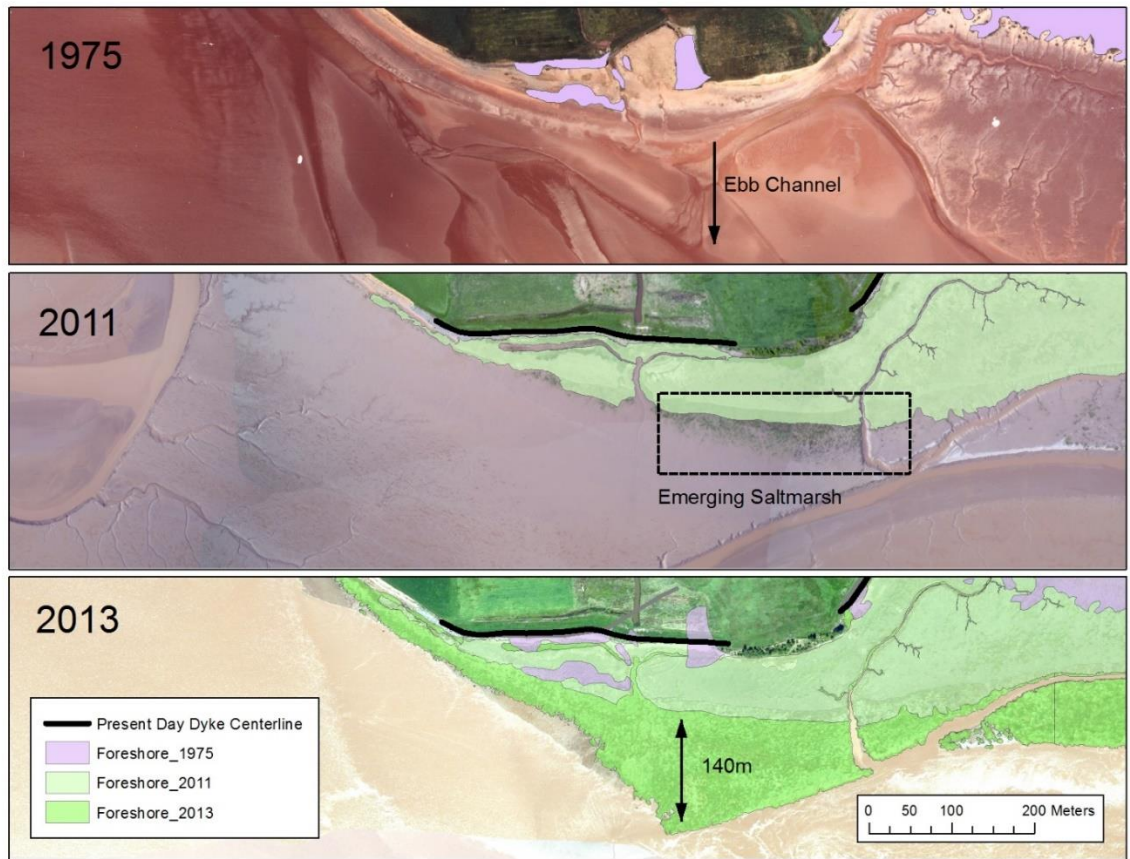


Figure 24: Extreme rates of progradation (>50m/yr) caused by the rapid colonization of an intertidal mudflat by *Spartina alterniflora*.

2.6 Conclusion

One of the primary ways healthy, robust saltmarshes enhance the resiliency of dykelands by mitigating or reducing incoming wave energy at the dyke (van Proosdij and Page, 2012; Vuik et al, 2016). Although there are many factors that determine the effectiveness of wave attenuation, the distance a wave travels over a saltmarsh is perhaps the most important (Sheppard et al, 2011; Vuik et al, 2016). By measuring end point change rates (EPR) along foreshore saltmarshes in front of dyke infrastructure, it is possible to qualify dykeland resiliency over time. Furthermore, if said changes can be linked to human implementations in the intertidal zone, inferences about their impacts on dykeland resiliency can be made as well. Overall, the saltmarsh EPR in the Cobequid Bay

Salmon River Estuary reflect trends found in saltmarshes outside of Atlantic Canada. Specifically, EPR trends show that saltmarshes are eroding in landscapes that are wave dominated and mixed (Montreuil and Bullard, 2012; McLaughlin et al, 2015). This is happening in the Cobequid Bay Salmon River Estuary despite an ample enough sediment supply to keep pace with sea level rise (SLR) (Kirwan et al, 2016). Much like the greater Minas Basin in which the Cobequid Bay Salmon River Estuary resides, erosional EPRs are increasing in response to SLR (Wilson et al, 2017). Rates have increased by nearly $0.5 \text{ m}\cdot\text{yr}^{-1}$ when comparing the time periods between 1970 – 2000, and 2000 to present. Dealing with an increase in foreshore saltmarsh erosion is a challenge in a landscape with a hardened backshore. While the dykes protect the upland from coastal flooding, they also prevent the saltmarshes to retreat in the face of accelerated rates of erosion (Wolters et al, 2005; Torio et al, 2013)

As this study focused on saltmarshes on the foreshore side of dykes, dykes and reclamation were inevitably found to have the largest impacts on saltmarshes in the Cobequid Bay Salmon River Estuary. Irrespective of foreshore changes, there has been a loss of over 1600ha of saltmarsh since 1938- mainly due to reclamation. Reclamation of saltmarsh habitat for agriculture and urban development has been the most significant cause of saltmarsh habitat loss, worldwide (Allen, 2000; van der Wal and Pye, 2004; van Proosdij and Page, 2012; Wang et al, 2013; Pye and Blott, 2014). If dykes and upland infrastructure were developed behind the natural extent of saltmarshes, they would be more resilient landscapes than they currently are. However, the reality of coastal communities and dykelands is different. Dykes were built in the intertidal zone and the land behind them was developed for a variety uses, reinforcing the necessity of the dyke infrastructure. As such, “grey” infrastructure is an important component of the green-grey

coastal defence systems (Sutton-Grier et al, 2015). Grey coastal protection structures are needed in high-energy systems where development has placed vital upland infrastructure or homes in reach of coastal storms. Although saltmarshes have the capacity to dissipate waves, they may not dissipate all wave energy during large storm events, especially those that occur during an over-marsh tide (Möller et al, 2014; Vuik et al, 2016).

Of all the structures and strategies examined in this thesis, kickers were found to be the only implementation that can actively increase dykeland resiliency. Kickers increase dykeland resiliency by promoting deposition at the foreshore edge of marshes that are colonized by saltmarsh habitat (Klingemann et al, 1984; van Proosdij and Matheson, 2015). In this study, kickers were found to precipitate saltmarsh progradation at a rate exceeding $2.5 \pm 0.1 \text{ m}\cdot\text{yr}^{-1}$. By increasing the width of the foreshore marsh, kickers effectively increase the capacity of the marsh to attenuate or mitigate wave interaction at the dyke infrastructure. Furthermore, despite promoting rapid sediment deposition, kickers do not interfere with the littoral movement of sediment to the extent foreshore rocking does (Schwimmer and Pizzuto, 2000). Hardening of shorelines can disrupt estuarine sediment transport, reducing sediment deposition in adjacent saltmarshes. Finally, scour created by kickers are limited to the immediate area upstream (which is minimized in tidal systems) and in the thalweg (Klingemann et al, 1984). Foreshore rocking was found to cause scour in the intertidal mudflat on either side of foreshore rocking as well as underneath (French, 2001; Bernatchez and Fraser, 2010). Kickers should be looked at as alternatives to foreshore rocking in low-to-medium energy areas where erosion has occurred due to channel movement. Apart from Klingemann et al (1984), who looked at how gabion groynes and spur dikes influenced deposition and scour in a flume laboratory, the literature on how these structures could be used in coastal

defence strategies, is scarce. The results from this study show that they could be a valuable method for creating saltmarsh habitat, decreasing flood risk, and enhancing dykeland resiliency.

Structures such as aboiteau, and strategies such as dredging and borrow pits can have impacts on the saltmarsh resiliency at the saltmarsh scale. Aboiteau are important structures for dykelands as they allow for upland drainage; however, dynamic aboiteau channels can cause unexpected rates of change at the foreshore edge. Furthermore, areas of the dyke adjacent to aboiteau channels are inherently more vulnerable to overtopping as there is no foreshore saltmarsh in these areas. Although dredging was cited as major contributor to sediment loss in other estuaries, (van der Wal and Pye, 2004; Blott et al, 2006; Wang et al, 2015), it did not impact foreshore width in the Cobequid Bay Salmon River Estuary due extreme suspended sediment concentrations and deposition rates in the fluvial zone where dredging was concentrated (Purcell, 2020). Furthermore, dredging is implemented for the purpose of expediting flood water away from nearby developed areas. As a result, it represents a very short-term increase in dykeland resiliency despite not being a viable long-term solution to flooding.

Ultimately, the Cobequid Bay Salmon River Estuary is mostly constrained by the presence of dyke infrastructure. This means there is a serious caveat to the concept of “natural variability” within this region. It is possible that the constraint placed on the estuary by the dyke infrastructure dampens natural channel migration. That being said, the largest drivers of EPR change in the Cobequid come from natural processes, particularly from the movement of tide and ebb channels. The dynamic movement of these channels resulted in some of the largest rates of erosion and progradation found in any saltmarsh, worldwide. Specifically, the 79 year mean of

$-6.5 \pm 0.1 \text{ m}\cdot\text{yr}^{-1}$, with a maximum erosion rate of $-26.5 \pm 0.9 \text{ m}\cdot\text{yr}^{-1}$, is a rate more comparable to the rapid rates of erosion found in arctic landscapes (Irrgang et al, 2018). Conversely, when ebb and tidal channels move away from the foreshore edge of saltmarshes, they can create conditions where significant deposition is possible. Saltmarsh progradation can happen rapidly when the elevation capital for saltmarsh growth is achieved. At NS040_05, this resulted in progradation rates as high as $77.3 \pm 2.0 \text{ m}\cdot\text{yr}^{-1}$ between 2011 and 2013, as the saltmarsh colonized the mudflat built by the changing ebb channel. However, it is important to reiterate that there was a latency between the developments of the mudflat and the progradation of the saltmarsh. Many of the observed changes in this study happen as a result of changes in the intertidal zone in front of the marsh, and are only observed in the foreshore saltmarsh once certain thresholds are passed (e.g. undercutting of foreshore cliff, accretion of mudflat) (Chauhan, 2009; Willemsen et al, 2018; Evans et al, 2019). Studies which endeavor to measure foreshore saltmarsh EPR should also examine changes in the intertidal zone in front of the marsh if inferences are to be made about future EPR trends and dykeland resiliency.

In order to enhance dykeland resiliency, dykeland managers should adapt to, and mitigate, the impacts of coastal flooding and erosion using a suite of coastal defence options. In the past, the focus in the Cobequid Bay Salmon River Estuary has been on implementing “grey” engineering solutions (Sherren et al, 2016). Protecting and promoting saltmarsh growth directly enhances dykeland resiliency, and in some instances, the resiliency of dykelands are contingent on healthy foreshore saltmarshes. Currently, saltmarshes are estimated to provide approximately \$400 million in ecosystem services annually, in Nova Scotia alone (Nova Scotia Wetlands Conversation Policy, 2019). This includes protection from coastal flooding and erosion, which Costanza et al (2008) valued

at US\$8236 ha·yr⁻¹ for reduced hurricane damages. Without the coastal protection, and other benefits (e.g. carbon sequestration, flood abatement) provided by saltmarshes the costs to keep dykelands safe from the hazards associated with climate change and SLR would be too great. As such, dykeland resilience is reliant on saltmarshes in the contemporary context of climate change. Therefore, understanding how human implementations in the intertidal zone affects the short and long-term evolution of foreshore saltmarsh is paramount if saltmarshes are to be considered an integral component of a green-grey hybrid coastal defence system (Sutton-Grier et al, 2015).

Chapter 3:

Application of unmanned aerial systems, structure-from-motion, and hydrodynamics to assess the sustainability of borrow pits for dykeland management.

3.1 Introduction

Climate change and an associated rise in sea level pose a significant threat to low-lying coastal areas worldwide (IPCC, 2014). Specifically, these areas face an exacerbation of coastal hazards such as flooding, erosion, saltwater intrusion and loss of habitat that could potentially put critical infrastructure and lives at risk (Nicholls and Cazenave, 2010). Perhaps the most commonly used method of coastal defence to protect low-lying areas from these hazards is the construction of dykes (i.e. dikes, levees, embankments). Historically, dykes were constructed to reclaim saltmarsh converting it to agricultural land. Currently, these dykes protect low-lying areas by acting as a physical barrier between the sea and the upland. A major concern for these low-lying areas (referred to dykelands hereon in) is that increases in sea level rise (SLR) and the impacts of these hazards require significant upgrades to dyke infrastructure if dykes are to provide adequate protection for the human activities in the historic floodplain. Improving dyke infrastructure not only requires the top of the dyke to be raised to keep water out but also requires a widening of the dyke footprint in order to accommodate the increased height, as well as armouring of the dyke itself if erosion is a major issue (van Proosdij and Page, 2012). The presence of a foreshore saltmarsh in front of a dyke can significantly reduce wave energies that reach it, effectively reducing the strain and maintenance costs (Möller and Spencer, 2002; Vuik et al, 2016). As a result, foreshore saltmarshes reduce the engineering requirements needed to keep pace with the increase in wave energy and the

frequency of large storm events precipitated by SLR (Vuik et al, 2016). In this context, saltmarshes are integral habitats in dykelands since dyke infrastructure improvements can constitute a major endeavor for coastal communities and often require a significant amount of money and raw material. In the Bay of Fundy, Nova Scotia, Canada, dyke builders have historically excavated swaths of in-situ saltmarsh seaward of the dyke, called borrow pits, for topping material to ease the financial and material costs. However, the question of whether this historic practice is sustainable in context of contemporary dykeland management has not been addressed.

The practice of excavating borrow pits can be traced back to the original Acadian dyke builders in the area during the 17th century (Bleakney, 2004). Before the mechanization of this process, dyke builders would excavate borrow pits with specialized dyking spades (Bleakney, 2004). Borrow pits provided early dyke builders with a renewable source of material, as the borrow pits would fill with sediment via the incoming tide over time. However, with SLR and expanding infrastructure behind the dykes, topping dykes require more material and bigger borrow pits. Today, borrow pits are dug using excavators and other heavy machinery. This practice sometimes provides 100% of the material requirements for dyke topping projects and dramatically reduces the overall costs compared to trucking in upland material. Since the costs associated with borrow pits can be 20% of the costs of importing upland sources, borrow pits allow dyke builders to "stretch their dollars", topping a greater length of dyke for reduced costs (D. Hingley, Aboiteau Superintendent, personal communication, April 30, 2018). In areas with high amounts of suspended sediment concentration these pits can infill within several years and be used again as a renewable source of material for future projects. Unfortunately, this practice can also lead to unwanted impacts on the integrity and

resilience of the saltmarsh by leaving large human-made tidal channels that can persist several decades (Burdick et al, 2019). Large borrow pits can negatively influence the morphodynamic processes which occur within, and adjacent to, the foreshore saltmarsh leading to erosion and/or slow infill rates within the borrow pits (Pye, 1995).

Furthermore, if local sediment dynamics and hydrology is not conducive to sedimentation, some borrow pits may never properly infill. If saltmarshes are to be used as a natural source of coastal protection that can augment the protection capacity of the dykes, then poorly functioning borrow pits can represent a negative influence to the overall resiliency of the dykeland – a topic relatively unexplored in the literature.

The primary objective of this chapter is to determine whether borrow pits recently excavated in the Bay of Fundy constitute a sustainable source of material for dyke topping, or will they remain unfilled and reduce the resiliency of the saltmarsh, and therefore, the dykeland behind them. To do this, several aerial surveys using unmanned aerial systems (UASs) were flown, producing high-quality orthomosaics and digital surface models (DSMs). Comparing DSMs in a geographical information system (GIS) allowed for an estimation of sedimentation rates (i.e. infill rates) in the borrow pits, which was used to estimate the long-term impact of the borrow pit on the saltmarsh. These infill rates were then compared to local hydrodynamic characteristics (e.g. SSC, water velocity) and borrow pit design to determine what factors contribute to the success and failure of borrow pits to infill. Finally, this chapter will explore the efficacy of UAS and structure from motion (SfM) software for performing volumetric analyses (including sediment budgets) in borrow pits. This will include a rigorous assessment of accuracy, identifying the minimal level of change detection, as well as recommendations for using UAS and SfM in intertidal areas such as creek networks, mudflats, or ditches.

3.1.1 Borrow Pits

As previously mentioned, borrow pits are excavated swaths of saltmarsh used as material for dyke building, topping, or maintenance (Figure 25). The impact borrow pits have on saltmarsh integrity is relatively unexplored in the literature. Only a few studies make mention of the impact of borrow pits on saltmarshes (Pye, 1995; Browne, 2017), with even fewer that have borrow pits as their primary focus (Browne, 2011). Regardless, all studies point out a direct indication that borrow pits lead to unwanted impacts on saltmarshes including increased rates of erosion (Pye, 1995; Browne, 2011). Specifically, Pye (1995) identified two different mechanisms associated with borrow pits that directly led to increased erosion within the saltmarsh. First, the integrity of the saltmarsh platform was compromised during the construction phase of the borrow pit (Pye, 1995). This was a result of the marsh platform being too low in the tidal frame, and perhaps too wet, to accommodate the machinery used in the excavation (Pye, 1995). In addition, the design was not properly implemented with the borrow pits being wider than necessary (i.e. more saltmarsh area lost or disturbed) (Pye, 1995). The second impact borrow pit construction had on saltmarsh erosion was that the borrow pits were tied into the pre-existing natural tidal creek network (Pye, 1995). This resulted in the natural creeks deepening and widening to accommodate the increase volume of water introduced by connecting them to the borrow pits (Pye, 1995). Finally, since borrow pits act as a sediment sink, there is less sediment available for accretion on the adjacent platform, as well as in natural tidal creeks and on other nearby marshes (Browne, 2011). Mitigating the undesirable morphodynamic responses of a saltmarsh to borrow pit implementation requires a careful consideration of the local hydrodynamic environment and how the design of the borrow pit will interact with, and influence, saltmarsh morphodynamics.

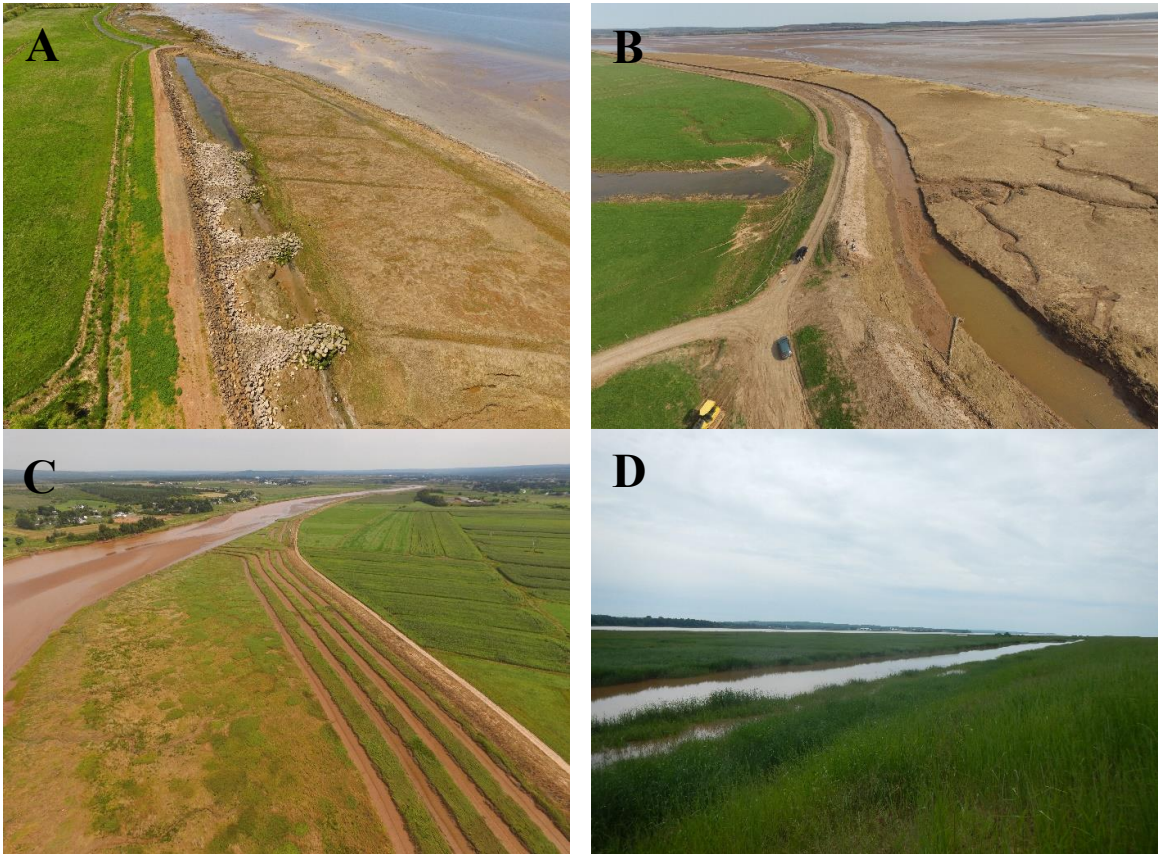


Figure 25: Aerial photographs of borrow pits. A) A borrow pit and dyke supported by a rock apron. B) A long borrow pit excavated near Masstown, Nova Scotia. C) A parallel borrow pit configuration excavated near Truro, Nova Scotia. D) A borrow pit inundated at high tide near Onslow, Nova Scotia.

Borrow pit design requires a consideration of the pre-existing nearshore and saltmarsh sediment dynamics, as well as a physical design that helps promote sediment deposition. In the Bay of Fundy, borrow pits are excavated parallel to dykes that require topping to meet a critical protection elevation (van Proosdij et al, 2013). Borrow pit dimensions are based primarily on the size and capabilities of the equipment being used for excavation (D. Hingley, personal communication, April 30, 2018). In other words, the reach of the excavator arm defines the width of the borrow pit (D. Hingley, and C. Esau, Engineer, personal communication, April 30, 2018) (Figure 26). Historically, this reach

was approximately 5m (smaller when excavated by dyke spade) but now borrow pits can reach 8-10m in width (D. Hingley, personal communication, April 30, 2018). Dykes are excavated to a depth of approximately 1.5m (5ft) so that the borrow pit will not slump, and for construction safety reasons (D. Hingley, personal communication, April 30, 2018). Before a borrow pit is excavated, the top 8" - 12" will be removed (i.e. grubbed) and discarded so that organics are not used as topping material (C. Esau, personal communication, April 20, 2018). Saltmarshes are typically drained months beforehand by excavating a small drainage ditch that extends to the foreshore edge. This is done to eliminate any areas where water can pond and allow for the platform and materials to consolidate – therefore, improving construction and decreasing the amount of damage to the saltmarsh by the construction equipment (D. Hingley and C. Esau, personal communication, April 30, 2018). In the end, these drainage outlets usually constitute the borrow pit outlet, which is the artificial channel that water enters and leaves the borrow pit. The number, size and orientation of the outlet channel is not a consideration in the borrow pit design, although anecdotal observations in the Bay of Fundy suggest that it should be, and efforts are being made to improve the design processes. Ultimately, the design of the borrow pit and the pre-existing hydrodynamic characteristics of the saltmarsh determine the capacity of borrow pits to infill sustainably.



Figure 26: Borrow pit excavation using a long-reach excavator. Photo credit - Carl Esau, NSDA, winter 2015.

Despite the scarcity of borrow pit studies that explore the impact of human-made tidal creeks and ditches on saltmarsh functioning provide a suitable analog (Vincent et al, 2013; Pieterse et al, 2017). According to Elsey-Quirk and Adamowicz (2016), over 90% of saltmarshes along the Northeastern Atlantic coast of the US are ditched. In the Bay of Fundy, restored saltmarshes still have relict ditches that are integrated into their drainage networks. However, the largest ditching artifacts are those created by borrow pit excavation (MacDonald et al, 2010). Ditching saltmarshes is a practice that dates back centuries and serves a variety of purposes from mosquito control, improving drainage of the marsh surface, the creation of bird habitat, and for re-introducing appropriate hydrology to restored saltmarshes (Wallace et al, 2005; Corman et al, 2012; Pieterse et al, 2017). The impacts of ditching a saltmarsh are variable. Implementing ditches into a saltmarsh can dramatically alter the drainage patterns on the marsh platform (Redfield,

1972). This can ultimately lead to the marsh being overly drained, leading to increased sedimentation in the constructed ditches, and a reduction of the saltmarsh's natural drainage system (Redfield, 1972). When these ditches become plugged they can unintentionally create shallow pools, or pannes, which have the potential to increase salinity, ammonia concentration, and the potential for methane creation (Elsley-Quirk and Adamowicz, 2015; Skinner, 2016). This, along with lowering bulk density and root-collapse, can negatively impact the success of vegetation on the marsh, decreasing the saltmarsh's integrity (Vincent et al, 2013; Skinner, 2016). Furthermore, ditches tend to erode saltmarshes at the peat level (unlike tidal creeks), which combined with the impacts of ditching, can lead to a lowering of the marsh platform (Burdick et al, 2019). If the lowering of the marsh platform from ditching impacts its ability to keep pace with SLR, then the ditches ultimately impact the resiliency of these saltmarsh and its usefulness as a source of coastal protection. It should be mentioned that the majority of the above studies were in micro and mesotidal marshes. The impacts of ditching on macro or hypertidal marshes has not been thoroughly explored. However, MacDonald et al, 2010 showed that in sediment-rich, hypertidal estuaries, relict ditches can sometimes infill, which can cut off areas of the marsh from the drainage networks, creating pannes. Skinner (2016) examined the impact of pannes on the biogeochemistry of saltmarshes in the Bay of Fundy and found that they reduce vegetation growth success and minimize rates of vertical platform change where present. Apart from the impact ditches or borrow pits have on saltmarshes, it is also important to understand how hydrodynamics in a human-made channel compare to those in natural systems.

A recent study by Pieterse et al (2017) examined erosion and deposition occurring on the bed of human-made ditches throughout the tidal cycle over a three-week period. Pieterse et al (2017) found that bed erosion occurred primarily during the flood tide, coinciding with the largest peaks in suspended sediment concentration (SSC). Bed accretion occurred primarily the ebb tide, while a secondary spike in SSC was also observed during the end of the ebb tide (Pieterse et al, 2017). Of interest, bed erosion and peak SSC did not occur simultaneously with peak sheer stress (Pieterse et al, 2017). These patterns were linked to the presence of a “fluffy” layer of sediment, which was easily re-suspended during the accelerating flood tide, leaving a more consolidated layer of sediment exposed during peak sheer stress (Pieterse et al, 2017). Ultimately, Pieterse et al (2017) conclude that both hydrodynamics and bed level changes in these human-made ditches resembled those of natural origin. Furthermore, they suggest that because of these similarities that how a channel is formed may not influence their evolution in the longer-term (Pieterse et al, 2017). A final point of interest was that the ditches that were further inland accreted (0.02-0.03m) over the course of the study, while those closer to the channel tended to erode (-0.01m). However, no insight is given as to how these rates translate to yearly changes in bed elevation (Pieterse et al, 2017). Corman et al (2012) measured mean sedimentation rates in mosquito ditches found on a New York saltmarsh to be $0.52\text{cm}\cdot\text{yr}^{-1}$. When examining rates of infill, Corman et al (2012) indicate the importance of comparing ditch sedimentation to marsh surface accretion. If the marsh is accreting at a rate faster than the ditches, then the ditches will never fully infill (Corman et al, 2012). This is an important factor overlooked in this study; however, it is known that borrow pits accrete at a rate much faster than the saltmarsh platform. This is likely related to flocculation rates that occur in hypertidal, high SSC creeks and will be

discussed below. A fundamental difference between the ditches examined in these papers and the borrow pits examined in this thesis is that borrow pits are typically much larger in both area and volume than these ditches. Furthermore, the borrow pits examined in this study exist in a hypertidal environment with much larger SSCs. It may be pertinent to investigate the long-term evolution of man-made ditches, or borrow pits, in an array of hydrodynamic conditions.

3.1.2 Sediment Dynamics

The study of sediment dynamics and ecomorphological feedbacks in tidal creeks and on saltmarsh platforms is paramount in understanding the future morphological evolution of the saltmarsh, itself (Poirier et al, 2017). These types of studies are particularly important if saltmarshes are considered as a source of coastal protection since current creek and marsh function is an indicator of how the marsh will fare in response to SLR (Cahoon, 2015; Kirwan et al, 2016). Specifically, the study of sediment dynamics can reveal whether a marsh is in an erosional state or a depositional state, and at what rate the marsh platform and creeks adjust to the changes in the drivers that control their evolution. As such, these studies require empirical measurements of sediment dynamics as well as topographic measurements to quantify any morphological changes that are taking place (Christiansen et al, 2000, van Proosdij et al, 2006, Poirier et al, 2017). In the context of borrow pits, it is vital that the hydrodynamic processes that govern the morphological adjustments within the borrow pits result in deposition, or infill (Dyer et al, 2000). For dykeland managers, understanding deposition (i.e. infill rates) can be a valuable tool for estimating when (or if) the borrow pits will refill if they are to be reused as material for future dyke topping projects.

Infill rates in borrow pits are contingent on creating an environment that is conducive to sediment deposition. Sediment deposition relies on the interaction of sediments, hydrology, vegetation, and topography, but is ultimately the product of the availability of sediment in the system and the opportunity for that sediment to settle (Reed, 1989; van Proosdij et al, 2006). In the context of borrow pits, availability includes suspended sediment concentration (Christiansen et al, 2000; Temmerman et al, 2004; Poirier et al, 2017), grain size, flocculation (Krank, 1981; Voulgaris and Meyers, 2004; O'Laughlin et al, 2014), and weather conditions. Opportunity factors that influence deposition in borrow pits include, flow velocity, turbulence, and presence of vegetation (Yang et al, 2008). A recent study by Poirier et al (2017) showed that SSC and flocculation play a very important role in sedimentation in hypertidal creek networks in the Bay of Fundy. Specifically, in marshes with high SSC and grain sizes less than 64 μ m, sediment will flocculate and settle very rapidly on the flood tide (Poirier et al, 2017). Since the ebb tide is typically not fast enough to re-suspend these aggregate sediments, these tidal creeks will accrete until a large event occurs with enough energy to erode the bed material (Pieterse et al, 2017). As a result, only a proportionally small amount of sediment that enters the creek is deposited on the marsh platform (Poirier et al, 2017). If these processes interact in a similar manner inside borrow pits, then the borrow pits should be primarily depositional. However, since borrow pits were not created by natural processes, it is unknown whether the same patterns of deposition occur within them since the hydrological conditions controlled by their design impact their morphological adjustment differently than natural systems.

Another component of sedimentation in borrow pits is that sediment deposition is seasonally variable (Poirier 2014, Poirier et al 2017). Poirier et al (2017) found that a

hypertidal marsh had higher deposition rates during the winter and spring months when SSC was higher due to higher tides, storminess and freshets. SSC is typically lower in tidal creeks and on the platform during over marsh tides in the calmer drier summer months (Poirier et al, 2017). This is especially important to note because the season in which measurements take place can ultimately impact the interpretation of the analysis if variability is not considered. When comparing two sets of measurements it is paramount to interpret the volumetric change (or infill rates) in the context of seasonality. The last aspect of sedimentation to consider is that sediment dynamics in borrow pits are directly influenced by the design of the pit, as design parameters (e.g. channel geometry) have a direct influence on both the availability of sediment in the pit and the opportunity for it to settle.

3.1.3 Unmanned Aerial Systems and Structure-from-Motion

Monitoring landscape change in the geosciences has long been reliant on creating accurate digital elevation models (DEMs) (Lane et al, 2003; Milan et al, 2011; Carrivick et al, 2015). Traditionally, DEMs would be created using 3D points obtained through in-situ surveying methods such as the total station (TS) or RTK-GPS (Fuller et al, 2003; Wheaton et al, 2010). Although accurate, these techniques are both time consuming and result in low DEM resolutions (i.e. $>1 - 5$ points per m^2 depending on study area) (Smith et al, 2016). More recently, airborne Light Detection and Ranging (LiDAR) and Terrestrial Laser Scanner (TLS) (i.e. Terrestrial LiDAR) have provided researchers with both accurate and high resolution DEMs that can be obtained remotely (Milan et al, 2007; Devereux and Amable, 2009; Cavalli et al, 2017). However, these techniques can be cost-prohibitive which can reduce the return frequency of successive surveys. Improvements

in UAS and SfM-MVS technology have potentially ushered in a new paradigm in monitoring landscapes by allowing geoscientists to obtain accurate, high resolution DSMs at a considerably lower cost to most alternatives (Smith et al, 2016; Kalacska et al, 2017). For an overview of the pros and cons of the various DEM creation techniques see Smith et al (2016) or Carrivick et al (2016).

“Structure from Motion as applied in the geosciences is not so much a single technique as a workflow employing multiple algorithms developed from three-dimensional computer vision, traditional photogrammetry, and more conventional survey techniques” (Carrivick et al, 2016, pg. 37). SfM software (e.g. Pix4D, AgiSoft Photoscan) employ feature detection algorithms, such as SIFT (Lowe, 2004) or LDAHash (Strecha et al, 2011) that identify common keypoints across a set of 2D images, which can be obtained via a UAS or any conventional camera (Carrivick et al, 2015; Smith et al, 2016). These key points are then used to match the images together using various keypoint correspondence and filtering algorithms (Carrivick et al, 2015; Smith et al, 2016). SfM algorithms then perform a bundle adjustment to reconstruct the 3D geometry captured in the 2D images using additional algorithms to estimate the pose, position and orientation of the camera (Carrivick et al, 2015). Ground control points obtained through surveying techniques (e.g. RTK-GPS, Total Station) are then used to georeference the 3D structure to real-world coordinates. The final step in the SfM workflow is the Multi-View Stereo (MVS) portion, which is used to further densify the point cloud (Carrivick et al, 2015). Carrivick et al (2015) and Smith et al (2016) both provide good general overviews of the SfM-MVS workflow for the nonprofessional user. For a more detailed description and a more in depth overview of the algorithms associated with SfM-MVS see Snavely (2008).

Recently, there has been a proliferation of studies using UASs and SfM-MVS to monitor change in a large variety of landscapes, including: urban areas (Unger et al, 2014), mine sites (Haas et al, 2016; Xiang et al, 2018), beach dunes (Mancini et al, 2013), glaciers (Gindraux et al, 2017), river systems (Bakker and Lane, 2017; Cook, 2017), badlands (Smith and Vericat, 2015), coastal areas (Goncalves and Henriques, 2015; Turner et al, 2016), and coral reefs (Murfitt et al, 2017). Saltmarsh landscapes (Kalacska et al, 2017) have been relatively unexplored in the UAS and SfM-MVS literature including their tidal creek networks and adjacent mudflats (Jaud et al, 2016; Dale et al, 2018). Kalacska et al (2017) showed that the application of UAS and SfM-MVS could produce high quality DEMs of saltmarsh platforms and their associated tidal network if flown before the re-emergence of vegetation. In that study, they found that the accuracy of these DEMs could potentially exceed the accuracy of LiDAR DEMs. Jaud et al (2016) found that UAS and SfM could create DEMs on intertidal mudflats suitable for analyzing sedimentary hydrodynamics and sediment budgets at various scales. However, Jaud et al (2016) also had a few concerns associated with SfM produced DEMs in intertidal mudflat environments, which will be discussed later. To date, there have been no studies which utilize UAS and SfM-MVS to measure deposition, or infill rates, in tidal creek networks. Typically, studies of deposition in tidal creeks require the use of an RTK-GPS or a TLS. Furthermore, in-situ measurements require the researcher to enter the tidal creek, which can influence the hydrodynamic processes in the creek.

Of the studies mentioned above, not all utilize UAS and SfM-MVS to measure volumetric changes in the landscape. Many of these studies focus on vertical change (i.e. erosion and deposition) only (Cook, 2017). Areas of erosion and deposition are calculated by subtracting two DEMs or Digital Surface Models (DSMs) in a Geographic Information

System (GIS), creating a DEM of difference (DoD) (Lane et al, 2003). Mapping erosion and deposition using these techniques allows researchers to understand the geomorphic processes that occur in the landscape by studying the patterns of change using DoDs. These studies are augmented by the use of level of detection (LoD) analysis, which help quantify significant change based on the accuracy of the DEMs produced and the level of significance required (Wheaton et al, 2010; Hugenholtz et al, 2013). LoD can also be used to refine volumetric change analyses by applying the same methods to the DoD.

Haas et al (2016) utilized LoD to compare changes between two DEMs in an iron ore mine. Using UAS and SfM-MVS Haas et al (2016), were able to quantify the volumetric change within the mine and identify areas of erosion and deposition. Furthermore, UAV and SfM-MVS allowed them to identify certain geomorphic processes, such as the formation of gullies (Haas et al, 2016). This is a major benefit to using UAS and SfM-MVS. Gillan et al (2017) also concluded that these technologies allow for an unprecedented synoptic understanding of erosion and deposition that occurs within the study area. A drawback to this analysis is that the accuracy of the DEMs produced by UAS and SfM-MVS were lower than TLS, and therefore, much of the data was excluded when the LoD was applied (Haas et al, 2016; Xiang et al, 2018). However, it should be noted that using DoD without the added step of LoD can be used to perform volumetric analyses. In fact, Lane et al (2003) recommends using all the cells available in a DoD to calculate a volumetric change. This method was used by Juad et al (2016) to create a short-term sediment budget on intertidal mudflats. The advantages of LoD is the high level of scrutiny applied to the accuracy of the DEMs, which helps the researcher avoid propagating volumetric changes that occur from changes outside the LoD (Hugenholtz et al, 2016; Cavelli et al, 2017). However, LoD can also hinder the analysis

by discarding all the small changes that may have occurred within the landscape that can be confirmed qualitatively or by additional measurements (Lane et al, 2003). As changes that occur within the borrow pits are suspected to be considerably small compared to most landscapes, both methods are applied and compared in this paper to help strengthen the analysis and infer conclusions.

3.2 Study Area

The Cobequid Bay – Salmon River Estuary is in the northeastern portion of the Bay of Fundy, in Nova Scotia, Canada (Figure 27 and 28). It is a hypertidal semi-diurnal estuary, with a tidal range exceeding 16m (Desplanque and Mossman, 2004). The Cobequid Bay – Salmon River Estuary is fetch-limited, protected from winds coming in from the Bay of Fundy by Cape Split and a cliff formation near Economy, NS. In the winter, ephemeral ice is present throughout the system. The primary fluvial contributions of the estuary come from the Salmon, Shubenacadie, and North Rivers, the Salmon River being the dominant source of freshwater flow. Finally, the sediment in the Cobequid Bay – Salmon River Estuary consists primarily of coarse and very coarse silt in the outer and mid-estuary (samples taken in May and September) (CBCL, 2015). The inner estuary consists predominantly of fine to medium gravel in the North River, and the Salmon River consists of medium gravel during the spring but shifts to medium silt by the fall (van Proosdij et al., 2014). The mid-estuary typically consists of fine sand (Crewe et al, 2004). Suspended sediment concentrations can exceed $250\text{g}\cdot\text{L}^{-1}$ near the turbidity maximum, and typically decrease moving to the mid and outer-estuary (Crewe et al, 2004; Purcell, 2020). In tidal channels and human-made saltmarsh creeks (i.e. borrow pits) suspended sediment concentrations range from $0.5\text{g}\cdot\text{L}^{-1}$ up to $>100\text{g}\cdot\text{L}^{-1}$, with the

greatest concentrations found near the turbidity maximum. The hypertidal tides in the Cobequid Bay Salmon River Estuary constitute the primary mechanism of net sediment transport (Dalrymple et al, 2012).

Current relative sea level rise projections (RCP 8.5) for Yarmouth, the closest station to the Annapolis Basin, and Truro, in the Cobequid Bay are 0.493m - 1.262m and 0.541m – 1.271m, for 2100, respectively (James et al, 2014). As a result, many dykes in the Bay of Fundy are at risk from overtopping (van Proosdij et al, 2018). With approximately 241km of dyke infrastructure in the province of Nova Scotia, topping dykes to meet 2050 SLR standards is a significant challenge. Borrow pits allow the Nova Scotia Department of Agriculture to top dykes for minimal costs. Although this practice dates back to Acadian dyke builders in the 17th Century, current borrow pits are excavated using large excavators and equipment (Bleakney, 2004). In this study there were five main borrow pit sites containing 13 borrow pits (Table 6 and 7): Masstown West (MTW), Masstown East (MTE), 3) Victoria Diamond Jubilee (VDJ), Lower Truro (LT), and Ryerson – Dugau (RD). These sites were chosen because they all had borrow pits that were excavated within the last 5 years. Furthermore, these borrow pits vary in their design and in their local hydrodynamic environments (Table 1 and Table 2). The borrow pits in this study were designed and constructed by the NSDA.

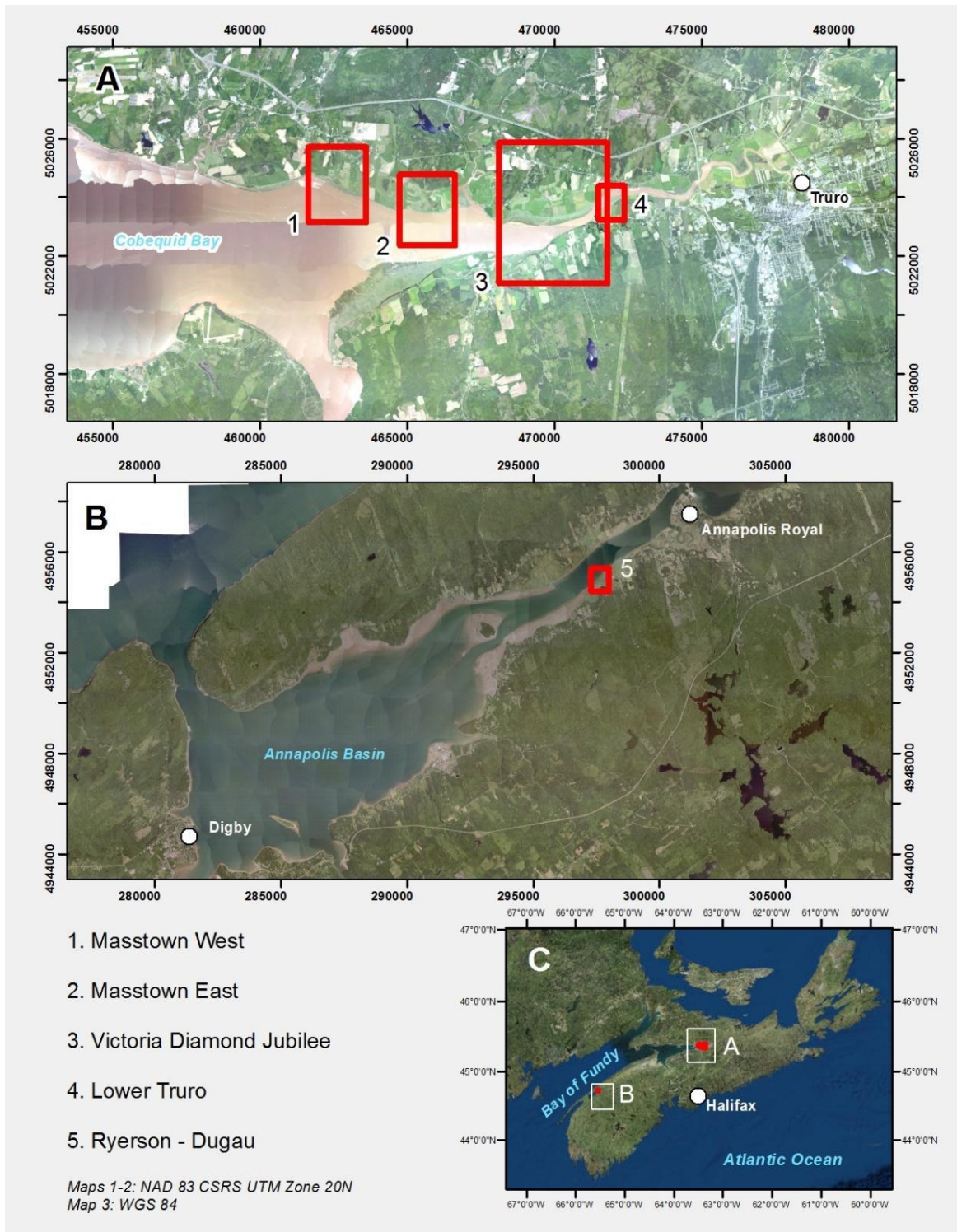


Figure 27: Study area map showing the locations of marshes with newly excavated borrow pits examined in this thesis. Masstown West, Masstown East, VDJ, and Lower Truro are all located in the Cobequid Bay Salmon River Estuary while Ryerson-Dugau is located in the lower Bay of Fundy in the Annapolis Basin.



Figure 28: Borrow pits at A) Masstown West, B) Masstown East, C) Ryerson-Dugau, D) VDJ, and E) Lower Truro marshes.

Table 6: Borrow pits on each marsh and the year they were constructed.

Site	Borrow Pit	Year Constructed
Masstown West (NS023w)	MTW_01	2016
	MTW_02	
Masstown East (NS023e)	MTE_03	2016
	MTE_04	
	MTE_05	
Victoria Diamond Jubilee (VDJ) (NS012)	VDJ_01	2016
	VDJ_02	
	VDJ_03	
Lower Truro (NS081)	LT_01	2015
	LT_02	
	LT_03	
	LT_04	
Ryerson- Dugau (NS005)	RD_01	2013

Table 7: General hydrodynamic characteristics of each marsh.

Site	Mean Platform Height (m CGVD2013)	As-built Borrow Pit Bottom Elevation (m CGVD2013)	SSC relative to Bay of Fundy.	Dominant estuarine Process zone	State of Foreshore Marsh
Masstown West	7.634m	6.085m	Moderate	Mixed-to-tidal	Historically eroding, currently eroding
Masstown East	7.729m	6.039m	Moderate	Mixed-to-tidal	Historically eroding, currently prograding
VDJ	7.829m	6.379m	Very high	Mixed	Historically prograding, currently prograding
Lower Truro	8.025m	N/A	High	Mixed-to-fluvial	Historically dynamic, currently prograding
Ryerson- Dugau	3.308m	N/A	Low	Mixed	Historically eroding, currently eroding.

3.3 Methods and Materials

Fieldwork was carried out in 2016 and 2017 between the months of May and November. The fieldwork in this paper can be split into two parts: 1) Change detection (i.e. DSMs of Difference and volumetric change) in the borrow pits using an Unmanned Aerial System (UAS) and Structure-from-Motion (SfM); and 2) empirical field measurements of hydrodynamics, including: suspended sediment concentrations, water levels, and water velocity in the borrow pits.

3.3.1 Change Detection using UAS-SfM

In order to determine infill rates and volumetric change in the borrow pits, 16 aerial surveys were performed over the five marshes between November 2015 and September 2017. Every marsh was surveyed twice except for Masstown East and Masstown West marshes which were surveyed 4 times each (Table 8).

Table 8: Dates each marsh was surveyed with a UAS.

Site	Dates surveyed
Masstown (East and West)	November 2015, May 2016, August 2016, August 2017
VDJ	November 2016, August 2017
Lower Truro	August 2016, September 2017
Ryerson – Dugau	May 2017, September 2017

Before each flight, a ground control point (GCP) network was designed to ensure optimal georeferencing results in the Structure-from-Motion (SfM) workflow (Figure 29). GCP networks were designed following the evolving recommendations found in the literature focusing on using UASs and SfM for change detection in various landscapes (Tonkin and Midgely, 2016; Raczynski, 2017). Ultimately, each GCP network contained a minimum of 4 GCPs for georeferencing (actual range 5 – 22), with the remaining used as check points for the accuracy of the georectification when available (Tonkin and Midgely, 2016). Furthermore, GCPs were well distributed and were designed to contain the area of interests (e.g. borrow pits) (Tonkin and Midgely, 2016; Raczynski, 2017). The Buffer tool was used to ensure the areas of interest were within 200m of a GCP when possible. Finally, the extent of the flights went well past the areas of interest to keep them away from the edges of the DSM where doming and bowling artefacts can negatively influence the DSM accuracy (James and Robson, 2014). Figure 29 shows the GCP network for

NS005 Ryerson – Dugau, which was the last, and most optimal, GCP network created during this thesis.

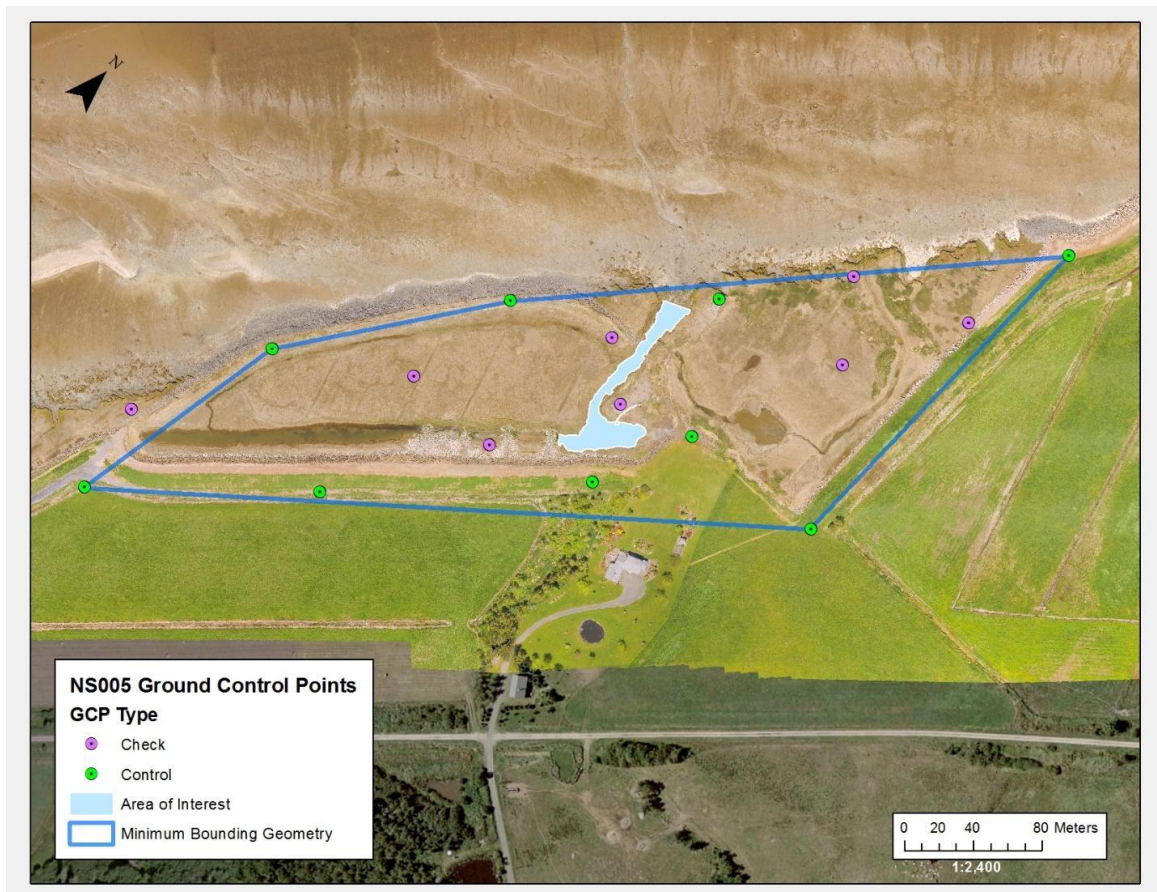


Figure 29: Idealized GCP network at Ryerson-Dugau Marsh. GCPs surround the study area and are evenly distributed throughout the site.

GCPs were installed and then surveyed using a Leica Geosystems GS14 dual-frequency GNSS receiver (Figure 30). The GNSS receiver received RTK corrections via the Leica SmartNet Network Correction Service over the TELUS cellular telephone network. The reported horizontal and vertical accuracies for the GS14 are 8mm and 15mm, respectively (Leica, 2016). However, an approximate accuracy for each collected point was provided by the corrections service. The actual approximate accuracies ranged from 5– 10mm horizontally, and 8–13mm vertically. The GCPs were surveyed in the NAD83 CSRS

UTM Zone 20N Epoch 2010 coordinate system. During this project, the standards of practice set by the Association of Nova Scotia Land Survey switched from using the CGVD28 vertical datum to the CGVD2013 (Acker et al, 2016). However, only the Masstown East and Masstown West marshes were surveyed using the CGVD28 datum (November 2015 and May 2016). These coordinates were converted to CGVD2013 using GPS H 3.3 software.



Figure 30: General method for installing GCPs.

The unmanned aerial vehicle (UAV) used in the aerial surveys was a DJI Phantom 3 Professional controlled using the Pix4D Capture App (Table 9). Every survey was flown at an approximate altitude of 90m above the study site at a speed of approximately 9 – 10m·s⁻¹. Sidelap and frontlap were set to 80% and 60%, respectively, and all pictures used

in the SfM software were nadir facing. The resulting pixel size of the imagery was approximately 4cm (3.7 - 3.9cm). Oblique imagery was obtained for supplementary qualitative analysis.

Table 9: Specifications for the DJI Phantom 3 Professional (dji.com, 2018).

DJI Phantom 3 Professional	Specifications
Weight	1280g
Size	350mm (diagonally)
Max Speed	16m·s ⁻¹
Satellite Positioning System	GPS/GLONASS
Battery	4480mAh LiPo 4s
Flight Time	~20min
Camera	1/2.3" CMOS Pixels: 12.4M
Lens	FOV 94° 20 mm (35 mm format equivalent) f/2.8 focus at ∞
Shutter Speed	8 - 1/8000 s

Once the images were obtained, they were exported to Pix4D in order to create the DSMs and orthomosaics. Pix4D is a structure-from-motion software program that utilizes a variation of the SfM- MVS workflow described above (Carrivick et al, 2016; pix4d.com, 2020). After some initial testing, it was decided to use the default settings in the Initial Settings, the Point Cloud and Mesh creation and the DSM and orthomosaic creation steps. However, the linear rolling shutter model was applied to the camera model because of the high speeds in which the flights were flown (9 – 10m·s⁻¹), which substantially reduced the average error in the borrow pits (Vautherin et al 2016; Raczynski, 2017). The accuracy reported by the RTK associated with measurement on the GCP was used as the value in the Horizontal and Vertical Accuracy columns in the GCP Manager. Once the DSMs and orthomosaics were created in Pix4D, they were exported to ArcGIS 10.5 for further analysis.

The first step in the volumetric and change analysis was to extract the borrow pits from the DSM. This isolated the analysis to just the parts of the DSM that constituted the borrow pits so that results were not influenced by changes outside the pits. This also significantly reduced processing time and storage requirements. Extraction was done by digitizing the outside edge of the borrow pit using the orthomosaic and the DSM for reference. This method is more accurate than traditional edge delineation using RTK-GPS or a Total Station due to the high resolution of the imagery. The digitized borrow pit polygon was then used as a mask in the *Extract by Mask* tool to clip the borrow pit away from the DSM.

In order to get an accurate estimate of volumetric change of the borrow pit and sediment budget, it was paramount to remove any parts of the borrow pit DSM that negatively influenced the accuracy of the analysis (Haas et al, 2016). Specifically, this meant removing the noise and the vegetation from the DSM. Noise can occur in the DSM when there is not an adequate number of keypoints to perform a quality bundle adjustment. This can result in large deviations in elevations within a small area, which are easily identifiable in the DSM. Vegetation impacts the quality of the analysis because the DSM does not penetrate through it, giving an over-estimation of the surface elevation. Several different methodologies were tested, including converting the LAS files to multipoints, erasing the erroneous points, and re-interpolating the DSM. Ultimately, it was decided to simply erase the noise from the DSMs and only use/compare the parts that were suitable for analysis. To do this, error masks were digitized using a combination of the DSMs, orthomosaics and LAS points symbolized to show points that were two standard deviations away from the local bed elevation. These error masks were then erased from the DSM. The *Intersect* and *Raster Calculator* tools were then used to only

include the common areas of each DSM that were suitable for analysis. Once suitable borrow pit DSMs were created, the volumetric change/infill rates between successive flights were calculated.

The volumetric change analysis was split into two parts: 1) calculating the change of the volume of the borrow pit, and 2) calculate the change of sediment entering and leaving the pits for the infill rate analyses. The volumetric change of the borrow pit was calculated in order to compare the values to the original as-built volume of the pit. Furthermore, the volume of the borrow pit can be used to calculate its tidal prism, and therefore, apply hydraulic geometry equations to anticipate whether the outlet channels will adjust. The sediment budget values were used to determine infill rates in $\text{m}\cdot\text{yr}^{-1}$

Volumetric Change

The volumetric change of each borrow pit was calculated the *Surface Volume* tool in ArcMap 10.5. The Surface Volume tool calculates a volume between a surface and a reference plane (Figure 31) (ESRI, 2018). The surfaces used were the edited DSMs described above, while the reference plane was calculated as the mean of "top of pit" shots measured with an RTK-GPS during the as-built survey. This method allows the bankfull elevation of the borrow pit to constitute the reference plane and allows for comparisons between two DSMs despite whatever dimensional changes occur (e.g. borrow pits become wider due to bank scour). Calculating the volume of the pit allows for the direct comparison of the as-built volume of the borrow pit.

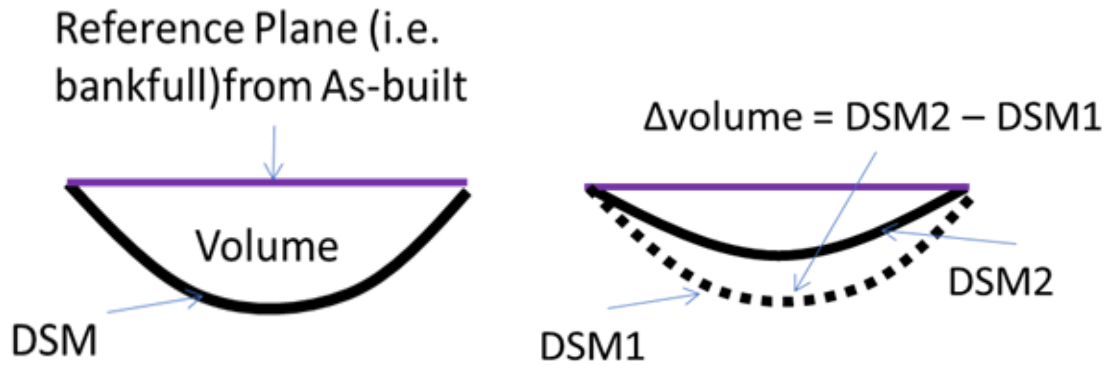


Figure 31: Generalized diagram of how the Surface Volume tool in ArcMap10.5 was used to determine volumetric change (ESRI, 2018).

Infill Rates and Sediment Budgets

In order to measure the amount of sediment that deposited, or eroded from, the borrow pit between two DSMs, a series of calculations were made using the *Raster Calculator* Tool. This method allows for the measurement of volumetric change without the use of a reference plane. Of the two methods, this methodology is more widely used in the UAS/DoD literature (Gómez-Gutiérrez et al, 2014; Turner et al, 2015). Essentially, the *Raster Calculator* is used to determine the change in elevation between two pixels, which is then multiplied by the area of a pixel to generate a raster that shows the volumetric change of each pixel. The *Zonal Statistics* tool is then used to summate the value of all the pixels of cell size c in the volumetric change raster to determine the overall volumetric change of the borrow pit.

Equation 5: Volumetric Change in sediment between two DSMs.

$$\sum [(DSM_{new} - DSM_{old}) c^2]$$

Finally, infill, or accretion rates, were determined by dividing the net volumetric change and normalizing the rates by dividing by borrow pit area and time. This allowed

rates of change to be compared between borrow pits regardless of their size and the time between flights in which measurements were taken.

DSM Accuracy Validation

One of the primary challenges with reporting volumetric change is reporting the level of uncertainty associated with said change. This paper examines two methods for reporting and quantifying volumetric uncertainty. The first method applies volumetric uncertainty equations based off work presented in Lane et al 2003, and Taylor 1997. Both equations utilize the accuracy of the DSMs, and the number and size of pixels to determine volumetric uncertainty. Lane et al 2003 add the errors in the DSM in quadrature under the assumption that errors form a Gaussian distribution, while Taylor 1997 does not, and is therefore considered the maximum possible error. The second method uses the level of detection method to determine “real” changes where volumetric change is based off 1 and 2 sigma probabilities. Accurate uncertainty reporting is paramount in interpreting the amount of volumetric change presented, but also in understanding the accuracy of the methodology used to determine change.

Determining which equation to apply to obtain the uncertainty in volumetric change between two DSMs requires some decisions to be made based on the nature of the error in the measurements. Chief amongst these is whether to assume that the errors in the DSMs are pairwise uncorrelated (i.e. random), or if the errors are spatially correlated (Taylor, 1997; Lane et al, 2003; Haas et al, 2016). This paper uses both to explore the possible range of error in the DSMs (Taylor, 1997; Lane et al, 2003; Haas et al. 2016; Xiang et al, 2018). In both methods, the error of each DSM can be reported as a standard deviation or $RSME_z$, which can be obtained from two primary methods: one, the stable area approach, which compares the variation between the two DSMs in areas that have

not changed over time (Westaway et al, 2000). The second approach involves using check points from an alternative source of measurement (e.g. RTK-GPS, TLS) and comparing measured values with those in the DSMs (Smith and Vericat, 2015). The values are then reported as a root mean square error value ($RMSE_Z$) of the vertical component of the DSMs. This paper primarily uses the latter method since there are little, to no, stable errors in the greater saltmarsh DSMs or the clipped borrow pit DSMs, as mentioned previously. However, the stable area approach was tested and used for NS081 Lower Truro, which had a hard, stable road adjacent to the marsh. For the second method, an RTK-GPS was used to measure areas of bare earth in the DSMs and the orthometric height was compared to the value in the DSMs using the *Extract Multi Values to Points* tool in ArcMap 10.5. This tool assigns each point (i.e. RTK-GPS point) the value (i.e. DSM Z-value) of the cell it intersects (arcgis.com. 2018). The differences were then subtracted and the $RMSE_Z$ value for each DSM was calculated using the equation:

Equation 6: Root mean square error of the vertical component (Hugenholtz et al, 2013).

$$RMSE_Z = \sqrt{\frac{1}{n} \sum_{i=1}^n (Z_{DSM_i} - Z_{RTK_i})^2}$$

For the stable area approach tested on NS081, a polygon was digitized around the stable area (i.e. road), and the *Random Points* tool in ArcMap 10.5 was used to randomly create 200 points within said polygon. The values between the two DSMs were compared and entered in the above equation (Equation 4) to determine a single $RMSE_Z$ value to characterize the error between them.

When a concurrent RTK-GPS evaluation was not possible, due to the lack of equipment availability, the accuracy of the DSM is assumed as a value three times the ground sample distance (GSD), or approximately 0.12 m (3 x 0.04m) (pix4d.com, 2018).

Most histograms created that compare the difference between the DSMs and the RTK values show that the errors in the DSMs follow a Gaussian distribution. Many studies have had similar results and have followed a simplified equation from Lane et al (2003), which adds the error in quadrature (Haas et al, 2016; Xiang et al, 2018):

Equation 7: Volumetric uncertainty added in quadrature (Lane et al, 2003).

$$\sigma_v = c^2 \sqrt{n (\delta DoD)^2}$$

Where σ_v is the total volumetric uncertainty of a DSM of difference (DoD) with n number of cells with a size of c, and δDoD equals:

Equation 8: Uncertainty between two DSMs based on their individual accuracies (Brasington et al, 2003; Lane et al, 2003).

$$\delta DoD = \sqrt{(RSME_{ZOld})^2 + (RSME_{ZNew})^2}$$

However, this equation was made using older DEM creation methods, such as total stations and RTK-GPS. When these equations are applied to DSMs created using UAS and SfM-MVS, the resultant error is too small to be a reasonable, or defensible, value compared to the magnitude of error in each DSM. In addition, even though most error histograms follow a Gaussian distribution, not all did. Furthermore, it is known that the distribution of error in UAV/SfM-MVS generated DSMs is not truly random. Errors are higher in areas with less variable surface characteristics (e.g. water, mud, shadows), and near vertical edges, especially with nadir facing imagery (Juad et al, 2016). This means that the errors are not pairwise uncorrelated and therefore should be calculated using Taylor (1997) equation for maximum volumetric uncertainty:

Equation 9: Maximum volumetric uncertainty (Taylor, 1997).

$$\sigma_{Vabs} = c^2 \times \delta DoD \times n$$

Recent DEM of Detection (DoD) literature have started to apply the use of Level of Detection (LoD) thresholds in determining volumetric change and its uncertainty (Wheaton et al, 2010; Milan et al, 2011; Haas et al, 2016; Xiang et al, 2018). That is because DSMs generated with SfM may contain spatially correlated errors due to the distribution of keypoints and their importance in the SfM-MVS algorithms. Since representing spatial distribution of error in a DSM is a significant challenge, many papers apply a LoD threshold to determine volumetric change (Wheaton et al, 2010). This method only utilizes pixels where significant changes have occurred between the two DSMs for calculating change. This can either be performed using a simple t-test, or through the use of Fuzzy Interface Systems (FIS) that utilize a number of data (e.g. point density, slope, surface roughness) to quantify the distribution of error in the DSM (Wheaton et al, 2010; Milan et al, 2011; Cavalli et al, 2017). This paper uses the simple approach to LoD.

LoD is determined by the applying a user-selected significance threshold using the equation:

Equation 10: Level of detection threshold determined by a "t" value and the uncertainty between two DSMs (Wheaton et al, 2010).

$$U_{crit} = t(\delta DoD)$$

Where t can equal 1.00 (68% confidence) or 1.96 (95% confidence) depending on the desired level of confidence (Brasington et al, 2003; Lane et al, 2003; Milan et al, 2011).

To utilize only the pixels that fall within the level of detection in the DSMs, the Reclassify tool is used to assign all the pixels in the $DoD \leq (-)U_{crit}$ or $\geq U_{crit}$ a value of

1, and a value of “NoData” that fall between $\pm U_{crit}$. The Raster Calculator is then applied using the same methodology outlined above except only utilizing the changes within the LoD. In this regard, this method provides a level of certainty that the change between the DSMs occurred as opposed to a volumetric uncertainty.

This thesis used a combination of Taylor’s (1997) equation and the recent LoD methods to determine a volumetric uncertainty with an increasing level of confidence that changes in the DoD are “real changes”. All changes were ultimately scrutinized using a variety of qualitative checks (e.g. field photos) and compared to the hydrodynamic information which can be used to verify if the processes in the borrow pits are conducive to erosion or deposition.

3.3.2 Empirical Measurements of Hydrodynamics

Empirical hydrodynamic measurements were made in the borrow pits to supplement the UAS-SfM data. These measurements were obtained to compare the hydrodynamic conditions within the borrow pits to their infill rates. Specifically, this study collected incoming SSC, SSC over the tidal period, SSC throughout the water column, resolved horizontal water velocity, hydroperiod and depth of water. Field measurements were completed on select spring tides during the late spring, summer, and fall of 2016 and 2017 (Table 3).

Although each marsh varied in the number and design of borrow pits, the setup for measuring hydrodynamics followed a consistent layout (Figure 32). Rising stage bottles were placed at the outlets, middle, and end of the borrow pits. The Nortek acoustic Doppler Current Profiler (ADCP) and Acoustic Doppler Velocimeters (ADV) were situated in the centre of the borrow pits away from the outlets and the end of the borrow

pit to measure an average velocity within the pit. Two level loggers and ISCO automated water samplers were deployed simultaneously; however, one set of each was located at a separate marsh as to compare sediment dynamics and tidal characteristics of two marshes during the same tide.

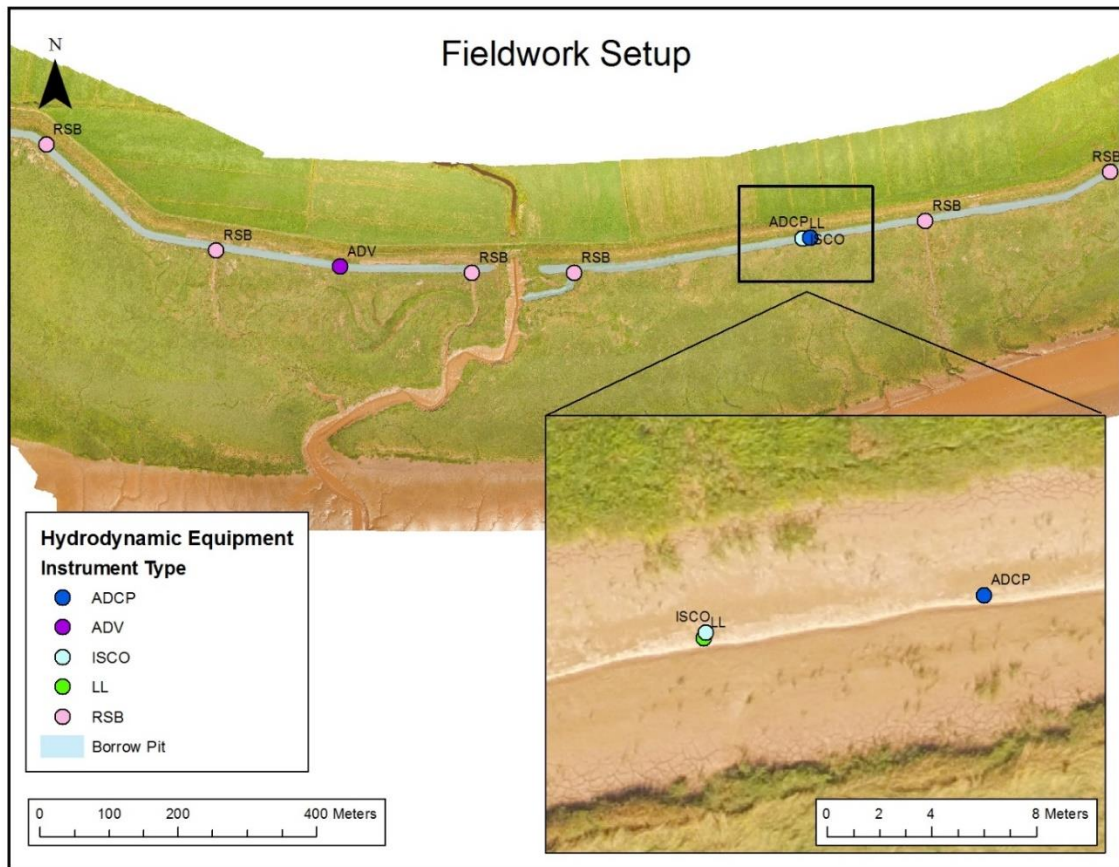


Figure 32: Fieldwork setup at VDJ Marsh showing the general layout of hydrodynamic equipment used at all sites, including: Acoustic Doppler Current Profiler (ADCP), Acoustic Doppler Velocimeter (ADV), Teledyne ISCO Water Sampler, Level Loggers (LL) and Rising Stage Bottles (RSB).

As mentioned previously, rising stage bottles were placed near the end and middle of every borrow pit, as well as at every major borrow pit outlet, to collect incoming SSC (Nolte et al, 2013) (Figure 33). Each rising stage bottle collected approximately 500ml samples. Furthermore, an ISCO automated water sampler was installed 20cm above the bed to collect SSC in 250ml samples throughout the tidal cycle. Comparing the incoming

and outgoing SSC in each borrow pit can help inform whether that material is being deposited, either in the borrow pit or on the marsh platform (Nolte et al, 2013). SSC was determined using standard suction filtration techniques using Whatman 42 filter papers with a pore size of 2.5 μ m. The papers were then dried and their post and pre filtration weights were compared to determine the SSC of each sample.



Figure 33: Rising stage bottles installed 20cm above the channel bed were used to measure incoming SSC.

To measure flow velocity within the borrow pits, an ADCP and two ADVs were used. Both were placed near the centre of the borrow pits, with the ADCP upward facing on the borrow pit bed adjacent to the pit thalweg, while the ADV's were placed over the pit thalweg, approximately 15cm above the bed and orientated in the +ve X direction of

flow (direction of flood tide). The resolved horizontal velocity obtained from the ADV was calculated using:

Equation 11: Resolved Horizontal Velocity (O’Laughlin and van Proosdij, 2013).

$$RVH = \sqrt{(u^2 + v^2)}$$

Finally, hydroperiod and depth of water in the pit were obtained using HOBO Level Loggers. The loggers were placed near the centre of selected borrow pits in two different marshes and left for a period of 30 days to compare any differences in hydroperiod that may occur between them. To determine the depth of water in the pit during each tide a barometer (i.e. barologger) was placed outside the borrow pits and the barometric pressure was subtracted from the pressure collected in the level loggers to isolate pressure in the pit. Following that, the depth of water was calculated using the equation:

Equation 12: Depth of water based on water and atmospheric pressures and the density of water (nasa.gov, 2014).

$$Depth = \frac{[(kpa_{LL} - kpa_{BL}) \times 1000]}{g \times r}$$

Where g is the acceleration of gravity and r is the density of saltwater (1025 kg/m³) (nasa.gov, 2014). Table 10 shows a list of when each of the above hydrodynamic instruments were deployed at each marsh.

Table 10: List of hydrodynamic equipment deployed during each field visit. All hydrodynamic data can be found in Appendix 2.

Date	Location	RSB	ISCO	ADCP	ADV	OBS	LL
July 2016	Masstown (East and West)	✓	✓ (MTW_01)	X	X	X	X
August 2016	Lower Truro	✓	✓ (LT_01)	X	X	X	X
September 2016	Ryerson – Dugau	✓	✓	X	X	X	X
May 2017	Masstown (East and West)	✓	✓ (MTW_01)	✓ (MTW_01)	✓ (MTE_03)	✓	✓
	Lower Truro	✓	✓ (LT_01)	✓ (LT_01)	✓ (LT_01)	✓	X
June 2017	Masstown (West)	✓	✓ (MTW_01)	✓ (MTW_01)	✓ (MTW_01)	✓	✓
	VDJ	✓	✓ (VDJ_03)	✓ (VDJ_03)	✓ (VDJ_02)	✓	✓
July 2017	Ryerson – Dugau	✓	✓	✓	✓	✓	✓

3.4 Results

3.4.1 Digital Surface Model Accuracy Validation

The point-to-raster validations of the DSMs reveal $RMSE_Z$ values ranging from 0.041m – 0.156m (**Table 11**). These values are consistent with $RMSE_Z$ -values published in other reports, especially when accounting for the ground sample distance (GSD) and the suboptimal surface characteristics within the borrow pits. Standard deviation (SD) had a similar range between 0.057m – 0.149m. Mean absolute error (MAE) values range from 0.042m – 0.135m. For DSMs with no associated validation data, all values are three times

the ground sample distance (GSD) (i.e. 0.120m) and are indicated as an “X” in Table 6 (pix4d.com, 2018).

Table 11: Accuracy validation for each DSM. "X" indicates when the accuracy assessment was not conducted due to equipment availability. For each flight the number of ground control points (GCPs) and independent check points (n) are listed, along with the mean, standard deviation (SD), root mean squared error of the vertical component (RMSE_Z), and the mean absolute error (MAE) for each validation.

Site	Date	GCPs (#)	n	Mean	SD	RMSE _Z	MAE
RD	May 2017	17	X	X	X	0.041m	X
	Sept 2017	9	36	0.023m	0.089m	0.072m	0.075m
VDJ	Nov 2016	16	41	0.024m	0.149m	0.156m	0.135m
	August 2017	18	85	0.018m	0.072m	0.074m	0.056m
MTW	May 2016	7	479	0.019m	0.105m	0.106m	0.076m
	August 2016	8	X	X	X	X	X
	August 2017	10	58	-0.012m	0.089m	0.090m	0.069m
MTE	May 2016	6	116	0.032m	0.063m	0.071m	0.058m
	August 2016	5	X	X	X	X	X
	August 2017	8	84	0.006m	0.096m	0.097m	0.080m

3.4.2 Infill Rates and Empirical Measurements of Hydrodynamics

Over the course of the study, nine out of the 13 borrow pits surveyed were accreting vertically (Table 12). Of the four remaining pits, two were actively eroding and two had zero net change. All of the borrow pits had infilled when comparing their as-built volume to the most recent aerial survey. The borrow pit with the greatest accretion rate during the study was MTE_02, which had an average accretion throughout the borrow pit of $0.19 \pm 0.10\text{m}\cdot\text{yr}^{-1}$ between May 2016 and August 2017. RD_01 had the greatest rate of

erosion at $-0.54 \pm 0.08 \text{ m}\cdot\text{yr}^{-1}$. The high rate of erosion at RD_01 corresponded with the lowest incoming and mean suspended sediment throughout the tidal cycle (Table 13). Borrow pits were grouped into three main categories (Not infilling, Adjusting or no change, and Infilling), and was based on the volumetric change measured during this study, the volumetric change from as-built volume, and observations from the field. This allowed for the identification of the unique hydrodynamics that contribute to borrow pit infill rates.

Table 12: Results of the volumetric change analysis for all borrow pits using all pixels and 68% confidence intervals. * represents a manually calculated as-built volume. ¹ represents an “Year 2” infill rate.

State	BP	All Pixels (m ³)			All Pixels (m ³ yr ⁻¹)	68% CI (m ³)			68% CI (m ³ yr ⁻¹)	All Pixels (m ³ yr ⁻¹)		BP Geometry			
		Deposition	Erosion	Net	Vertical Accretion Rate during study	Deposition	Erosion	Net	Vertical Accretion Rate during study	Volumetric Change from as-built	Vertical Accretion Rate from as-built	Length (m)	Width (m)	Ratio (L:W)	Number of Outlets
Will not infill	RD_01	0.83 ± 0.89	-188.53 ± 84.95	-187.70 ± 84.95	-0.54 ± 0.08	0.60 ± 0.31	-185.21 ± 80.29	-184.67 ± 80.29	-0.54 ± 0.08	N/A	N/A	121	8	15	1
Adjusting or no change	VDJ_01	228.52 ± 607.68	-257.92 ± 627.42	-29.40 ± 873.46	0.00 ± 0.12	53.09 ± 31.67	-80.07 ± 45.98	-27.09 ± 55.83	0.00 ± 0.01	2008.27	0.20	766	11.6	66	1
	VDJ_03	431.28 ± 959.15	-546.88 ± 728.19	-115.60 ± 1204.25	-0.03 ± 0.12	66.79 ± 48.84	-355.51 ± 196.27	-288.72 ± 202.26	-0.03 ± 0.02	1726.17	0.13	948	11.6	82	2
	MTW_01	378.46 ± 364.41	-377 ± 347.50	0.86 ± 503.54	0.00 ± 0.10	275.56 ± 134.56	-278.13 ± 116.62	-2.57 ± 178.06	0.00 ± 0.03	4604.76	0.23	1148	8.5	135	3
	MTW_02	338.97 ± 277.28	-198.30 ± 200.79	140.67 ± 342.35	0.03 ± 0.10	277.91 ± 148.50	-134.85 ± 76.72	143.06 ± 167.15	0.04 ± 0.05	N/A	N/A	384	8.5	45	1
Infilling	LT_01	383.19 ± 206.96	-44.86 ± 44.73	338.33 ± 211.74	0.09 ± 0.06	352.00 ± 145.95	-33.44 ± 13.08	318.56 ± 146.53	0.09 ± 0.04	4759.02*	0.40* ⁱ	824	6.1	135	2
	LT_02	298.70 ± 178.89	-20.39 ± 21.86	278.31 ± 180.21	0.10 ± 0.06	265.58 ± 121.66	-14.74 ± 6.14	250.84 ± 121.81	0.09 ± 0.04	4475.52*	0.47* ⁱ	763	6.1	125	2
	LT_03	306.92 ± 170.22	-35.56 ± 21.33	271.36 ± 171.55	0.10 ± 0.06	281.02 ± 128.45	-31.08 ± 10.89	249.94 ± 128.91	0.09 ± 0.05	4852.15*	0.45* ⁱ	697	6.1	114	2
	LT_04	219.30 ± 165.79	-29.06 ± 30.90	190.24 ± 168.64	0.07 ± 0.06	184.55 ± 105.21	-20.92 ± 10.90	163.63 ± 105.77	0.06 ± 0.04	2849.57*	0.39* ⁱ	543	6.1	89	1
	MTE_01	190.03 ± 137.93	-11.90 ± 14.19	181.13 ± 138.65	0.14 ± 0.11	164.50 ± 92.81	-8.29 ± 4.56	156.21 ± 92.92	0.12 ± 0.07	741.66	0.47	129	8.5	15	1
	MTE_02	727.03 ± 338.86	-75.57 ± 73.44	648.46 ± 346.73	0.19 ± 0.10	688.04 ± 265.17	-59.33 ± 28.38	628.71 ± 266.67	0.18 ± 0.08	4828.26	0.40	546	7.5	73	1
	MTE_03	402.54 ± 254.10	-46.96 ± 25.46	355.58 ± 255.37	0.16 ± 0.11	363.31 ± 180.56	-42.24 ± 12.25	321.07 ± 180.98	0.14 ± 0.08	1847.83	0.63	244	9.5	26	1
	VDJ_02	780.81 ± 871.14	-300.26 ± 528.51	480.55 ± 1018.92	0.06 ± 0.13	569.95 ± 401.26	-92.07 ± 74.56	477.88 ± 408.13	0.06 ± 0.05	6393.81	0.55	784	11.6	68	2

Table 13: Results of the empirical hydrodynamic measurements in each borrow pit.

State	BP	68% CI (m ³)	RSB (g·l ⁻¹)		ISCO (g·l ⁻¹)		ADCP (m·s ⁻¹)			
		Infill Rate	SSC Range	SSC Mean ± SD	SSC Range	SSC Mean ± SD	RHV (flood)	RHV (ebb)	Max (flood)	Max (ebb)
Not Infilling	RD_01	-0.54 ± 0.08	0.036 - 0.240	0.091 ± 0.049	0.044 - 0.159	0.092 ± 0.021	0.08	0.04	0.45	0.39
Adjusting or no change	VDJ_01	0.00 ± 0.01	1.250 - 7.670	3.830 ± 2.147	X	X	X	X	X	X
	VDJ_03	-0.03 ± 0.02	4.770 - 51.072	26.497 ± 13.086	2.973 - 92.458	32.440 ± 29.466	0.27	0.43	1.36	1.25
	MTW_01	0.00 ± 0.03	0.202 - 6.280	2.675 ± 1.723	0.058 - 1.429	0.366 ± 0.244	0.28	0.10	0.51	0.36
	MTW_02	0.04 ± 0.05	0.455 - 4.568	2.527 ± 1.345	X	X	X	X	X	X
Infilling	LT_01	0.09 ± 0.04	4.918 - 5.978	5.230 ± 0.390	0.041 - 4.262	1.472 ± 1.050	0.24*	0.30*	0.67*	0.58*
	LT_02	0.09 ± 0.04	2.072 - 8.249	4.518 ± 1.983	X	X	X	X	X	X
	LT_03	0.09 ± 0.05	2.596 - 7.273	5.136 ± 1.720	X	X	X	X	X	X
	LT_04	0.06 ± 0.04	5.295 - 10.054	7.413 ± 1.714	X	X	X	X	X	X
	MTE_01	0.12 ± 0.07	0.638 - 1.226	0.977 ± 0.284	X	X	X	X	X	X
	MTE_02	0.18 ± 0.08	0.299 - 8.929	3.213 ± 3.120	X	X	X	X	X	X
	MTE_03	0.14 ± 0.08	0.658 - 4.509	1.972 ± 1.230	X	X	0.37*	0.23*	0.61*	0.57*
	VDJ_02	0.06 ± 0.05	1.774 - 16.988	9.232 ± 4.616	X	X	X	X	X	X

Not Infilling

RD_01 was surveyed between May 2017 and September 2017. It lost a total of $-187.70 \pm 84.95\text{m}^3$ of sediment during this time, which equates an accretion rate of $-0.54 \pm 0.08\text{m}\cdot\text{yr}^{-1}$ after normalizing for area. The greatest vertical erosion in RD_01 occurred at the mouth of the borrow pit outlet and adjacent to a rock apron where the hydrodynamic equipment was installed (Figure 34). RD_01 had the lowest mean incoming suspended sediment concentration (SSC), as well as the lowest mean SSC throughout the tidal cycle at $0.091 \pm 0.049\text{g}\cdot\text{l}^{-1}$ and $0.092 \pm 0.021\text{g}\cdot\text{l}^{-1}$, respectively (Figure 35). RD_01 also had the least variability of SSC throughout the tidal cycle. While other borrow pits had higher concentrations during the initial flood tide and at the end of the ebb tide, RD_01 had a relatively flat SSC signal during the tidal period. Note that the vertical scales for SSC is different for each borrow pit. This is because of the high range between the lowest and highest concentrations and the importance the SSC pattern throughout the tidal period.

With a long tidal period that exceeded three hours, depth average velocities in the borrow pit throughout the tidal cycle were also lower than in any other borrow pit. On the flood tide, depth averaged velocities were $0.08\text{m}\cdot\text{s}^{-1}$, while the ebb tide averaged $0.04\text{m}\cdot\text{s}^{-1}$ over the three tides the ADCP was deployed. However, the maximum flood and ebb tides measured were comparable to other borrow pits peaking at $0.45\text{m}\cdot\text{s}^{-1}$ and $0.39\text{m}\cdot\text{s}^{-1}$, respectively. The maximum recorded velocities both coincided when flood and ebb tides passed through bankfull elevation (Figure 36).

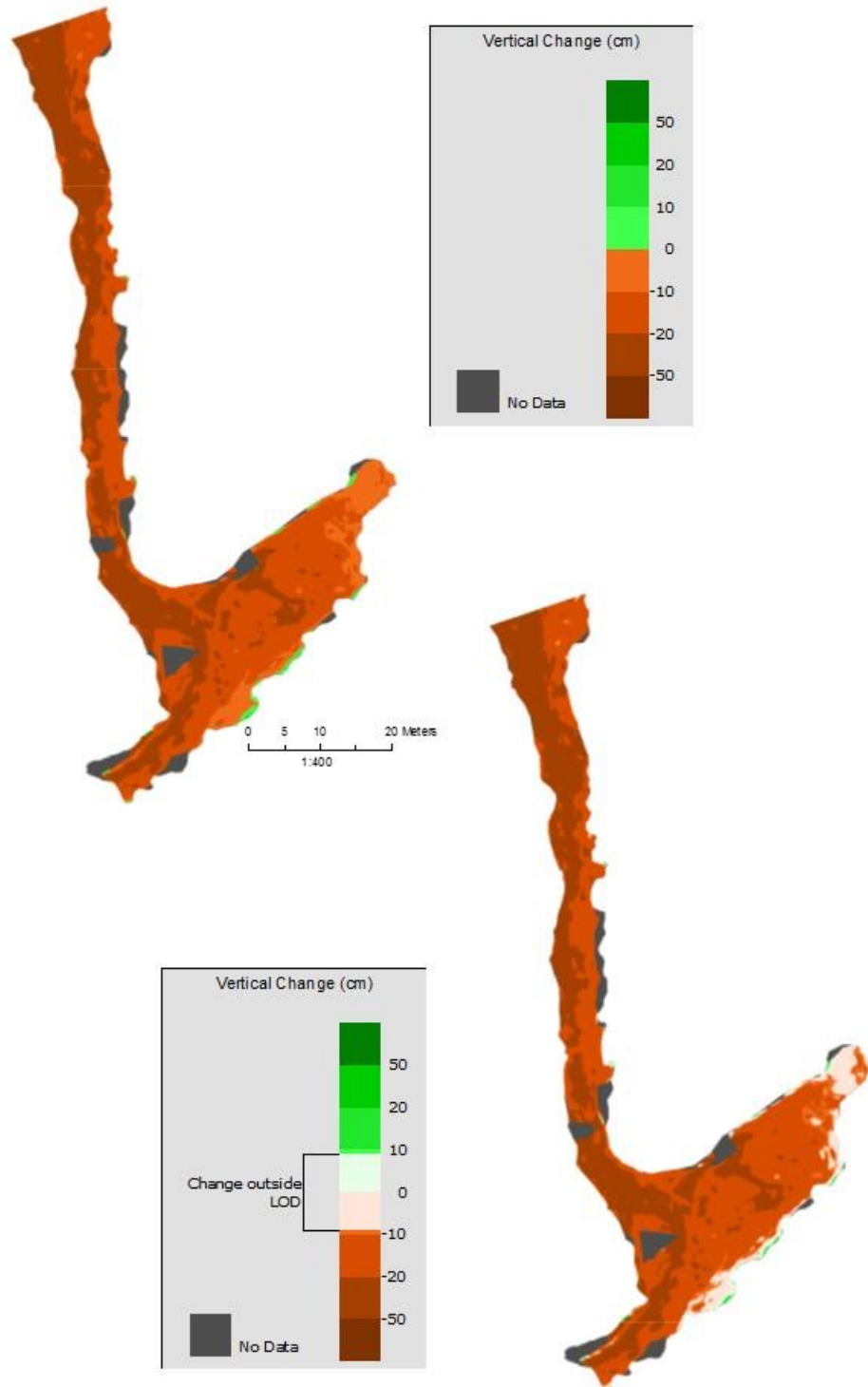


Figure 34: DoD showing vertical change at RD_01. Green represents vertical accretion and red represents erosion. The top figure uses all pixels, the bottom shows changes that occurred with 68% confidence (LoD = 0.080m).

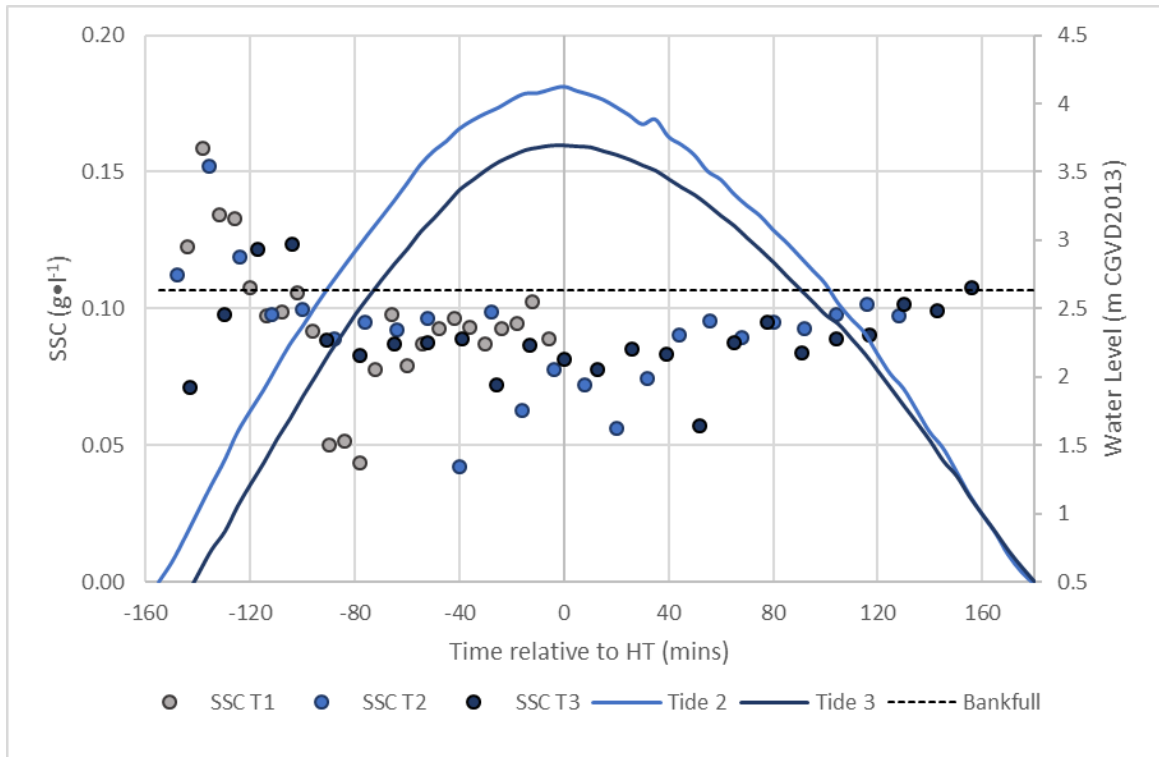


Figure 35: SSC vs water level over the tidal period. RD_01 July deployment. Time is relative to the recorded high tide (HT).

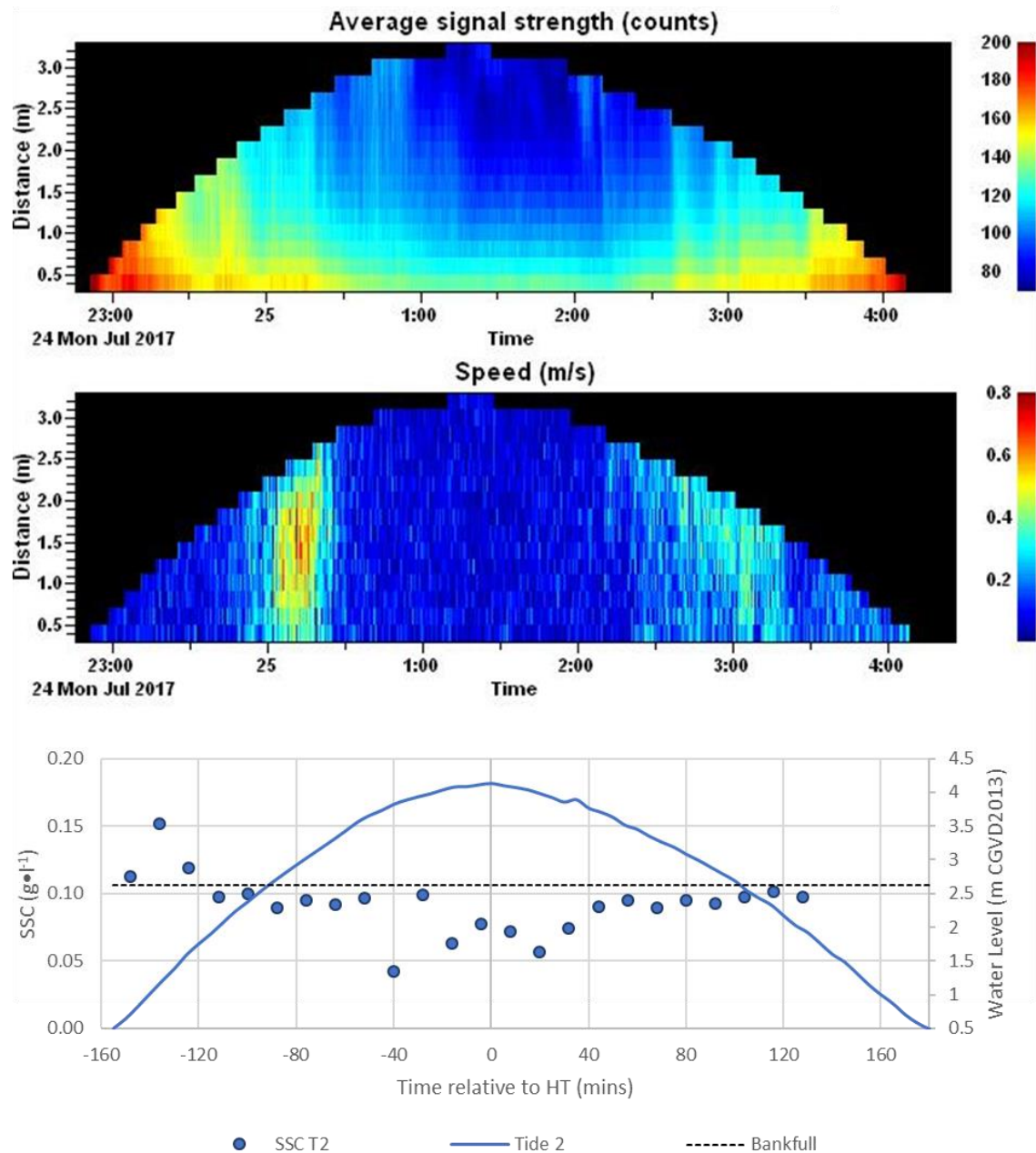


Figure 36: Hydrodynamics during July deployment (T2) at RD_01. Backscatter proxy (top), resolved horizontal velocity (middle), and SSC vs water level (bottom).

Adjusting or No Change

Borrow pits were classified as adjusting or having no change if their vertical accretion rate throughout the study was less than $0.05 \text{ m}\cdot\text{yr}^{-1}$. In total, four borrow pits were deemed to fall in this category. Vertical accretion ranged from $-0.03 \pm 0.02 \text{ m}\cdot\text{yr}^{-1}$ to $0.04 \pm 0.05 \text{ m}\cdot\text{yr}^{-1}$ in VDJ_03 and MTW_02, respectively. These low accretion values during the study are substantially slower than the accretion rates measured from the original as-built volumes. Compared to the infilling borrow pits, the adjusting borrow pits were accreting at a rate 21% - 58% of the infilling borrow pits. This suggests that the borrow pit is adjusting to a new depositional state or is approaching an equilibrium.

All borrow pits in this category had a mean incoming SSC greater than $2.50 \text{ g}\cdot\text{l}^{-1}$, with VDJ_03 having the greatest incoming SSC of any borrow pit measured at $26.497 \pm 13.086 \text{ g}\cdot\text{l}^{-1}$. Sediment throughout the tidal cycle did vary between the borrow pits, however (Figure 37 and 38). VDJ_03 had a mean SSC throughout the tidal cycle of $32.440 \pm 29.466 \text{ g}\cdot\text{l}^{-1}$, while MTW_01 was much lower at $0.366 \pm 0.244 \text{ g}\cdot\text{l}^{-1}$. The pattern of SSC throughout the tidal cycle also differed between MTW_01 and VDJ_03. During June 2017, an ISCO was placed in both MTW_01 and VDJ_03 during the same three tides. Figure 39 shows SSC in MTW_01 settled quickly following the initial influx of sediment on the flood tide, with a slight resuspension as water levels fell below bankfull. In VDJ_03, SSC stayed in suspension much longer, falling only after water levels moved below bankfull on the ebb tide. However, when tide level did not exceed bankfull, both SSC patterns show a steady rate of settling following the initial flood tide. An ISCO was not deployed in either MTW_02 or VDJ_01.

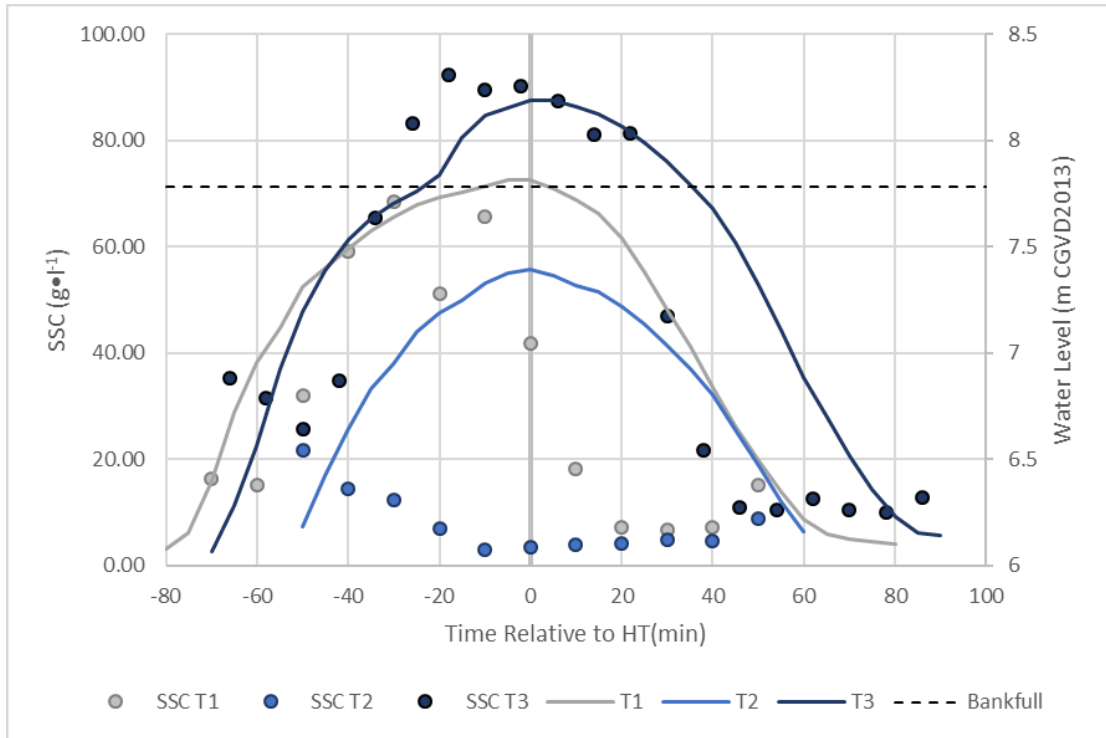


Figure 37: SSC vs water level over the tidal period. VDJ_03 June deployment. Time is relative to the recorded high tide (HT).

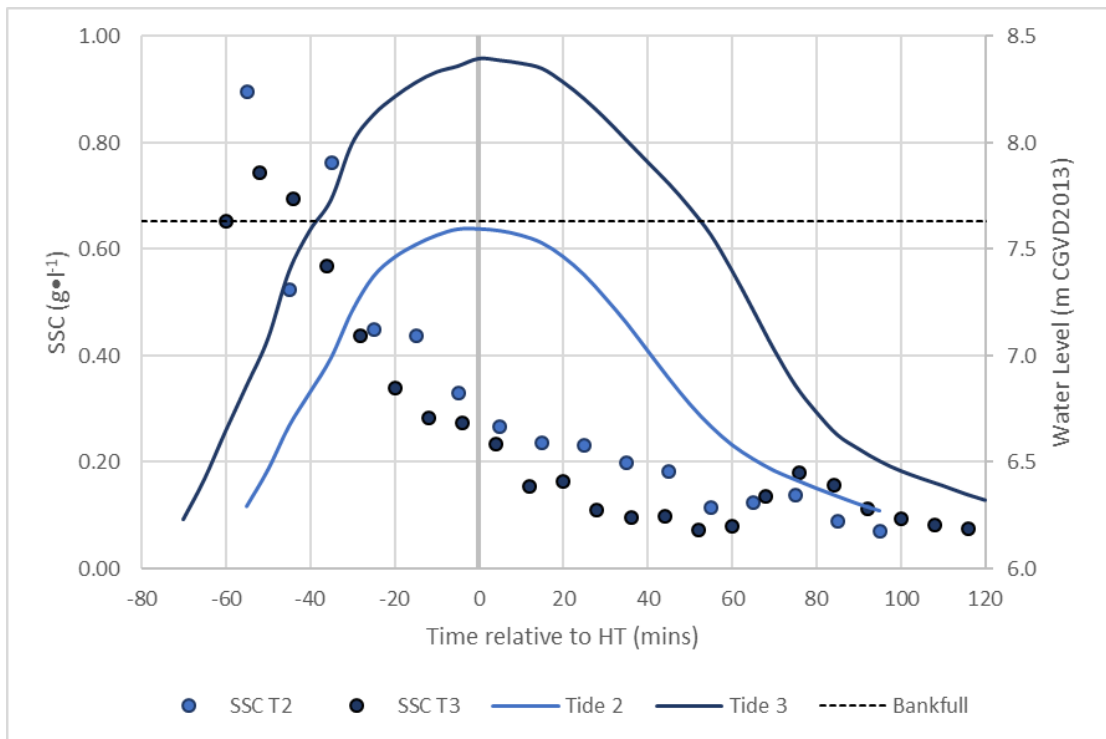


Figure 38: SSC vs water level over the tidal period. MTW_01 June deployment. Time is relative to the recorded high tide (HT).

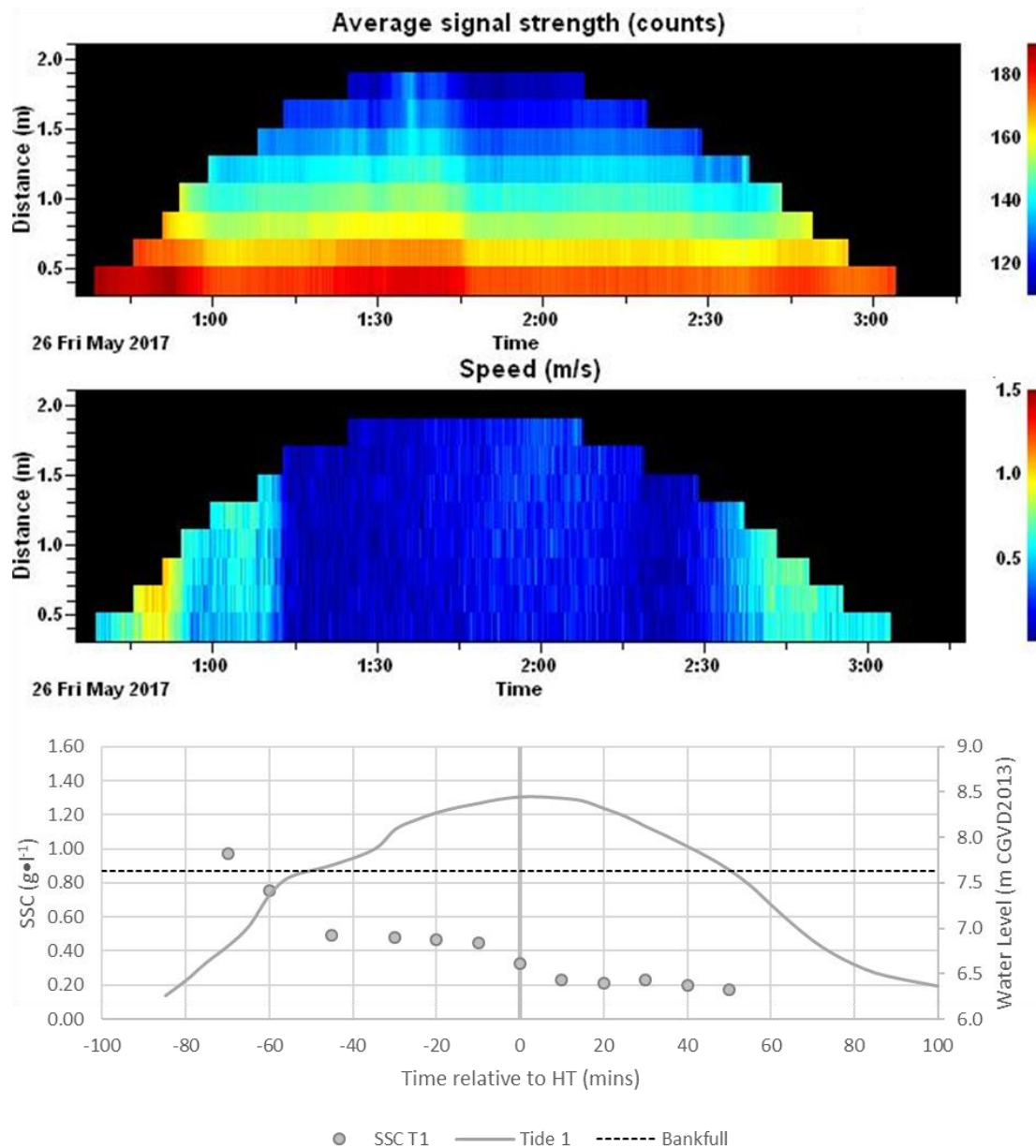


Figure 39: Hydrodynamics during May deployment (T1) at MTW_01. Backscatter proxy (top), resolved horizontal velocity (middle), and SSC vs water level (bottom).

Where the borrow pits in this category differ the most is in their hydrology. Resolved horizontal velocity (RHV) measured from the ADCP suggest that MTW_01 is slightly flood dominated, while VDJ_03 is ebb dominated. MTW_01 had a mean RHV of

0.28 $\text{m}\cdot\text{s}^{-1}$ on the flood tide and a mean RHV of 0.10 $\text{m}\cdot\text{s}^{-1}$ on the ebb tide. VDJ_03 had an RHV of 0.27 $\text{m}\cdot\text{s}^{-1}$ and 0.43 $\text{m}\cdot\text{s}^{-1}$ on the flood and ebb tide, respectively. The maximum recorded velocities in VDJ_03 were also high, reaching 1.36 $\text{m}\cdot\text{s}^{-1}$ on the flood tide and 1.25 $\text{m}\cdot\text{s}^{-1}$ on the ebb tide. These velocities would be higher if the instruments were placed in the outlet channel where flow is more confined.

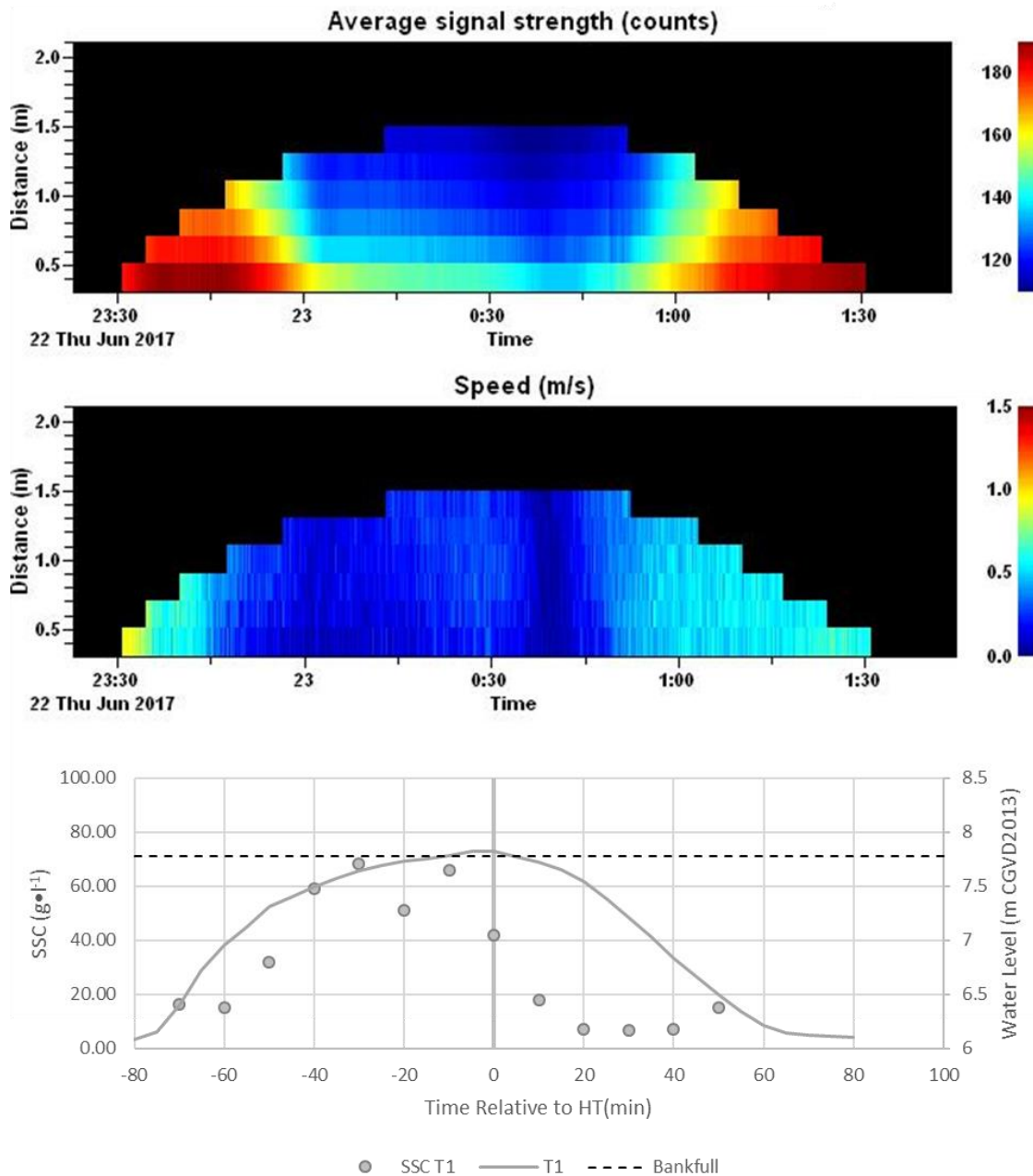
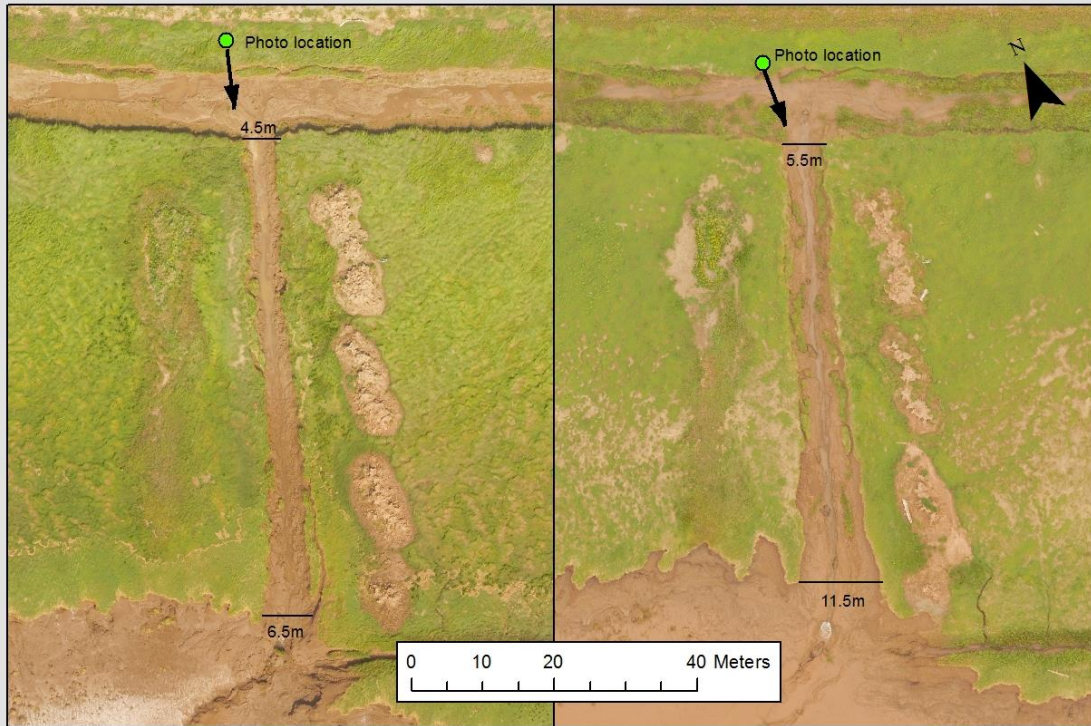


Figure 40: Hydrodynamics during June deployment (T1) at VDJ_03. Backscatter proxy (top), resolved horizontal velocity (middle), and SSC vs water level (bottom).

Significant erosion in the outlet channel was observed in all four borrow pits (Figure 42 – 45). For example, the mouth of the main outlet channel in MTW_01 had nearly doubled in width, expanding from 6.5m to 11.5m wide, between August 2016 and

August 2017. This widening coincided with bed erosion exceeding 0.75m in some areas. The outlet at VDJ_03 also experienced bed erosion greater than 0.75m during the study, however, the erosion here expanded approximately 400m into the borrow pit. MTW_02 had pronounced gradient of bed surface change, with large amounts of erosion in, and near the outlet, and deposition at the middle and end of the borrow pit (Figure 41).



August 2016

Width of outlet at borrow pit = 4.5m
Width of outlet at mouth = 6.5m

August 2017

Width of outlet at borrow pit = 5.5m
Width of outlet at mouth = 11.5m



June 2016



August 2017

Figure 41: The borrow pit outlet at MTW_01 significantly widened at either end, or experienced bed scour. This is a result of the volume of the pit being out of hydraulic equilibrium with the size of the outlet channel.

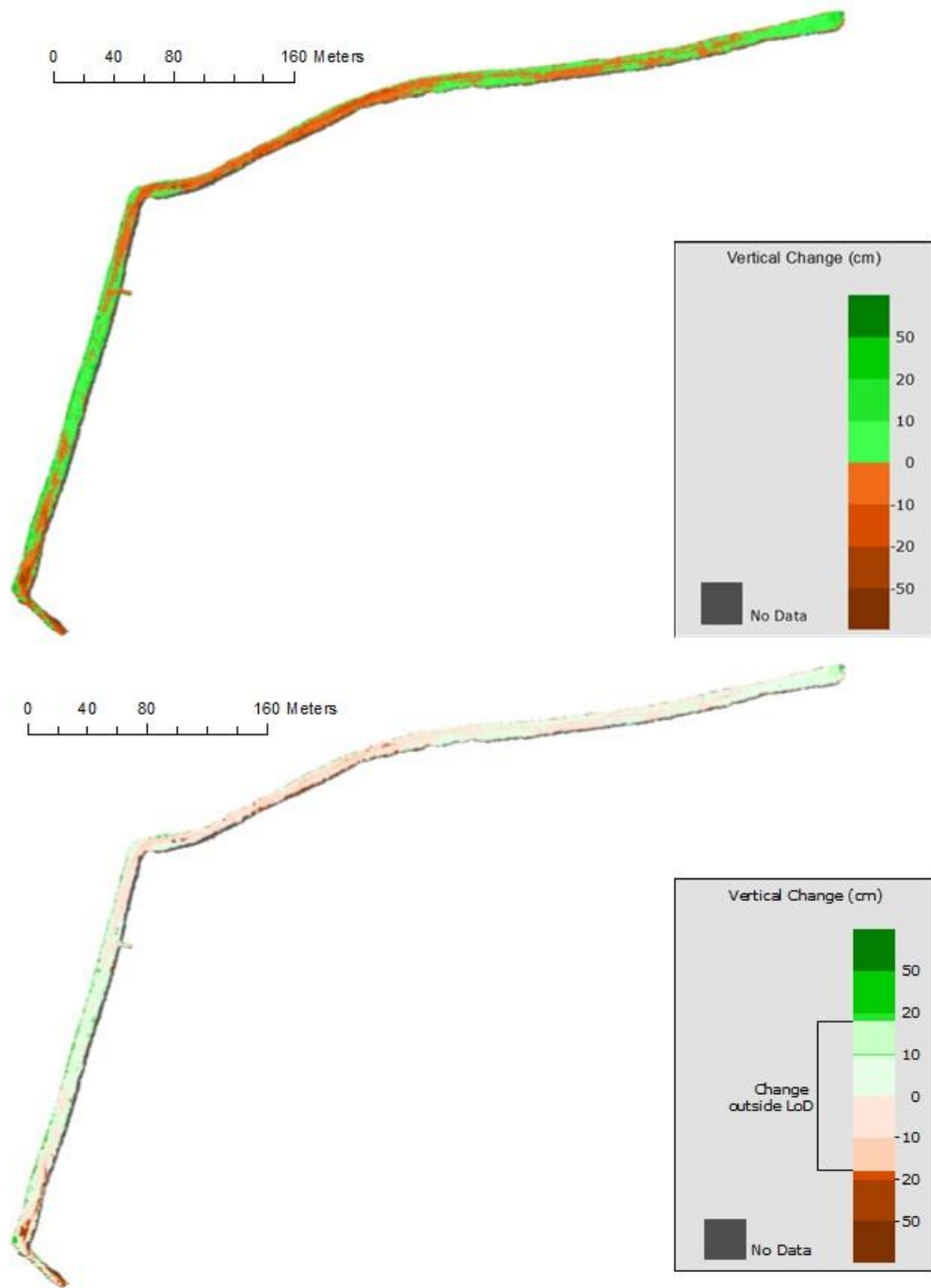


Figure 42: DoD showing vertical change at VDJ_01. Green represents vertical accretion and red represents erosion. The top figure uses all pixels, the bottom shows changes that occurred with 68% confidence ($LoD = 0.170m$).

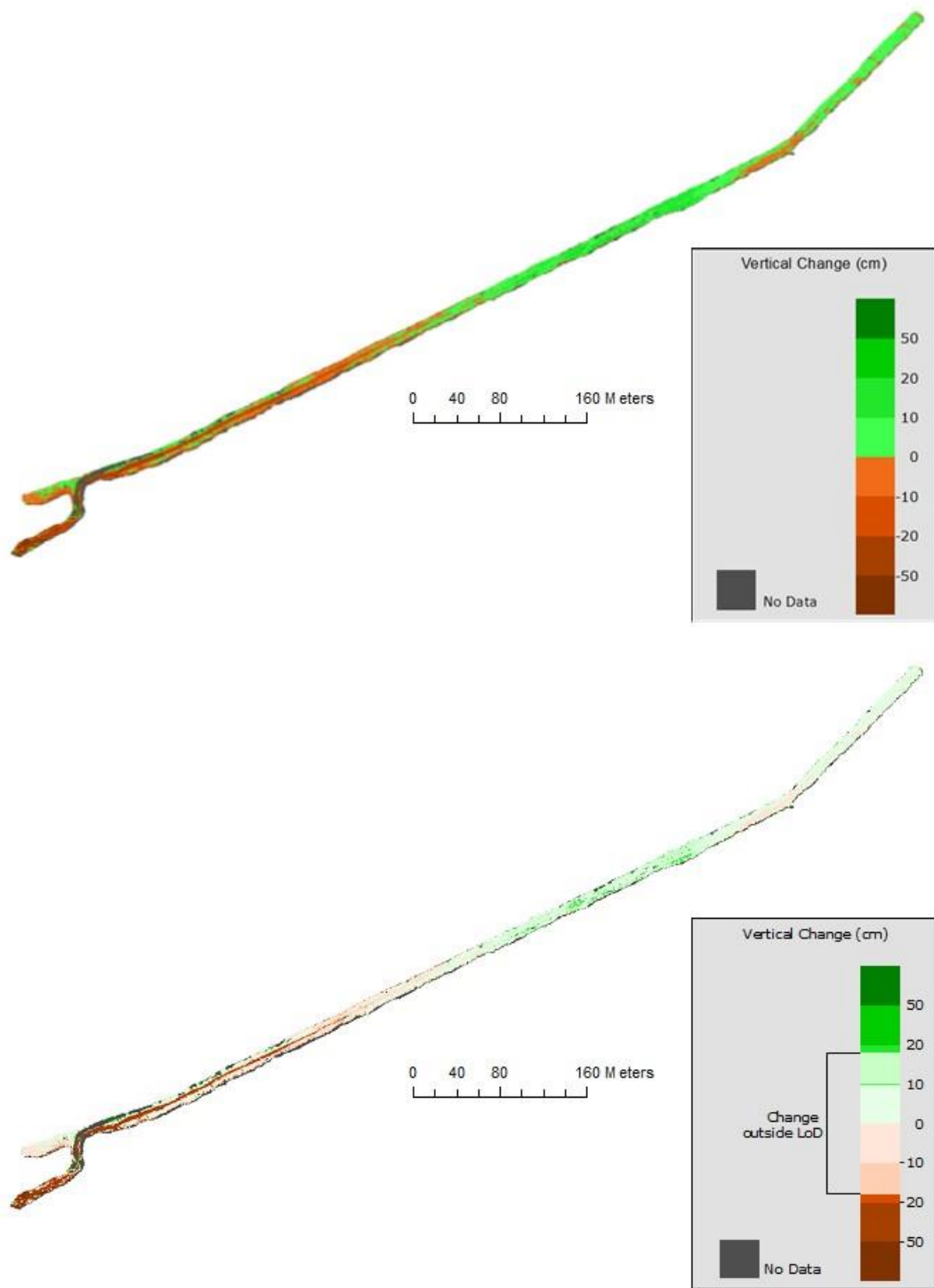


Figure 43: DoD showing vertical change at VDJ_03. Green represents vertical accretion and red represents erosion. The top figure uses all pixels, the bottom shows changes that occurred with 68% confidence ($LoD = 0.170m$).

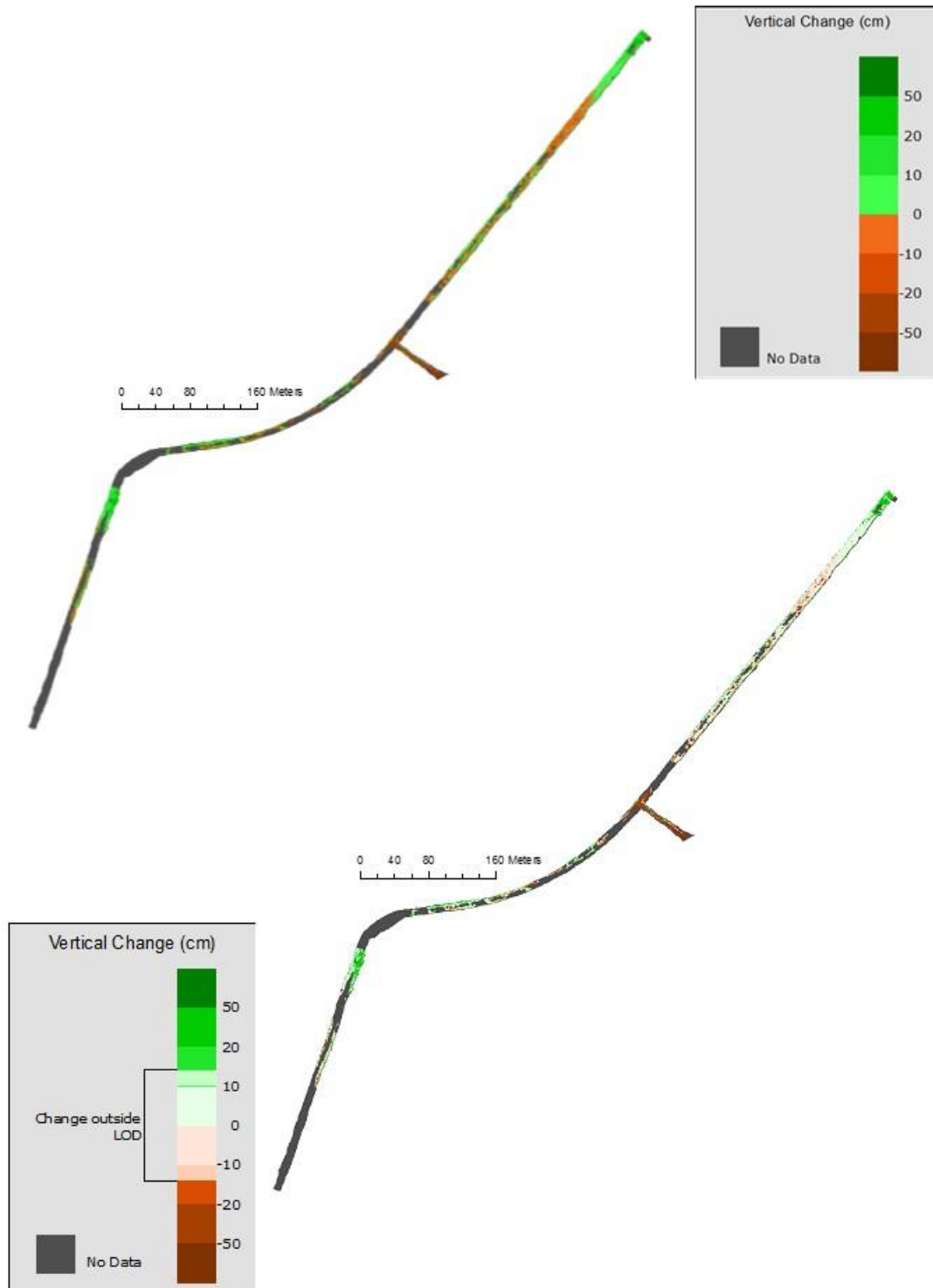


Figure 44: DoD showing vertical change at MTW_01. Green represents vertical accretion and red represents erosion. The top figure uses all pixels, the bottom shows changes that occurred with 68% confidence ($LoD = 0.140m$).

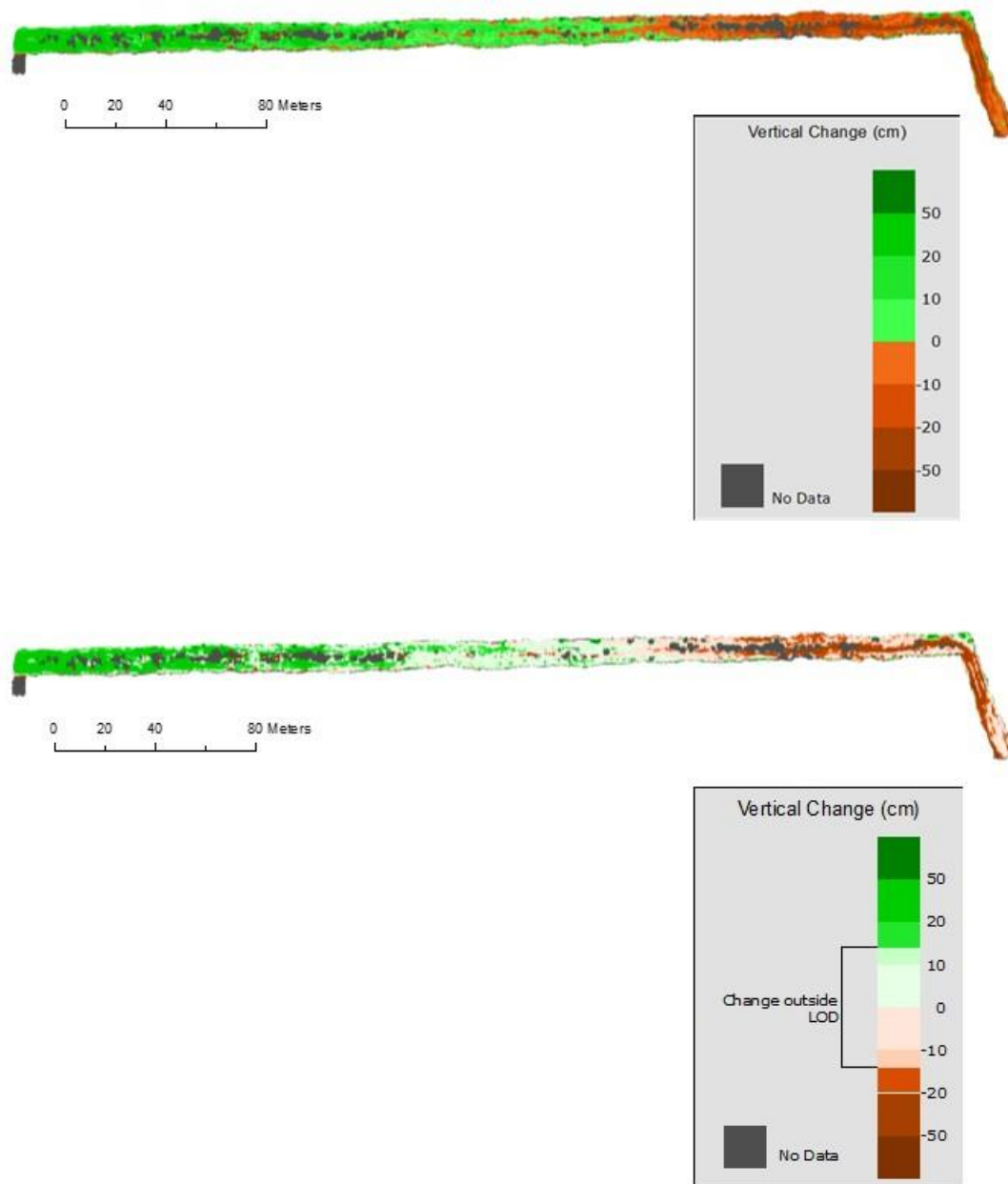


Figure 45: DoD showing vertical change at MTW_02. Green represents vertical accretion and red represents erosion. The top figure uses all pixels, the bottom shows changes that occurred with 68% confidence ($LoD = 0.140m$).

Infilling

The infilling borrow pits had a vertical accretion rate ranging from $0.06 \pm 0.05 \text{m}\cdot\text{yr}^{-1}$ to $0.18 \pm 0.08 \text{m}\cdot\text{yr}^{-1}$, at 68% confidence; the latter, MTE_02, having the greatest rate of any borrow pit during the study period (Figure 46 – 50). This accretion rate correlated with a net gain of $628.71 \pm 266.67 \text{m}^3$, again, the most of any borrow pit. MTE_03 had the greatest vertical accretion rate compared to the original as-built volume, at an approximate rate of $0.63 \text{m}\cdot\text{yr}^{-1}$. Overall, the borrow pits in the Masstown East marsh had the three highest rates of vertical accretion – followed by the four borrow pits in the Lower Truro marsh. The only borrow pit outside these two sites that fell into the infilling category was VDJ_02, which had the second greatest net gain in sediment at $477.88 \pm 408.13 \text{m}^3$ (68% CI). However, since the area of VDJ_02 is much larger than the other borrow pits in this category, this large deposition of sediment translated to a smaller vertical accretion rate of $0.06 \pm 0.05 \text{m}\cdot\text{yr}^{-1}$.

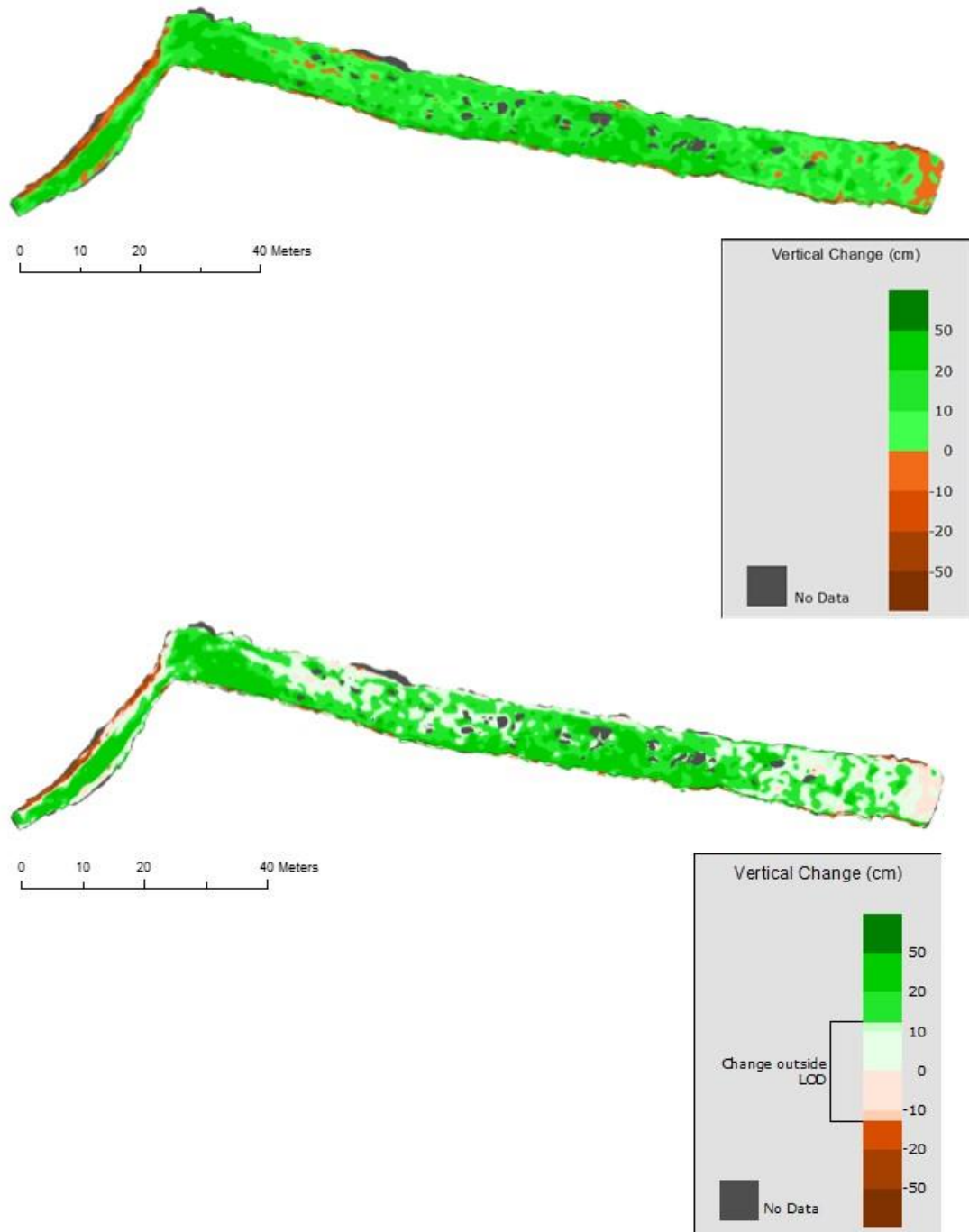


Figure 46: DoD showing vertical change at MTE_01. Green represents vertical accretion and red represents erosion. The top figure uses all pixels, the bottom shows changes that occurred with 68% confidence ($LoD = 0.120m$).

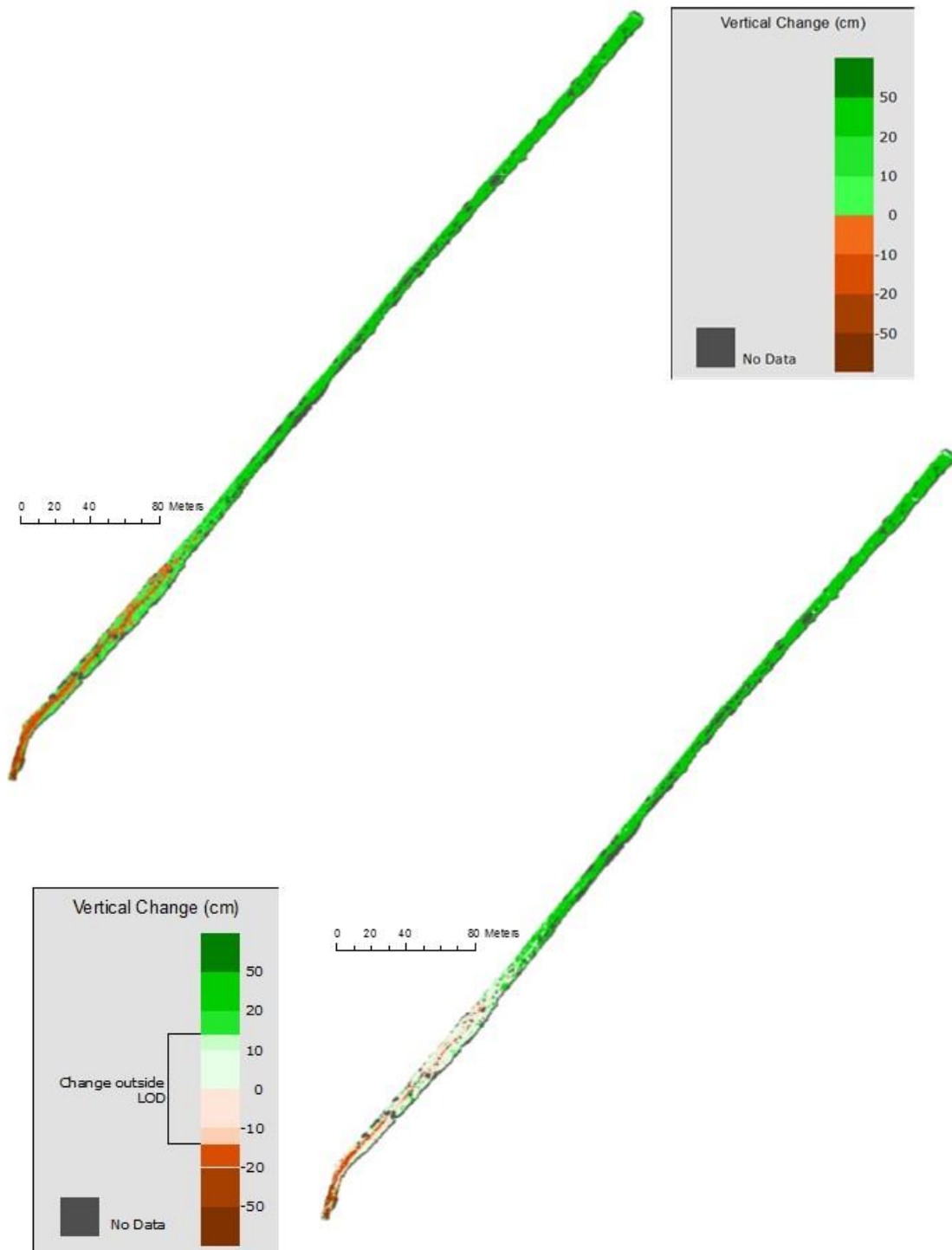


Figure 47: DoD showing vertical change at MTE_02. Green represents vertical accretion and red represents erosion. The top figure uses all pixels, the bottom shows changes that occurred with 68% confidence (LoD = 0.120m).

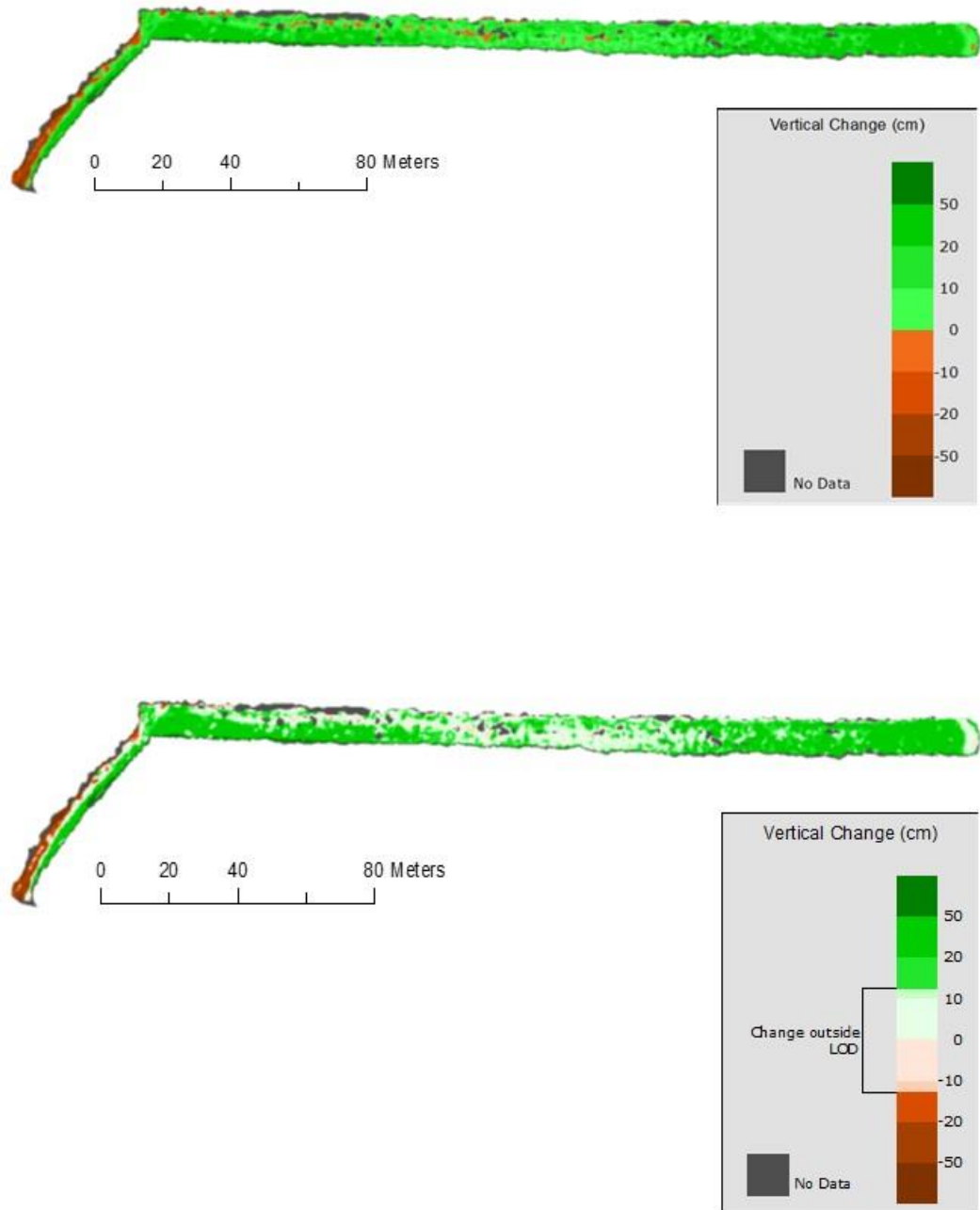


Figure 48: DoD showing vertical change at MTE_03. Green represents vertical accretion and red represents erosion. The top figure uses all pixels, the bottom shows changes that occurred with 68% confidence (LoD = 0.120m).

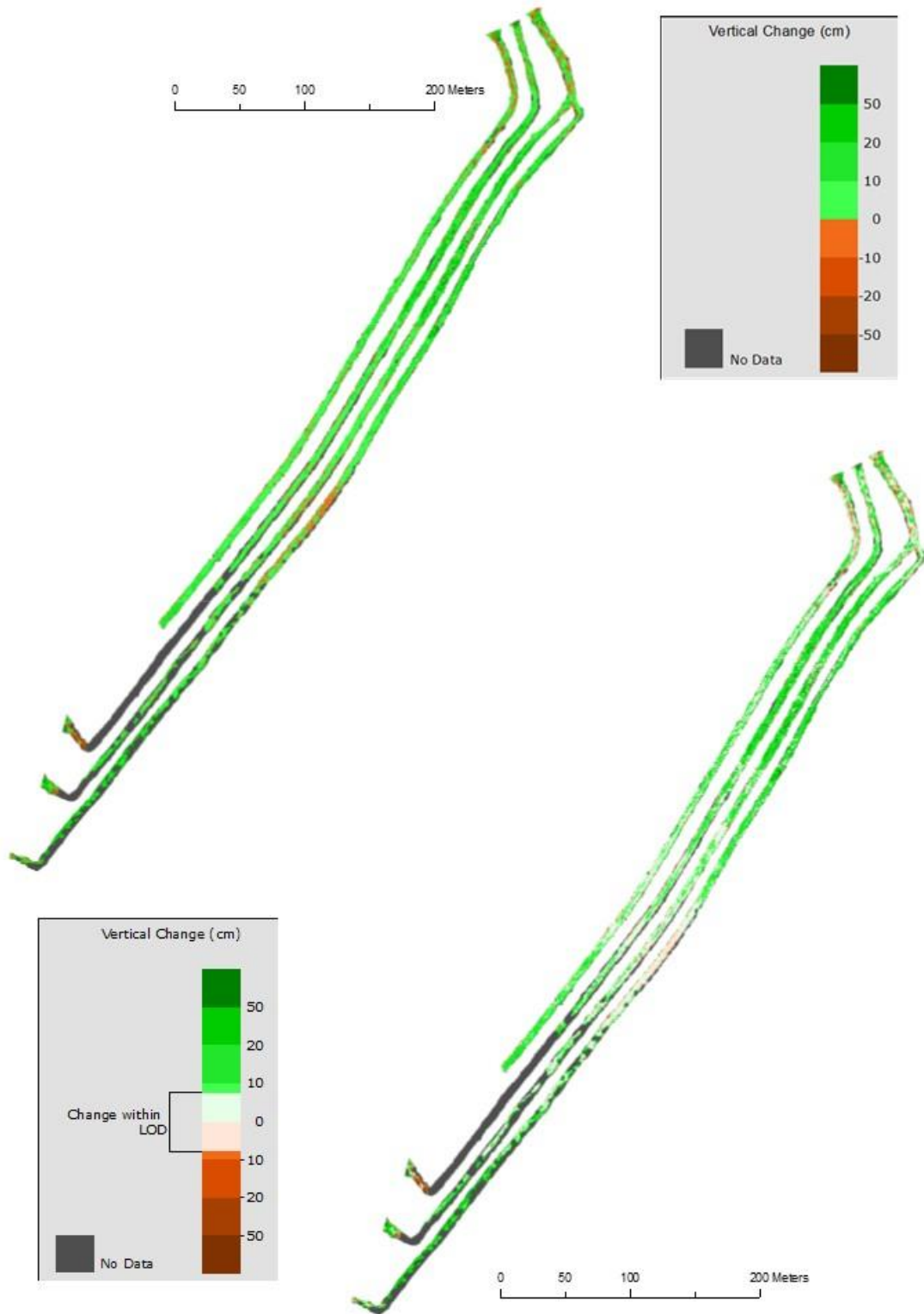


Figure 49: DoD showing vertical change at LT_01, LT_02, LT_03, and LT_04. Green represents vertical accretion and red represents erosion. The top figure uses all pixels, the bottom shows changes that occurred with 68% confidence (LoD = 0.070m).



0 40 80 160 Meters



0 40 80 160 Meters

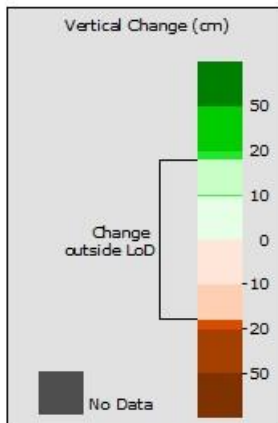


Figure 50: DoD showing vertical change at VDJ_02. Green represents vertical accretion and red represents erosion. The top figure uses all pixels, the bottom shows changes that occurred with 68% confidence (LoD = 0.170m).

Of the eight borrow pits in this category, only LT_01 had an ISCO deployed during this study (Figure 51). However, incoming SSC was measured in all borrow pits. Overall, incoming SSC in these borrow pits ranged from $0.977 \pm 0.284 \text{ g}\cdot\text{l}^{-1}$ to $9.232 \pm 4.616 \text{ g}\cdot\text{l}^{-1}$. The borrow pits in Masstown East marsh had the lowest incoming SSC, followed by Lower Truro marsh, with VDJ_02 having the highest incoming SSC in this category. The mean SSC throughout the tidal cycle in LT_01, as measured with an ISCO, was $1.472 \pm 1.050 \text{ g}\cdot\text{l}^{-1}$. This was the second highest mean SSC measured throughout the tidal cycle behind VDJ_03. The pattern of SSC throughout the tidal period was similar to that of MTW_01, with an initial influx of sediment in suspension as water enters the borrow pit followed by rapid settlement as water approaches, or exceeds, bankfull. SSC then reaches a low shortly after slack tide with a slight resuspension on the ebb tide. Tide 3 had more resuspension on the ebb tide due to a rain event creating turbidity in the borrow pit.

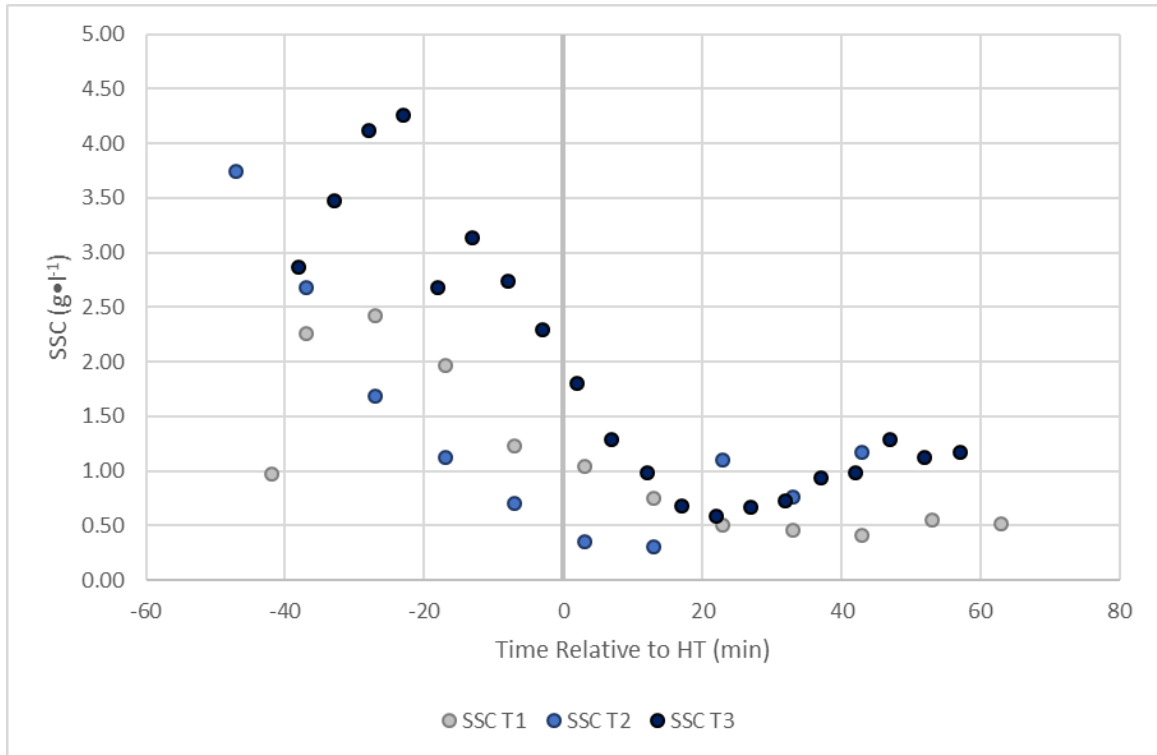


Figure 51: SSC throughout the tidal period in LT_01. There is no water depth in this graph due to an equipment malfunction. Time is relative to high tide (HT).

An ADCP was not deployed in any of the borrow pits that fell into this category.

However, an ADV was deployed in May 2017 in both LT_01 and MTE_03.

Unfortunately, the ADV did not capture the full extent of any of the three tides it was deployed for. From the data available, LT_01 had a mean RHV of $0.30 \text{ m}\cdot\text{s}^{-1}$ on the ebb tide, slightly more than the $0.24 \text{ m}\cdot\text{s}^{-1}$ on the flood. Max recorded velocities were $0.67 \text{ m}\cdot\text{s}^{-1}$ and $0.58 \text{ m}\cdot\text{s}^{-1}$ on the flood and ebb tides, respectively. MTE_03 was more flood dominant with a mean RHV of $0.37 \text{ m}\cdot\text{s}^{-1}$, and a mean RHV of $0.27 \text{ m}\cdot\text{s}^{-1}$ on the ebb tide. Maximum recorded velocities were similar to LT_01 at $0.61 \text{ m}\cdot\text{s}^{-1}$ on the flood tide and $0.57 \text{ m}\cdot\text{s}^{-1}$ on the ebb tide.

3.5 Discussion

Borrow pit infill rates are typically higher than those found in natural creeks, human-made ditches, or restoration sites. While natural creeks are often in dynamic equilibrium and may have very little net annual change, despite seasonal variability in deposition, borrow pits are not (Poirier, 2014; Poirier et al, 2017). Ideally, if the hydrodynamic conditions are suitable for borrow pit excavation, borrow pits will be in a state of continual deposition until a “natural” state is achieved. This is similar to mosquito or drainage ditches, and in managed realignment or saltmarsh restoration sites. Brunetta et al (2019) measured an average accretion rate of $0.06 \text{ m}\cdot\text{yr}^{-1}$ following the managed realignment of a formerly reclaimed site in the Perkpolder Basin, Netherlands. When comparing to the original borrow pit volumes (i.e. as-built volume), the lowest measured infill rate was $0.13 \text{ m}\cdot\text{yr}^{-1}$, in VDJ_03. However, a direct comparison is challenging to make since Brunetta et al (2019) looked at accretion throughout the entire site, including channels and platform. Channels in a cross-section measured at the backshore, in a similar location to where borrow pits are located, appear to have accreted by 0.30m to 0.70m over a two year period (Brunetta et al, 2019), which is comparable to the accretion found at the end of borrow pits (i.e. opposite end from outlet).

One of the biggest differences between the borrow pits this study and the restored tidal flat in Brunetta et al (2019) is that suspended sediment concentrations (SSC) in Perkpolder are much lower than the those found in the Cobequid Bay borrow pits, and comparable to those found in RD_01.

3.5.1 Importance of Suspended Sediment Concentration

The borrow pit at Ryerson – Dugau (RD_01) had a net erosion of -187.70m^3 . This equates to a loss 0.150m loss in surface elevation within the borrow pit when normalizing for area. There were several factors that contributed to RD_01 eroding, including: low suspended sediment concentration (SSC), very high inundation period, an eroding foreshore, and the presence of rock aprons that release water into the pit after tidal waters leave the pit.

As previously mentioned, sediment deposition in tidal creeks and in human-made borrow pits is a product of the availability of sediment and the opportunity to deposit (Reed, 1989; van Proosdij et al, 2006). The hydrodynamic data measured RD_01 revealed that it lacked available sediment and had little to no opportunity to settle. To start, suspended sediment concentrations (SSC) ranged from $0.07\text{-}0.12\text{ g}\cdot\text{l}^{-1}$ which is significantly lower than the borrow pits located in the Cobequid Bay Salmon River estuary. In fact, the SSC at RD_01 was 100 – 1000 times less than the SSC measured in VDJ_03. This is especially important since flocculation plays such a vital role in sediment deposition in hypertidal creek networks (Poirier et al, 2017). Low SSC means there is less availability of sediment to aggregate and settle on the borrow pit bed (O’Laughlin et al, 2014; Poirier et al, 2017). This low rate of settling is compounded by the presence of the rock aprons, which release water from the marsh platform, into the borrow pit, once the tide levels recede below them (Figure 52). This created extended periods of relatively high ebb velocities within the borrow pit, specifically within the borrow pit thalweg. For material to have an opportunity to settle it is paramount that ebb velocities are not fast enough to re-suspend the sediment (Pieterse et al, 2017). Velocity measurements from the ADCP show a consistent period, starting when tide recedes below bankfull, and

continuing for approximately an hour, where velocities range between $0.3\text{m}\cdot\text{s}^{-1} - 0.5\text{m}\cdot\text{s}^{-1}$. This corresponds to a flux in sediment throughout the entire water column, which suggests that more sediment is being re-suspended than deposited. Furthermore, since there is always water moving out of the borrow pit at low tide, rain events can wash sediment into the thalweg and remove it from the borrow pit.



Figure 52: Rock aprons implemented across the borrow pit at RD_01 (right). Ebb tide moving over the rock aprons in RD_01 (left).

The ideal SSC pattern throughout the tidal period is present in the ISCO data measured at LT_01 in the Lower Truro marsh (Figure 53). Poirier et al, 2017 described this pattern in natural hypertidal tidal creeks with high concentrations of suspended sediment. This includes high relative SSC on the incoming tides, which flocculated and settle out of suspension quickly before bankfull, with ebb velocities insufficient to re-suspend sediment. The pattern of SSC in MTW_01 was flatter than LT_01. The SSC on the flood tide was approximately two to three times less than LT_01 and settles to a similar range under calm meteorological conditions. This shows the importance of high SSC, as LT_01 had an infill rate of $0.09 \pm 0.04\text{m}\cdot\text{yr}^{-1}$ versus of $0.00 \pm 0.03\text{m}\cdot\text{yr}^{-1}$ despite

being inundated 21 fewer times out of 46 measured tides than MTW_01. The hydrological conditions in MTW_01 may also be less conducive to deposition as well.

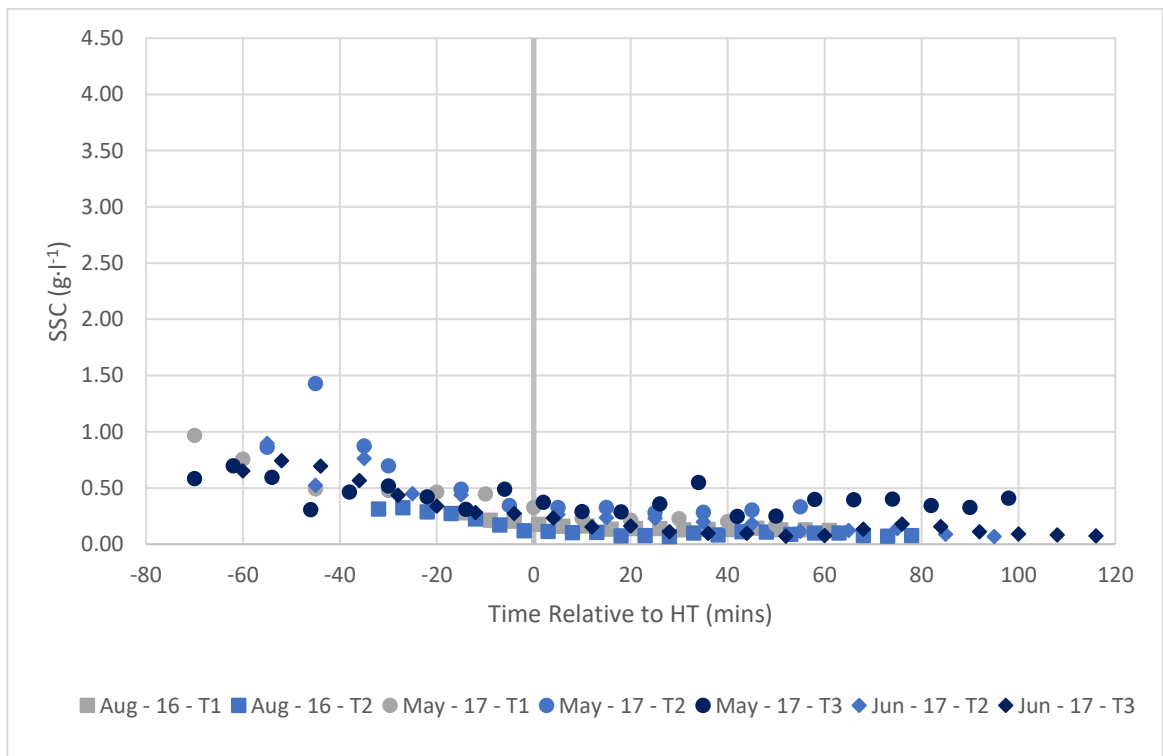
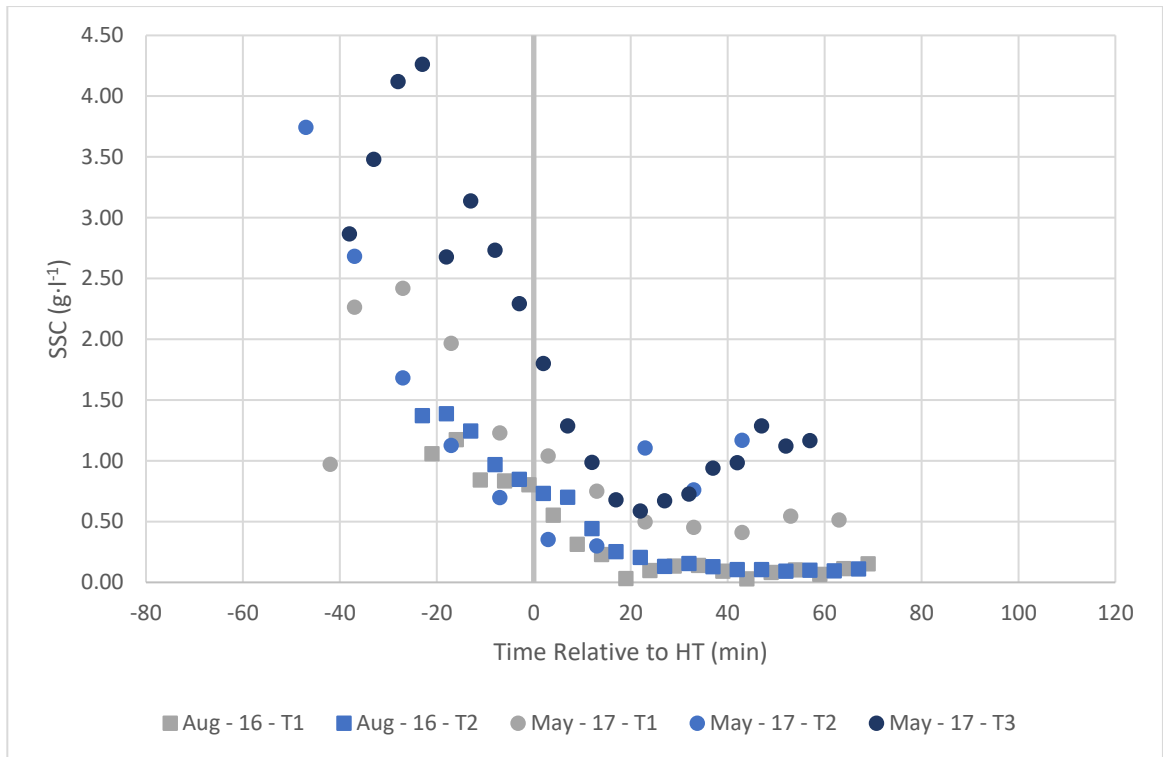


Figure 53: SSC throughout the tidal period for LT_01 (top) and MTW_01 (bottom). Measurements were taking August 2016, May 2017, and June 2017 (MTW_01 only). LT_01 not only had a higher incoming SSC (before high tide), it had similar SSC on the ebb tide except for Tide 3, May 2017, which occurred during a large storm.

3.5.2 Borrow Pit Hydrology

Whereas SSC is the major control on the availability of sediment for borrow pit deposition, hydrology in the borrow pit controls the opportunity for that sediment to settle. Three borrow pits (MTW_01, RD_01, and VDJ_03) had full suite of hydrodynamic instrumentation installed, all three had hydrological conditions that were not conducive to deposition.

Despite the highest suspended sediment concentrations measured in any borrow pit, VDJ_03 experienced a net loss of sediment of -115.60m^3 between November 2016 and August 2017. The high SSC was partially a result of significant erosion occurring in the borrow pit outlet and the areas of the borrow pit near the outlet (Figure 38). This correlated with the greatest bed scour measured in the DoD's, with over 0.60m of bed elevation lost in approximately eight months in some areas. Velocity measurements from the ADCP and water levels from the level logger suggest that VDJ_03 can be slightly ebb dominant when tides exceed bankfull (Figure 40). Ebb dominance is associated with a net transport of sediment out of an estuary or channel (Dronkers, 1986). Furthermore, the mean resolved horizontal velocities (RHV) recorded on the ebb tide are higher than those on the flood tide, at $0.43\text{m}\cdot\text{s}^{-1}$ and $0.24\text{m}\cdot\text{s}^{-1}$, respectively. This is corroborated by the backscatter proxy for SSC from the ADCP which shows a similar incoming and outgoing SSC to be equal. It is possible that ice build-up or a large storm event altered the internal topography within the borrow pit, or the greater saltmarsh, which caused a shift from a regime flood dominance and infill, to one of slight ebb dominance and net sediment loss. It is also possible that the marsh platform drains into the borrow pit following an over marsh tide, leading to an increase in ebb period and velocities.

3.5.3 Role of scour in borrow pit re-vegetation.

Field observations of borrow pits suggest that the borrow pits with the most scour and slumping tend to see the quickest regeneration of vegetation growth. MTW_01 and VDJ_03 had the most extensive vegetation cover of the borrow pits excavated in 2016. Since saltmarsh species, particularly *Spartina alterniflora* can colonize mudflats and tidal creeks through rhizome growth, the direct introduction of pieces of saltmarsh to the borrow pits can precipitate plant growth within the borrow pits. It is unknown how much this will benefit the borrow pit in terms of future infill rates. However, the presence of saltmarsh species is known to increase sedimentation rates both by slowing tidal velocities, decreasing bed turbulence and through sediment sticking to the vegetation (Leonard and Luther, 1995). There was significant bed accretion between patches of vegetation measured in the borrow pits at Lower Truro marsh. However, the re-emergence of vegetation in Lower Truro was probably not due to the scour in the borrow pits, but from scour elsewhere in the estuary or by seeds dispersing into the borrow pit from the saltmarsh platform. A caveat to this is that if the saltmarsh grows sporadically within the borrow pit, it can lead to scour between patches by intensifying channelization of water moving through it (Schwarz et al, 2015).

3.5.4 The potential impact of seasonal variability.

One of the more important considerations when examining infill rate, whether in borrow pits or natural tidal creeks, is the role of seasonal variability in sediment deposition (Poirier et al, 2017). Due to seasonal differences in sediment availability and hydrodynamics, borrow pits volumes may vary throughout the year. Poirier (2014) found that the volume of a natural creek, in the Bay of Fundy, was lowest during the summer

months. In other words, the sediment deposition increased during this time, increasing the bed elevation, and lowering the volume Poirier (2014). Although this study was not setup in a manner to fully address this question, it is hypothesized that having the final aerial surveys take place during the late summer months may increase the amount of measured deposition if the original survey was flown during other months of the year.

3.5.5 Efficacy of UAS for saltmarshes and tidal environments.

Overall, combining unmanned aerial systems (UAS) and structure-from-motion (SfM) is both an efficient and powerful method for obtaining digital surface models (DSMs) for monitoring tidal channels. However, there are still some challenges with these techniques that are specific to tidal environments. The challenge that affected the outcome of this thesis the most was the lack of stable areas to compare between the separate flights (Westaway et al, 2000). Having no stable areas meant that the uncertainty between the two DSMs were derived from propagating the vertical error using both DSMs (Taylor, 1997; Lane et al, 2003). The stable area approach allows for a single value to quantify the deviance between the DSMs, which typically lowers the uncertainty used in the volumetric error calculations. Furthermore, having a stable area allows for the co-registration of the DSMs, which lowers the uncertainty between them even more. In DoD analysis, the absolute accuracy of the two DSMs is less important than the relative accuracy (i.e. co-registration) (Martha et al, 2010; Turner et al, 2015). This is apparent when comparing the propagated error between the two Lower Truro DSMs (0.133m) and the stable area approach (0.068m). This is comparable to Turner et al (2015), who were able to reduce their uncertainty to 0.07m from DSMs with RSME ranging from 0.061m – 0.109m, by co-registering and using a stable area approach. This thesis did not use any

co-registering software (e.g. CloudCompare) which could have further improved the volumetric uncertainty for the Lower Truro site (Turner et al, 2015; Stocker et al, 2015; Dewez et al, 2016). In saltmarshes, to overcome this challenge, it is paramount that an extra emphasis is placed on GCP number and placement, as well as carrying out a vertical accuracy assessment of the bare earth areas in the DSM. This will help quantify and reduce the uncertainty of the individual DSMs.

The average vertical DSM uncertainty, not including the DSMs with no assessments that were given a 0.120m value, was 0.085m, which is consistent with other studies using UAS and SfM to monitor landscape change (Juad et al, 2016; Tonkin and Midgely, 2016; Cook, 2017; Gindraux et al, 2017; Raczynski, 2017). With this average level of accuracy, UAS and SfM can reliably detect vertical changes between two DSMs of 0.120m at 68% confidence and 0.236m at 95% confidence. Compared to LiDAR, which has a standardized vertical accuracy for sandy beaches of 0.150m (Sallenger et al, 2003; Young and Ashford, 2006). This means that LiDAR can detect changes of 0.212m and 0.416m at 68% and 95% CI, respectively, which is double the reliable detection threshold of the average DoD in this thesis. The caveat to this being that the method for determining the uncertainty between the two DEMs is obtained by propagating the individual uncertainties and not by the co-registration, stable area approach.

Due to the nature of deposition in borrow pits and natural tidal channels, which is relatively evenly distributed throughout their area compared to other landscapes, measuring vertical change still represents a challenge. For example, in the borrow pit VDJ_01 only 6.9% and 1.4% of the pixels had changes that exceeded 68% and 95% confidence, respectively. To detect changes less than or equal to 0.100m the average uncertainty between the two DSMs would need to equal 0.071m. The simplest way to

achieve this accuracy is to fly low or increase the resolution of the camera on the drone (Juad et al, 2016; Cook, 2017; Raczynski, 2017). Raczynski (2017) shows that a 50% reduction in GSD size can lead to a similar reduction in uncertainty. Reducing the flight altitude to 40m – 50m would have led to lower DSM uncertainties. However, lower altitude flights take longer to complete and require more GCPs. This can constitute a safety hazard or time issue in hypertidal environments. This also would have meant that the foreshore edge would not have been collected, which was needed for Chapter 2 of this thesis.

Working in a hypertidal environment provides unique challenges when employing UAS and SfM techniques for monitoring landscape change. Having a safety window approximately six hours long limits the comprehensiveness of the aerial survey and the steps to ensure and measure DSM accuracy. To compound this, optimal low tide would be early afternoon so that shadowing is not an issue in the DSM. Furthermore, neap tides are preferable because they may not inundate the platform or the borrow pits/tidal channels. This allows for a subsequent vertical accuracy assessment the following day without having to worry if any changes occurred after the aerial survey. Unfortunately, neap tides in the middle of the day with low wind and no rain do not occur regularly throughout a single season. This means that compromises are made, whether it is fewer GCPs or forgoing robust accuracy assessments.

One of the benefits, and perhaps drawbacks, of using emerging technology is that it advances rapidly. This thesis alone saw the introduction of automatic flight grids, rolling shutter models, UAVs with much higher camera resolution, and UAS that utilize RTK or post processing kinematic (PPK) technology. Using a UAV-RTK Turner et al (2016) were able to achieve an uncertainty of 0.068m without the use of GCPs. Not

having to deploy GCPs, which is the most time-consuming aspect of the workflow, would allow for aerial surveys to be flown at a lower altitude and for a more robust accuracy assessment.

3.5.6 Volumetric Uncertainty

One of the most challenging questions when addressing the efficacy of UAS is the quantifying volumetric uncertainty. As mentioned previously, there are two equations in the literature that are used to quantify volumetric uncertainty between two DSMs. The first is Taylor's (1997) equation for total volumetric uncertainty and the second is Lane et al (2003) equation which adds errors in quadrature. This paper utilizes Taylor's equation since error is spatially variable, and therefore, not entirely pairwise uncorrelated (Milan et al, 2011). The result is a higher estimate of volumetric uncertainty that is reported in papers that use a variation of Lane's equation, such as Haas et al (2016) and Xiang et al (2018). Table 14 compares volumetric uncertainty using both equations. For the below equations, c equals pixel size (0.040m) and n equals the number of pixels. There are no Level of Detection (LoD) thresholds applied below.

Table 14: Table comparing Lane et al (2003) and Taylor (1997) equations for volumetric uncertainty.

DSMs	RSME _Z	δDoD	Lane et al (2003) (m ³)	Taylor (1997) (m ³)
MTW_01 May 2016 and August 2017	=0.106m = 0.090m	0.139m	0.86 ± 0.33	0.86 ± 503.34
MTE_02 May 2016 and August 2017	=0.071m =0.097m	0.120m	648.46 ± 0.74	648.46 ± 346.73
VDJ_03 November 2016 and August 2017	=0.156m =0.074m	0.173m	-115.60 ± 1.39	-115.60 ± 1204.25
RD May 2017 and September 2017	=0.041m =0.072m	0.083m	-187.70 ± 0.37	-187.70 ± 84.95

Using the equation from Lane et al (2003), the resultant uncertainty is significantly lower than when using the equation from Taylor (1997). Using MTW_01 as an example, the Lane et al (2003) equation results in a volumetric uncertainty of 0.33m³ between two DSMs with a vertical uncertainty of 0.139m between them, which have an area of 3621.15m². This value is too low when the accuracy of the DSMs (0.106m and 0.090m) are considered. However, the equation from Taylor (1997) used in this paper is an overestimation of volumetric uncertainty since it assumes all the uncertainty is one direction. This disregards the distribution of errors in the DSM (compared to RTK) which are both positive and negative, resulting in a conservative estimate of error. Adding a LoD provides a better estimation of volumetric uncertainty as it eliminates changes too small to detect when taking the accuracy of the DSMs into account.

The application of a LoD improves the volumetric uncertainty, however, it does have an impact on the calculated volume of change related to the types of processes occurring in the borrow pit. Specifically, applying an LoD can increase or decrease the calculated volumetric change depending on how erosion and deposition is occurring in

the borrow pits, most commonly favouring erosion. For example, using all pixels, VDJ_03 had a volumetric change of $-115.60 \pm 1204.25\text{m}^3$. After applying a LoD (68% CI) to exclude changes below 0.173m, the volumetric change increased to $-288.72 \pm 202.26\text{m}^3$ in the erosional direction. This is because the large vertical changes are happening in concentrated areas within the borrow pit, specifically the bed erosion of the outlet channel and borrow pit thalweg. When that material settles after it is entrained, it is distributed over a much larger areas within the borrow pit, resulting in a change too small to pass the LoD threshold. 12 out of the 13 borrow pits had their net changes decreased after applying an LoD threshold. MTW_02, had a small increase in net change, which can be attributed to the slumps from the borrow pit wall settling in the middle of the pit. When comparing to other papers, applying LoD thresholds had a less biased impact on net change. In Milan et al (2011), applying a uniform 0.20m LoD resulted in an increase in net change twice (deposition favoured), and a decrease in net change twice (erosion favoured). If LoD thresholds are applied in future studies, it would be pertinent to consider how changes are occurring and examining the results with how said changes impact results in mind.

3.6 Conclusion

In the context of dykeland management, borrow pits can be a sustainable practice if implemented strategically. Of the 13 borrow pits studied, eight were infilling at a rate that would allow them to be reused for future dyke topping projects. However, their sustainability depends on being implemented in saltmarshes with optimal hydrodynamic characteristics (e.g. very high SSC). The results in this study show that an incoming SSC greater than $1.00\text{g}\cdot\text{l}^{-1}$ is needed to achieve an infill rate greater than $0.3\text{m}\cdot\text{yr}^{-1}$. In areas

where optimal hydrodynamics are not present, borrow pits are not only unsustainable as a source of material, they also decrease dykeland resiliency by reducing the effective distance in which waves can be dissipated and by introducing unpredictable patterns of erosion in the backshore which otherwise would not occur. The loss of wave attenuation from losing a robust foreshore marsh could be offset by the amount the dyke was topped using the borrow pit depending on the width of the marsh. Dykeland managers must weigh the need to top the dyke against the loss of saltmarsh habitat and the ecosystem services that come with it. To avoid this, it is paramount to implement a comprehensive study of hydrodynamics before any borrow pit excavation is done. Ultimately, borrow pits should only be excavated in saltmarshes that have high suspended sediment concentrations.

The results in this study show that an incoming SSC greater than $1.00\text{g}\cdot\text{l}^{-1}$ and borrow pits should be designed in a manner that minimizes flow velocity. Borrow pits should also not be implemented if natural channels are ebb dominated in the planned areas of excavation. Finally, smaller borrow pits can reduce the amount of bed erosion and scour in the outlet channel. Borrow pits should be monitored continuously following excavation. This includes using unmanned aerial systems (UAS) and structure-from-motion (SfM) to monitor sedimentation and to identify areas of scour.

As demonstrated by this study, UAS combined with structure-from-motion represents a powerful workflow for measuring change in borrow pits, mudflats, and un-vegetated natural tidal creeks. However, there are some drawbacks to the technology, the foremost being the inability to penetrate vegetation. This study shows that changes less than 0.10m can be reliably measured; a number that is steadily decreasing as the technology improves. Another issue that needs to be properly addressed is the

quantification of volumetric uncertainty. The stable area approach should be used when possible, although in hypertidal saltmarshes that remains a significant challenge. The assumption that error is pairwise correlated may also not be appropriated when using UAS-SfM as there is a definite spatial distribution of error in the DSMs, particularly at steep edges and in shadowed areas. Using the equation from Taylor (1997) combined with the application of a level of detection (LoD) threshold may be the best way to properly assess volumetric uncertainty. This is especially important in areas such as borrow pits that do not have large vertical changes, and less important in landscapes that experience large changes, such as eroding cliff faces or in mining. It may be important to design a methodology with the technological limitations of UAS-SfM in mind.

Ultimately, dykeland resiliency is inextricably linked to the maintenance, or even promotion, of saltmarsh habitat in front of dyke infrastructure. This is especially true in the context of green-grey coastal defence systems (Sutton-Grier et al, 2015; Vuik et al, 2016). Borrow pits are an inexpensive method of acquiring material for much needed dyke topping projects, which can keep dykelands from experience coastal flooding. However, saltmarsh integrity is temporarily hindered as the borrow pit is in the process of infilling. If it is able to infill to provide protection, then the practice is sustainable in the context of dykeland management. To ensure this, it is paramount that a scientific framework for implementing borrow pits be established if further excavation of saltmarsh is to continue. This not only requires measurements of hydrodynamics, but of volumetric change within the borrow pit using a non-intrusive, remote sensing technique such as unmanned aerial vehicles and structure-from-motion software.

Chapter 4: Enhancing dykeland resiliency: Guiding principles for dykeland management in a “green-grey” coastal defence system.

A robust foreshore saltmarsh in front of dyke infrastructure makes dykelands more resilient to the impacts of climate change. Not only does the saltmarsh help dykelands adapt to exacerbated coastal hazards by reducing incoming wave energy, they can also help mitigate climate change by sequestering carbon from the atmosphere (Möller et al, 2014; Vuik et al, 2016; Wollenburg et al, 2018). Furthermore, saltmarshes can reduce the cost of maintaining and topping dykes allowing dykeland managers to focus capital on efforts to make dykelands less vulnerable to other issues associated with climate change (e.g. drought, upland flooding). However, in a hybrid coastal defence system there needs to be synergy between green and grey coastal defence structures and strategies. While a fully green coastal defence system is ideal, and in most cases preferable, it is not feasible in some systems. This could be because of unmovable infrastructure within the flood extent, or because of predominant high wave energies. Ultimately, the amount of “green” and the amount of “grey” in a coastal defence system should be assessed on a case-by-case basis. The following chapter constitutes guiding principles regarding the management of foreshore saltmarsh and the implementations of certain structures and strategies for hybrid coastal defence systems in a macrotidal estuary.

4.1 No foreshore saltmarsh should be destroyed to implement coastal defence structures.

In order to increase, or even maintain, dykeland resiliency it is paramount that foreshore saltmarsh is not permanently destroyed in the process of implementing grey

coastal defence structures or strategies. This includes a complete restriction on reclamation projects aimed to turn saltmarsh into agricultural land or land for urban development (van Proosdij and Page, 2012). Foreshore saltmarsh losses constitute a loss of dykeland resiliency. Saltmarsh reclamation in the context of climate change and rising sea levels not only leads to the creation of un-resilient dykelands, it compromises the resiliency of existing dykelands, often in unforeseen ways. For example, reclamation could significantly alter the local tidal prism causing unforeseen patterns of progradation and erosion elsewhere in the estuary (van der Wal et al, 2002). Although dyke construction can sometimes precipitate lateral saltmarsh growth towards the intertidal zone, this progradation does not constitute an enhancement in dykeland resiliency due to the loss of overall foreshore width. Finally, reclamation also contributes to the intensification of climate change by disturbing and destroying saltmarshes, which are valuable carbon sinks (Wollenburg et al, 2018).

4.2 Green and hybrid coastal defence schemes should be implemented wherever possible.

When implementing foreshore protection dykeland managers have a range of options that span the spectrum from green to grey solutions. Green options, such as living shorelines or oyster reefs tend to promote vegetation growth and work to trap and retain soils on foreshore saltmarsh edges or intertidal zone, while maintaining or enhancing ecosystem services (Moody et al, 2013; Gittman et al, 2016; Polk and Eulie, 2018). Grey options, such as foreshore rocking or seawalls, attempt to limit the interaction of wave energy with the foreshore edge (French, 2001). Each option has its own advantages and disadvantages. For example, grey infrastructure can withstand higher energy storms but

are expensive to rebuild once they begin to deteriorate (Sutton-Grier et al, 2015). Seawalls and foreshore rockings also deflect incoming wave energy resulting in significant scour below and adjacent to the structures (Bernatchez and Fraser, 2012; Sutton-Grier et al, 2015). While living shorelines cannot withstand the same magnitude of energy that grey defences can, they typically last longer in the face of smaller, repeated events due to their ability to self-repair (Sutton-Grier et al, 2015). Knowing when to implement which defence is an important aspect of dykeland management.

Kickers are an example of a hybrid defence structure that has shown to enhance dykeland resiliency in the mixed and fluvial zones of the Cobequid Bay – Salmon River Estuary. Kickers are built structures, yet they promote deposition like some green coastal defence implementations. By creating conditions conducive to sediment deposition, saltmarshes can prograde into a former intertidal mudflat whereas rockings restricts foreshore movement in either direction (van Proosdij and Matheson, 2015). For example, rockings were implemented on the foreshore adjacent to NS081_02 (Lower Truro) in 2013. Between 2013 and 2015 the average end point rate along transects in this area was $0.0\text{m} \pm 2.3 \cdot \text{yr}^{-1}$. In the area immediately downstream where a kicker was implemented the average EPR $1.5\text{m} \pm 2.3\text{m} \cdot \text{yr}^{-1}$.

Implementing kickers, as opposed to foreshore rockings, will enhance dykeland resiliency by promoting the progradation of foreshore saltmarshes in fluvial dominant and mixed zones. It is also important that dykeland managers are cognizant of the return on investment for each defence strategy. While implementing foreshore rockings may provide more protection up front, it may also be significantly more expensive, require replacement much sooner and yield only a marginal return on investment. Furthermore, while the cost of implementing kickers has not been established, it is posited that they

would be significantly cheaper per metre of protection offered opposed to foreshore rocking. In low-energy areas (i.e. fluvial dominant), kickers supplemented with living shorelines, and some minor rocking may provide a cheap, green alternative to large-scale foreshore rocking. In this regard, dykelands are made more resilient by integrating green and grey techniques in a hybrid coastal defence system (Sutton-Grier et al, 2015). This provides a tangible example of how dykeland managers can implement green and grey foreshore protection appropriately based on the processes, hydrodynamics and energies in the intertidal zone and the value of the adjacent upland infrastructure.

While human implementations can affect dykeland resiliency by impacting changes in foreshore saltmarsh width, most of the significant change occurs as a result of natural drivers such as channel migration or wave action. In order to successfully manage dykelands in the context of climate change, dykeland managers must have a strong understanding of ecomorphodynamics and processes in the intertidal zone (Bouma et al, 2014). Structures and strategies that are designed to work these processes rather than fighting them are a viable option (Sutton-Grier et al, 2015; van der Nat et al, 2016; Polk and Eulie, 2018). In the Cobequid Bay Salmon River Estuary, some of these options including the managed realignment of dyke infrastructure is now being explored (Sherren et al, 2019). This project will provide flood abatement for the nearby town of Truro, while restoring several hectares of saltmarsh habitat and mitigating climate change by sequestering carbon (Sherren et al, 2019). This could free up capital to supplement existing coastal defences that protect vital infrastructure within Truro with both green and grey structures and strategies.

4.3 Borrow Pits

When it comes to the management of dyke infrastructure regarding the adaptation to sea level rise (SLR) there are three primary options for dykeland managers:

- 1) Hold the line: maintaining the position of dyke infrastructure and raising it to meet future SLR protection standards.
- 2) Managed Realignment: strategic removal, repositioning, or setback of dyke infrastructure, allowing saltmarsh to recolonize the intertidal zone.
- 3) Saltmarsh Restoration: removal of grey coastal protection structures to allow saltmarsh to restore to its complete natural extent.

In the Bay of Fundy, holding the line and managed realignment are the most commonly used options as the presence of infrastructure and high-value agriculture in the natural flood plain limits the possibilities for full-scale saltmarsh restoration. Both holding the line and managed realignment requires significant capital and material costs to implement. In both cases borrow pits represent a cheap alternative to upland material, allowing dykeland managers to address more critical coastal defence and climate change adaptation needs and increasing the length of dykes they can top. However, as mentioned previously, any removal of foreshore saltmarsh represents a loss of dykeland resiliency; therefore, if borrow pits are to be used for dyke topping material their implementation should be based off a rigorous study of local hydrodynamics. This will ensure that borrow pits are a sustainable source of inexpensive dyke topping material, while only reducing dykeland resiliency in the short-term (i.e. <10 years).

4.3.1 Dyke topping material should be borrowed from upland source whenever possible.

The easiest way to top a dyke to climate change standards while maintaining dykeland resiliency is to obtain the dyke topping material from an upland source. Although more expensive than borrow pits, the Nova Scotia Department of Agriculture (NSDA) will source their material from the upland whenever possible. Upland material has several advantages over material derived from foreshore saltmarsh borrow pits. One, the moisture content is much lower in upland sources. This allows for the material to be formed immediately on the dyke, whereas saltmarsh borrow pit material needs to sit on the dyke for a season to allow the moisture and salt content to leech out (D. Hingley, personal communication, April 30, 2018). Also, due to the higher salt content in borrow pit material, vegetation grows on the dyke quicker when upland material is used. This helps reinforce the dyke material and minimizes erosion on the dyke side and toe (D. Hingley, personal communication, April 30, 2018). Most importantly, sourcing upland material for dyke topping allows dykeland managers to maintain the integrity of the foreshore saltmarsh, maximizing its potential for wave attenuation (Vuik et al, 2016).

4.3.2 Borrow pits should only be implemented on robust foreshore saltmarshes with a history of progradation and static change patterns.

Pye (1995) determined that borrow pits can lead to unwanted erosion within the natural tidal networks connected to the borrow pits, as well as near the backshore where the borrow pits are located. Therefore, it is expected that significant, unpredictable erosion may occur if the foreshore edge erodes into an unfilled borrow pit. In this context, borrow pits can reduce the resiliency of a dykeland. Since foreshore width is a key control

on a saltmarsh's capacity to attenuate wave energy, an unfilled borrow pit represents a loss of protection and less resilient intertidal landscape (Vuik et al, 2016). If borrow pits are to be implemented and be a sustainable practice, it is imperative to consider processes both on the marsh platform, and on the foreshore edge. Using tide level data collected in the borrow pits and the infill rate from the as-built volume, a simplified predictive infill curve can be created to determine when the borrow pits will accrete to the original marsh platform elevation. Specifically, infill curves were created based off the changing inundation frequency in the borrow pits as the borrow pit accretes over time. Infill rates decrease over time with inundation frequency as the elevation of the borrow pit grows within the tidal frame. Equations and detailed results for infill curves are available in Appendix 3. The duration for a borrow pit to infill can be compared to the end point change rate (EPR) of the foreshore edge using the results from Chapter 2.

Using foreshore position data as far back as 1938, the EPR rates on the four borrow pit sites in the Cobequid Bay ranged from $-8.18 \pm 1.22 \text{ m}\cdot\text{yr}^{-1}$ to $1.17 \pm 0.82 \text{ m}\cdot\text{yr}^{-1}$. Of the four sites, only MTW_01 in Masstown West marsh is cause for concern. The mean years before urgency (i.e. years before the foreshore erodes into the borrow pit) for MTW_01 was 14.63 years. One section of the borrow pit may be eroded into within 7.91 years if historic rates of erosion continue into the future. Using a "Year 1" infill rate of $0.23 \text{ m}\cdot\text{yr}^{-1}$, the predicted infill duration for MTW_01 is, at a minimum, 18 years, well after the predicted erosion period of 14.63 years (Figure 54). Since the infill rate for MTW_01 during the study period is much lower than the infill rate from the original as-built, it is expected that MTW_01 will most likely not infill within 25 years.

Table 15: Results of EPR in front of borrow pits (BP). Mean, minimum and maximum years before urgency (YBU) was calculated by dividing the width of the foreshore by EPR in the same location. Prograding marshes do not yield an YBU date.

Marsh (Marsh#) Borrow Pit	Mean EPR (in front of BP)	Mean Foreshore Width (to BP)	Mean Y.B.U	Min Y.B.U	Max Y.B.U
Masstown West (NS023w) MTW_01	-8.18 ± 1.22	117.10 ± 24.77	14.63	7.91	23.12
Masstown East (NS023e) MTE_03	0.23 ± 0.21	71.55 ± 12.41	Prograding	224.54	Prograding
VDJ (NS012) VDJ_03	-0.60 ± 0.80	248.12 ± 35.20	531.97	120.14	Prograding
Lower Truro (NS081) LT_01	1.17 ± 0.82	113.01 ± 48.45	Prograding	787.50	Prograding

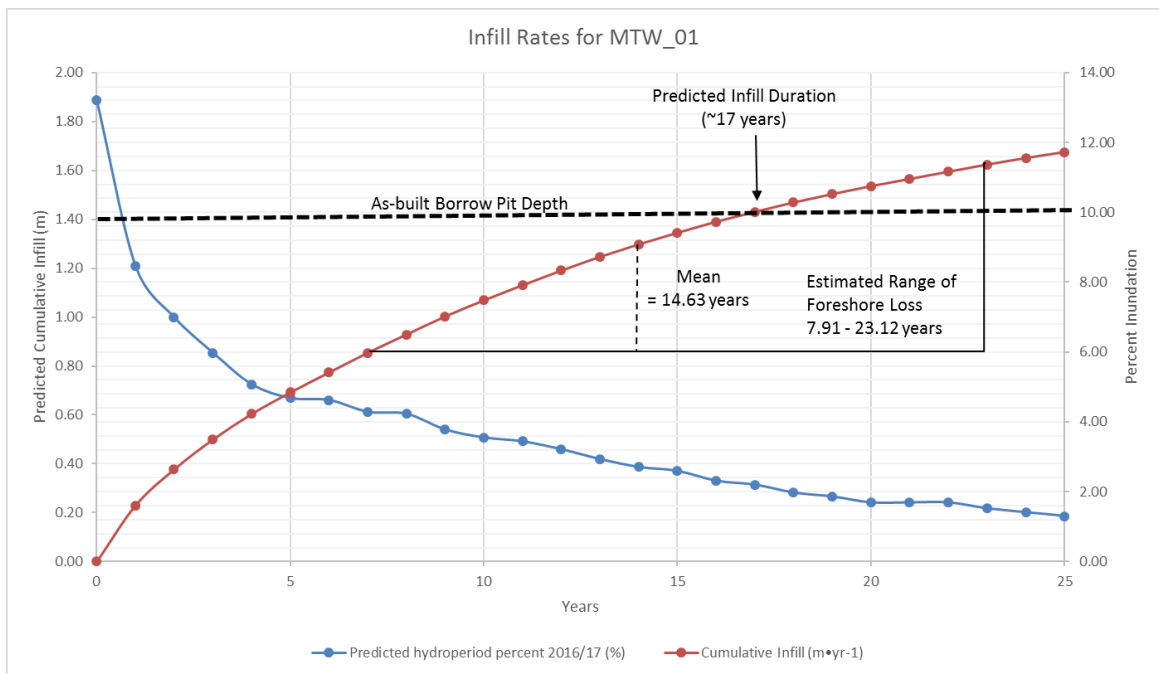


Figure 54: Predicted cumulative infill and hydroperiod for MTW_01.

This shows that borrow pit excavation can be maladaptive irrespective of optimal hydrodynamics for deposition. If borrow pit excavation is to be a sustainable practice for providing dyke topping material, without detracting from dykeland resiliency, it is imperative to consider the state of foreshore change. For example, the mean foreshore width in front of VDJ_03 is 248.12 ± 35.20m, was historically prograding, and now the

foreshore edge is mostly static. If the hydrodynamic conditions improve, VDJ_03 would prove to be a suitable location for borrow pit excavation. As it stands, VDJ_03 will not infill for approximately 33 years (Figure 55).

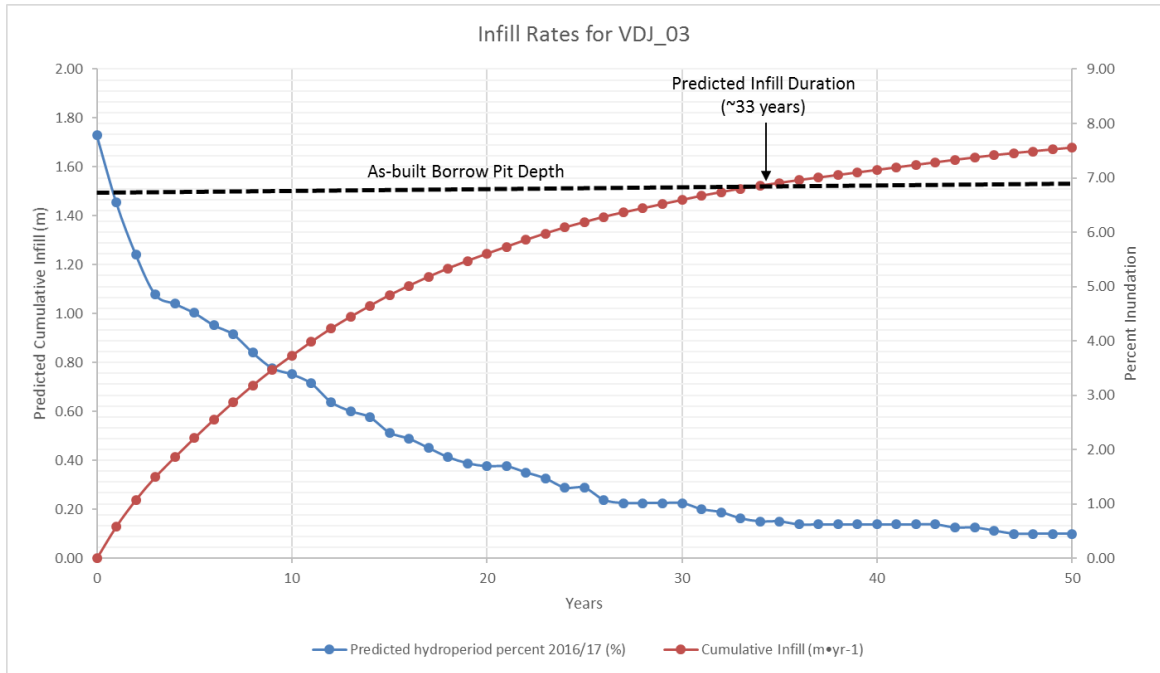


Figure 55: Predicted cumulative infill and hydroperiod for VDJ_03.

4.3.3 Borrow pits should only be implemented in low-energy, highly-turbid systems.

Results from Chapter 3, as well as observations in the field, suggest that borrow pits are successful in low-energy, highly turbid parts of an estuary. Specifically, borrow pits were found to be much more successful in the fluvial zones of estuaries than mixed and wave dominated sections. Anecdotally, the closer to the turbidity maxima the borrow pit is located, the quicker the infill. Two borrow pits that weren't examined in this study were located at NS067 North Onslow (excavated in 2012) and NS024 Noel Shore (excavated before 1966). NS067 North Onslow is located at the turbidity maxima of the Cobequid Bay Salmon River Estuary, while NS024 Noel Shore is in the wave dominated

zone of the estuary, approximately 3600m downstream (Dalrymple et al, 2012). Table 16 shows the hydrodynamic characteristics near each borrow pit.

Table 16: The hydrodynamic characteristics near NS024 Noel Shore and NS067 North Onslow.

Borrow Pit	NS024 Noel Shore	NS067 North Onslow
Process Dominated Zone	Wave	Fluvial
SSC	<0.5 g·l ⁻¹	94.09 g·l ⁻¹ (Purcell, 2020)
Max Fetch	~1500m	<50m
Max Tidal Range	>16m	>5m

Figure 56 shows that after three years the borrow pit at NS067 has infilled significantly and is full of vegetation, while NS024 has infilled very little over the 47 years between images (Figure 57). As a result, borrow pits excavated in areas with similar hydrodynamic conditions as the borrow pit at NS067 should only impact the integrity of the foreshore saltmarsh, and therefore dykeland resiliency, for a short period of time.

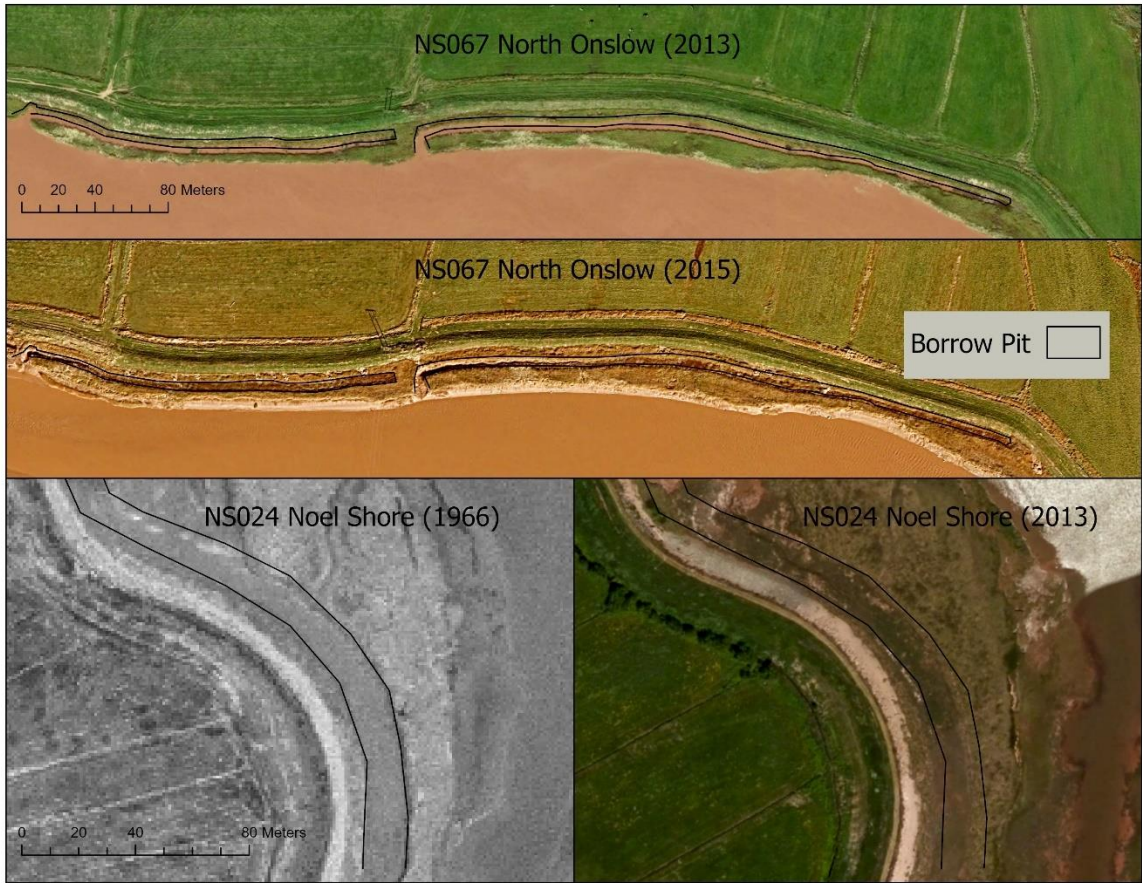


Figure 56: A map showing the deposition of sediment and the recovery of vegetation in two borrow pits in NS024 Noel Shore and NS067 North Onslow marshes.



Figure 57: The borrow pit at NS024 Noel Shore (CBWES, 2019).

LT_01 is less than a kilometer downstream from NS067 North Onslow. Results from Chapter 3 suggest that LT_01 should only have a short-to-medium impact on dykeland resiliency due to their high infill rates. The mean incoming suspended sediment concentration (SSC) was $5.230 \pm 0.390 \text{ g}\cdot\text{l}^{-1}$ and the inundation frequency during this time was 2.97%. Ultimately, this led to a predicted infill duration of approximately nine years after an initial infill rate of $0.40 \text{ m}\cdot\text{yr}^{-1}$ (Figure 58). At this rate, the borrow pit should infill in nine years, meaning it will be at an elevation in which it can provide a similar level of wave attenuation prior to borrow pit excavation. Borrow pits that behave like LT_01 are sustainable in the context of dykeland management.

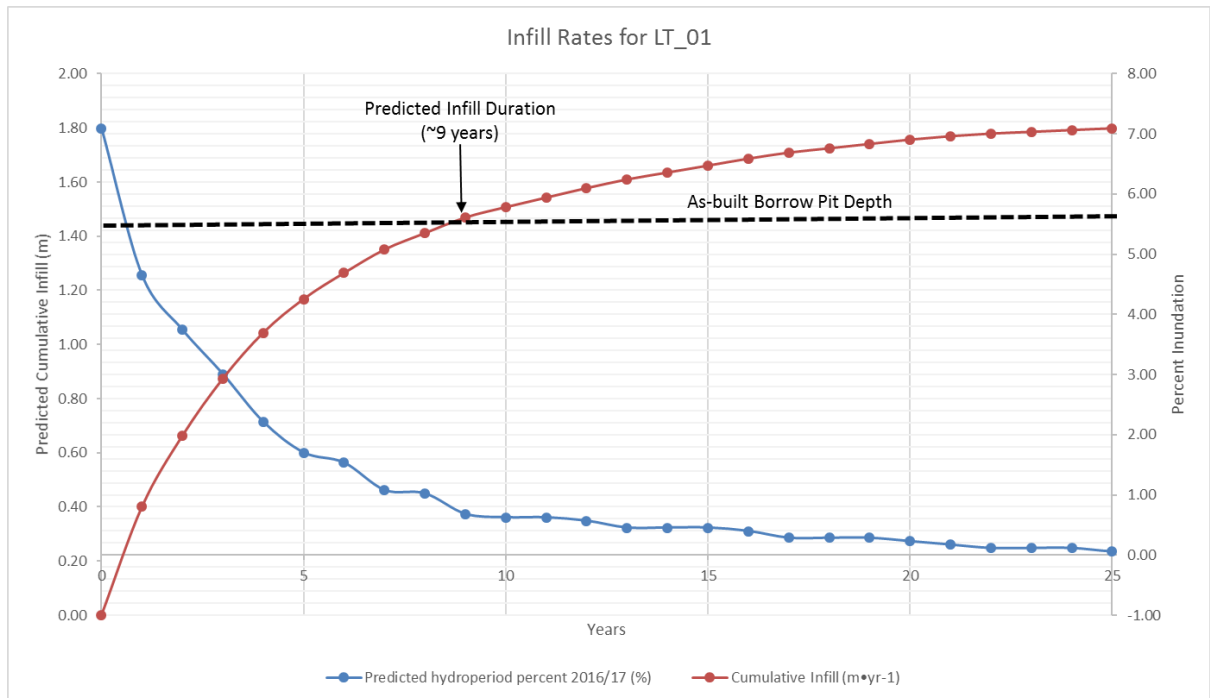


Figure 58: Predicted cumulative infill and hydroperiod for LT_01.

4.3.4 Borrow pits should be based off a scientific framework for implementation.

The success of borrow pit infill is function of the availability of sediment entering the pit, and the opportunity for that sediment to deposit (Reed, 1989; van Proosdij et al, 2006). Availability is influenced by the amount of sediment in the water, flocculation rate, and the number of times the borrow pit is inundated (Christiansen et al, 2000; Temmerman et al, 2004; Poirier et al, 2017). Opportunity is impacted by hydrological factors such as flow velocity, turbulence, presence of vegetation, and whether flow is ebb or flood dominated (Voulgaris and Meyers, 2004; Yang et al, 2008). Decisions regarding borrow pit implementation must be made following a rigorous study of hydrodynamics and end point change rate. The study should address the following:

- **Foreshore width** for the entire length of borrow pit. Should be greater than 50m in mixed and wave-dominated areas within an estuary (van Proosdij and Page, 2012). In fluvial areas width can be less than 50m but more investigation is

required. A caveat to this is that EPR should not predict erosion of the foreshore edge into the borrow pit within 50 years.

- **Foreshore erosion rates:** Historical and contemporary erosion rates of the foreshore edge. Borrow pits perform better in progradational saltmarshes and they tend to be depositional in nature. Furthermore, if the current state of the foreshore edge is erosional, it may not be a suitable location for a borrow pit depending on the foreshore width.
- **Suspended sediment concentration** dictates the availability of sediment for deposition in borrow pits (Christiansen et al, 2000). An ISCO automated water sampler employed in the channel that the borrow pit will be connected to would be able to determine the average SSC, but also the pattern of SSC throughout the tidal cycle (Poirer et al, 2017). This can identify fluxes of resuspension that can help determine whether channel is depositional or erosional. This should be supplemented by an Acoustic Doppler Current Profiler (ADCP) which can measure SSC and velocity throughout the water column. Rising stage bottles (RSBs) in the channel can help determine the initial SSC during flood tide. SSC should exceed $1 \text{ g}\cdot\text{l}^{-1}$.
- ADCP and ISCO data can also determine whether the channel is **flood or ebb dominated**. Flood dominated channels are preferable as they tend to have a net import of sediment throughout a single tidal cycle (Dronkers, 1986). It should be noted that dominance can change depending on hydrological factors such as tide height (e.g. exceeding bankfull) and storm events.
- **Level loggers and platform elevation** can provide the inundation frequency of the borrow pit, which is another component on availability. Level loggers should be deployed in the channel at an elevation equal to the planned bed elevation of the borrow pit.
- **Planned as-built volume** obtained through conventional survey methods or with an unmanned aerial system and structure-from-motion.
- **Georeferenced orthomosaic** of saltmarsh where borrow pit is to be excavated to compare the baseline condition of the marsh. Pye (1995) found that construction practices that occurred when excavating a borrow pit were a significant factor in reducing saltmarsh integrity.

Only if all the factors above show that the saltmarsh is suitable for borrow pit excavation should a borrow pit be implemented. However, following the excavation of a borrow pit, constant monitoring is required and adaptive management must be implemented if the borrow pit is not showing signs of adequate deposition.

4.3.5 Adaptive management strategies for failing borrow pits.

While no research currently exists on adaptive management for borrow pits, there are a number of studies and initiatives centred on enhancing elevation capital in anthropogenically modified marshes and restoration sites that could be applied to failing borrow pits (Burdick et al, 2019; Vuik et al, 2019). These adaptive management approaches typically revolve around slowing down water velocity, establishing vegetation, and promoting deposition. One method to do this is to build brushwood fences/dams or brush treatments (Burdick et al, 2019; Vuik et al, 2019). Brush treatments have been used in marshes in New England, U.S.A. to elevate mosquito ditches (Burdick et al, 2019). These treatments typically consist of mowed saltmarsh plants which are placed and secured within the ditches (Burdick et al, 2019). The treatments not only slow the velocities within the ditches, they promote the regrowth of saltmarsh vegetation (Burdick et al, 2019). This could easily be used in borrow pits as grubbed material (including saltmarsh plants) is often stockpiled on the marsh platform. If it those piles were redistributed within the borrow pits it is possible that it would slow velocities within the borrow pits, promoting deposition, and re-introduce saltmarsh vegetation within the borrow pits. This would create a positive feedback for deposition as more sediment and vegetation is introduced to the borrow pit. A similar approach would be to use brushwood dams at the entrance of the outlet channels and in strategic positions along the borrow pit where bed scour occurs. Brushwood dams work like brush treatments by slowing velocities and trapping sediment behind them (Vuik et al, 2019). Finally, the last adaptive management approach that could be used it to plant seeds, seedlings, or sprigs in the borrow pit. This method has been used in restoration sites around the world in order to promote sedimentation (Broome et al, 1987; Zelder, 2017). Seeding or planting saltmarsh

species within a failing borrow pit would introduce vegetation and promote sedimentation (Broome et al, 1987). Planting could also be applied to stabilize scoured borrow pit walls, which could prevent them from eroding into the dyke infrastructure. Ensuring borrow pits infill is paramount in regards to dykeland resiliency as an unfilled borrow pit reduces the effective width the foreshore can attenuate wave energies and possibly introduce scour near the dyke structure.

4.4 Conclusion

Ultimately, dykeland resilience is contingent on a variety of factors including the existence of vital infrastructure, socioeconomics, and the capacity to respond if a significant flooding or erosion event occurs (Cutter et al, 2009, IPCC, 2014). Many of these factors are beyond the scope of dykeland managers. However, dykeland managers can control how the flood and erosion adaptation structures and strategies they implement interact with the foreshore saltmarsh. If dykeland managers wish to enhance the resiliency of their dykelands it is paramount they work to maintain or even promote the robustness of saltmarshes on the foreshore of their dykes (Vuik et al, 2016). This means utilizing green structures and strategies in hybrid coastal defence systems whenever possible (Sutton-Grier et al, 2015). It also means recognizing where hard grey structures and strategies need to be implemented in order to protect the dykelands from coastal flooding and erosion. This requires rigorous studies to find the best solutions to address climate change and the associated rise in sea levels.

References

- Acker, S., Ash, R., Bond, J., Lewis, P., & Morse, A. (2016). *Association of Nova Scotia Land Surveyors: NAD83 User Guide*. Association of Nova Scotia Land Surveyors.
- Allen, J. R. (2000). Morphodynamics of Holocene salt marshes: a review sketch from the Atlantic and Southern North Sea coasts of Europe. *Quaternary Science Reviews*, *19*(12), 1155 - 1231.
- Allen, J. R., & Haslett, S. K. (2014). Salt-marsh evolution at Northwick and Aust warths, Severn Estuary, UK; a case of constrained autocyclicality. *Atlantic Geology*, *50*, 1-16.
- Anderson, M. E., & Smith, J. M. (2014). Wave attenuation by flexible, idealized salt marsh vegetation. *Coastal Engineering*, *83*, 83-92.
- Andrews, J. E., Burgess, D., Cave, R. R., Coombes, E. G., Jickells, T. D., Parkes, D. J., & Turner, R. K. (2006). Biogeochemical value of managed realignment, Humber estuary, UK. *Science of the Total Environment*, *371*(1-3), 19-30.
- Bakker, M., & Lane, S. N. (2017). Archival photogrammetric analysis of river–floodplain systems using Structure from Motion (SfM) methods. *Earth Surface Processes and Landforms*, *42*(8), 1274-1286.
- Barbier, E. B., Hacker, S. D., Kennedy, C., Koch, E. W., Stier, A. C., & Silliman, B. R. (2011). The value of estuarine and coastal ecosystem services. *Ecological monographs*, *81*(2), 169-193.
- Bernatchez, P., & Fraser, C. (2012). Evolution of coastal defence structures and consequences for beach width trends, Québec, Canada. *Journal of Coastal Research*, *28*(6), 1550-1556.
- Bleakney, J. S. (2004). *Sods, soil, and spades: the Acadians at Grand Pre and their dykeland legacy*. McGill-Queen's University Press.

- Blott, S. J., Pye, K., van der Wal, D., & Neal, A. (2006). Long-term morphological change and its causes in the Mersey Estuary, NW England. *Geomorphology*, 81(1-2), 185-206.
- Bouma, T. J., van Belzen, J., Balke, T., Zhu, Z., Airoidi, L., Blight, A. J., . . . Lara, J. L. (2014). Identifying knowledge gaps hampering application of intertidal habitats in coastal protection: Opportunities & steps to take. *Coastal Engineering*, 87, 147-157.
- Brasington, J., Langham, J., & Rumsby, B. (2003). Methodological sensitivity of morphometric estimates of coarse fluvial sediment transport. *Geomorphology*, 53(3-4), 299-316.
- Broome, S.W., Seneca, E.D., and Woodhouse Jr., W.W. (1987). Tidal salt marsh restoration. *Aquatic Botany*, 32, 1-22.
- Browne, J. P. (2011). Impacts on *Spartina alterniflora*: Factors Affecting Salt Marsh Edge Loss (Doctoral Dissertation).
- Browne, J. P. (2017). Long-term erosional trends along channelized salt marsh edges. *Estuaries and Coasts*, 40(6), 1566-1575.
- Brunetta, R., Ciavola, P., & De Paiva, J. S. (2019). Morphological evolution of an intertidal area following a set-back scheme: a case study from the Perkpolder Basin (The Netherlands). *Frontiers in Earth Science*, 7, 228.
- Burdick, D. M., Moore, G. E., Adamowicz, S. C., Wilson, G. M., & Peter, C. R. (2019). Mitigating the Legacy Effects of Ditching in a New England Salt Marsh. *Estuaries and Coasts*, 1-8.
- Cahoon, D. R. (2015). Estimating relative sea-level rise and submergence potential at a coastal wetland. *Estuaries and Coasts*, 38(3), 1077-1084.
- Carrivick, J. L., Smith, M. W., & Carrivick, D. M. (2015). Terrestrial laser scanning to deliver high-resolution topography of the upper Tarfala valley, arctic Sweden. *GFF*, 137(4), 383-396.

- Carrivick, J. L., Smith, M. W., & Quincey, D. J. (2016). *Structure from Motion in the Geosciences*. John Wiley & Sons.
- Cavalli, M., Goldin, B., Comiti, F., Brardinoni, F., & Marchi, L. (2017). Assessment of erosion and deposition in steep mountain basins by differencing sequential digital terrain models. *Geomorphology*, *291*, 4-16.
- CBCL (van Proosdij, D., Leys, V., Smith, G., Forbes, J., Wilson, A., Fernandez, V., . . . Thibault, A. (2015). *Truro Flood Risk Study*. Final report submitted to the Joint Flood Advisory Committee Colchester County, Town of Truro and Millbrook First Nations. 150 pp.
- Chauhan, P. P. (2009). Autocyclic erosion in tidal marshes. *Geomorphology*, *110*(3-4), 45-57.
- Chmura, G. L., Ainsfeld, S. C., Cahoon, D. R., & Lynch, J. C. (2003). Global carbon sequestration in tidal, saline wetland soils. *Global Biogeochemical Cycles*, *17*(4), 1-12.
- Christiansen, T., Wilberg, P. L., & Milligan, T. G. (2000). Flow and sediment transport on a tidal salt marsh surface. *Estuarine, Coastal and Shelf Science*, *50*(3), 315-331.
- Cook, K. L. (2017). An evaluation of the effectiveness of low-cost UAVs and structure from motion for geomorphic change detection. *Geomorphology*, *278*, 195-208.
- Corman, S. S., Roman, C. T., King, J. W., & Appleby, P. G. (2012). Salt marsh mosquito-control ditches: sedimentation, landscape change, and restoration implications. *Coastal Research*, *28*(4), 874-880.
- Costanza, R., Pérez-Maqueo, O., Martinez, M. L., Sutton, P., Anderson, S. J., & Mulker, K. (2008). The value of coastal wetlands for hurricane protection. *AMBIO: A Journal of the Human Environment*, *37*(4), 241-248.
- Crain, C. M., & Bertness, M. D. (2006). Ecosystem engineering across environmental gradients: implications for conservation and management. *Bioscience*, *56*(3), 211-218.

- Crewe, B. (2004). Characterization of sediment in the Salmon River Estuary (Master's Thesis). Dalhousie University, Halifax, Nova Scotia.
- Dale, J., Burgess, H. M., Burnside, N. G., Kilkie, P., Nash, D. J., & Kundy, A. B. (2018). The evolution of embryonic creek systems in a recently inundated large open coast managed realignment site. *Anthropocene Coasts*, 1(1), 16-33.
- Dalrymple, R. W., Knight, R. J., Zaitlin, B. A., & Middleton, G. (1990). Dynamics and facies model of a macrotidal sand-bar complex, Cobequid Bay—Salmon River Estuary (Bay of Fundy). *Sedimentology*, 37(4), 577-612.
- Dalrymple, R. W., Mackay, D. A., Ichaso, A. A., & Choi, K. S. (2012). Processes, morphodynamics, and facies of tide-dominated estuaries. In *Principles of Tidal Sedimentology* (pp. 79-107). Dordrecht: Springer.
- Daniel, J. F. (1971). *Channel Movement of Meandering Indiana Streams*. US Government Printing Office.
- Desplanque, C., & Mossman, D. J. (2004). Tides and their seminal impact on the geology, geography, history, and socio-economics of the Bay of Fundy, eastern Canada. *Atlantic Geology*, 40(1), 65. doi:10.4138/729
- Devereux, B., & Amble, G. (2009). Airborne LiDAR: instrumentation, data acquisition and handling. *Laser Scanning for the Environmental Sciences*, 102-114.
- Dewez, T., Girardeau-Montaut, D., Allanic, C., & Rohmer, J. (2016). Facets: A cloudcompare plugin to extract geological planes from unstructured 3d point clouds. *XXIII ISPRS Congress, Jul 2016, Prague, Czech Republic*, 799-804.
- Doney, S. C., Ruckelshaus, M., Duffy, M. E., Barry, J. P., Chan, F., English, C. A., . . . Polvina, J. (2012). Climate change impacts on marine ecosystems. *Annual Review of Marine Science*, 4, 11-37.
- Doody, J. P. (2004). 'Coastal squeeze'—an historical perspective. *Journal of Coastal Conservation*, 10(1), 129-138.

- Doody, J. P. (2008). *Saltmarsh Conservation, Management and Restoration*. Brampton: Springer.
- Dronkers, J. (1986). Tidal asymmetry and estuarine morphology. *Netherlands Journal of Sea Research*, 20(2-3), 117-131.
- Dyer, K. R., & Taylor, P. A. (1973). A simple, segmented prism model of tidal mixing in well-mixed estuaries. *Estuarine and Coastal Marine Science*, 1(4), 411-418.
- Dyer, K. R., Christie, M. C., Feates, N., Fennessy, M. J., Perjup, M., & van der Lee, W. (2000). An Investigation into Processes Influencing the Morphodynamics of an Intertidal Mudflat, the Dollard Estuary, The Netherlands: I. Hydrodynamics and Suspended Sediment. *Estuarine Coastal and Shelf Science*, 50, 607-625.
- Elsley-Quirk, T., & Adamowicz, S. C. (2016). Influence of physical manipulations on short-term salt marsh morphodynamics: Examples from the North and Mid-Atlantic Coast, USA. *Estuaries and Coasts*, 39(2), 423-439.
- ESRI. (n.d.). *Surface Volume (3D Analyst)*. Retrieved 2018, from <https://pro.arcgis.com/en/pro-app/tool-reference/3d-analyst/surface-volume.htm>
- French, J. R., Benson, T., & Burningham, H. (2005). Morphodynamics and Sediment Flux in the Blyth Estuary, Suffolk, UK. In *High Resolution Morphodynamics and Sedimentary Evolution of Estuaries* (pp. 143-171). Dordrecht: Springer.
- French, P. W. (2001). *Coastal Defences: processes, problems and solutions*. New York: Routledge.
- Friedrichs, C. T., & Perry, J. E. (2001). Tidal salt marsh morphodynamics: a synthesis. *Journal of Coastal Research*, [Special Issue] 27, 7-37.
- Friess, D. A., Möller, I., Spencer, T., Smith, G. M., Thomson, A. G., & Hill, R. A. (2014). Coastal saltmarsh managed realignment drives rapid breach inlet and external creek evolution, Freiston Shore (UK). *Geomorphology*, 208, 22-33.
- Fuller, I. C., Large, A. R., Charlton, M. E., Heritage, G. L., & Milan, D. J. (2003). Reach-scale sediment transfers: an evaluation of two morphological budgeting

- approaches. *Earth Surface Processes and Landforms: The Journal of the British Geomorphological Research Group*, 28(8), 889-903.
- Gabet, E. J. (1998). Lateral migration and bank erosion in a saltmarsh tidal channel in San Francisco Bay, California. *Estuaries*, 21(4), 745-753.
- Garbutt, R. A., Reading, C. J., Wolters, M., Gray, A. J., & Rothery, P. (2006). Monitoring the development of intertidal habitats on former agricultural land after the managed realignment of coastal defences at Tollesbury, Essex, UK. *Marine Pollution Bulletin*, 53(1-4), 155-164.
- Gedan, K., Kirwan, M. L., Wolanski, E., Barbier, E. B., & Silliman, B. R. (2011). The present and future role of coastal wetland vegetation in protecting shorelines: answering recent challenges to the paradigm. *Climate Change*, 106(1), 7 - 29.
- Gindraux, S., Boesch, R., & Farinott, D. (2017). Accuracy assessment of digital surface models from unmanned aerial vehicles' imagery on glaciers. *Remote Sensing*, 9(2), 186.
- Gittman, R. K., Peterson, C. H., Currin, C. A., Joel Fodrie, F., Piehler, M. F., & Bruno, J. F. (2016). Living shorelines can enhance the nursery role of threatened estuarine habitats. *Ecological Applications*, 26(1), 249-263.
- Gómez-Gutiérrez, Á., Schnabel, S., Berenguer-Sempere, F., Lavado-Contador, F., & Rubio-Delgado, J. (2014). Using 3D photo-reconstruction methods to estimate gully headcut erosion. *Catena*, 120, 91-101.
- Gonçalves, J. A., & Henriques, R. (2015). UAV photogrammetry for topographic monitoring of coastal areas. *ISPRS Journal of Photogrammetry and Remote Sensing*, 104, 101-111.
- Greenburg, D. A., Blanchard, W., Smith, B., & Barrow, E. (2012). Climate change, mean sea level and high tides in the Bay of Fundy. *Atmosphere-Ocean*, 50(3), 261-276.
- Haas, F., Hilger, L., Neugirg, F., Umstädter, K., Bretiung, C., Fischer, P., . . . Schmidt, J. (2016). Quantification and analysis of geomorphic processes on a recultivated iron

ore mine on the Italian island of Elba using long-term ground-based lidar and photogrammetric SfM data by a UAV. *Natural Hazards and Earth System Sciences*, 16(5), 1269-1288.

Hugenholtz, C. H., Whitehead, K., B. O., Barchyn, T. E., Moorman, B. J., LeClair, A., . . . Hamilton, T. (2013). Geomorphological mapping with a small unmanned aircraft system (sUAS): Feature detection and accuracy assessment of a photogrammetrically-derived digital terrain model. *Geomorphology*, 194, 16-24.

Hugenholtz, C., Brown, O., Walker, J., Barchyn, T., Nesbit, P., Kucharczyk, M., & Myshak, S. (2016). Spatial accuracy of UAV-derived orthoimagery and topography: Comparing photogrammetric models processed with direct georeferencing and ground control points. *Geomatica*, 70(1), 21-30.

IPCC, 2013: *Climate Change 2013: The Physical Science Basis. Contribution of Working Group I to the Fifth Assessment Report of the Intergovernmental Panel on Climate Change*. Stocker, T.F., D. Qin, G.-K. Plattner, M. Tignor, S.K. Allen, J. Boschung, A. Nauels, Y. Xia, V. Bex and P.M. Midgley. Cambridge University Press, Cambridge, United Kingdom and New York, NY, USA, 1535 pp, doi:10.1017/CBO9781107415324.

IPCC, 2014a: *Climate Change 2014: Impacts, Adaptation, and Vulnerability. Part B: Regional Aspects. Contribution of Working Group II to the Fifth Assessment Report of the Intergovernmental Panel on Climate Change*. Barros, V.R., C.B. Field, D.J. Dokken, M.D. Mastrandrea, K.J. Mach, T.E. Bilir, M. Chatterjee, K.L. Ebi, Y.O. Estrada, R.C. Genova, B. Girma, E.S. Kissel, A.N. Levy, S. MacCracken, P.R. Mastrandrea, and L.L. White. Cambridge University Press, Cambridge, United Kingdom and New York, NY, USA, 688 pp.

Irrgang, A. M., Lantuit, H., Manson, G. K., Günther, F., Grosse, G., & Overduin, P. P. (2018). Variability in rates of coastal change along the Yukon coast, 1951 to 2015. *Journal of Geophysical Research: Earth Surface*, 123(4), 779-800.

Jackson, C. W. (2009). *The Ambur project: Analyzing Moving Boundaries Using R*. Department of Geology & Geography Georgia Southern University.

James, M. R., & Robson, S. (2014). Mitigating systematic error in topographic models derived from UAV and ground-based image networks. *Earth Surface Processes and Landforms*, 39(10), 1413-1420.

- James, T. S. (2014). *Relative sea-level projections in Canada and the adjacent mainland United States*. Natural Resources Canada.
- Jaud, M., Grasso, F., Le Dantec, N., Verney, R., Delacourt, C., Ammann, D. J., & Grandjean, P. (2016). Potential of UAVs for monitoring mudflat morphodynamics (application to the seine estuary, France). *ISPRS International Journal of Geo-Information*, 5(4), 50.
- Kalacska, M., Chmura, G., Lucanus, O., Bérubé, D., & Arroyo-Mora, J. P. (2017). Structure from motion will revolutionize analyses of tidal wetland landscapes. *Remote Sensing of Environment*, 199, 14-24.
- Kirwan, M. L., Temmerman, S., Skeeahan, E. E., Guntenspergen, G. R., & Fagherazzi, S. (2016). Tidal salt marsh morphodynamics: a synthesis. *Nature Climate Change*, 6(3), 253-260.
- Klingeman, P. C., Kehe, S. M., & Owusu, Y. A. (1984). *Streambank erosion protection and channel scour manipulation using rockfill dikes and gabions*. Oregon State University, Department of Civil Engineering. Corvallis: Water Resources Research Institute.
- Kranck, K. (1981). Particulate matter grain-size characteristics and flocculation in a partially mixed estuary. *Sedimentology*, 28, 107-114.
- Lane, S. N., Westaway, R. M., & Murray-Hicks, D. (2003). Estimation of erosion and deposition volumes in a large, gravel-bed, braided river using synoptic remote sensing. *Earth Surface Processes and Landforms: The Journal of the British Geomorphological Research Group*, 28(3), 249-271.
- Leonard, L. A., & Luther, M. E. (1995). Flow hydrodynamics in tidal marsh canopies. *Limnology and oceanography*, 40(8), 1474-1484.
- Leonardi, N., & Fagherazzi, S. (2014). How waves shape salt marshes. *Geology*, 42(10), 887-890.

- Leonardi, N., Defne, Z., Ganju, N. K., & Fagherazzi, S. (2016). Salt marsh erosion rates and boundary features in a shallow Bay. *Journal of Geophysical Research: Earth Surface*, *121*(10), 1861-1875.
- Lowe, D. G. (2004). Distinctive image features from scale-invariant keypoints. *International journal of computer vision*, *60*(2), 91-110.
- Luketina, D. (1998). Simple tidal prism models revisited. *Estuarine, Coastal and Shelf Science*, *1*, 77-84.
- MacDonald, G. K., Noel, P. E., van Proosdij, G., & Chmura, G. L. (2010). The legacy of agricultural reclamation on channel and pool networks of Bay of Fundy salt marshes. *Estuaries and Coasts*, *33*(1), 151-160.
- Mancini, F., Dubbini, M., Gattelli, M., Stecchi, F., Fabbri, S., & Gabianelli, G. (2013). Using unmanned aerial vehicles (UAV) for high-resolution reconstruction of topography: The structure from motion approach on coastal environments. *Remote Sensing*, *5*(12), 6880-6898.
- Martha, T. R., Kerle, N., Jetten, V., van Westen, C. J., & Kumar, K. V. (2010). Landslide volumetric analysis using Cartosat-1-derived DEMs. *IEEE Geoscience and remote sensing letters*, *7*(3), 582-586.
- McLoughlin, S. M., Wiberg, P. L., Safak, I., & McGlathery, K. J. (2015). Rates and forcing of marsh edge erosion in a shallow coastal bay. *Estuaries and Coasts*, *38*(2), 620-638.
- Milan, D. J., Heritage, G. L., & Hetherington, D. (2007). Application of a 3D laser scanner in the assessment of erosion and deposition volumes and channel change in a proglacial river. *Earth Surface Processes and Landforms: The Journal of the British Geomorphological Research Group*, *32*(11), 1657-1674.
- Milan, D. J., Heritage, G. L., Large, A. R., & Fuller, I. C. (2011). Filtering spatial error from DEMs: Implications for morphological change estimation. *Geomorphology*, *125*(1), 160-171.

- Milligan, D. C. (1987). *Martime Dykelands: The 350 Year Struggle*.
- Möller, I., & Spencer, T. (2002). Wave dissipation over macro-tidal saltmarshes: Effects of marsh edge typology and vegetation change. *Journal of Coastal Research*, 36(sp.1), 506-521.
- Möller, I., Kudella, M., Rupprecht, F., Spencer, T., van Wesenbeeck, B. K., Wolters, G., . . . Schimmels, S. (2014). Wave attenuation over coastal salt marshes under storm surge conditions. *Nature Geoscience*, 7(10), 727 - 731.
- Möller, I., Spencer, T., & French, J. R. (2016). Wind wave attenuation over saltmarsh surfaces: preliminary results from Norfolk, England. *Journal of Coastal Research*, 12(4), 1009-1016.
- Montreuil, A. L., & Bullard, J. E. (2012). A 150-year record of coastline dynamics within a sediment cell: Eastern England. *Geomorphology*, 179, 169-185.
- Moody, R. M., Cebrian, J., Kerner, S. M., Heck, K. L., Powers, S. P., & Ferraro, C. (2013). Effects of shoreline erosion on salt-marsh floral zonation. *Marine Ecology Progress Series*, 488, 145-155.
- Murfitt, S. L., Allan, B. M., Bellgrove, A., Rattray, A., Young, M. A., & Ierodiaconou, D. (2017). Applications of unmanned aerial vehicles in intertidal reef monitoring. *Scientific Reports*, 7(1), 1-11.
- Narayan, S., Beck, M. W., Reguero, B. G., Losada, I. J., van Wesenbeeck, B., Pontee, N., . . . Burks-Copes, K. A. (2016). The effectiveness, costs and coastal protection benefits of natural and nature-based defences. *PloS one*, 11(5), 1-17.
- NASA. (2014, June 12). Retrieved May 01, 2018, from Fluids Pressure and Depth: https://www.grc.nasa.gov/WWW/K-12/WindTunnel/Activities/fluid_pressure.html
- Nicholls, R. J., & Cazenave, A. (2010). Sea-level rise and its impact on coastal zones. *Science*, 328(5985), 1517 - 1520.

- Nolte, S., Koppenaar, E. C., Esselink, P., Dijkema, K. S., Schuerch, M., De Groot, A. V., . . . Temmerman, S. (2013). Measuring sedimentation in tidal marshes: a review on methods and their applicability in biogeomorphological studies. *Journal of Coastal Conservation*, 17(3), 301-325.
- O’Laughlin, C., van Proosdij, D., & Milligan, T. G. (2014). Flocculation and sediment deposition in a hypertidal creek. *Continental Shelf Research*, 82, 72-84.
- O’Laughlin, C., & van Proosdij, D. (2013). Influence of varying tidal prism on hydrodynamics and sedimentary processes in a hypertidal salt marsh creek. *Earth Surface Processes and Landforms*, 38(5), 534-546.
- Pederson, J. B., & Bartholdy, J. (2007). Exposed salt marsh morphodynamics: an example from the Danish Wadden Sea. *Geomorphology*, 1-2, 115-125.
- Pieterse, A., Puleo, J. A., McKenna, T. E., & Figlus, J. (2017). In situ measurements of shear stress, erosion and deposition in man-made tidal channels within a tidal saltmarsh. *Estuarine, Coastal and Shelf Science*, 192, 29-41.
- Pix4D. (2020). Retrieved May 01, 2018, from Pix4D: <https://www.pix4d.com/>
- Poirier. (2014). Seasonal influences on the ecomorphodynamics of a hypertidal salt marsh and tidal creek system (Master's Thesis). Saint Mary's University, Halifax, Nova Scotia.
- Poirier, E., van Proosdij, D., & Milligan, T. G. (2017). The effect of source suspended sediment concentration on the sediment dynamics of a macrotidal creek and salt marsh. *Continental Shelf Research*, 148, 130-138.
- Polk, M. A., & Eulie, D. O. (2018). Effectiveness of Living Shorelines as an Erosion Control Method in North Carolina. *Estuaries and Coasts*, 41(8), 2212-2222.
- Pringle, A. W. (1995). Erosion of a cyclic saltmarsh in Morecambe Bay, north-west England. *Earth Surface Processes and Landforms*, 20(5), 387-405.

- Province of Nova Scotia. (2000). *Agricultural Marshlands Conservation Act c. 22, s. 1*. Retrieved from <https://nslegislature.ca/sites/default/files/legc/statutes/agricmar.htm>
- Province of Nova Scotia. (2017, December 10). *Historic Wetland Loss in Nova Scotia*. Retrieved 10 01, 2019, from Government of Nova Scotia: <https://www.novascotia.ca/nse/wetland/historic-wetland-loss-ns.asp>
- Province of Nova Scotia. (2018, August 14). *Fundy Dykelands and Wildlife*. Retrieved October 1, 2019, from Lands and Forestry: <https://novascotia.ca/natr/wildlife/habitats/dykelands/>
- Purcell, J. (2020). *Application of managed dyke realignment and hydrodynamic modelling for flood mitigation in a hypertidal estuary in Truro, Nova Scotia (Unpublished master's thesis)*. Halifax, Nova Scotia, Canada: Saint Mary's University.
- Pye, K. (1995). Controls on long-term saltmarsh accretion and erosion in the Wash, eastern England. *Journal of Coastal Research*, 11(2), 337-356.
- Pye, K., & Blott, S. J. (2010). The geomorphology of UK estuaries: the role of geological controls, antecedent conditions and human activities. *Estuarine, Coastal and Shelf Science*, 150, 196-214.
- Pye, K., & French, P. (1993). *Erosion & Accretion Processes on British Salt Marshes. Volume Three: National survey of Accretion & Erosion Status (Vol. 3)*. Cambridge: Cambridge Environmental Research Consultants.
- Raczynski, R. J. (2017). *Accuracy analysis of products obtained from UAV-borne photogrammetry influenced by various flight parameters*. Master's Thesis, NTNU.
- Redfield, A. C. (1972). Development of a New England salt marsh. *Ecological Monographs*, 42(2), 201-237.
- Reed, D. J. (1989). Patterns of sediment deposition in subsiding coastal salt marshes, Terrebonne Bay, Louisiana: the role of winter storms. *Estuaries*, 12(4), 222-227.

- Rendón, O. R., Garbutt, A., Skov, M., Möller, I., Alexander, M., Ballinger, R., . . .
Beaumont, N. (2019). A framework linking ecosystem services and human well-being: Saltmarsh as a case study. *People and Nature*, *1*(4), 486-496.
- Sallenger Jr, A. H., Krabill, W. B., Swift, R. N., Brock, J., List, J., Hansen, M., & Morgan, K. (2003). Evaluation of airborne topographic lidar for quantifying beach changes. *Journal of Coastal Research*, *19*(1), 125-133.
- Sanchez-Arcilla, A., Garcia, M., Garcia, V., & Sierra, J. P. (2017). Flocculation and Settling Velocity Within a *Spartina Anglica* Canopy. *Proceedings of Coastal Dynamics 2017*, (pp. 727-738). Helsingør.
- Schwarz, C., Bouma, T. J., Zhang, L. Q., Temmerman, S., Ysebaert, T., & Herman, P. M. (2015). Interactions between plant traits and sediment characteristics influencing species establishment and scale-dependent feedbacks in salt marsh ecosystems. *Geomorphology*, *250*, 298-307.
- Shepard, C. C., Crain, C. M., & Beck, M. W. (2011). The protective role of coastal marshes: a systematic review and meta-analysis. *PloS one*, *6*(11), 1-11.
- Sherren, K., Bowron, T., Graham, J. T., Rahman, H. M., & van Proosdij, D. (2019). Coastal infrastructure realignment and salt marsh restoration in Nova Scotia, Canada. Chapter 5. In *Responding to Rising Seas: OECD Country Approaches to Tackling Coastal Risks* (pp. 111-135). Paris: OCED Publishing.
- Sherren, K., Loik, L., & A., D. J. (2016). Climate adaptation in 'new world' cultural landscapes: The case of Bay of Fundy agricultural dykelands (Nova Scotia, Canada). *Land Use Policy*, *51*, 267-280.
- Singh, K., Walters, B. B., & Ollerhead, J. (2007). Climate change, sea-level rise and the case for salt marsh restoration in the Bay of Fundy, Canada. *Environments*, *35*(2), 71-84.
- Skinner, C. (2016). The biogeochemistry of a restoring macrotidal salt marsh: Cheverie Creek, Nova Scotia (Master's Thesis). Saint Mary's University, Halifax, Nova Scotia.

- Smith, M. W., & Vericat, D. (2015). From experimental plots to experimental landscapes: topography, erosion and deposition in sub-humid badlands from structure-from-motion photogrammetry. *Earth Surface Processes and Landforms*, 40(12), 1656-1671.
- Smith, M. W., Carrivick, J. L., & Quincey, D. J. (2016). Structure from motion photogrammetry in physical geography. *Progress in Physical Geography*, 40(2), 247-275.
- Snavely, N., Seitz, S. M., & Szeliski, R. (2008). Modeling the world from internet photo collections. *International journal of computer vision*, 80(2), 189-210.
- Stöcker, C., Eltner, A., & Karrasch, P. (2015). Measuring gullies by synergetic application of UAV and close range photogrammetry—A case study from Andalusia, Spain. *Cantena*, 132, 1-11.
- Strecha, C., Bronstein, A., Bronstien, M., & Fua, P. (2011). LDAHash: Improved matching with smaller descriptors. *IEEE transactions on pattern analysis and machine intelligence*, 34(1), 66-78.
- Stronkhorst, J., & Mulder, J. (2014). Considerations on managed realignment in The Netherlands. In *Managed Realignment: A Viable Long-Term Coastal Management Strategy?* (pp. 61-68). Dordrecht: Springer.
- Sutton-Grier, A., Wowk, K., & Bamford, H. (2015). Future of our coasts: The potential for natural and hybrid infrastructure to enhance the resilience of our coastal communities, economies and ecosystems. *Environmental Science & Policy*, 51, 137-148.
- Taylor, J. (1997). *Introduction to Error Analysis, the Study of Uncertainties in Physical Measurements*. New York: University Science Books.
- Temmerman, S., Govers, G., Wartel, S., & Meire, P. (2004). Modelling estuarine variations in tidal marsh sedimentation: response to changing sea level and suspended sediment concentrations. *Marine Geology*, 212, 1-19.

- Temmerman, S., Meire, P., Bouma, T. J., Herman, P. M., Ysebaert, T., & De Vriend, H. J. (2013). Ecosystem-based coastal defence in the face of global change. *Nature*, *504*(7478), 79-83.
- Thieler, E. R., Himmelstoss, E. A., Zichichi, J. L., & Ergul, A. (2009). *e Digital Shoreline Analysis System (DSAS) version 4.0-an ArcGIS extension for calculating shoreline change*. U.S. Geological Survey.
- Tibbetts, J., & van Proosdij, D. (2013). Development of a relative coastal vulnerability index in a macro-tidal environment for climate change adaptation. *Journal of Coastal Conservation*, *17*(4), 775-797.
- Tide Facts: The Humber Estuary*. (n.d.). Retrieved 11 01, 2019, from http://www.tide-project.eu/downloads/TIDE_Facts-Humber_Estuary.pdf
- Tonkin, T. N., & Midgley, N. G. (2016). Ground-control networks for image based surface reconstruction: An investigation of optimum survey designs using UAV derived imagery and structure-from-motion photogrammetry. *Remote Sensing*, *8*(9), 786.
- Torio, D. D., & Chmura, G. L. (2013). Assessing coastal squeeze of tidal wetlands. *Journal of Coastal Research*, *29*(5), 1049-1061.
- Turner, I. L., Harley, M. D., & Drummond, C. D. (2016). UAVs for coastal surveying. *Coastal Engineering*, *114*, 19-24.
- Unger, J., Reich, M., & Heipke, C. (2014). UAV-based photogrammetry: monitoring of a building zone. *International Archives of the Photogrammetry, Remote Sensing and Spatial Information Sciences-ISPRS Archives 40 (2014)*, *40*(5), 601-606.
- van der Nat, A., Vellinga, P., Leemans, R., & van Slobbe, E. (2016). Ranking coastal flood protection designs from engineered to nature-based. *Ecological Engineering*, *87*, 80-90.
- van der Wal, D., & Pye, K. (2004). Patterns, rates and possible causes of saltmarsh erosion in the Greater Thames area (UK). *Geomorphology*, *61*(3-4), 373-391.

- van der Wal, D., Pye, K., & Neal, A. (2002). Long-term morphological change in the Ribble Estuary, northwest England. *Marine Geology*, 189(3-4), 249-266.
- van Proosdij, D., & Baker, G. (2007). *Intertidal morphodynamics of the Avon River estuary*. Nova Scotia Department of Transportation.
- van Proosdij, D., & Matheson, G. (2015). *Truro Flood Sub Consultant Report: Historical Morphodynamics & Dykeland Management*.
- van Proosdij, D., & Page, S. (2012). *Best Management Practices for Climate Change Adaptation in Dykelands: Recommendations for Fundy ACAS Sites*. Saint Mary's University, Department of Geography, Halifax, Nova Scotia, Canada.
- van Proosdij, D., Davidson-Arnott, R. G., & Ollerhead, J. (2006). Controls on spatial patterns of sediment deposition across a macro-tidal salt marsh surface over single tidal cycles. *Estuarine, Coastal and Shelf Science*, 69(1-2), 64-86.
- van Proosdij, D., Milligan, T., Bugden, G., & Butler, K. (2009). A tale of two macro tidal estuaries: differential morphodynamic response of the intertidal zone to causeway construction. *Journal of Coastal Research*, 772-776.
- van Proosdij, D., Perrott, B., & Carrol, K. (2013). Development and application of a geo-temporal atlas for climate change adaptation in Bay of Fundy dykelands. *Journal of Coastal Research*, 1069-1074.
- van Proosdij, D., Ross, C., & Matheson, G. (2018). *Risk Proofing Nova Scotia Agriculture: A Risk Assessment System Pilot (AgriRisk)*. Maritime Provinces Spatial Analysis Research Centre, Department of Geography and Environmental Studies. Halifax: Saint Mary's University.
- Vautherin, J., Rutishauser, S., Schneider-Zapp, K., Choi, H. F., Chovancova, V., Glass, A., & Strecha, C. (2016). Photogrammetric accuracy and modeling of rolling shutter cameras. *ISPRS Annals of Photogrammetry, Remote Sensing & Spatial Information Sciences*, 3, 139-146.

- Vincent, R. E., Burdick, D. M., & Dionne, M. (2013). Ditching and ditch-plugging in New England salt marshes: effects on hydrology, elevation, and soil characteristics. *Estuaries and Coasts*, 36(3), 610-625.
- Voulgaris, G., & Meyers, S. T. (2004). Temporal variability of hydrodynamics, sediment concentration and sediment settling velocity in a tidal creek. *Continental Shelf Research*, 24, 1659-1683.
- Vuik, V., Jonkman, S. N., Borsje, B. W., & Suzuki, T. (2016). The efficiency of vegetated foreshores for reducing wave loads on coastal dikes. *Coastal Engineering*, 116, 42 - 56.
- Vuik, V., Borsje, B. W., Willemsen, P.W.J.M., Jonkman, S. N. (2019). Salt marshes for flood risk reduction: Quantifying long-term effectiveness and life-cycle costs. *Ocean and Coastal Management*, 171, 96 – 110.
- Wallace, K. J., Callaway, J. C., & Zedler, J. B. (2005). Evolution of tidal creek networks in a high sedimentation environment: a 5-year experiment at Tijuana Estuary, California. *Estuaries*, 28(6), 795-811.
- Wang, Z. B., van Maren, D. S., Ding, P. X., Yan, S. L., van Prooijen, B. C., de Vet, P. L., . . . He, Q. (2015). Human impacts on morphodynamic thresholds in estuarine systems. *Continental Shelf Research*, 111, 174-183.
- Westoby, M. J., Brasington, J., Glasser, N. F., Hambrey, M. J., & Reynolds, J. M. (2012). Structure-from-Motion' photogrammetry: A low-cost, effective tool for geoscience applications. *Geomorphology*, 179, 300-314.
- Wheaton, J. M., Brasington, J., Darby, S. E., & Sear, D. A. (2010). Accounting for uncertainty in DEMs from repeat topographic surveys: improved sediment budgets. *Earth surface processes and landforms: the journal of the British Geomorphological Research Group*, 35(2), 136-156.
- Willemsen, P. W., Borsje, B. W., Hulscher, S. J., van der Wal, D., Zhu, Z., Ottenman, B., . . . Bouma, T. J. (2018). Quantifying bed level change at the transition of tidal

- flat and salt marsh: can we understand the lateral location of the marsh edge?
Journal of Geophysical Research: Earth Surface, 123(10), 2509-2524.
- Wilson, E. (2017). Coastal retreat rates and sediment input to the Minas Basin, Nova Scotia. *Canadian Journal of Earth Sciences*, 54(4), 370-378.
- Wollenburg, J. T., Ollerhead, J., & Chmura, G. (2018). Rapid carbon accumulation following managed realignment on the Bay of Fundy. *PLOS ONE*, 13(3), 1-14.
- Wolters, M., Bakker, J. P., Bertness, M. D., Jeffereies, R. L., & Möller, I. (2005). Saltmarsh erosion and restoration in south-east England: squeezing the evidence requires realignment. *ournal of Applied Ecology*, 42(5), 844-851.
- Xiang, J., Chen, J., Sofia, G., Tian, Y., & Tarpolli, P. (2018). Open-pit mine geomorphic changes analysis using multi-temporal UAV survey. *Environmental earth sciences*, 77(6), 220.
- Yang, S. L., Li, H., Ysebart, T., Bouma, T. J., Zhang, W. X., Zhang, W. X., . . . Ding, P. X. (2008). Spatial and temporal variations in sediment grain size in tidal wetlands, Yangtze Delta: On the role of physical and biotic controls. *Estuarine, Coastal and Shelf Science*, 77, 657-671.
- Young, A., & Ashford, S. A. (2006). Application of airborne LIDAR for seacliff volumetric change and beach-sediment budget contributions. *Journal of Coastal Research*, 22(2), 307-318.
- Zelder, J.B. (2017). What's new in adaptive management and restoration of coasts and estuaries? *Estuaries and Coasts*, 40(1), 1-21.

Appendix I – EPR Images and Shoreline Position Error.

Image or Mosaic	Year	Type	Resolution (m)	RMS (m)	Digitizing Error (m)	Shoreline Proxy Offset (m)	Shoreline Position Error (m)
Truro_1938	1938	Aerial Photographs	1.00	5.00	1.00	2.00	5.48
Truro_1964	1964	Aerial Photographs	0.25	5.00	1.00	2.00	5.48
Hants_1964	1964	Aerial Photographs	1.00	5.00	1.00	2.00	5.48
Colchester_1964	1964	Aerial Photographs	1.00	5.00	1.00	2.00	5.48
Hants_1966	1966	Aerial Photographs	1.00	5.00	1.00	2.00	5.48
Colchester_1966	1966	Aerial Photographs	1.00	5.00	1.00	2.00	5.48
Truro_1975	1975	Aerial Photographs	1.00	5.00	1.00	2.00	5.48
Truro_1994	1994	Aerial Photographs	1.00	5.00	1.00	2.00	5.48
Colchester_1994	1994	Aerial Photographs	1.00	5.00	1.00	2.00	5.48
O2002	2002	Aerial Imagery	0.60	2.50	1.00	2.00	3.35
O2003JUAN	2003	Aerial Imagery	0.50	5.00	1.00	2.00	5.48
NS111_2004	2004	Aerial Photographs	0.50	5.00	1.00	2.00	5.48
NS097_2004	2004	Aerial Photographs	0.50	5.00	1.00	2.00	5.48
O2007	2007	Aerial Imagery	0.25	2.50	1.00	2.00	3.35
O2008_2K	2008	Aerial Imagery	0.15	1.00	1.00	2.00	2.45
O2011CBCL	2011	Aerial Imagery	0.15	0.30	1.00	2.00	2.26
O2013	2013	Aerial Imagery	0.25	2.50	1.00	2.00	3.35
O2015	2015	Aerial Imagery	0.25	2.50	1.00	2.00	3.35
MasstownSite1_112015	2015	UAV Imagery	0.04	0.10	1.00	2.00	2.24
MasstownSite2_112015	2015	UAV Imagery	0.04	0.10	1.00	2.00	2.24
MasstownSite3_112015	2015	UAV Imagery	0.04	0.10	1.00	2.00	2.24
LowerTruro_082016	2016	UAV Imagery	0.04	0.10	1.00	2.00	2.24
MasstownEast_052016	2016	UAV Imagery	0.04	0.10	1.00	2.00	2.24

MasstownWest_052016	2016	UAV Imagery	0.04	0.10	1.00	2.00	2.24
MasstownWest_082016	2016	UAV Imagery	0.04	0.10	1.00	2.00	2.24
NS012VDJ_112016	2016	UAV Imagery	0.04	0.10	1.00	2.00	2.24
MasstownEast_082016	2016	UAV Imagery	0.04	0.10	1.00	2.00	2.24
MasstownWest_082017	2017	UAV Imagery	0.04	0.10	1.00	2.00	2.24
MasstownEast_082017	2017	UAV Imagery	0.04	0.10	1.00	2.00	2.24
NS012VDJ_082017	2017	UAV Imagery	0.04	0.10	1.00	2.00	2.24
OnslowNorthRiver_072017	2017	UAV Imagery	0.04	0.10	1.00	2.00	2.24
LowerTruro_092017	2017	UAV Imagery	0.04	0.10	1.00	2.00	2.24

Appendix II – Hydrodynamic Tables by Borrow Pit

Borrow Pit	Mean Incoming SSC	Mean SSC	Min SSC	Max SSC	RHV (flood)	RHV (ebb)
RD_01						
MTW_01						
MTW_02		X	X	X	X	X
MTE_01		X	X	X	X	X
MTE_02		X	X	X	X	X
MTE_03		X	X	X		
VDJ_01		X	X	X	X	X
VDJ_02		X	X	X	X	X
VDJ_03						
LT_01		X	X	X	X	X
LT_02		X	X	X	X	X
LT_03		X	X	X	X	X
LT_04		X	X	X	X	X

RD_01 July 2017

Tide (m)	Mean Incoming SSC (g·l ⁻¹)	Mean SSC throughout tidal cycle (g·l ⁻¹)	Min SSC (g·l ⁻¹)	Max SSC (g·l ⁻¹)	RHV (flood) (m·s ⁻¹)	RHV (ebb) (m·s ⁻¹)	Max (flood) (m·s ⁻¹)	Max (ebb) (m·s ⁻¹)
T1 (3.79m)	0.065	0.095	0.044	0.159	0.05	0.05	0.45	0.39
T2 (4.12m)	0.123	0.091	0.042	0.152	0.09	0.03	0.44	0.43
T3 (3.69m)	0.084	0.089	0.057	0.124	0.10	0.03	0.45	0.36

MTW_01 May 2017

Tide (m)	Mean Incoming SSC (g·l ⁻¹)	Mean SSC throughout tidal cycle (g·l ⁻¹)	Min SSC (g·l ⁻¹)	Max SSC (g·l ⁻¹)	RHV (flood) (m·s ⁻¹)	RHV (ebb) (m·s ⁻¹)	Max (flood) (m·s ⁻¹)	Max (ebb) (m·s ⁻¹)
T1 (8.45m)	1.711	0.415	0.173	0.969	0.24	0.04	0.46	0.41
T2 (7.96m)	3.081	0.547	0.282	1.429	0.35	0.21	0.48	0.29
T3 (8.67m)	4.026	0.410	0.247	0.698	0.24	0.05	0.51	0.36

MTW_01 June 2017

Tide (m)	Mean Incoming SSC (g·l ⁻¹)	Mean SSC throughout tidal cycle (g·l ⁻¹)	Min SSC (g·l ⁻¹)	Max SSC (g·l ⁻¹)	RHV (flood) (m·s ⁻¹)	RHV (ebb) (m·s ⁻¹)	Max (flood) (m·s ⁻¹)	Max (ebb) (m·s ⁻¹)
T1 (N/A)	4.123	X	X	X	X	X	X	X
T2 (7.63m)	0.874	0.316	X	X	X	X	X	X
T3 (8.40m)	3.492	0.246	X	X	X	X	X	X

MTW_02 May 2017

Tide (m)	Mean Incoming SSC (g·l ⁻¹)	Mean SSC throughout tidal cycle (g·l ⁻¹)	Min SSC (g·l ⁻¹)	Max SSC (g·l ⁻¹)	RHV (flood) (m·s ⁻¹)	RHV (ebb) (m·s ⁻¹)	Max (flood) (m·s ⁻¹)	Max (ebb) (m·s ⁻¹)
T1 (8.45m)	1.650	X	X	X	X	X	X	X
T2 (7.96m)	3.679	X	X	X	X	X	X	X
T3 (8.67m)	2.328	X	X	X	X	X	X	X

MTW_02 June 2017

Tide (m)	Mean Incoming SSC (g·l ⁻¹)	Mean SSC throughout tidal cycle (g·l ⁻¹)	Min SSC (g·l ⁻¹)	Max SSC (g·l ⁻¹)	RHV (flood) (m·s ⁻¹)	RHV (ebb) (m·s ⁻¹)	Max (flood) (m·s ⁻¹)	Max (ebb) (m·s ⁻¹)
T1 (N/A)	4.123	X	X	X	X	X	X	X
T2 (7.63m)	0.874	X	X	X	X	X	X	X
T3 (8.40m)	3.492	X	X	X	X	X	X	X

MTE_01 May 2017

Tide (m)	Mean Incoming SSC (g·l ⁻¹)	Mean SSC throughout tidal cycle (g·l ⁻¹)	Min SSC (g·l ⁻¹)	Max SSC (g·l ⁻¹)	RHV (flood) (m·s ⁻¹)	RHV (ebb) (m·s ⁻¹)	Max (flood) (m·s ⁻¹)	Max (ebb) (m·s ⁻¹)
T1 (8.45m)	0.638	X	X	X	X	X	X	X
T2 (7.96m)	1.076	X	X	X	X	X	X	X
T3 (8.67m)	1.226	X	X	X	X	X	X	X

MTE_02 May 2017

Tide (m)	Mean Incoming SSC (g·l ⁻¹)	Mean SSC throughout tidal cycle (g·l ⁻¹)	Min SSC (g·l ⁻¹)	Max SSC (g·l ⁻¹)	RHV (flood) (m·s ⁻¹)	RHV (ebb) (m·s ⁻¹)	Max (flood) (m·s ⁻¹)	Max (ebb) (m·s ⁻¹)
T1 (8.45m)	1.002	X	X	X	X	X	X	X
T2 (7.96m)	2.959	X	X	X	X	X	X	X
T3 (8.67m)	5.663	X	X	X	X	X	X	X

MTE_03 May 2017

Tide (m)	Mean Incoming SSC (g·l ⁻¹)	Mean SSC throughout tidal cycle (g·l ⁻¹)	Min SSC (g·l ⁻¹)	Max SSC (g·l ⁻¹)	RHV (flood) (m·s ⁻¹)	RHV (ebb) (m·s ⁻¹)	Max (flood) (m·s ⁻¹)	Max (ebb) (m·s ⁻¹)
T1 (8.45m)	1.002	X	X	X	0.34	0.26	0.61	0.57
T2 (7.96m)	2.032	X	X	X	0.31	0.20	0.59	0.52
T3 (8.67m)	2.883	X	X	X	0.30	0.27	0.59	0.50

VDJ_01 June 2017

Tide (m)	Mean Incoming SSC (g·l ⁻¹)	Mean SSC throughout tidal cycle (g·l ⁻¹)	Min SSC (g·l ⁻¹)	Max SSC (g·l ⁻¹)	RHV (flood) (m·s ⁻¹)	RHV (ebb) (m·s ⁻¹)	Max (flood) (m·s ⁻¹)	Max (ebb) (m·s ⁻¹)
T1 (8.19m)	3.533	X	X	X	X	X	X	X
T2 (7.80m)	1.708	X	X	X	X	X	X	X
T3 (8.60m)	6.249	X	X	X	X	X	X	X

VDJ_02 June 2017

Tide (m)	Mean Incoming SSC (g·l ⁻¹)	Mean SSC throughout tidal cycle (g·l ⁻¹)	Min SSC (g·l ⁻¹)	Max SSC (g·l ⁻¹)	RHV (flood) (m·s ⁻¹)	RHV (ebb) (m·s ⁻¹)	Max (flood) (m·s ⁻¹)	Max (ebb) (m·s ⁻¹)
T1 (8.19m)	8.316	X	X	X	X	X	X	X
T2 (7.80m)	4.771	X	X	X	X	X	X	X
T3 (8.60m)	14.608	X	X	X	X	X	X	X

VDJ_03 June 2017

Tide (m)	Mean Incoming SSC (g·l ⁻¹)	Mean SSC throughout tidal cycle (g·l ⁻¹)	Min SSC (g·l ⁻¹)	Max SSC (g·l ⁻¹)	RHV (flood) (m·s ⁻¹)	RHV (ebb) (m·s ⁻¹)	Max (flood) (m·s ⁻¹)	Max (ebb) (m·s ⁻¹)
T1 (8.19m)	27.899	31.108	6.822	68.385	0.30	0.55	1.25	0.95
T2 (7.80m)	20.307	8.022	2.973	21.605	0.23	0.30	1.36	0.86
T3 (8.60m)	31.284	46.735	9.997	92.458	X	X	X	X

LT_01 May 2017

Tide (m)	Mean Incoming SSC (g·l ⁻¹)	Mean SSC throughout tidal cycle (g·l ⁻¹)	Min SSC (g·l ⁻¹)	Max SSC (g·l ⁻¹)	RHV (flood) (m·s ⁻¹)	RHV (ebb) (m·s ⁻¹)	Max (flood) (m·s ⁻¹)	Max (ebb) (m·s ⁻¹)
T1 (N/A)	4.965	1.057	0.041	2.263	0.23	0.32	0.59	0.57
T2 (N/A)	4.980	1.097	0.301	2.682	X	X	X	X
T3 (N/A)	5.746	1.890	0.588	4.262	0.26	0.33	0.67	0.58

LT_02 May 2017

Tide (m)	Mean Incoming SSC (g·l ⁻¹)	Mean SSC throughout tidal cycle (g·l ⁻¹)	Min SSC (g·l ⁻¹)	Max SSC (g·l ⁻¹)	RHV (flood) (m·s ⁻¹)	RHV (ebb) (m·s ⁻¹)	Max (flood) (m·s ⁻¹)	Max (ebb) (m·s ⁻¹)
T1 (N/A)	2.970	X	X	X	X	X	X	X
T2 (N/A)	5.987	X	X	X	X	X	X	X
T3 (N/A)	4.599	X	X	X	X	X	X	X

LT_03 May 2017

Tide (m)	Mean Incoming SSC (g·l ⁻¹)	Mean SSC throughout tidal cycle (g·l ⁻¹)	Min SSC (g·l ⁻¹)	Max SSC (g·l ⁻¹)	RHV (flood) (m·s ⁻¹)	RHV (ebb) (m·s ⁻¹)	Max (flood) (m·s ⁻¹)	Max (ebb) (m·s ⁻¹)
T1 (N/A)	4.147	X	X	X	X	X	X	X
T2 (N/A)	5.932	X	X	X	X	X	X	X
T3 (N/A)	5.307	X	X	X	X	X	X	X

LT_04 May 2017

Tide (m)	Mean Incoming SSC ($\text{g}\cdot\text{l}^{-1}$)	Mean SSC throughout tidal cycle ($\text{g}\cdot\text{l}^{-1}$)	Min SSC ($\text{g}\cdot\text{l}^{-1}$)	Max SSC ($\text{g}\cdot\text{l}^{-1}$)	RHV (flood) ($\text{m}\cdot\text{s}^{-1}$)	RHV (ebb) ($\text{m}\cdot\text{s}^{-1}$)	Max (flood) ($\text{m}\cdot\text{s}^{-1}$)	Max (ebb) ($\text{m}\cdot\text{s}^{-1}$)
T1 (N/A)	6.634	X	X	X	X	X	X	X
T2 (N/A)	5.945	X	X	X	X	X	X	X
T3 (N/A)	9.660	X	X	X	X	X	X	X

Appendix III – Predicted cumulative infill and hydroperiod.

Year	Elev (m CGVD2013)	Predicted hydroperiod 2017(min/year)	Predicted hydroperiod percent 2016/17 (%)	Infill Rate	Cumulative Infill (m•yr ⁻¹)
		=countif(Predicted tide height > elev)*5	=(Hydroperiod minutes) / (total min/year) * 100		
0	6.060	8110	4.63		0.00
1	6.180	7035	4.02	0.12	0.12
2	6.284	6200	3.54	0.10	0.22
3	6.376	5490	3.13	0.09	0.32
4	6.457	4985	2.85	0.08	0.40
5	6.531	4475	2.55	0.07	0.47
6	6.597	4010	2.29	0.07	0.54
7	6.656	3695	2.11	0.06	0.60
8	6.711	3400	1.94	0.05	0.65
9	6.761	3120	1.78	0.05	0.70
10	6.808	2855	1.63	0.05	0.75
11	6.850	2715	1.55	0.04	0.79
12	6.890	2570	1.47	0.04	0.83
13	6.928	2385	1.36	0.04	0.87
14	6.963	2205	1.26	0.04	0.90
15	6.996	2070	1.18	0.03	0.94
16	7.027	1980	1.13	0.03	0.97
17	7.056	1875	1.07	0.03	1.00
18	7.084	1790	1.02	0.03	1.02
19	7.110	1680	0.96	0.03	1.05
20	7.135	1590	0.91	0.02	1.07
21	7.158	1525	0.87	0.02	1.10
22	7.181	1425	0.81	0.02	1.12
23	7.202	1330	0.76	0.02	1.14
24	7.222	1260	0.72	0.02	1.16
25	7.240	1220	0.70	0.02	1.18

Year	Elev (m CGVD2013)	Predicted hydroperiod 2016/17 (min/year)	Predicted hydroperiod percent 2016/17 (%)	Infill Rate	Cumulative Infill (m•yr ⁻¹)
		=countif(Predicted tide height > elev)*5	=(Hydroperiod minutes) / (total min/year) * 100		
0	6.425	5195	2.97		0.00
1	6.895	2560	1.46	0.47	0.47
2	7.127	1625	0.93	0.23	0.70
3	7.274	1130	0.64	0.15	0.85
4	7.376	905	0.52	0.10	0.95
5	7.458	720	0.41	0.08	1.03
6	7.523	585	0.33	0.07	1.10
7	7.576	480	0.27	0.05	1.15
8	7.619	400	0.23	0.04	1.19
9	7.655	345	0.20	0.04	1.23
10	7.687	300	0.17	0.03	1.26
11	7.714	275	0.16	0.03	1.29
12	7.739	240	0.14	0.02	1.31
13	7.760	220	0.13	0.02	1.34
14	7.780	205	0.12	0.02	1.36
15	7.799	180	0.10	0.02	1.37
16	7.815	175	0.10	0.02	1.39
17	7.831	160	0.09	0.02	1.41
18	7.845	145	0.08	0.01	1.42
19	7.859	140	0.08	0.01	1.43
20	7.871	130	0.07	0.01	1.45
21	7.883	120	0.07	0.01	1.46
22	7.894	110	0.06	0.01	1.47
23	7.904	110	0.06	0.01	1.48
24	7.914	105	0.06	0.01	1.49
25	7.923	105	0.06	0.01	1.50

Year	Elev (m CGVD2013)	Predicted hydroperiod 2017 (min/year)	Predicted hydroperiod percent 2016/17 (%)	Infill Rate	Cumulative Infill (m•yr ⁻¹)
		=countif(Predicted tide height > elev)*5	=(Hydroperiod minutes) / (total min/year) * 100		
0	6.370	5530	3.16		0.00
1	6.460	4970	2.84	0.09	0.09
2	6.541	4370	2.49	0.08	0.17
3	6.612	3960	2.26	0.07	0.24
4	6.676	3595	2.05	0.06	0.31
5	6.735	3250	1.86	0.06	0.36
6	6.788	2950	1.68	0.05	0.42
7	6.836	2750	1.57	0.05	0.47
8	6.881	2605	1.49	0.04	0.51
9	6.923	2400	1.37	0.04	0.55
10	6.962	2210	1.26	0.04	0.59
11	6.998	2050	1.17	0.04	0.63
12	7.031	1965	1.12	0.03	0.66
13	7.063	1855	1.06	0.03	0.69
14	7.094	1760	1.00	0.03	0.72
15	7.122	1630	0.93	0.03	0.75
16	7.149	1550	0.88	0.03	0.78
17	7.174	1435	0.82	0.03	0.80
18	7.197	1345	0.77	0.02	0.83
19	7.219	1270	0.72	0.02	0.85
20	7.240	1220	0.70	0.02	0.87
21	7.260	1190	0.68	0.02	0.89
22	7.279	1110	0.63	0.02	0.91
23	7.297	1075	0.61	0.02	0.93
24	7.315	1035	0.59	0.02	0.94
25	7.332	995	0.57	0.02	0.96

Year	Elev (m CGVD2013)	Predicted hydroperiod 2017 (min/year)	Predicted hydroperiod percent 2016/17 (%)	Infill Rate	Cumulative Infill (m•yr ⁻¹)
		=countif(Predicted tide height > elev)*5	=(Hydroperiod minutes) / (total min/year) * 100		
0	6.030	8325	4.75		0.00
1	6.310	6005	3.43	0.28	0.28
2	6.512	4605	2.63	0.20	0.48
3	6.667	3660	2.09	0.15	0.64
4	6.790	2945	1.68	0.12	0.76
5	6.889	2570	1.47	0.10	0.86
6	6.975	2145	1.22	0.09	0.95
7	7.048	1910	1.09	0.07	1.02
8	7.112	1675	0.96	0.06	1.08
9	7.168	1480	0.84	0.06	1.14
10	7.218	1270	0.72	0.05	1.19
11	7.261	1190	0.68	0.04	1.23
12	7.301	1075	0.61	0.04	1.27
13	7.337	990	0.57	0.04	1.31
14	7.370	925	0.53	0.03	1.34
15	7.401	855	0.49	0.03	1.37
16	7.430	780	0.45	0.03	1.40
17	7.456	720	0.41	0.03	1.43
18	7.480	670	0.38	0.02	1.45
19	7.503	620	0.35	0.02	1.47
20	7.524	585	0.33	0.02	1.49
21	7.544	530	0.30	0.02	1.51
22	7.561	505	0.29	0.02	1.53
23	7.578	475	0.27	0.02	1.55
24	7.594	440	0.25	0.02	1.56
25	7.609	420	0.24	0.01	1.58

Equation X is used to determine the change in elevation between two successive years, where Z is bed elevation, R_0 is the year one infill rate obtained from Chapter 3, and H is hydroperiod.

To determine the infill rate between two years Equation X is used:

Finally, cumulative infill (CI) is determined by adding each successive infill rate to the original as-built borrow pit bed elevation (Equation X):

End point erosion rates (EPR) from transects that intersect the borrow pits were used to determine a mean EPR for each individual borrow pits. 10 metres were subtracted from each transect foreshore width to determine the distance from the borrow pit to the foreshore edge. The borrow pit foreshore width and EPR rates were used to determine how long before the foreshore would erode into the borrow pit.